On the nature of structural fluctuations in complex liquids

Martina Požar

Sorbonne Université

L'Université de Split

École doctorale “Physique en Île-de-France” et “Doctoral school of Biophysics”

Laboratoire de physique théorique de la matière condensée (LPTMC), Sorbonne Université et Faculté de Science, Université de Split

On the nature of structural fluctuations in complex liquids

Sur la nature des fluctuations structurelles dans les liquides complexes

par Martina POŽAR

Thèse de doctorat de la physique

Dirigée par Aurélien PERERA et Larisa ZORANIĆ

Présentée et soutenue publiquement le 16eme Novembre 2018

Devant un jury composé de :

M	Jean-François DUFRÊCHE	(rapporteur)
M	Jadran VRABEC	(rapporteur)
Mme	Hélène GERARD	(examinatrice)
Mme	Sanja TOMIĆ	(examinatrice)
Mme	Leandra VRANJEŠ-MARKIĆ	(examinatrice)
M	Dražen ZANCHI	(examinateur)
Mme	Larisa ZORANIĆ	(co-directrice de thèse)
M	Aurélien PERERA	(co-directeur de thèse)

Summary

The analysis of different types of structuring, present in simple and complex liquids and their mixtures, was done using the method of molecular dynamics. Complex mixtures have at least one associative component, such as water, alcohols (mono-ols and diols) and amines. The supra-molecular structuring in these mixtures is detected, described, quantified and connected with the atom-atom interactions is the molecules. These systems have interesting fluctuation behaviors, as shown through Kirkwood-Buff integrals. Their correlation functions behave in a complex way, depending on the component, concentration and temperature. The pre-peak at small k values in the site-site structure factor is defined as a signature of molecular domains in these mixtures. A special focus is placed on long-range structuring, which is a novelty considering the majority of the work in the field of the physics of liquids. This thesis contributes to a better understanding of micro-heterogeneous structures in molecular liquids, and gives new links to structural heterogeneities in soft and bio-matter.

Keywords: liquids, binary-mixtures, molecular-dynamics, structural-properties, microheterogeneity, water, alcohols, amines, non-polar-solvents

---

Resumé

L'analyse de différents types de structuration, présents dans des liquides simples et complexes et leurs mélanges, a été réalisée en utilisant la méthode de la dynamique moléculaire. Les mélanges complexes ont au moins un composant associatif, tel que l'eau, les alcools (mono-ols et diols) et les amines. La structuration supra-moléculaire dans ces mélanges est détectée, décrite, quantifiée et liée aux interactions atome-atome entre les molécules. Ces systèmes ont des fluctuations aux comportements intéressants, comme le montrent les intégrales de Kirkwood-Buff. Leurs fonctions de corrélation se comportent d'une manière complexe, en fonction du composant, de la concentration et de la température. Le pré-pic aux petites valeurs de k dans les facteurs de structure site-site est défini comme une signature de la ségrégation en domaines dans ces mélanges. Une attention particulière est mise sur la structuration à longue portée, ce qui est une nouveauté compte tenu de la majorité des travaux dans le domaine de la physique des liquides. Cette thèse contribue à une meilleure compréhension des structures micro-hétérogènes dans les liquides moléculaires et permet d'établir des liens avec les hétérogénéités structurelles dans la matière molle et de la bio-matière.

Mots-clés: liquides, mélanges-binaires, dynamique-moléculaire, propriétés-structurelles, microhétérogénéité, eau, alcools, amines, solvants-non-polaires

Acknowledgments

Writing a thesis is never a solitary endeavour. In my case, it has been an incredible journey, made all the richer by the host of people who contributed in a myriad of ways. Regardless of their individual styles of support, these people have my immense gratitude.

First and foremost, I would like to thank my supervisors, doc. dr.sc. Larisa Zoranić and dr.sc. Aurélien Perera. Both of them were instrumental in the making of this thesis and it's impossible to itemize all the ways they've helped me. Larisa Zoranić not only gave me a chance on her project, but also much of her own time and care - I will never forget that. Aurélien Perera, whose drive and passion for science are remarkable, has been there for me from the first days of the joint PhD study, for which I'm forever grateful.

Special thanks go to other members of the Split group, namely prof. Franjo Sokolić, doc. dr.sc. Bernarda Lovrinčević and Tomislav Primorac, for all the scientific discussions and other activities shared together. Prof. Tomaž Urbič, a dear collaborator and co-author, also deserves a big thank you.

Assistance provided by the Doctoral School of Biophysics in Split, heralded by prof. emeritus Davor Juretić, prof. Paško Županović and dr.sc. Irena Bitunjac, was greatly appreciated.

I would like to express my gratitude to the kind folks from Laboratoire de Physique Théorique de la Matière Condensée (LPTMC) at Sorbonne Université (formerly known as Université Pierre et Marie Curie), especially the former and current directors, Pascal Viot and Bertrand Delamotte. My *parrain*, Maria Barbi, and *tuteur*, Daniel Borgis, also deserve my appreciation.

I want to acknowledge all the organizations which funded me during the course of my PhD program: the Croatian Science Foundation (through their Young reasearchers project), the French government (for allocating two research grants) and L'Oréal ADRIA d.o.o. together with the Croatian jury for UNESCO (the grant "For women in science").

Heartfelt thanks go to all my friends for their patience and encouragement (especially Dijana, who bore the brunt of it). Last but not least, I thank my parents Marica and Borislav, to whom I dedicate this thesis. Their love and support cannot be overstated.

Contents

1. Introduction **1**

2. Theory and methodology **9**
2.1. Molecular dynamics 10
2.1.1. Potentials in MD 11
2.1.2. Interaction computation 12
2.1.3. MD and statistical mechanics 15
2.1.4. Temperature and pressure coupling 16
2.1.5. The GROMACS program package 18
2.2. Structural analysis 19
2.2.1. Pair correlation functions 19
2.2.2. Structure factors 21
2.2.3. Scattering intensity 22
2.2.4. Cluster probability distributions 24
2.3. Kirkwood-Buff integrals 25

Results and discussion **31**

3. Simple and complex disorder **31**
3.1. Mixtures with benzene as a common solvent 33
3.1.1. Benzene-alkane mixture 33
3.1.2. Benzene-acetone mixture 36
3.1.3. Benzene-ethanol mixture 38
3.2. The influence of solvent shape on disorder 42
3.2.1. Mixtures with acetone 42
3.3. Conclusions 44

4. The ethanol-methanol mixture **47**
4.1. Structural analysis 48
4.1.1. Snapshots 48
4.1.2. Cluster distribution probabilities 49
4.1.3. Pair correlation functions 51
4.1.4. Structure factors 52
4.2. Thermodynamical analysis 54
4.2.1. Volumes and energies 54
4.2.2. Kirkwood-Buff integrals 55

4.3. The methanol-1-propanol mixture 57
4.4. Conclusions 58

5. Microheterogeneity versus clustering 61
5.1. Snapshot analysis 63
5.2. Correlation function analysis 64
5.3. Structure factor analysis 66
5.4. Cluster distribution analysis 68
5.5. Conclusions 71

6. Aqueous alcohol mixtures in cold conditions 73
6.1. Aqueous methanol mixture 74
6.1.1. Correlation functions 74
6.1.2. Cluster probability distributions 76
6.1.3. Structure factors 76
6.1.4. Kirkwood-Buff integrals 78
6.2. Aqueous ethanol and aqueous tert-butanol mixture 79
6.2.1. Correlation functions 79
6.2.2. Cluster probability distributions 81
6.2.3. Structure factors 81
6.2.4. Kirkwood-Buff integrals 83
6.3. Conclusions 84

7. The case of the aqueous propylamine mixture 85
7.1. Neat propylamine 86
7.2. Aqueous propylamine 88
7.2.1. Snapshots 88
7.2.2. Cluster probability distributions 89
7.2.3. Pair correlation functions 90
7.2.4. Structure factors 91
7.2.5. Kirkwood-Buff integrals 93
7.3. Conclusions 94

8. The microstructure of neat 1,n-diols and their mixtures 97
8.1. Neat 1,n-diols 99
8.1.1. Cluster distribution probabilities 100
8.1.2. Pair correlation functions 101
8.1.3. Structure factors 102
8.1.4. Scattering intensity 104
8.2. Mixtures with 1,n-diols 105
8.2.1. Mixtures with water 105
8.2.2. Mixtures with mono-ols 109
8.3. Conclusions 113

9. Conclusions and outlook **115**

A. Supplementary simulation results for neat liquids **121**
A.1. Simulation protocol . . . 121
A.2. Neat liquids - various results . . . 122
A.2.1. Benzene . . . 122
A.2.2. Acetone . . . 124
A.2.3. Alcohols . . . 126
A.2.4. Water . . . 131
A.2.5. Other neat liquids . . . 131
A.2.6. Pyridine and piperidine . . . 132

B. Supplementary simulation data for mixtures **133**
B.1. Simulation protocol, system size and simulation time . . . 133
B.2. Mixtures with benzene as the common solvent . . . 134
B.2.1. LP shift . . . 134
B.3. The ethanol-methanol mixture . . . 135
B.3.1. LP shift . . . 135
B.4. Aqueous alcohol mixtures in cold conditions . . . 135
B.4.1. Simulations at low temperatures . . . 135
B.4.2. Cluster distribution probabilities . . . 137
B.5. Propylamine-water mixture . . . 138
B.5.1. LP shift . . . 138
B.6. Mixtures with 1,n-diols . . . 138
B.6.1. LP shift . . . 138
B.6.2. Cluster distribution probabilities . . . 139
B.6.3. Thermodynamic results . . . 140

Summary **145**

Sažetak **149**

Resumé **153**

List of Figures **153**

List of Tables **159**

Curriculum vitae **162**

List of Publications **164**

Bibliography **165**

1. Introduction

The general purpose of this thesis is to analyze the rich variety of disorder present in liquids, especially binary mixtures involving at least one hydrogen bonding component. The liquid state, as an intermediate state between the gas and the solid, is very wide, encompassing also soft matter, such as liquid crystals and micro-emulsions [1]. Liquids in the soft matter category constitute of large molecules, larger than water or alcohols. For example, N-(4-Methoxybenzylidene)-4-butylaniline (MBBA), a molecule which makes up liquid crystals (Figure 1.1, upper panel), is much larger than the molecules of water, acetone or mono-ol alcohols [2]. Similarly, surfactant molecules such as sodium stearate (Figure 1.1, lower panel), which sit at the interfaces between water and oil in micro-emulsions, are very similar to MBBA in size [3, 4, 5]. These two liquids are characterized by the appearance of of mesoscopic formations, which can go up to the size of 100 nm. These formations include ordered mono-domains in liquid crystals or micellar supra-structures in micro-emulsions [6, 7, 8].

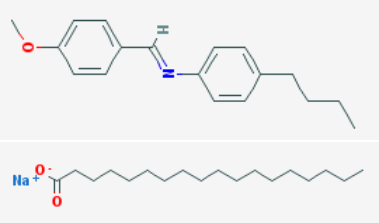

Figure 1.1.: The 2D structures of: MBBA (upper panel) and sodium stearate (lower panel). Both figures are taken from PubChem [9, 10].

However, in this thesis we study liquids in which the structuring is in the 1-10 nm range at most, and is also lacking any of the regular geometric features which can be found in self-assembly. One of the goals of this study is to consider them as precursor states to more organised forms of liquids, in which they would share the same property of being "complex" liquids. The building block for this complexity is the hydrogen bond. Associative liquids such as water or alcohols, thanks to their hydrogen bonding properties, certainly fall into the category of complex liquids. On the other hand, liquid argon is the classic example of a simple liquid [1]. There are detailed studies of simple liquids, such as the famous textbook "Theory of Simple Liquids" by Hansen and MacDonald [11], as well as many others on soft-matter, such as "Soft matter physics: an introduction" by Kleman and Lavrentovich [12]. However, there are almost no specific studies of the complex liquids we mention in this work. Even though water is notoriously known as a mysterious liquid [13], with more than 60 anomalies in the liquid state alone [14, 15], aqueous mixtures are often considered as a straightforward extension of "simple liquids". It would be even hard

to prove, in a classical way, why one should pay any specific attention to water and aqueous mixtures, aside from the complexity brought by angle dependent interactions. Indeed, the majority of studies of such liquids uses the same statistical tool as in simple liquids - the pair correlation function [16, 17, 18, 19, 20, 21, 22, 23]. This poses the question if complex liquids require the study of higher rank correlation functions, such as 3-body or higher correlations. In the absence of any explicit indication requiring these hard-to-compute quantities, it would indeed seem that both simple and complex liquids can be satisfactorily understood from pair interactions and pair correlations. In this work, we show that it is not so much the fact that pair correlations are studied, but rather how the complexity manifests itself in an entirely novel and unexpected fashion with the same statistical tools used to study simple liquids.

At the heart of this complexity lie fluctuations, which make an important difference between classical thermodynamics and statistical thermodynamics. Classical thermodynamics cannot explain fluctuations, since it consider matter as a continuum endowed with field type properties, such as heat and energy. Statistical mechanics introduces interacting particles and allow the computation of energy and heat as emergent quantities [24]. For example, for a simple monoatomic liquid, the excess internal energy is written as a weighted average of the pair interaction $v(r)$ [11]:

$$\frac{E_{ex}}{N} = \frac{\rho}{2} \int g(r) v(r) d\vec{r}$$

where $g(r)$ is the radial distribution function which plays the role of the statistical weight function. Similarly, temperature is related to the average kinetic energy of the particles through:

$$\frac{E_{kin}}{N} = \frac{3}{2} k_B T$$

and the total energy is $E = E_{kin} + E_{ex}$. The expression for the excess internal energy above has the same mathematical structure for complex liquids, and would depend on the orientational properties of the molecules, described by the molecular pair interaction $v(1,2) = v(r, \Omega_1, \Omega_2)$, where Ω_i describes the orientation of molecule 1. For each additional (orientational) degree of freedom, the kinetic energy would contain orientational degrees of freedom as additional $\frac{1}{k_B T}$ terms [11]. From these expressions, one sees that the final numerical values for E_{ex} may not explicitly allow to differentiate one type of liquid from another, if it is only for the magnitude of this value. Energy is a collective thermodynamic property, so it cannot be invoked to characterize the type of local structure we wish to analyze. In fact, none of the thermodynamic properties can directly lead us to a pertinent analysis, since they can only reflect averages over the entire system [24]. This is precisely the crux of the

problem that we meet here. Statistical average is a very convenient tool to analyse the large number of molecules in a system. However, that same statistical tool seems to be an inconvenient obstacle for analyzing the heterogeneity which appears in associating mixtures.

In order to better pinpoint the nature of this problem, we can compare a liquid of flexible polymers with a gas of strong dipolar spheres. Such spheres tend to assemble into chains [25], which are not of the same nature as the flexible polymers, since they are labile. And the crucial question would be: how to describe such chains? As polymers or in terms of individual particles? This problem does not seem to be properly adressed in the current state of knowledge in liquids. Yet, this is the type of problem which seems to be relevant for biological systems, where the constant assembly and dissociation of many types of molecules and macromolecules happens in a highly concerted fashion. In view of this problem, one may ask what are exactly the difficulties with the current statistical description of liquids, which do not allow one to investigate complex systems? It seems that the complexity is hidden inside the statistical quantities, and the problem is to figure out how it is hidden, where it is hidden, but also "what" is hidden. Indeed, we do not know how to characterize this complexity in the first place.

To illustrate, let us refer to one of the most apparent problem that has emerged in the past decades, the nature of the fluctuations in binary aqueous mixtures. This problem appeared through the unusually large values of the so-called Kirkwood-Buff integrals (KBI) [26, 27, 28, 29]. These quantities combine the integrals of the species-species correlation functions $g_{ij}(r)$ with thermodynamic quantities such as the total and partial molar volumes, V and V_i, the isothermal compressibility κ_T and the derivative of the chemical potentials by the mole fraction of one of the components $\frac{\partial \mu_i}{\partial x_i}$ (the corresponding expressions are given in section 2.3) [30]. The derivation of Kirkwood and Buff indicates that these quantities reflect the concentration fluctuations in the system [31]. However, this leads to a new issue: why do some stable aqueous mixtures, such as *tert*-butanol-water, have concentration fluctuations as high as those which are close to demixing, like 1-butanol-water [26]? This is further complicated by the fact that the KBIs for some aqueous mixtures are rather small, e.g. in aqueous DMSO [26].

Figure 1.2 shows the differences in the experimental KBIs of the aqueous TBA and DMSO systems. Concentration fluctuations by themselves are not enough to characterize such a big diversity in the magnitude and trend of the KBIs, given the relatively small molecular differences between the two solvents (Figure 1.2). Both molecules have a significant non-polar part in the molecule, but TBA has a hydroxyl group which is a donor and acceptor, while DMSO has a single oxygen atom which acts as an acceptor [32]. These are considerations at the single molecule level, which prompts the question of how these small differences become magnified at the mixture level. To better understand what is happening in terms of structuring, we turn to the snapshots of the mixtures in Figure 1.3.

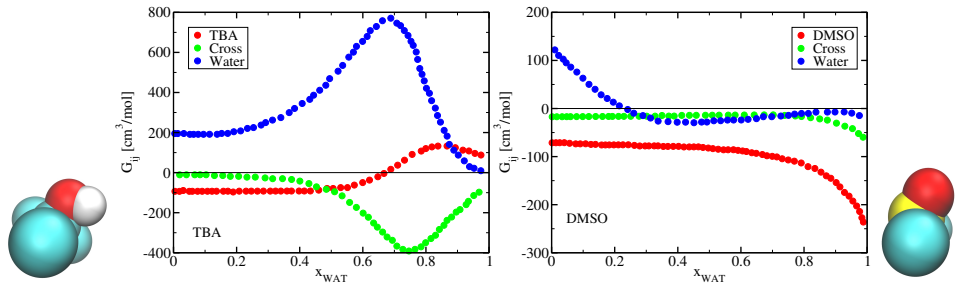

Figure 1.2.: KBIs of aqueous TBA (left) and aqueous DMSO (right) as function of water mole fraction (taken from Matteoli and Lepori [26]). The TBA and DMSO molecules are shown to scale.

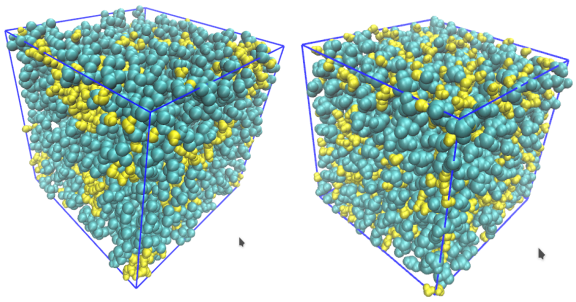

Figure 1.3.: Snapshpot of equimolar aqueous TBA system (left panel) and aqueous DMSO (right panel). Both systems contain 2048 molecules. Water molecules are shown in yellow and the solute molecules in cyan.

Figure 1.3 indicates that that there is a difference in the organization of these mixtures. TBA-water seems to be more heterogeneous than aqueous-DMSO, which is particularly noticeable when observing water molecules. Water molecules in TBA-water are grouped together in large, almost globular patches, while in aqueous DMSO the same molecules forms chain-like clusters. Investigations of these systems in our group [33, 34] have shown that the structuring of water has a crucial effect on the concentration fluctuations. The fact that water forms chain-like clusters in DMSO-water is the reason why the concentration fluctuations are so low, as witnessed by the KBIs [34]. These studies have implied that concentration fluctuations are subordinate to local aggregative structures. The latter are detectable through pre-peaks in atom-atom structure factors. The statistical study of such pre-peaks is highly difficult because of the two spatial and temporal scales involved: one of individual molecules, which move at the sub-pico-second scale, and the other of the heterogeneity, which "moves" at nano-second scale [35]. Returning to Figure 1.3, the hidden feature we were looking for is the heterogeneity. Previous studies have hinted that this is a very moving feature, which shows different facets in different systems [36, 37, 38, 39, 40, 41].

As hinted in the paragraphs above, the problems explored in this thesis are rooted in the physico-chemical aspects of the constituent molecules, such as the nature of

their interactions, but emerge in the collective properties of their liquid state. For this reason, this thesis will study many different liquid mixtures, in order to pinpoint how concentration fluctuations coarsen into the specific heterogeneity we are interested in, and how this depends on the nature of the components. Its aim is to describe realistic mixtures, but mostly from a structural point of view. This may appear very restrictive, especially when considering all the other properties which are usually studied in physical chemistry, both experimentally and theoretically, and one may wonder about the position of the present study within the general physical chemistry and chemical physics areas. However, physical chemistry strives to understand either macroscopic properties or properties of single/very few molecules. Individual molecules have many properties related to their electronic distribution and its coupling with the internal nuclear distributions [42]. Usually, this type of property is studied through quantum mechanics. The same methodology allows the study of small clusters of molecules, in order to understand how they bind and act in this context. While this is supposed to give an idea of how the same molecules would behave in condensed liquid phases, it is also often not the case. One good example is the polarisation of water molecules, which is very different in the gas phase, in small clusters and in neat water [43, 44]. The description of the polarisation of water in the liquid phase has garnered controversies ever since early water models were proposed [44, 45, 46].

At the opposite end of the spectrum, macroscopic properties represent spatial averages over many local distributions and tend to wash out such details. The relevance of such details is then to be found in some anomalies developed by macroscopic measures. Once again, the anomalous properties of water are a good example [15, 14, 47]. Its properties stem from specific microscopic dispositions of the water molecules at the local level [48, 49, 50]. Water molecules tend to form Hbonds, but a continuous paving of the entire liquid with these bonds is not possible, unless it is in the solid ice form [47] [1]. Since the Hbond connected form cannot pave the entire volume, it must have only some local extent, which must also come in a variety of forms, buried within more disordered forms of water. The notion about water existing in two forms has surfaced right at the start of the scientific interest for this substance, with Röngten in 1892 [52]. Since then, several studies have tried to prove or disprove this idea [48, 53, 54, 55, 56]. In a way, neat water itself appears as a micro-heterogeneous liquid. Incidentally, the 2005 issue of Science, mentioning all the unsolved problems in Science, ranging from pure Mathematics all the way to social sciences, positioned the structure of water as the 21st problem, between superfluidity and the glass transition [57]. Since then, this particular problem has not been really solved.

The nature of this problem perfectly describes the weakness of the current position in the understanding of liquids. The amount to which local heterogeneity influences

[1] On a sidenote, there are more than a dozen forms of ice, mostly depending on applied pressure, indicating that even the ordered form has several frustrations under pressure, which when releaved lead to other forms of ice [51].

the macroscopic properties is largely misunderstood. The Split and Paris groups have brought a new understanding to this problem, based on the idea that micro-heterogeneity was a k-fluctuation, with $k \neq 0$, and to be differentiated from fluctuations which correspond to macroscopic observables (principally through the KBI). This is a novelty in the field of molecular liquids and their mixtures, for the vast majority of authors, even when dealing with complex mixtures like aqueous methanol or aqueous ethanol, concentrate their efforts on ellucidating the short range organization [58, 22, 19, 59, 20, 18, 16, 60, 61], thermodynamic [61, 60, 58, 62, 20, 63] or transport properties [64, 58, 20, 16, 65, 66]. In contrast, the work presented in this thesis pays particular attention to the medium to long range ordering.

This research also has tentative tangents towards biophysics, as micro-heterogeneity could play an important role in the way various large molecules exist inside biosystems. Perhaps such macromolecules could be considered as active forms of micro-heterogeneity, as opposed to the passive micro-heterogeneity found in aqueous and non-aqueous mixtures, but that is to be defined by subsequent investigations. Either way, the present study may be a stepping stone towards ellucidating the microscopic mechanisms for self-assembly and giving a more fleshed out description of bio-matter in general.

The main tools used in this thesis are statistical tools issued from the theory of liquids, wherein the data are obtained by molecular dynamics (MD) computer simulations. MD is done within the framework of classical mechanics, relying on solving the equation of motion of all the particles in a simulation box, hence follow their individual trajectories for a given time frame [67]. Of course, this means that quantum aspects are not considered in our study. Furthermore, the principal interest of this research is the analysis of static properties, such as pair correlation functions, and thermodynamic properties. Dynamic quantities, like diffusion coefficients or time dependent van Hove correlation functions, are not featured. This may bring up the question of using Monte Carlo methods, which are simpler since they are limited to the calculation of energy [68]. However, the necessity of simulating large systems for long simulation times, in order to track the evolution of micro-heterogeneity, requires the use of fast and efficient programs. It's much more practical to use an already available program package, like Gromacs [69, 70, 71], for a homemade Monte Carlo code is too slow at the current stage of development to be an efficient rival.

The details of the chapters can be summarised and put into perspective of the ideas that fed into the present work, in the following way.

Chapter 2 is an exposé of the theoretical foundations relevant for this work. First, the computer simulation methodology is detailed as it is the main tool utilized. Then, important results of the statistical theory of liquids are covered, pertaining to the structural analysis, such as pair correlation functions and site-site structure factors. The connection between site-site structure factors and X-ray radiation scattering is detailed. Finally, through the Kirkwood-Buff integrals, results related to density and concentration fluctuations are elucidated.

Chapter 3 presents the concept of simple and complex disorder in mixtures, exemplified through binary mixtures with benzene as the common solvent. The chapter is based on one publication [72], clarifying issues such as what generates MH, is water necessary to have MH in the system and the influence of solute shape on MH. Chapter 4 discusses the concept of ideal mixtures, concerning specifically mixtures of small monohydric alcohols (mono-ols). When mixed with water, methanol and ethanol exhibit very different structural properties, but when mixed with each other, the picture changes. This is the material from one publication [73]. In Chapter 5, the difference between clustering and MH is revealed by a detailed structural analysis, contrasting the results of site-site structure factors and cluster distribution probabilities in two different MH mixtures. The content of this chapter stems from [74]. Chapter 6 concerns three aqueous mono-ol mixtures in cold conditions and investigates the temperature dependence of the structural properties. This research is featured in two publications [75, 76].

The following two chapters shift their focus from mixtures with mono-ols and explore changes in structure when a different type of co-solvent is added. Chapter 7 studies the structural properties of neat propylamine and its aqueous mixture, in comparison with previous mono-ol investigations. Its content is the basis of one paper [77]. In Chapter 8, the attention is centered on dihidric alcohols (diols), both as neat liquids and related mixtures. This research was published in two papers [78, 79].

Chapter 9 is the Conclusion. Some of the work in current completion is briefly discussed, as well as other projects. Some of the latter couldn't be fully investigated for a variety of reasons and might be explored at a later stage, while others exceeded the temporal limits of this thesis. Finally, Appendices A and B contain all the relevant simulation details on neat liquids and liquid mixtures, respectively. They also contain supplementary results and more technical discussions not featured elsewhere.

2. Theory and methodology

The theoretical groundwork about the statistical theory of liquids and simulation methodology is laid out in this chapter. It covers the basics in brief, as details can be found in many excellent textbooks, such as "Theory of simple liquids" by Hansen and MacDonald [11], "Computer simulations of liquids" by Allen and Tildesley [68], "Theory of Molecular Fluids" [80] by Gray and Gubbins and many others[1, 81, 82].

However, the majority of these works focuses heavily on simple systems, such as monoatomic liquids and/or their binary mixtures. As mentioned in the Introduction, both the statistical theory and computer simulations face challenges when encountering a systematic non-uniformity in liquids - micro-heterogeneity (MH). This problem is closely linked to the appearance of density (in single component) or concentration fluctuations (CF) (in mixtures). Fluctuations are at the very heart of the statistical approach, since they signal the first departure from the average homogeneity. When a mixture is close to a macroscopic phase transition, it exhibits high concentration fluctuations, which are an indicator that the components would prefer to phase separate rather than being in a homogeneous mixture. MH systems may have high CF, as shown by the KBI experimental results published by Matteoli and Lepori [26]. However, MH systems are proven to be stable in ambient conditions, and the question of how MH helps the stability of a mixture is not quite resolved.

Furthermore, a wide variety of KBI behaviour can be noticed for co-solvents which have points in common. To take the example from the Introduction, *tert*-butanol and DMSO are both large molecules with a considerable non-polar part. Yet, aqueous-DMSO displays near-ideal KBIs, while aqueous-TBA has a strongly non-ideal trend in the KBIs, which is leaning towards demixing. This illustrates the fact that differences in the interactions could be dramatically enhanced in the fluctuations, all while being far from the critical point. This is the most important idea here.

These large experimental KBIs also pose many problems in computer simulations. When dealing with systems where there is considerable segregation, yet no demixing, it's a prerequisite to have a reliable robust force field description, in order to avoid finding demixing in simulation conditions. Also, it is necessary to simulate very large systems for a long time, to ensure the proper sampling of the complex motion of the labile segregated domains, which are of the nanometer scale. Currently, simulation box sizes may go up to 128 or 256 thousand molecules, which is considered exceptionally large for such small molecules and comes at a considerable computational cost. The majority of the simulations for complex systems in this

work are performed for 16 thousand molecules, which is sufficient for the systems studied herein.

The present chapter reviews the theoretical context in order to clarify the points which are relevant to the study of the micro-heterogeneity. After a brief account of molecular dynamics as a method and the program package Gromacs as the main tool for simulation, we step over to the main means of analysis. The site-site correlation functions are the principal descriptor tool for the structural distribution of molecules and are directly obtainable from simulations. From a theoretical point of view, the main quantity should be the molecular correlation function. However, this quantity contains angular contributions [11], which are not suitable for analysis of directed Hbond correlations. It is necessary to sum several angular projections of the molecular correlation to achieve this [11], which is very cumbersome. Therefore, we will restrict ourselves to site-site correlations.

From site-site correlation functions, we can access the site-site structure factors, and from them the scattering intensity, which can be obtained from radiation experiments. Thus, site-site correlation functions have a link to experimental observables. This will be derived later in the chapter.

Returning to the structure factor, the statistical theory of liquids relates the $k = 0$ behavior of the structure factor to concentration fluctuations. At $k = 0$, it's not important whether the site-site or species-species (center-of-mass) structure factors are used, for they will lead to the same value. Finally, this is connected to the oft-mentioned Kirkwood-Buff integrals, which are a measure of concentration fluctuations and are calculated from the integral of the pair correlation function. This integral is independent of the choice of the center of integration, and for this reason, KBIs can be evaluated from any atom-atom correlation function. As will be shown later in the thesis, the emphasis will be put on distingushing KBIs, which represent macroscopic thermodynamic concentration fluctuations, from the small-k behaviour of the structure factor, which represents k-dependent concentration fluctuations. The latter embodies the inhomogeneity we would like to describe in this work.

Last but not least, another type of structural analysis - cluster probability distributions - will also be presented.

2.1. Molecular dynamics

The conception of molecular dynamics can be traced back to the pioneering works of Alder and Wainwright. Even though the duo employed the method for simulating hard spheres in 1957 [83], they gave the detailed outline of MD in their seminal article from 1959 [84]. Alder and Wainwright recognized MD's limitations (due to the lack of computational power back then, the main issue was the small number of particles contained in the simulated systems), but have also pointed it out as an alternative to the then-known Monte Carlo (MC) method. Unlike MC simulations, which are

basically sampling experiments which use accumulation of random numbers followed by a limited number of arithmetic and logical operations [68], MD has the advantage of allowing the study of time-dependent processes [11].

Alder and Wainwright later extended their simulations to elastic discs [85], but the next advance in simulation was Rahman's work on liquid argon in 1964 [86]. It took ten years before Stillinger and Rahman joined forces to simulate the first realistic liquid system: water [87].

Afterwards, MD rapidly developed as a method, encompassing more versatile and complex systems such as proteins [88] and nucleic acids [89]. However, the basic MD procedure hasn't changed from the early days. The first step in the MD simulation is to choose a force field which will define the interaction between the particles in the system [90]. Afterwards, it is necessary to designate a set of initial coordinates within a cell of fixed volume for each particle of the N-particle system. A set of velocities, derived from the Maxwell distribution at the desired temperature, is then assigned so that the net linear momentum of the system is zero. The motion of the particles is then described by numerical integration of the classical equations of motion [11]:

$$m_i \frac{d^2 \vec{r}_i}{dt^2} = \vec{F}_i, i = 1...N \tag{2.1}$$

Leaving a system to run and develop for a period of time is necessary so that the system can reach equilibrium at the new state point [68]. Usually, information from an MD simulation is extracted by taking the time averages of the equilibrium properties of the system over the whole dynamical history of the system [11].

2.1.1. Potentials in MD

The starting point to replicating macroscopic systems in silico is the interaction of the particles. The potential is vitally important for obtaining reliable results in particle simulations, because forces are calculated from it in the course of the simulation [68]:

$$\vec{F}_i = -\nabla_i U,\ i = 1...N \tag{2.2}$$

To calculate the potential energy of a system, one needs to define the potential energy function $U(r^N)$. This function usually has two contributions: intramolecular interactions, which come from the atoms on the same molecule, and intermolecular interactions, which are calculated from atoms on different molecules [68].

The intramolecular interaction of a simple molecular model will contain terms for "bound" atoms in a molecule: $U_{intra} = U_{bonds} + U_{angles} + U_{dihedrals}$, where the terms describe the deviation of bond lengths, bond angles and torsion angles (dihedrals) away from equilibrium values. The intermolecular interactions will be made up of contributions from non-bonded pairs of atoms describing van der Waals and electrostatic interactions: $U_{inter} = U_{vdW} + U_{El}$. Usually, the van der Waals interaction is described with the Lennard-Jones potential, while the electrostatics is handled via the Coulomb potential [90]:

$$U_{inter} = \sum_{i}^{N} \sum_{j}^{N} \left\{ 4\epsilon_{ij} \left[\left(\frac{\sigma_{ij}}{r_{ij}} \right)^{12} - \left(\frac{\sigma_{ij}}{r_{ij}} \right)^{6} \right] + \frac{q_i q_j}{4\pi\varepsilon_0 r_{ij}} \right\} \tag{2.3}$$

where σ and ϵ are characteristic length and energy of the pair potential, while q represents the partial electric charge on a particle. These pair potentials are taken to be pairwise-additive (apart from long-range Coulomb forces), so the sum of non-bonded pair interactions will give rise to non-bonded forces.

However, different systems require different bond lengths, bond angles, force constants, van der Waals parameters and partial charges. A set of such parameters, together with the adequate equation for the potential energy of the system, is collectively called a force field. There are many force fields available today, the majority of which were developed by taking into consideration quantum mechanical calculations, and/or experimental data obtained by thermodynamic and spectroscopic measurements [91].

2.1.2. Interaction computation

There are several approaches to the interaction computation (Figure 2.1). First we have the all pairs method (simple to implement, but not very efficient when the cut-off radius is small compared with the linear size of the simulation region [91]), then cell subdivision (where the simulation domain is divided into cells with an edge length greater than or equal to the cut-off radius of the interaction to be computed. The particles are sorted into these cells and the interactions are computed between particles in the same or neighboring cells [91].) and at last neighbor lists (where for each particle a list is constructed that lists all other particles within the potential cut-off distance, beyond which particle interactions are ignored [92]). From all those listed above, the most popular one is the neighbor list, thanks to its efficiency [91].

So far it's established that the potential, which is a function of the atomic positions (3N) of all the atoms in the system, is necessary for solving the equations of motion. The more complex the simulated system is, the more complex the potential functions of its atoms, and the only way to solve them is using a numerical method. Many numerical algorithms have been developed for integrating the equations of motion

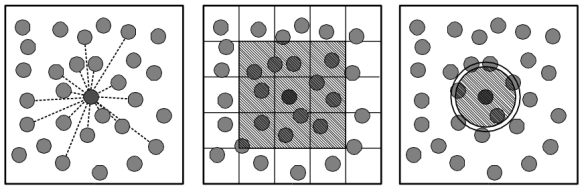

Figure 2.1.: The different approaches to computing interactions: all pairs (left panel), cell subdivision (middle panel), and neighbor lists (right panel). Illustration taken from [91].

like Verlet [92], velocity Verlet [93], Leapfrog [94] and the predictor-corrector (PC) type (Beeman's algorithm [95] is a Verlet-type algorithm modified with the PC part).

Both have advantages and disadvantages. While the PC type algorithm is more flexible, it requires more work and storage than Leapfrog or Verlet [91]. Their accuracies are discussed in more detail elsewhere [91, 96]. As an example, we will take the Leapfrog algorithm and explain the way it operates [94]. The velocity is always a half-step ahead of positions and forces (hence the name). The first velocity at a half time step is calculated as:

$$\vec{v}(t + \frac{1}{2}\Delta t) = \vec{v}(t - \frac{1}{2}\Delta t) + \vec{a}(t)\Delta t \tag{2.4}$$

and then the position advances for the full time step:

$$\vec{r}(t + \Delta t) = \vec{r}(t) + \vec{v}(t + \frac{1}{2}\Delta t)\Delta t \tag{2.5}$$

During the full step, the current velocities are calculated for they are necessary for energy calculation:

$$\vec{v}(t) = \frac{1}{2}\left(\vec{v}(t + \frac{1}{2}\Delta t) + \vec{v}(t - \frac{1}{2}\Delta t)\right) \tag{2.6}$$

After that step, the algorithm loops again and again, until the desired number of steps is reached.

To cut down the simulation time, it's advantageous to use geometric constraints that tie bond lengths and angles to given values, because that will fixate lengths of the chemical bonds and the values of the angles within the molecules and thus eliminate the degrees of freedom for the bond and angle potentials, which are the high-frequency degrees of freedom. There are various methods for incorporating geometric constraints, and the popular algorithms are SHAKE [97], RATTLE [98]

and LINCS [99]. There are several ways to introduce constraints into the numerical intergation schemes. In the case of SHAKE, the numerical integration step without constraints is done first, in order to get new particle coordinates. Then, the new coordinates are modified in regards to the constraints in the second step, using an iterative method [97]. LINCS operates in a similar way, however, it uses a non-iterative single step procedure to acquire the constrained distances after an unconstrained step [99]. This makes it faster and more stable than SHAKE, though it's most suited for bond length constraints and isolated angle constraints.

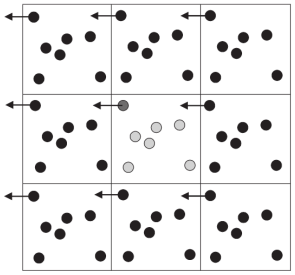

Figure 2.2.: Illustration of the periodic boundary conditons, taken from [90]

To simulate a system which closely resembles a macroscopic system, it's necessary to minimize surface effects and this is done by using periodic boundary conditions [11], which basically means having an infinite array of copies of the simulation region [91], as illustrated in Figure 2.2. Since each cell is surrounded by its images, the particles that immigrate have the same relative position and momenta in all cells [11]. The direct consequence of periodicity is the fact that if a particle leaves the "cell" through one side, it immediately appears through the opposite side. Also, particles positioned within the cut-off distance of a boundary interact with particles in an adjacent copy of the system, or with particles near the opposite boundary [91].

It's worth mentioning how long-range interactions are dealt with in MD. "Long-range" often denotes the case where the spatial interaction decays slower than r^{-d}, where d is the dimensionality of the system. An example of this type of interaction is the Coulomb interaction, which has a r^{-1}dependence. The slow decay of that interaction means that one cannot truncate the potential after a cut-off distance; it has to be accounted for with different means.

One method for the treatment of such potentials relies on Ewald summation, where the potential is split into its short-range and long-range part, each of which can be computed efficiently with a specific separate approach [96]. The original charge distribution, represented by a set of delta functions, is screened by a new charge distribution (described by Gaussian functions) which has the same magnitude but the opposite charge as the original distribution. Then, a set of compensating Gaussians is added to cancel the effect of the screening Gaussians, with the compensating ones being equal in magnitude and opposite in charge as the screened ones.

The screened interactions become short ranged, and their contributions to the total potential are summed over all of the sites in the central cell and their images in the real space. The cancelling Gaussian distributions are added together in the reciprocal space. Also, an additional correction term is required, to exclude the

interaction of the Gaussian with itself. The total Coulomb energy can then be written as [67]:

$$U_{Coul} = U_{SR} + U_{LR} - U_{self} = \\ = \frac{1}{2}\sum_{j\neq i=1}^{N}\frac{q_i q_j}{r_{ij}} erfc\left(\sqrt{\alpha} r_{ij}\right) + \frac{1}{2V}\sum_{\vec{k}\neq 0}\frac{4\pi}{k^2}\left(e^{-\frac{k^2}{4\alpha}}|\rho(\vec{k})|^2\right) - \sqrt{\left(\frac{\alpha}{\pi}\right)}\sum_{i=1}^{N} q_i^2 \tag{2.7}$$

where q are the charges, r_{ij} the distance between the charges, α is the parameter of convergence, k is the wave vector and $\rho(\vec{k}) = \sum_{i=1}^{N} q_i e^{i\vec{k}\vec{r}_i}$.

Mesh Ewald methods approximate the reciprocal part of the Ewald sum through a discrete convolution on the mesh, which is solved with fast Fourier transform (FFT). If the parameter α is chosen well, the computational cost goes down from $\mathcal{O}(N^{3/2})$ to $\mathcal{O}(NlogN)$. There are different mesh methods, like particle-mesh Ewald (PME) [100], smooth-particle-mesh Ewald (SPME) [101] and particle-particle-particle mesh (PPPM) [102]. However, all mesh methods produce errors during the interpolation, FFT and differentiation. If time is more important than precision, though, mesh methods are the way to go.

2.1.3. MD and statistical mechanics

It's important to note how closely MD is linked to statistical mechanics. MD generates information about atomic positions, velocities and interactions, i.e. the microscopic level, but gives output in the form of macroscopic properties such as pressure and temperature [67]. That gap between the microscopic and macroscopic properties of a system is bridged by statistical mechanics. Statistical mechanics deals with systems with a vast multitude of particles, where it's difficult to track the precise changes in state in a system. Furthermore, there is some knowledge of the system, but insufficient to precisely define a state. To combat that problem, statistical mechanics studies the behavior of an ensemble (collection) of system representations (all of which are similar to the system of interest), which is distributed over a range of precise states [24]. The system representations in the ensemble are not identical at the molecular level; it's vital that their thermodynamic properties are the same [90]. According to the ergodic hypothesis [24], the average calculated over a large number of system representations in the ensemble is exactly the same as the time average that would be calculated by studying the time evolution of the system of interest. Knowing the average behavior of the system representations in the ensemble, it's possible to predict what will, on average, happen with the system of interest [24]. An ensemble is classified by the (bulk) thermodynamic properties kept constant in each system the ensemble contains [90]. Following that classification, there are:

1. the canonical ensemble, where the number of particles N, volume V and temperature T are constant;

2. the microcanonical ensemble, where N, V and energy E are constant;
3. the isothermal-isobaric ensemble, where N, T and pressure p are constant and
4. the grand canonical ensemble, where the chemical potential μ, V and T are constant. [67]

All ensembles are equivalent in the thermodynamic limit, so the thermodynamic properties of a model system can be calculated in averages in any ensemble (or the most convenient one) [68]. Behind each ensemble there are mathematically derived expressions such as their respective partition functions [11], which in turn can be used to calculate thermodynamic properties (shown in detail in [11] and [24]), in terms of ensemble averages that correspond to experimental observables.

2.1.4. Temperature and pressure coupling

Performing an MD simulation in any other ensemble than microcanonical requires a means to keep at least one quantity constant (on average) during the simulation. There are two ways of attaining that - applying a hard boundary (more information in [68]) or a soft boundary, which leaves room for fluctuations in the instantaneous observable, only requiring its average to remain equal to the macroscopic value. Soft boundary methods include weak-coupling, stochastic-coupling and so on [103].

In terms ot temperature coupling algorithms, or thermostats, an example of weak-coupling is the Berendsen thermostat [104], where the simulated system is coupled with a heat bath of a desired temperature T_0. The temperature of the system is controlled by scaling the velocities to every time step with a factor:

$$\lambda = \sqrt{1 + \frac{\Delta t}{\tau_T}\left(\frac{T_0}{T} - 1\right)} \tag{2.8}$$

where T_0 is the desired temperature, T is the actual temperature, Δt is the time step of the integration algorithm and τ_T is a constant. Since this thermostat suppresses kinetic energy fluctuations, it doesn't generate trajectories in the canonical ensemble and cannot be used to calculate properties. However, it's a very efficient algorithm to get a system to a desired temperature, so it's widely used for system equilibration. For production runs, thermostats like Nosé-Hoover [105, 106] are more appropriate since they reproduce the behavior of a canonical ensemble. It does so by introducing a dynamical variable ζ, the thermodynamic friction coefficient, which has the role of accelerating or deccelerating particles until the temperature reaches the desired value. The equation of motion is thus modified in the following way:

$$\frac{d\vec{v}(t)}{dt} = \frac{\vec{F}(t)}{m} - \zeta\vec{v}(t) \tag{2.9}$$

where ζ is defined as:

$$\frac{d\zeta\vec{v}(t)}{dt} = \frac{1}{Q}\left(\sum \frac{m\vec{v}(t)^2}{2} - \frac{N_{df}}{2}k_B T\right) \tag{2.10}$$

where Q is a parameter that determines the relaxation of the dynamics of the friction, T is the desired temperature and N_{df} refers to the number of degrees of freedom in the system.

Barostats are algorithms used to attain and control the pressure of the system. An example of a such an algorithm is the Berendsen barostat [104], which is analogous to its temperature counterpart in the sense that it couples the system to a pressure bath. It introduces an extra term to to the equations of motion which affects the change in pressure:

$$\frac{dP}{dt} = \frac{(P_{ext} - P)}{\tau_P} \tag{2.11}$$

where P_{ext} is the pressure of the external bath, P is the instantaneous pressure and τ_P is the time constant.

At every step of the simulation, the coordinates and the box sides are rescaled with the factor η:

$$\eta = 1 - \frac{\kappa_T \Delta t}{3\tau_P}(P_{ext} - P) \tag{2.12}$$

where κ_T is the isothermal compressibility of the system. Since κ_T affects only the time constant of the pressure relaxation and not the average pressure itself, its value can be estimated. For example, many molecular dynamics program packages use the compressibility of water ($\kappa_T = 4.5 \cdot 10^{-5}$ bar^{-1} at ambient conditions [107]). However, the fluctuations in instantaneous pressure produced by the Berendsen thermostat are not accounted for accurately.

The Parrinello-Rahman barostat [108, 109] is the analogue of the previously described Nosé-Hover thermostat because it also introduces an extra degree of freedom to simulate the effect of weak coupling to a pressure bath. The additional degree of freedom imitates a piston which corrects the pressure toward its desired value. The simulation cell is modelled by a second order differential equation which depends on the difference between the desired pressure tensor and instantaneous pressure tensor. Also, the equations of motions are modified to based on the dynamics of the cell size. Typically, the Parrinello-Rahman barostat takes four to five times longer to obtain the desired pressure than the Berendsen barostat, so the two barostats can be used in tandem, i.e. Berendsen to bring a system quickly to the designated pressure and Parrinello-Rahman to construct accurate trajectories.

2.1.5. The GROMACS program package

All of the simulations presented in this work have been performed by the program package GROMACS [69, 70, 71]. GROMACS is the acronym for 'GROningen MAchine for Chemical Simulations', as it was conceived at the University of Groningen in the 1990s. Nowadays, the program package is develped by scientists from the Royal Institute of Technology and Uppsala University, Sweden, and counts more than 1,5 milion lines of code [110].

GROMACS was mainly developed as a tool for simulating biomacromolecules, such as proteins, lipids and nucleic acids, but it's versatile enough to perform simulations of liquids and non-biological systems, such as polymers. One of its main advantages is high performance - due to algorithmic and processor-specific optimizing, it runs several times faster than many simulation programs. Simulations can be run on CPUs or GPUs, and they can be executed in parallel, using the Message Passing Interface (MPI) or threads.

Another advantage is that it is very flexible in terms of force fields, supporting many different force fields and having an extensive built-in parameter library. Since the package is geared towards biomacromolecule simulation, it includes a fully automated topology builder for proteins. However, as the topology and parameter files are written in clear text format, it's convenient to write topologies for small molecules. It's also possible to have conditional parts in the topology and include other files, since a C preprocessor is used.

GROMACS handles every part of simulation process, from setting up the initial configuration of the system, minimizing the energy of the system, running the actual simulation and calculating the results. The input configuration files can be of many formats, for example the Protein Data Bank (PDB) format, which is then converted into the internal file format.

During the course of the simulation, the trajectory data can be stored compactly, using lossy compression, with the precision being designated by the user. Gromacs also offers a number of trajectory analysis tools, with the output provided in the .xvg format, suitable for plotting in the Xmgr/Grace program. These tools include the calculation of the pair correlation function, cluster probability distribution, root mean square displacement, radius of gyration and many more. The output configurations and trajectory can be visualized with a number of visualization programs, like VMD [111] and Pymol [112].

2.2. Structural analysis

2.2.1. Pair correlation functions

As mentioned in the introduction of this chapter, the principal quantity which we study is the pair correlation function $g(r)$. For the case of a homogenous, isotropic liquid, $g(r)$ is oftentimes referred to as the radial distribution function (RDF) [30]. A detailed derivation of the pair correlation function is provided in textbooks [11, 30], so we will briefly mention the most important points.

The N-particle distribution function $g_N^{(n)}(\vec{r}^n)$ is defined in terms of the corresponding particle density $\rho_N^{(n)}(\vec{r}_1, ...\vec{r}_n)$ by [11]:

$$g_N^{(n)}(\vec{r}^n) = \frac{\rho_N^{(n)}(\vec{r}_1, ...\vec{r}_n)}{\prod_{i=1}^n \rho_N^{(1)}(\vec{r}_i)} \tag{2.13}$$

where N is the number of particles.

In the case of homogenous systems, the particle distribution function measures the which extent the structure of a fluid deviates from the complete randomness. In a homogenous, isotropic system, the pair distribution function $g_N(r_1, r_2)$ is a function of $r_{1,2} = |r_1 - r_2|$:

$$g_N^{(2)} = \frac{\rho_N^{(2)}(\vec{r}_1, \vec{r}_2)}{\rho^2} \equiv g(r) \tag{2.14}$$

Particle densities can also be expressed through delta functions as an ensemble average over pairs[68]:

$$g_{ij}(r) = \frac{1}{\rho N} \left\langle \sum_i^N \sum_{j \neq i} \delta(\vec{r} - \vec{r}_{ij}) \right\rangle \tag{2.15}$$

However, as we're primarily concerned with the long-range behavior of studied systems, we must look into the $g(r)$ when the distance between the particles is sufficiently large ($r \to \infty$). In systems of finite size, such as those in computer simulation (despite being pseudo-infinite through periodic boundary conditions), the exact limit of the $g(r)$ for a system of finite size with N particles is [113]:

$$lim_{r \to \infty} g_{ij}(r) = 1 - \frac{\varepsilon_{ij}}{N} \tag{2.16}$$

where ε_{ij} is [72]:

$$\varepsilon_{ij} = \frac{1}{\rho x_i x_j} \left(\frac{\partial \rho_i}{\partial \beta \mu_i} \right)_{TV\mu_k} \tag{2.17}$$

In Equation 2.17, ρ_i is the number density of species i, μ_i is the chemical potential of the said species and $\beta = \frac{1}{k_B T}$ (k_B being the Boltzmann constant and T the temperature). If we were to have an infinite system, $N \to \infty$, Equation 2.16 would go to unity.

Equation 2.16 was first derived by Lebowitz and Percus in 1961[113], while a more intuitive derivation of the LP asymptote correction for both neat liquids and mixtures has been published by Požar *et al.* [72].

It's important to mention that the LP correction is often presented for the ideal mixture case, where $\varepsilon_{ij} = 1$, and consequentially, $g(r) \to 1 - \frac{1}{N}$. This is especially relevant for the systems studied in this thesis, for a good deal of them doesn't fall into the category of ideal mixtures.

For large systems ($N \sim 10^3$ particles and more), Equation 2.16 is not very important for the calculation of quantities such as the excess internal energy, which involve multiplying with the pair interaction which is often very short ranged. On the other hand, if the integration of the $g(r)$ over the volume of the system is necessary, the fact that the $g(r)$ doesn't oscillate around 1 as the horizontal asymptote will become amplified. We proposed to correct this problem by multiplying $g(r)$ by the factor $1/\left(1 - \frac{\varepsilon_{ij}}{N}\right) \approx 1 + \frac{\varepsilon_{ij}}{N}$, which leads to the correct asymptote of 1.

We also note that Equation 2.17 holds only for simulations in the NVT ensemble, while Equation 2.16 holds both in the canonical and in the isobaric-isothermal ensemble that we use in our simulations. Since we use a numerical method to shift the asymptote, the differences for the asymptote correction between the NVT and NpT ensemble are implicitly addressed. The numerical procedure for shifting is discussed in depth in previous papers by Perera *et al.* [40, 114]. An example of the LP correction can be seen in Figure 2.3, which features the carbon united atom correlations in benzene, for the benzene-pentane mixture at low benzene content. If one were to judge from the main panel, it would seem like the uncorrected $g(r)$ (thick black line) asymptotically goes to unity, just as the corrected $g(r)$ (dashed red line). However, the inset of Figure 2.3 zooms in on the tails of both $g(r)$, demonstrating that the uncorrected correlation function doesn't go to unity, while the corrected $g(r)$ does. This will be particularly relevant for the mixtures studied in the following chapters. The LP corrections for these systems are given in Appendix B.

Finally, we will mention a quantity closely related to $g(r)$, and that is the coordination number [30]:

$$N_{CN}(R_M) = \rho \int_0^{R_M} g(r) 4\pi r^2 dr \tag{2.18}$$

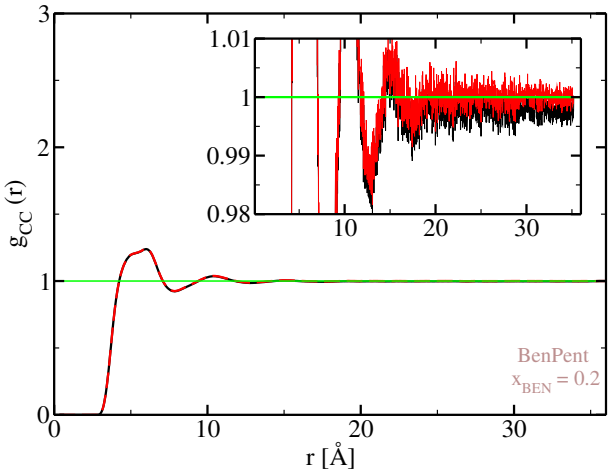

Figure 2.3.: An example of the LP shift for the case of carbon united atom correlations in benzene, for the benzene-pentane mixture at $x_{BEN} = 0.2$. Main panel: uncorrected *g(r)* (black) and corrected *g(r)* (dashed red). Inset: zoom of the tails of the *g(r)*s.

The coordination number represents the average number of particles in a sphere of radius R_M (the particle at the center is excluded). Depending on the choice of R_M, one can obtain the coordination numbers for shells of interest.

2.2.2. Structure factors

The pair correlation function $g(r)$ introduces another important quantity in liquid state physics - the structure factor $S(k)$. The structure factor can be defined in terms of species-species ($S_{\alpha\beta}(k)$, where α,β are the indices of species) or, for molecular species, in terms of atom-atom structure factors. In the latter case, the structure factor is $S_{i_\alpha j_\beta}(k)$, where i_α designates the i-th atom of molecule type α and j_β the j-th atom of molecule type β. The general definition of the structure factor is [11]:

$$S_{uv}(k) = \delta_{uv} + \rho\sqrt{x_u x_v}\int d\vec{r}[g_{uv}(r) - 1]e^{-i\vec{k}\vec{r}} \tag{2.19}$$

where u,v are the indices of any of the nature above ($u = \alpha$ or $u = i_\alpha$) , ρ is the total number density and x_u the mole fraction of species u.

The importance of the structure factor lies in the fact that it can be obtained from diffraction experiments [81], thus becoming invaluable for assessing the microstructure of liquids. However, that is not the only link the structure factor has with experiments. According to the statistical physics, the fluctuations in the number of particles contained in a given volume can also be connected to the long wavelength

limit of the structure factor [82]. In that case, the structure factor going to $k \to 0$ can be written as:

$$S_{uv}(k=0) = \frac{\langle N_u N_v \rangle - \langle N_u \rangle \langle N_v \rangle}{\sqrt{\langle N_u N_v \rangle}} = \rho k_B T \kappa_T \tag{2.20}$$

where ρ is the number density and κ_T the isothermal compressibility. Equation 2.20 simply shows that the mean square fluctuation in the number of atoms contained in a given volume is proportional to $S_{uv}(k=0)$, which is also measured by the isothermal compressibility. Thus, the $S(k=0)$ also contains thermodynamic information, which can be procured from experiments using thermodynamic or ultracoustic techniques [81]. This is a useful feature for dense liquids, since the results of diffraction measurements, *S(k)*, have to continuously join with the limit $S(k=0)$.

2.2.3. Scattering intensity

The intensity of scattered X-rays is calculated as [115]:

$$I(k) = \langle A(k) A^*(k) \rangle \tag{2.21}$$

where where k is the scattering wave vector and $A(k)$ is the scattering amplitude for the whole sample.

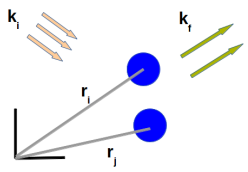

Figure 2.4.: Schematic of X-ray scattering on a sample.

The scattering wave vector k is defined as the difference between the initial wave vector k_i and final wave vector k_f of a diffraction probe, and it can be calculated as $k = 4\pi sin\frac{\theta}{\lambda}$, where λ is the wavelength of the incident X-ray [81] (Figure 2.4). The scattering amplitude is defined as $A(k) = \sum_{i=1}^{N} a_i(k)$, where a_i is the scattering amplitude of a single atom: $a_i(k) = f_i(k) e^{i\vec{k}\vec{r}}$. In the latter expression, $f_i(k)$ corresponds to the atomic form factor of the atom in question.

Inserting the expressions for the scattering amplitude in Equation 2.21, one can obtain the Debye formula when it's taken into account that $\left\langle e^{i\vec{k}\vec{r}_{ij}} \right\rangle_\Omega = \frac{sin(kr_{ij})}{kr_{ij}}$:

$$
\begin{aligned}
I(k) &= \left\langle \sum_{i,j} f_i(k) f_j(k) e^{i\vec{k}(\vec{r}_i - \vec{r}_j)} \right\rangle \\
&= \sum_{i,j} f_i(k) f_j(k) \left\langle e^{i\vec{k}\vec{r}_{ij}} \right\rangle_{\Omega} \\
&= \sum_{i,j} f_i(k) f_j(k) \frac{sin(kr_{ij})}{kr_{ij}}
\end{aligned} \tag{2.22}
$$

while the sum runs over all pairs of atoms i and j in the sample. The latter indicates that Equation 2.22 can be re-expressed in terms of the various site-site correlation functions.

2.2.3.1. Scattering intensity of an atomic liquid

If we consider the sample as a mixture of free atoms, with no geometrical constraints between them, the structure factor is equal to that of a species-species structure factor from Equation 2.19:

$$
S_{\alpha\beta}(k) = \delta_{\alpha\beta} + \rho\sqrt{x_\alpha x_\beta} \int d\vec{r} \left[g_{\alpha\beta}(\vec{r}) - 1 \right] e^{i\vec{k}\vec{r}} \tag{2.23}
$$

where α and β indicate atoms/species. The scattering intensity for that sample will be:

$$
I(k) = \rho \sum_{\alpha\beta} \sqrt{x_\alpha x_\beta} f_\alpha(k) f_\beta(k) S_{\alpha\beta}(k) \tag{2.24}
$$

2.2.3.2. Scattering intensity of a molecular liquid

However, in the case of a sample containing molecules, we have to take into account the fact that certain sites are connected with each other. That's why we need to split the contribution to the structure factor into intramolecular (for the sites in one molecule) and intermolecular (for sites on different molecules):

$$
\begin{aligned}
S_{i_\alpha j_\beta}(k) &= \left\langle \sum_{i_\alpha j_\beta} e^{i\vec{k}(\vec{r}_{i_\alpha} - \vec{r}_{j_\beta})} \right\rangle \\
&= \left\langle \sum_{i_\alpha j_\beta}^{\alpha=\beta} e^{i\vec{k}(\vec{r}_{i_\alpha} - \vec{r}_{j_\beta})} \right\rangle_{intra} + \left\langle \sum_{i_\alpha j_\beta}^{\alpha\neq\beta} e^{i\vec{k}(\vec{r}_{i_\alpha} - \vec{r}_{j_\beta})} \right\rangle_{inter}
\end{aligned} \tag{2.25}
$$

where α and β indicate molecular species and i_α and j_β sites belonging to each type of molecule. The intramolecular contributions can be rewritten, taking into account the fixed distances between the sites:

$$\left\langle \sum_{i_\alpha j_\beta}^{\alpha=\beta} e^{i\vec{k}(\vec{r}_{i_\alpha}-\vec{r}_{j\beta})} \right\rangle_{intra} = \left\langle \sum_{\alpha} \sum_{ij} e^{i\vec{k}\vec{d}_{ij}} \right\rangle \tag{2.26}$$

In a sample of N molecules, the intramolecular contributions will yield $N \sum_{ij} \frac{sin(kd_{ij})}{kd_{ij}}$, and we can define $w_{ij}(k) = \frac{sin(kd_{ij})}{kd_{ij}}$. The structure factor will then be:

$$S_{i_\alpha j_\beta}(k) = w_{ij}(k) + \rho\sqrt{x_\alpha x_\beta} \int d\vec{r} \left[g_{i_\alpha j_\beta}(r) - 1 \right] e^{i\vec{k}\vec{r}} \tag{2.27}$$

where x_α is the mole fraction of species α. And the scattering intensity will equal to:

$$I(k) = \rho \sum_{\alpha\beta} \sum_{i_\alpha j_\beta} \sqrt{x_\alpha x_\beta} f_{i_\alpha}(k) f_{j_\beta}(k) S_{i_\alpha j_\beta}(k) \tag{2.28}$$

Even though Equation 2.24 and Equation 2.28 are basically the same, the idea of the structure factors contributing to it are significantly different. Neglecting the intramolecular part of the structure factor (i.e. using Equation 2.23) will actually lead to the Pings-Waser (PW) expression for the scattering intensity [116]. Although frequently used in the literature [117, 118, 119, 120], the PW formula does not provide the proper result for the calculated scattering intensity of a molecular sample.

2.2.4. Cluster probability distributions

Besides the analyses based on pair correlation functions, we consistently feature results obtained by another type of structural analysis - cluster probability distributions. This type of calculation is fairly well represented in studies of neat liquids [121, 122, 123, 124, 125] and mixtures [18, 20, 36, 41, 126, 127, 128, 129, 130], making it a staple in liquid matter studies.

Usually, a cluster is defined as the group of particles where each particle has at least one connection with the neighboring particles. This connection can be defined through energetic or geometric criteria. An example of the former is the Hill's energetic criteria where particles are considered to be connected if their attractive interaction energy is higher than their relative kinetic energy [131]. However, for the calculations in the subsequent chapters, the latter criterion is employed, in the

form of Stillinger's distance criterion [132]. In that approach, sites are considered to be a part of the cluster if they are positioned within a certain cut-off distance from one another. The cut-off distance is defined by the first minimum of the site-site radial distribution function. The idea is to count how many particles are connected in a cluster of a given size n for each configuration k. This way, the interactions between bonded particles are indirectly related to their interactions through the pair correlation function. The cluster size distributions are calculated for the clustering of the like–like sites, using several different statistical approaches. We show the results for the cluster size probability functions:

$$P_n = \frac{\sum_k s\,(n,k)}{\sum_k \sum_n s\,(n,k)} \tag{2.29}$$

where P_n is the probability for the cluster formed of n sites, $s\,(n,k)$ represents the number of clusters of the size n in the configuration k. P_n is obtained by averaging the number $s\,(n,k)$ of clusters of size n over several such configurations.

As mentioned above, the choice of the cut-off distance (r_c) for a calculation depends on the first minimum in the pair correlation function of the site in question. Throughout the thesis, several molecules were used frequently, which means that certain sites from those molecules frequently underwent cluster calculations. If not stated otherwise, the r_c defined for sites were: 3.5 Å for the oxygens in water molecules; 3.7 Å for the oxygens in alcohol molecules; 4.5 Å between the carbon united atom sites in alcohol molecules and 6 Å between the carbon united atom sites in various non-polar solvents (*e.g.* benzene). However, it has been shown in previous group publications [124, 125] that varying the r_c around the first minimum won't change the resulting cluster distributions significantly.

2.3. Kirkwood-Buff integrals

The Kirkwood–Buff (KB) theory of solutions defines the relationship between thermodynamic quantities and molecular distribution functions for multicomponent systems in the grand canonical ensemble [31]. Although first derived in 1951., it laid dormant for decades, until Ben-Naim postulated the inverse procedure [27].

In the original paper, the main idea is to connect the derivatives of the components' chemical potentials with the integrals of the species' radial distribution functions via concentration fluctuations, which are then eliminated from the respective relations, thus providing a direct link between macroscopic and microscopic quantities [31].

The KB integrals (KBI) are defined as:

$$G_{ij_{\mu VT}} = \int_0^\infty [g_{ij}(r) - 1]\, 4\pi r^2 dr \tag{2.30}$$

where $g_{ij}(r)$ is the pair correlation function defined in the μ, V, T system for the two species i and j. Thus, the theory may be used to compute the thermodynamic quantities based on our knowledge of the pair correlation function [31]. Although KBI is a property of the grand canonical ensemble, it can be applied to the N-constant ensembles under a couple of approximations. First, the simulation data can represent an open system; second, the KBI at infinity is equal to the running KBI (rKBI) up to certain range r, beyond which there are no correlations due to intermolecular forces diminishing [30]:

$$G_{ij_{NpT}} = \int_0^r [g(r) - 1]\, 4\pi r^2 dr \tag{2.31}$$

Using relation Equation 2.31, it's possible to calculate the values for the rKBI from the data collected during the simulation. However, as mentioned in subsection 2.2.1, the fact that the $g(r)$ doesn't asymptotically go to unity for N-constant ensembles will cause problems for the calculation of volume integrals of the $g(r)$, such as the KBIs. In that case, we use the LP correction to shift the tail of the $g(r)$ to oscillate around unity, which results in the rKBI oscillating around the proper value (Figure 2.5).

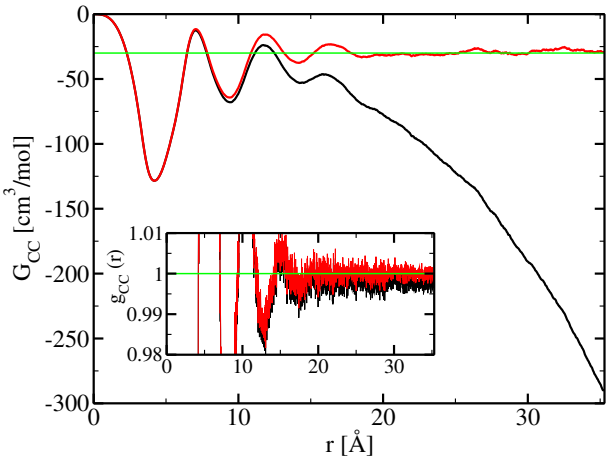

Figure 2.5.: rKBIs results for the carbon united atom correlation function of benzene, from the benzene-pentane mixture at $x_{BEN} = 0.2$. Main panel: rKBIs calculated from the corrected (red line) and uncorrected (black line) *g(r)*, which were presented in Figure 2.3. Inset: the same as in Figure 2.3, showing the zoomed-in tails of the *g(r)*s for the sake of completeness.

Technically, the two rKBIs depicted in Figure 2.5 are not the same. Using the LP shift, we empirically corrected the $g(r)$, transforming it from that of the NpT ensemble to that of a pseudo-μVT ensemble. We consider the pseudo-μVT ensemble to be close to the real μVT ensemble.

As mentioned above, the beauty of the KB theory of solutions lies in the fact that it defines the relationship between molecular distribution functions and thermodynamic quantities [31, 30], which means that the KBIs can be calculated using the thermodynamic approach [26, 31, 30]. In the case of a two-component system, the KBIs would correspond to:

$$G_{ij} = \left[k_B T \kappa_T - \frac{\bar{V}_i \bar{V}_j}{VD}\right](1 - \delta_{ij}) + \left[G_{12} + \frac{1}{x_i}\left(\frac{\bar{V}_j}{D} - V\right)\right]\delta_{ij} \tag{2.32}$$

where κ_T represents the isothermal compressibility (k_B is Boltzmann constant and T the temperature), $\bar{V}_i$ the partial molar volume of species i, V the total volume and x_i the mole fraction of species i. The D is related to the concentration fluctuations through the expression[31, 30, 26]:

$$D = x_i \left(\frac{\partial \beta \mu_i}{\partial x_i}\right)_{TP} \tag{2.33}$$

where μ_i is the chemical potential of species i ($\beta = 1/kT$ is the Boltzmann factor).

When several approximations are considered, Equation 2.32 can be reduced. The isothermal compressibility can be neglected since it's smaller in magnitude in comparison with the other terms. Then, the partial molar volumes of the components can be replaced by the molar volumes of the neat components, because the variations of excess volume with concentration can be ignored. (Also, the excess volume is at least one order of magnitude smaller than the volumes.) Finally, the KBI from Equation 2.32 can be connected to the components' mole fractions and volumes. The D term depends on the chemical potential, which can be split into three different contributions: (reference, ideal and excess parts): $\mu_i = \mu_i^{(0)} + k_B T \ln(\rho x_i) + \mu_i^{excess}$, and can be written as [26, 27]:

$$D = 1 + x_i \left(\frac{\partial \beta \mu_i^{excess}}{\partial x_i}\right)_{TP} \tag{2.34}$$

If we consider only the ideal part of the chemical potential and neglect the excess contribution and, that would correspond to $D = 1$. When $D = 1$ is inserted into Equation 2.32, one obtains the ideal KBIs, which is characteristic of weakly interacting species. As the interactions of at least one species become more pronounced, the expression for D becomes more sophisticated. This notion will be fleshed out in subsequent chapters with examples of different systems and their corresponding $D(x)$. However, for complex systems, it's difficult to determine this function from both experiments and simulations, which has been discussed in the literature [26, 30, 133, 134]. This problem is either non-existant or not so pronounced for simple systems, as we shall see further on.

Results and discussion

3. Simple and complex disorder

As we described in the Introduction, concentration fluctuations differ widely from simple to associated liquids. In this chapter, we study in detail how this happens by analyzing the principal structural descriptors, namely the pair correlation function, or site-site correlation function, as well the associated structure factors.

In the textbook sense, atomic liquids such as argon, nitrogen and oxygen are considered to be simple liquids [1]. Liquids with multiple atoms, such as CH_4, belong to the complex liquids, since orientational degrees of freedom need to be described. However, in this chapter we will reevaluate this definition, making a basic distinction between liquids which have charged atomic sites and those which have chargeless ones. Charged liquids, such as molten salts of NaCl, exhibit a very particular type of disorder, named charge order, where various atoms sit in charge alternated order, almost like in a disordered crystal [135, 136, 137, 138]. When such charged atoms are inside a molecule, the charge order they would impose is influenced by the molecular constraints. This way, atoms of opposite charge across different molecules tend to be next to each other in a dense liquid, which leads to weak or strong charge association. Molecular association is mostly based on charge association, and this is particularly true for classical force field models [139, 140, 141, 142, 143].

In this and all subsequent studies, we will consider liquids without atomic charges as simple liquids and those with atomic charges will exhibit complex disorder. That being said, we still need to confirm that the molecular shapes do not play an important role by enforcing shape order. For example this is the case in liquid crystalline order, where it is the elongated shape of the molecules which impose this type of order [144]. We will not consider such order here.

Instead, we shall turn to binary mixtures with different types of constituents and study the relationship between the local order generated by different types of molecular interactions and the nature of the global disorder. In the past, the group focused heavily on aqueous mixtures [37, 38, 114, 145, 134, 146, 147, 148, 149], which revealed considerable microheterogeneity, accompanied by the problems it posed in statistical analysis [35]. In order to obtain a clearer picture of the structuring in a mixture, we are bypassing water, an associating liquid, and using a much simpler solvent - benzene.

Benzene is the simplest and most widely known aromatic compound. It contains a six-membered ring and three double bonds. The molecular formula for benzene is C_6H_6 - every carbon has only one hydrogen atom. It's a planar molecule [32]. The

physical properties of aromatic hydrocarbons are similar to other hydrocarbons - they have low melting points and boiling points, on top of being miscible with water in very small proportions [32]. Even though benzene has its share of complexities on the submolecular level, it can be modelled in different ways as a molecular liquid. The questions of modeling benzene and choosing the appropriate benzene model are covered in Appendix A, but suffice to say, we chose the chargeless, united-atom model.

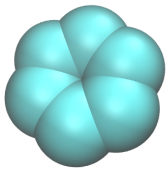

Figure 3.1.: The model of the benzene molecule.

Solvents of similar nature, like carbon tetrachloride, can be used as a replacement for benzene. The key is to have the solvent inert, so that it can essentially act as a backdrop against which we can observe the structuring (or lack thereof) the other component exhibits. For that reason, benzene has been mixed with substances of different physico-chemical makeup: an alkane (pentane), a ketone (acetone) and an alcohol (ethanol), shown in Figure 3.2. The simulation protocol and modeling details for the neat liquids and binary mixtures are covered in Appendices A and B, respectively.

In the following chapter, we present the results yielded by the mixtures with benzene as a common solvent and analyze the relationship between the concentration fluctuations and the correlation functions with their associated structure factors. It will be shown that systems with benzene contain much less of the problems encountered when studying aqueous mixtures and allow better insights into the nature of the disorder in liquids.

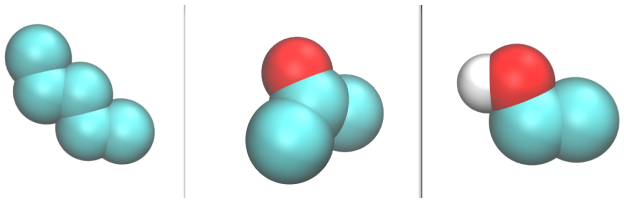

Figure 3.2.: Models of molecules: pentane (left), acetone (center) and ethanol (right). Atom colors: blue - carbon; red - oxygen; white - hydrogen. The sizes of the molecules are not properly proportioned in relation to one another, but are here solely for illustrative purposes. The molar volumes of the molecules are actually: $V_{PENT} = 115.3\ \frac{cm^3}{mol}$, $V_{ACE} = 74.1\ \frac{cm^3}{mol}$ and $V_{ETL} = 58.4\ \frac{cm^3}{mol}$.

The majority of the content of this chapter, which concerns mixtures with benzene, is taken from our PCCP paper [72]. The same part of the study has been presented as a poster at the 14th International summer school of Biophysics "Greta Pifat Mrzljak" (October 2014), and as a talk at the 9th meeting of the Croatian physical society

(October 2015). The remainder of the chapter, which discusses solvent shapes, is the subject of a pending publication.

3.1. Mixtures with benzene as a common solvent

3.1.1. Benzene-alkane mixture

The first mixture considered was the benzene-alkane system. Alkanes are hydrocarbons which have only C-C and C-H single bonds, and which can be joined together to form chains or rings of atoms [32]. The alkane in our case denotes two linear hydrocarbon chains which only differ in length: pentane (consisting of five methyl or methylene groups) and heptane (consisting of seven groups).

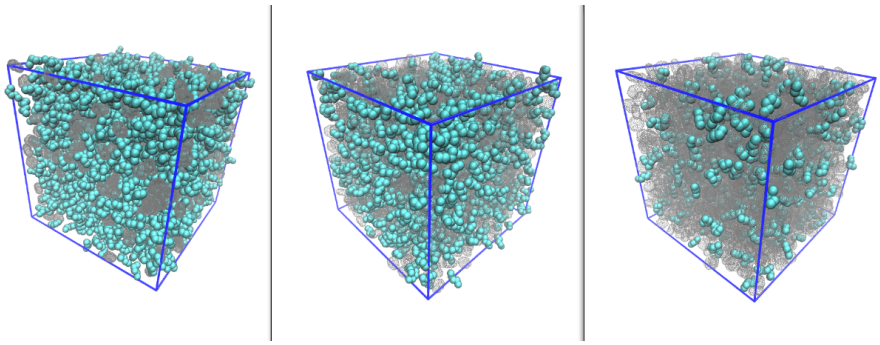

Figure 3.3.: Snapshots of the benzene-pentane mixture at three different mole fractions: $x_{BEN} = 0.2$ (left panel), $x_{BEN} = 0.5$ (middle) and $x_{BEN} = 0.8$ (right panel). Benzene is shown in transparent gray, while pentane is in cyan.

Both components are hydrocarbons which were modeled the same way in terms of van der Waals and electrostatic interactions (more on model details in the Appendix A). Therefore, the nature of the interactions between the components is the same and the only differences stem from the molecules' shapes (as seen in Figure 3.1 and the left panel of Figure 3.2).

In Figure 3.3, we can see the representative snapshots of the system, taken for three different mole fractions of benzene. Though it may be difficult to tell from a static image, the pentane and benzene molecules are evenly mixed, betraying no particular global order.

Figure 3.4 displays the the site–site correlations of the carbon united atoms of benzene $g_{BB}(r)$ (upper panel) and the end methyl groups of pentane $g_{MM}(r)$ (lower panel) for $x_B = 0.2$, 0.5 and 0.8 mole fractions of benzene in the benzene–pentane mixtures. The correlation functions of both species look similar, which is due to the site–site Lennard-Jones interactions being also similar. The subtle differences in the shape of the first neighbour peak are caused by the different geometries of

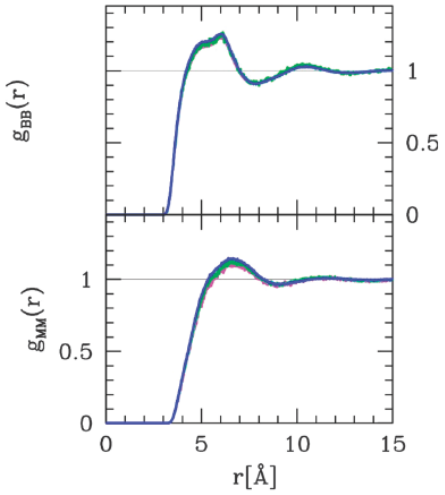

Figure 3.4.: Site–site correlations between the carbon atoms of benzene (upper panel) and between the end methyl groups of heptane (lower panel), and for 3 benzene mole fractions of $x_{BEN} = 0.2$ (magenta), $x_{BEN} = 0.5$ (green) and $x_{BEN} = 0.8$ (blue).

the species. However, the most striking feature is that there is little to no difference between correlation functions for all three concentrations. Hence, there are very few structural changes when the concentrations are varied, implying that the species see a similar environment despite the change in concentration.

The KBIs for the benzene-pentane (upper panel) and benzene-heptane systems (lower panel) are shown in Figure 3.5. The points represent data obtained from the simulation, while curves are a product of equations from Chapter 2. We set $D = 1$, which corresponds to the hypothetical ''ideal'' mixtures. The KBIs for the benzene-alkane systems are rather small and they follow the trend of the calculated theoretical curves. However, the agreement is not perfect, which may originate from: (a) the fact that the volume of neat benzene is not exactly that of the real system and (b) the neglected compressibility κ_T in Equation 2.32 may play a more important role, since both types of liquids are rather volatile.

The rKBIs and site-site structure factors are presented in Figure 3.6 for the equimolar concentration of the benzene-pentane mixture. The rKBIs (upper panel of Figure 3.6) reveal the oscillatory behavior typical of the carbon groups. As for the *S(k)*s (lower panel of Figure 3.6), we see that all three curves are characterized by only one feature - the main peak, which falls roughly at the same position for all three correlation functions. Since the main peak reflects the oscillations in the correlation functions, brought on by the size of the object, this result is expected, as in this case the carbon united atoms have a similar size. The concentration fluctuations, as noticed in the KBI Figure 3.5 are small and similar for all species. We also note the presence of a weak shoulder in $S_{PP}(k)$, which shows the dual short range ordering of the pentane molecules: parallel and cross, which is typical of small rods.

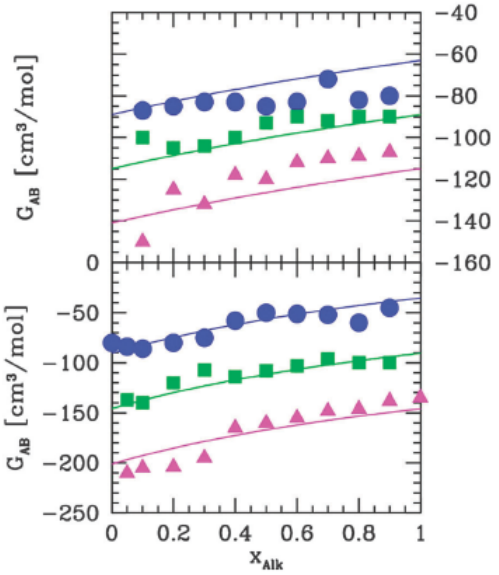

Figure 3.5.: Kirkwood–Buff integrals G_{AB} for the benzene–pentane system (upper panel) and benzene heptane system (lower panel), with the following color conventions: blue dots for G_{SS} (S for solute), magenta triangles for benzene G_{BB} and cross functions G_{BS} in green squares. The lines are the theoretical results assuming ideal mixtures.

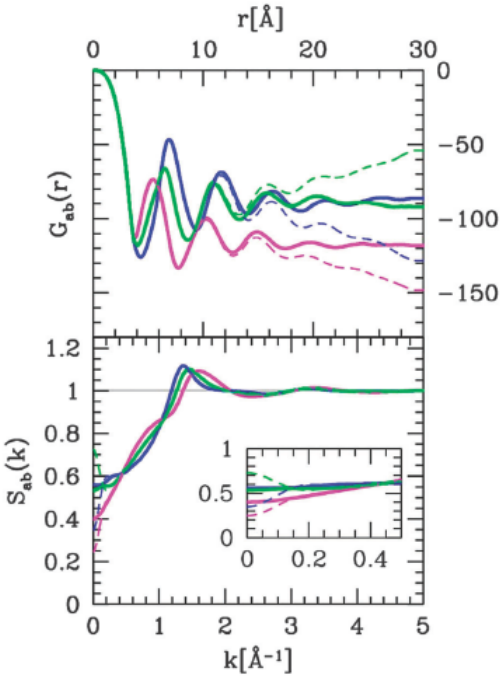

Figure 3.6.: Upper panel: running Kirkwood–Buff integrals $G_{AB}(r)$ for the benzene-pentane system. Lower panel: site-site structure factors corresponding to the rKBIs in the upper panel. Inset: Zoomed-in depiction of the site-site structure factors featured in the lower panel. The color code is: $g_{BB}(r)$ in blue, $g_{PP}(r)$ in magenta and $g_{BP}(r)$ in green. For all panels, the full lines denote data after the LP correction and the dashed lines uncorrected data.

3.1.2. Benzene-acetone mixture

Unlike benzene and alkanes, the acetone molecule has different chemical makeup [150]. Acetone (IUPAC name: propanone) is a ketone - a compound with bivalent carbonyl group bonded to two carbon substituents [151].

The acetone molecule force field has partial charges on both the oxygen and the central carbon atoms, which cancel each other out to achieve total electro–neutrality. Therefore, the oxygen atom of one acetone molecule will be attracted by the opposite charge of another molecule's carbon atom. The Coulomb interaction, being about a factor of $6{\cdot}10^2$ larger than the Lennard-Jones interaction between the sites, will dominate and the two acetone molecules will tend to form a dimer in an antiparallel configuration. That kind of the near neighbour dipolar interaction is a characteristic of the real acetone molecule [152]. So, in the benzene-acetone mixture, acetone's propensity for dimer association will promote the segregation of acetone molecules into pockets. This is something we can observe from the snapshots of the system, especially for low acetone content in Figure 3.7.

Since the association of acetones is energy driven, their pockets will have an internal energy that is, on average, more negative than in a random, entropically driven mixture. That is hinted with the KBI values in Figure 3.8. When considering the change of KBIs over mole fraction of benzene, it's apparent that this type of behavior differs from the benzene-alkane mixture in Figure 3.5. Not only do the KBI values differ in magnitude, but the benzene-acetone mixture shows a small non-ideality, as shown by the behaviour of the fitted D in the inset. The D behaves as $D(x) = 1 - \alpha x(1-x)$, where $\alpha = 2$. This type of function, and the resulting KBI behavior, is in line with a weak non-ideality. It also confirms enthalpic nature of acetone associations that are formed in the mixture.

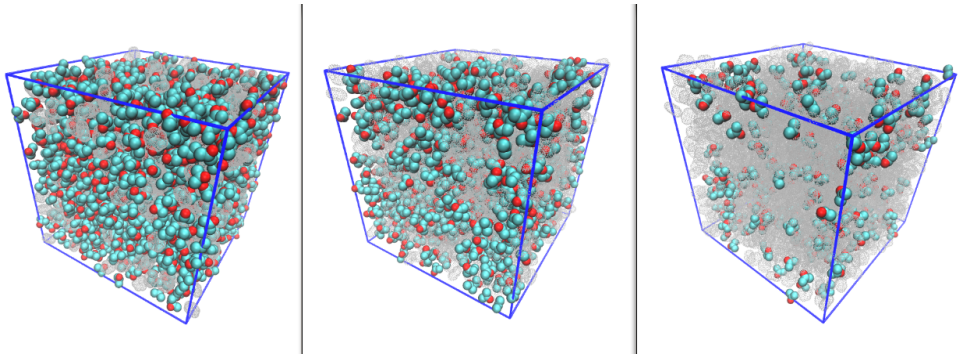

Figure 3.7.: Snapshots of the benzene-acetone mixture, for three different benzene mole fractions: $x_{BEN} = 0.2$ (left), $x_{BEN} = 0.5$ (middle) and $x_{BEN} = 0.8$ (right panel). Acetone is represented in red (oxygen) and cyan (carbon), while benzene is shown in transparent gray.

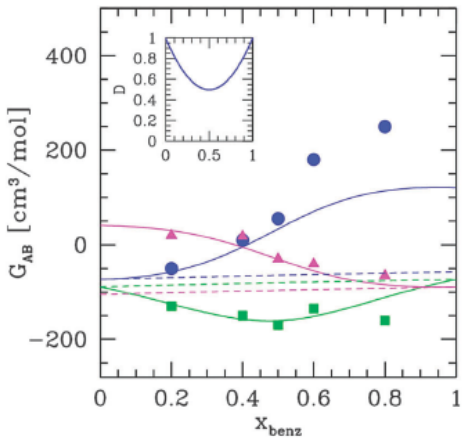

Figure 3.8.: Kirkwood–Buff integrals for the benzene–acetone system with same color conventions as Figure 3.5. Dashed lines represent the ideal behaviour and full lines the KBIs obtained through the expression for the regular mixture given in the text and shown in the inset.

However, solely from looking at the KBIs, which correspond to fluctuations at $k = 0$ [82], we cannot tell what is happening at small k values. That is, we cannot say if these acetone associations are merely concentration fluctuations or pseudo-particles. To answer that, we look into the correlations shown in Figure 3.9 for the equimolar mixture case.

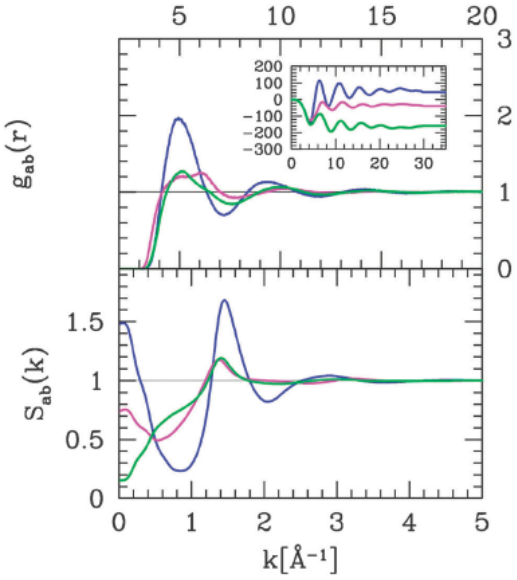

Figure 3.9.: Site–site correlations (top) for the equimolar benzene–acetone mixtures; blue lines for $g_{OO}(r)$ correlations between oxygen molecules on acetone, magenta lines for $g_{CC}(r)$ carbon–carbon correlations in benzene and green for cross correlations $g_{OC}(r)$. Corresponding structure factors in the lower panel. The inset in the upper panel shows the RKBI and the corresponding asymptotical values for the KBIs.

The upper panel displays the acetone oxygen–oxygen correlations $g_{OO}(r)$, the benzene carbon–carbon $g_{CC}(r)$ and the cross correlations $g_{OC}(r)$. The analysis of first neighbor correlations reveals the significant difference in height between acetone and benzene, implying the existence of acetone associations. That notion is furthered by the corresponding running KBIs, which are shown in the inset of the upper panel. The OO correlations are higher in magnitude than all others, confirming the enthalpic association picture.

The lower panel shows the structure factors for the g(r)s shown in the upper panel. We notice that the acetone $S_{OO}(k)$ has a strong $k = 0$ raise, indicating large concentration fluctuations. The only other feature in $S_{OO}(k)$ is the main peak at $k = 1.4$ Å^{-1}, so we can conclude that the raise is due to concentration fluctuations. We note that benzene has less fluctuations than acetone, which again confirms that it is acetone that drives the self-segregation.

Finally, we observe from the KBIs in Figure 3.8 that the simulation results for G_{OO} for large acetone concentrations are somewhat higher than that predicted by the analytical expression. This is due to an overestimation of G_{OO} from the simulations due to the fact that the tail of $g_{OO}(r)$ is not stabilized at a perfectly horizontal value. It is likely that a simulation of a larger system will provide a smaller value of the KBIs, more compatible with the theoretical prediction.

3.1.3. Benzene-ethanol mixture

Then there comes ethanol, a primary alcohol. Alcohols contain a hydroxyl group (OH group) bonded to a tetrahedral carbon atom, while the primary denotes to which carbon atom is the OH group attached [32]. The oxygen atom is more electronegative than carbon or hydrogen, rendering the the C-O and O-H bonds polar. With two polar bonds and a bent shape, an alcohol has a net dipole [151]. Since they possess a hydrogen atom bonded to an oxygen, alcohols have the ability of intermolecular hydrogen bonding. Therefore, alcohols are associating liquids and they have much stronger intermolecular forces than the hydrocarbons [32].

Ethanol is modeled in such a way that the hydrogen bond effect is reproduced. The partial charged are distributed between the oxygen and the hydrogen atom. Unlike in the case of acetone, the distribution of the charges allows for a favorable direct pairing between the oxygen and hydrogen atoms of two different ethanol molecules. This way, the Coulomb ordering of the ethanol molecules is not induced by dipolar ordering, as in the case of acetone, but by a classical equivalent of hydrogen bonding: ethanol molecules can form chains of the form O–H–O–H–O–, with the methyl groups randomly distributed outside the Hbonded chain.

In pure ethanol, this ordering is decreased by both thermal agitation and the multitude of binding possibilities [153]. In a benzene mixture, however, the presence of surrounding benzene diminishes the binding choices, and previously bonded clusters

are stabilized. Benzene as such offsets ethanol's structuring, which can be observed through all the properties analysed as in the previous two mixtures.

Figure 3.10 shows several features of the correlation functions for 3 different benzene concentrations, $x_{BEN} = 0.2$, 0.5 and 0.8, as well as for neat ethanol. The main panel, top and middle inset show the properties of $g_{OO}(r)$ for the ethanol molecules. It can be seen in the top inset and main panel that the OO correlations increase significantly as the concentration of ethanol is diminished, which points to the formation of Hbonded specific clusters when ethanol becomes isolated. The second inset shows the tail of the $g_{OO}(r)$. We see that, as the concentration of ethanol is decreased, long range oscillations become more and more pronounced. This long range modulation is difficult to observe in systems of 2000 particles, solely because the box side length is not enough to capture these oscillations. For that reason, it's necessary to simulate systems of ∼16000 particles (which take up double the box side as the 2000 particle system) for cases of complex disorder.

The third inset in Figure 3.10 shows the $g_{CC}(r)$ benzene correlations for the concentrations $x_{BEN} = 0.2$, 0.5, 0.8 and pure benzene. The benzene correlations retain the first neighbor structure as in the pure liquid and they change very little with concentration variations, which is radically different than the behavior of ethanol.

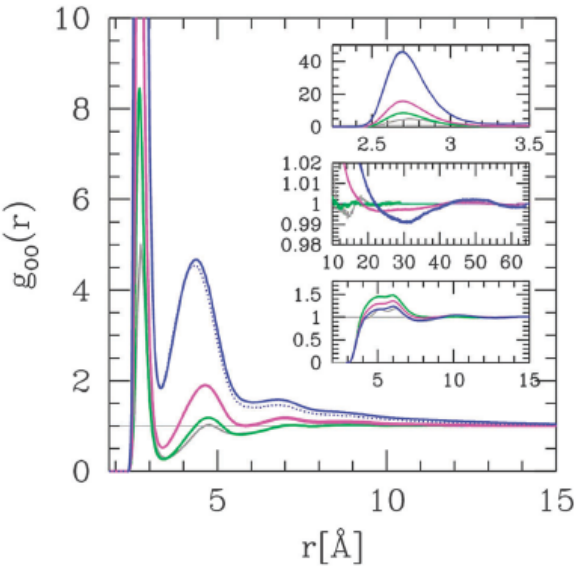

Figure 3.10.: (Main panel) Ethanol oxygen–oxygen correlations $g_{OO}(r)$ in benzene–ethanol mixtures, for benzene concentration x = 0 (gray curve), x = 0.2 (green), x = 0.5 (magenta) and x = 0.8 (dotted blue N = 2048, thick blue N = 16 384). Insets: (top inset) zoom on the first peak of $g_{OO}(r)$; (middle inset) zoom on the large separation behaviour of $g_{OO}(r)$ of the main panel: (lower inset) $g_{CC}(r)$ for benzene–benzene correlations for the same concentrations x as the main panel and the same color code.

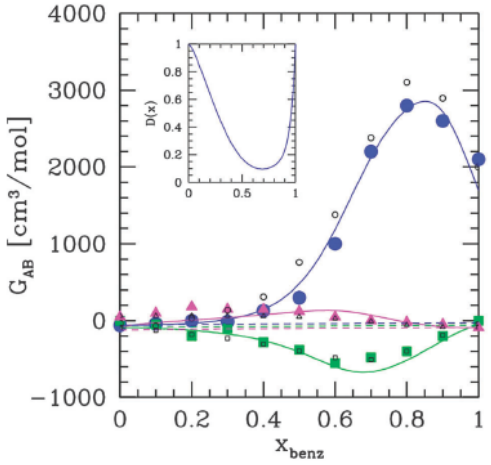

Figure 3.11.: Kirkwood–Buff integrals for the benzene–ethanol system with same color conventions as in Figure 3.5. Dashed lines for the ideal behaviour and full lines for the expression for D given in the text and shown in the inset. The open symbols are experimental KBIs for the benzene–methanol system given in [154].

Figure 3.11 shows the dramatic difference between the KBIs' behavior for benzene-ethanol and the two other examples. Not only is the behavioral trend of all species different, but the values are larger by almost 2 orders of magnitude. The dashed lines in Figure 3.11 show the ideal KBIs, and they are very small compared to the actual values.

Also, there is a noticeable contrast between the high ethanol KBIs and the comparatively small benzene KBIs for this mixture. However, one would expect that the benzene KBIs would be similar to the ideal KBIs, since benzene is not affected by ethanol's charge-induced clustering. It turns out that one cannot have inhomogeneity in the distribution of ethanol without influencing that of the benzene. Hence the fluctuations in the distribution of benzene are forced to follow those of ethanol, even though they are not concerned by the Coulomb induced clustering. These finding indicate that, besides information about concentration fluctuations, KBIs can hint at the nature of the components' interactions in the system.

Figure 3.12 shows the structure factors $S_{OO}(k)$ (top panel) and $S_{CC}(k)$ (lower panel) for various benzene concentrations. $S_{OO}(k)$ shows a remarkable evolution as the ethanol concentration diminishes. Pure ethanol (the gray line) shows the existence of a pre-peak at $k_P \approx 0.8$ Å^{-1}, which corresponds to an ethanol domain of the size d = $2\pi/\ k_P \approx 7.5$ Å - an elementary ring structure present in ethanol [155, 153]. However, as ethanol become the minority, that cluster peak at $k_P \approx 0.8$ Å^{-1}is absorbed by another pre-peak, positioned at $k_P \approx 0.1$ Å^{-1}. The latter pre-peak corresponds to a domain size of d = $2\pi/\ k_P \approx 60$ Å, which would contain approximately 10 ethanol molecules. Interestingly, this pre-peak position does not shift so much between x_{BEN} = 0.5 and x_{BEN} = 0.8. The reason for this behavior can be gleaned by looking at the snapshots of particular concentrations (Figure 3.13).

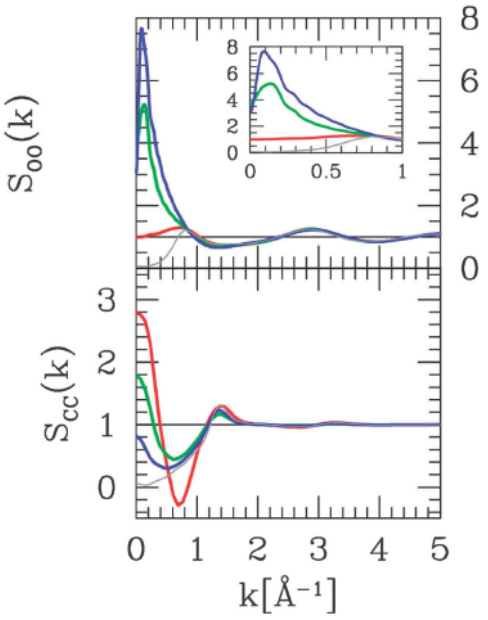

Figure 3.12.: Structure factors for the benzene–ethanol system: (top) oxygen– oxygen $S_{OO}(k)$ for the benzene mole fractions x = 0, 0.2, 0.5 and 0.8 with same color code as in Figure 3.10; (bottom) benzene carbon–carbon $S_{CC}(k)$ with same color codes as for above, except for x = 1 (pure benzene) in thin grey line.

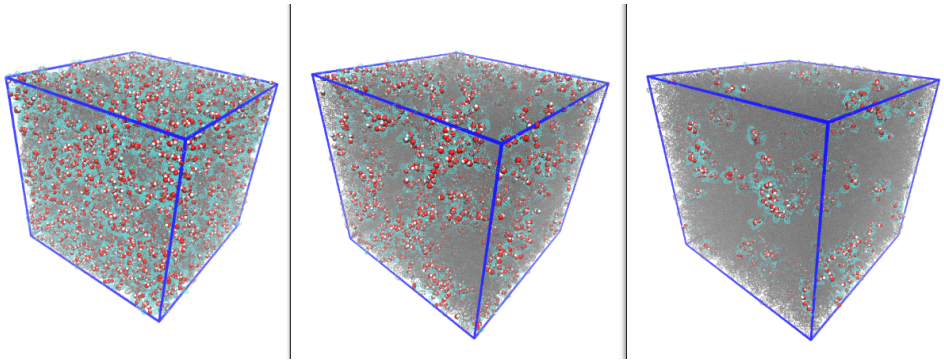

Figure 3.13.: Snapshots of the benzene-ethanol system for the following benzene mole fractions: x_{BEN} = 0.2 (left), 0.5 (middle) and 0.8 (right panel). Benzene is shown in transparent gray, while ethanol is shown by elements: oxygen in red, hydrogen in white and the carbon united atoms is transparent blue.

At x_{BEN} = 0.2, we observe ethanol chains which resemble the structures seen in neat ethanol [124, 125]. As ethanol is rarified, one can notice the occurrence of Hbonded rings which are especially visible for isolated aggregates. Besides the occasional lone ring, there are larger aggregates made out of piles of such smaller elementary aggregates, which is visible for both x_{BEN} = 0.5 and x_{BEN} = 0.8. This ties in with evolution of $S_{OO}(k)$, where the cluster peak of pure ethanol is being gradually

absorbed into the domain pre-peak, a feature present for $x_{BEN} = 0.5$ and $x_{BEN} = 0.8$.

The $S_{CC}(k)$ of benzene shows large concentration fluctuations at $k = 0$ when benzene is in the minority. However, $S_{CC}(k)$ does not show a pre-peak. This is clearly related to the absence of specific benzene clusters, which indicates that there is a significant difference between concentration fluctuations and micro-heterogeneity.

3.2. The influence of solvent shape on disorder

So far we've established the importance of molecular interactions in generating different types of disorder. But what happens when we have non-polar solvents which are characterized by different molecular shapes? For that reason, we're looking into binary mixtures of acetone or ethanol with pentane and carbon tetrachloride (CCl_4). Unlike benzene, which is a planar, plate-shaped molecule, pentane is linear while CCl_4 is globular (Figure 3.14).

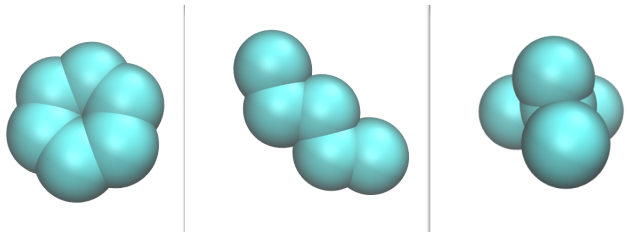

Figure 3.14.: Models of solvent molecules: benzene (left), pentane (center) and CCl_4 (right). The models are shown for illustrative purposes only, for their sizes are not depicted in proper proportions. The molar volumes of the molecules are: $V_{BEN} = 89.2\ \frac{cm^3}{mol}$, $V_{PENT} = 115.3\ \frac{cm^3}{mol}$ and $V_{CCL} = 96.7\ \frac{cm^3}{mol}$.

The chemical properties of the three non-polar molecules are very similar, as is the way that they are modeled (more details are in Appendix 1). That way we can monitor the steric effects different shapes may have in mixtures with species such as alcohols and ketones.

3.2.1. Mixtures with acetone

Just like in the case of the benzene mixture, acetone was mixed with both pentane and CCl_4 following the same protocol. We expect that acetone, having dipolar interactions, will tend to behave as it did in benzene - it will prefer to aggregate in small pockets in order to form dimers. The only question is if, and how much, will the other solvent hinder that?

The answer to that is partially answered by Figure 3.15. This image contains KBIs over molar fraction of solvent for both acetone-pentane (left panel) and acetone-CCl_4

(right panel). As expected, both mixtures exhibit a weak non-ideality in terms of KBI, confirming that acetone interactions are enthalpic in nature. The fitted D, used for obtaining the G_{AB}, is the same as in the case of benzene-acetone: $D(x) = 1 - \alpha x(1-x)$, where $\alpha = 2$. That function, shown in the inset of Figure 3.15, yields G_{AB}which match the trend of the simulated KBIs. Furthermore, when comparing the KBIs from Figure 3.15 to those in Figure 3.8, we see the similarity between all three acetone binary mixtures. Despite the difference between the solvents in terms of geometry, the concentration fluctuations in the systems are strikingly similar, not only for acetone, but also for the non-polar solvent. This finding implies that acetone's interactions are the driving force behind this behavior.

The discrepancies present (especially in the case of CCl_4 in the right panel) result from the fact that the simulated pure liquids (acetone and CCl_4) don't have the exact volume of the real systems. Also, system size may play a role in the slightly exaggerated value of the KBIs.

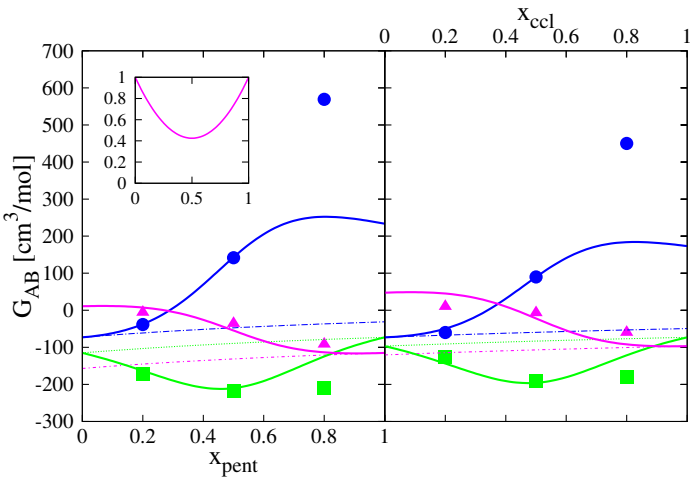

Figure 3.15.: Kirkwood–Buff integrals for the acetone-pentane (left) and acetone-CCl_4 system (right) with same color conventions as Figure 3.16. Dashed lines represent the ideal behaviour and full lines the KBIs obtained through the expression for the regular mixture given in the text and shown in the inset.

More information can be gathered from Figure 3.16, where the correlation functions and corresponding site-site structure factors are shown for acetone-CCl_4 (upper part) and acetone-pentane (lower part). This figure mimics Figure 3.8 and from the first glance it can be noticed that the behavior of acetone is almost identical in all three mixtures. Not only do acetone's correlations functions nearly overlap, but its structure factors show the same position and height of the main peak, and an almost identical raise at $k = 0$. This confirms that acetone's structuring, whether in terms of first neighbors or long range, is a result of acetone's interactions and the characteristics of the non-polar environment will have negligible influence upon it.

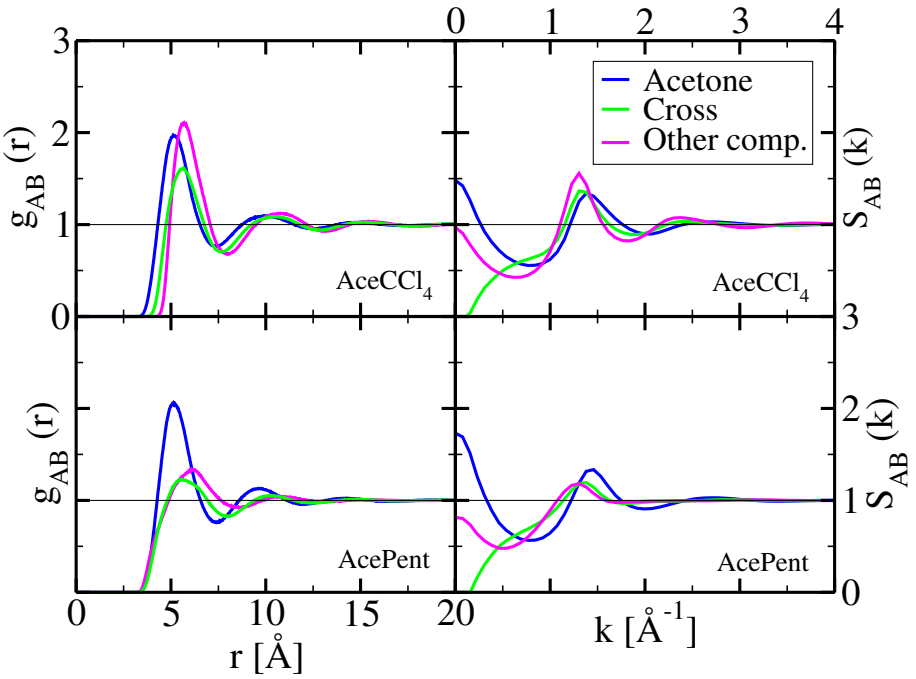

Figure 3.16.: Top row: correlation functions (left) and their corresponding structure factors (right) for the equimolar acetone-CCl_4 mixture. Bottom row: correlation functions (left) and their corresponding structure factors (right) for the equimolar acetone-pentane mixture.

The non-polar solvents show the same trends of behavior, but there are subtle differences among them, witnessed principally by their correlation functions. Even though all solvents have the first neighbour peak positioned at $r = 6$ Å, benzene's and pentane's $g_{CC}(r)$ have similar height and shape. The $g_{CC}(r)$ in CCl_4, on the other hand, shows that the carbon atoms are more correlated than benzene's or pentane's. In fact, the correlation function of CCl_4 resembles more the model Lennard-Jones system than benzene or pentane, which is due to close packing enabled by the molecular shape. These findings are mirrored by the $S_{CC}(k)$ functions. All three solvents have the characteristic main peak, positioned at $k = 1.25$ Å^{-1}, which corresponds to the particle size. That main peak in the $S(k)$ is of the same height for benzene and pentane, and somewhat higher for CCl_4. The structure factors for all three solvents also show a raise at $k = 0$, with CCl_4 having a slightly higher raise, which was expected from the KBI results in Figure 3.15.

3.3. Conclusions

In this chapter, we have shown how different types of interactions control local ordering, and in turn control the nature of the fluctuations that occur in the middle of the corresponding systems. We ellucidated the difference between different types

of disorder.

Simple disorder systems, i.e. simple mixtures, have components with similar interactions which are essentially dominated by excluded volume effects. They are characterized by near ideal concentration fluctuations and no noticeable local or global ordering.

If one component of a mixture has more pronounced interactions, such as dipolar interactions (e.g. acetone), then the concentration fluctuations will deviate from the ideal case. However, such a system will have some short range ordering and will lack large and more permanent structures, placing itself between simple and complex disorder. These are so called regular mixtures.

But if the system has one species with stronger interactions, such as the Hbond interaction, that will result in extensive clustering and domain formation. Such mixtures are termed complex disorder. Their signatures include large concentration fluctuations (especially for the associating species) and the occurrence of peaks at small k values of the site-site structure factors. These two characteristics are closely bound, but it's imporant to make a difference between them. Concentration fluctuations are macroscopic observables measured through the KBIs [31, 27], the latter corresponding to the $k = 0$ part of the structure factor. On the other hand, the small k region of the structure factor gives information about the microscopic structure of the mixture. A pre-peak in the structure factor at small k, as well as high KBIs, indicate the existence of domains.

The domains occuring in complex mixtures have their own share of intricacies. The temporal evolution of domains and fluctuations in domain number and size are issues which may cause statistical problems in computer simulations. Those problems are known, and have been reported before, especially for cases of water mixtures [114, 148]. However, it's shown that even mixtures with one associating species and the other inert, can have typical complex mixture behavior and to this associated statistical problems. The issues pertaining to correct system size and simulation time are addressed in Appendix B.

We have also shown that, in cases of complex disorder, the interaction is the key player. The interactions between one species generates complex disorder, while the influence of the molecular shape of the inert solvent is almost negligible.

4. The ethanol-methanol mixture

The concept of ideal mixtures is important in physical chemistry as they set the reference frame for analyzing mixtures with departures from ideal behavior [156]. Ideal mixtures are detected through the quasi linear dependence of a given mixing property:

$$A_{ideal}(x) = A_0(1-x) + A_1(x) \tag{4.1}$$

where $A_0 = A(x=0)$ and $A_1 = A(x=1)$ are the properties of the respective neat liquids "0" and "1". This simple equation states that the excess property $\Delta A(x) = 0$ in the general relation:

$$A(x) = A_{ideal}(x) + \Delta A(x) \tag{4.2}$$

What constituates ideal mixtures? It is not enough to suppress the van der Waals interactions to obtain an ideal mixture, since the hard core effect remain strongly non-ideal. This is seen in the case of hard sphere mixtures [157, 158], which show a non-ideal behavior, exemplified in the non-zero excess volume dependence [1].

For realistic liquids, it's said that a mixture will be ideal if its species are of similar shapes, sizes and molecular interactions with one another [156, 159]. A frequent textbook example of that is the benzene-toluene mixture, because the two molecules are very similar in size, shape, and chemical properties [156]. However, a mixture much more complex in terms of interactions, that of two alcohols, is considered an ideal mixture [160], because it obeys the relation above.

In the current chapter, we zoom in on the ethanol-methanol mixture and illustrate how ideality appears in correlations and thermodynamic properties, while the interactions are very strongly non-ideal. The signatures of ideality, particularly in the KBI results, will help us reevaluate the role of interactions and concentration fluctuations while defining an ideal mixture. Since we wish to mix two compounds with near similar properties, we capitalize on the fact that the alcohols' hydroxyl groups are modelled in the same way. This renders the interactions between all the functional groups in the system identical. However, there is a mismatch in the length of the alcohols' alkyl tails, which will compete with the hydroxyl group interactions.

As we don't expect this effect to be very pronounced in the ethanol-methanol mixture, we're also examining the methanol-1-propanol mixture, where there's a bigger difference in the alkyl tail lengths. Furthermore, we will be comparing the realistic ethanol-methanol system with a binary Lennard-Jones mixture, which is an example of an ideal mixture. The components of this LJ mixture are tailored to have volumes corresponding to those of the ethanol and methanol molecules, respectively. That way we can contrast a binary mixture of two alcohols with a true ideal mixture and put it into perspective considering the concepts of simple and complex disorder introduced in the previous chapter. The interest of this chapter is to revisit ideal mixtures with the same tools we use to investigate concentration fluctuations and micro-heterogeneity.

The results of this work are the subject of one publication [73]. The simulation protocol, models and other details can be found in Appendix A (for neat liquids) and Appendix B (for binary mixtures).

4.1. Structural analysis

4.1.1. Snapshots

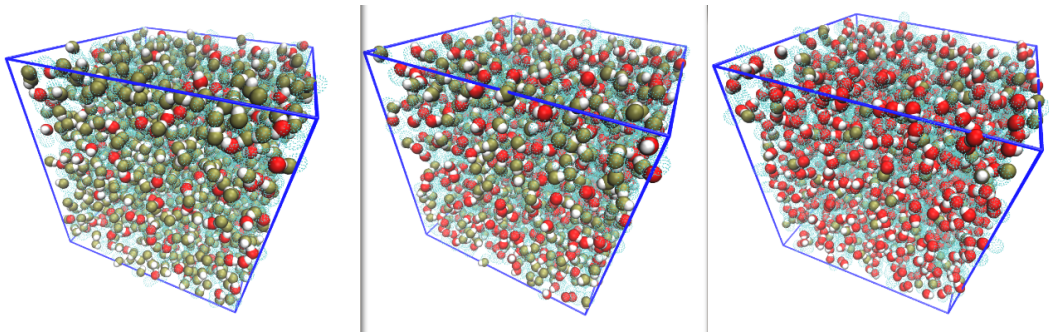

Figure 4.1.: Snapshots for the ethanol-methanol mixture for the following ethanol mole fractions: $x_E = 0.2$ (left), $x_E = 0.5$ (middle) and $x_E = 0.8$ (right). The methyl sites of both species are shown in transparent cyan, while the hydroxyl groups are represented in full. Ethanol's oxygen and hydrogen are featured in red and white, while methanol's are in olive and white.

Figure 4.1 shows the typical configurations for three typical mole fractions of the ethanol-methanol mixture. Only the bonding sites were represented in full (oxygen and hydrogen, with the oxygen shown in red for ethanol and olive for methanol), while the methyl sites are in transparent cyan. We can observe chain-like clustering for all mole fractions, with the hydroxyl groups of the alcohols intermingling into one uniform network which spans the whole box. This is most visible when rotating the

box when only the hydroxyl groups are shown. Since the hydroxyl groups of both molecules have the same partial charges, the hydroxyl groups are interchangeable. Hence, there is no micro-segregation of the two types of groups.

In Figure 4.2 we can see the global behavior of the ethanol-methanol mixture, but also for the two-component Lennard-Jones mixture. Neither one of the mixtures shows any form of local heterogeneity. That is to be expected of the LJ mixture, and is very telling for the alcohol mixture. The hydrogen bonding present in the latter system concerns only the hydroxyl groups, while the methyl groups are randomly arranged around the existing Hbond clusters. Micro-heterogeneity, on the other hand, affects the whole molecule.

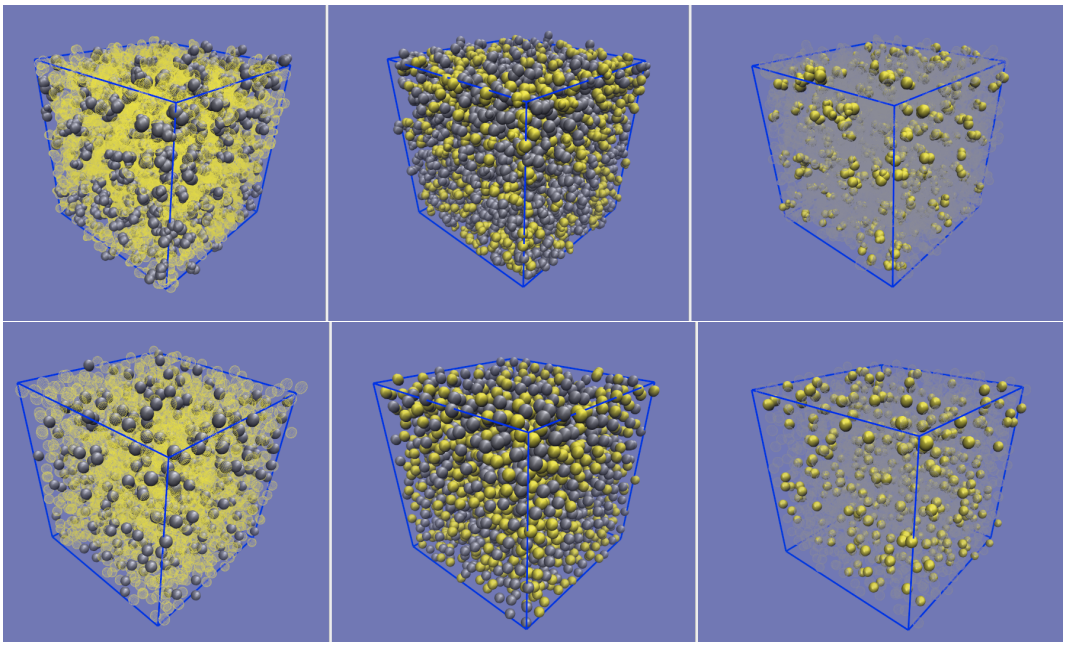

Figure 4.2.: Snapshots for the ethanol-methanol mixture (upper row) and Lennard-Jones mixture (lower row), for the same concentrations as in Figure 4.1. Methanol in shown in yellow and ethanol in gray. Their analogues in the LJ mixture are also shown in yellow and gray, respectively.

The upper panel illustrates the global heterogeneity (ethanol in grey and methanol in yellow, with similar conventions for the LJ system shown in the bottom panel). The global observation is that the hydrogen bonding does not bring out any specific form of local heterogeneity. In other words, both the alcohol and the LJ mixture look very similar. This enforces the impression of ideality of both systems.

4.1.2. Cluster distribution probabilities

The cluster distributions probabilities of different pairs of sites are displayed in Figure 4.3. In this case, the oxygen atoms of ethanol and methanol are considered

to be separate species, and are treated accordingly. These results are shown in the main panel of Figure 4.3 (methanol in dotted-dashed lines and ethanol in full lines), alongside the cluster distributions of neat ethanol and methanol (dotted black and brown lines, respectively). The curves representing neat ethanol and methanol are strongly non-monotonous and have a specific peak at about cluster size 3-5 [124, 125], which is consistent with the chain and loop clusters found in these alcohols [153, 161, 162]. This specific peak disappears as the solvent molecules are added, yielding fully monotonous distributions. As the peak present in neat alcohols corresponds to a specific cluster geometrical shape, its disappearance in mixing conditions does not mean that these chain structures have disappeared. In fact, the chains are now made of mixed methanol-ethanol hydroxyl groups, so this disappearance of the specific peak is an indication of the perfect mixing of methanol and ethanol.

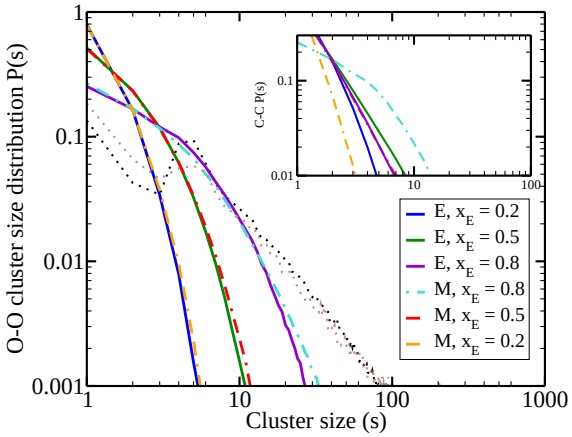

Figure 4.3.: Cluster distribution of the oxygen atoms (main panel) and carbon atoms (inset), for different ethanol mole fractions. Dot-dashed lines for methanol (labelled M) and full lines for ethanol (labelled E). Pure ethanol and methanol are shown in dotted lines, in black and grey, respectively.

However, we can consider another case, where all of the oxygen atoms in the system are taken to be of the same species. The results from this calculation are presented in Figure 4.4, with the curves assigned to the mole fraction of ethanol for the sake of reference. We observe that the cluster peak is present for all three concentrations, with the height and shape of the peak being close to identical in all three cases. As expected, this peak is located just like in its neat constituents, around the cluster size of 3-5. Since this peak is detectable via cluster calculation only when the entirety of oxygen atoms is considered, that proves that the clusters in the mixture are made out of the hydroxyl groups of both alcohols in equal measure. Mass spectrometry experiments done on the ethanol-methanol mixture indicate that tetramers are the preferential size of "mixed" clusters [163], which corresponds well with our results.

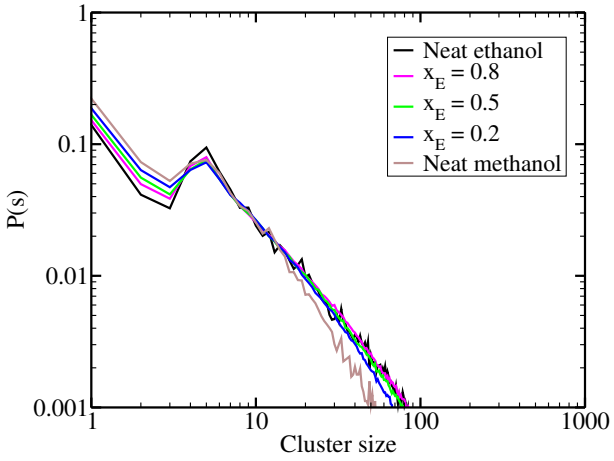

Figure 4.4.: Cluster probability distributions calculated for all oxygen atoms in the system, regardless of the molecule. For a point of reference, each curve is assigned the mole fraction of ethanol (color code is in the legend). Cluster distributions for neat ethanol and methanol are shown in black and brown.

As for the behavior of carbon united atoms, their cluster distributions are featured in the inset of Figure 4.3. The distributions in question are decaying functions typical of simple liquids. This result is expected since these atoms are randomly distributed in the mixture, just as they are in neat alcohols [124, 125].

4.1.3. Pair correlation functions

The correlation functions for the most important atom pairs are shown in Figure 4.5 for the same three molar fractions as in the previous sections. The main panel contains the oxygen-oxygen correlation functions, while the inset has the carbon-carbon correlation in alcohols (full lines) and those in the LJ mixtures (dashed lines).

All OO correlations have a high and narrow first peak characteristic for hydrogen bonding. Regardless of which species is in question, the first peaks of OO correlations look very much alike and independent of the concentration. That is due to the fact that the partial charges on the oxygen and hydrogen atoms are the same for both alcohols. This finding enforces the interpretation of perfect mixing between the two alcohols. However, the difference in the alcohols' non-polar parts clearly affects the second neighbors. Methanol has only one carbon united atom which doesn't hinder the arrangement of the oxygens' second neighbors. As a result, methanol's OO correlations are not depleted in the region of the second neighbors. On the other hand, ethanol's additional carbon group will lead to depletion of the second neighbors, for both ethanol and, to a lesser extent, cross OO correlations.

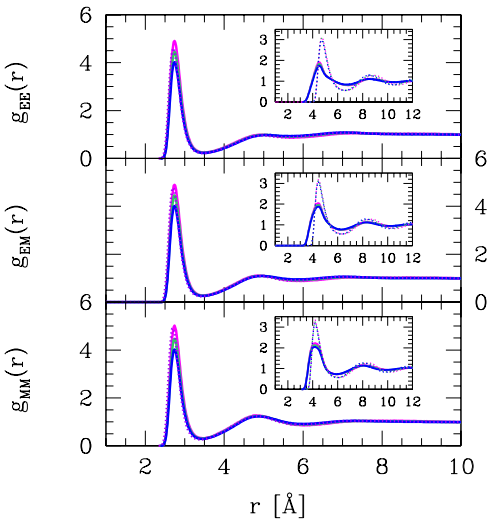

Figure 4.5.: Selected site-site correlation functions. Main panel: oxygen-oxygen correlations; inset: carbon-carbon correlations as well as the LJ correlations (dashes). The two top panels show the ethanol-ethanol oxygen correlations, the two middle show the ethanol-methanol oxygen correlations, and the two lower the methanol-methanol oxygen correlations. Each data set is shown for 3 solute concentrations x_E = 0.2 (blue), 0.5 (green), and 0.8 (magenta). The TraPPE model correlations are shown only for x_E = 0.5 in dotted purple lines (only on main panels).

As for the carbon group correlations in the inset, their shapes and positions resemble very much those between the Lennard-Jonesium. This demonstates that hydrogen bonding between the hydroxyl groups can create strong local order, but which doesn't affect the whole molecule, hence the unfettered non-polar groups.

In closing, we note that the OO correlations for the TraPPE model, shown in dotted purple the main panels, are indistinguishable from the OPLS data.

4.1.4. Structure factors

Figure 4.6 shows the site-site structure factors corresponding to the correlation functions from Figure 4.5. In the left panels of Figure 4.6 the OO structure factors are presented for all three species, for all three typical mole fractions. These curves have two distinct peaks. The main peak is located at $k_{MP} \approx 3\,\mathring{A}^{-1}$for all three species, and it represents the hydrogen bonding distance between the oxygen atoms, $r_{HB} \approx 2$ Å. The main peak varies with concentration in the cases of O_EO_E and O_MO_M structure factors simply because of the increase or decrease of the number of like molecules. The O_EO_M structure factors stay the same, indicating the constancy of cross bonding in the system. In this sense, the main peak witnesses the site-site interactions.

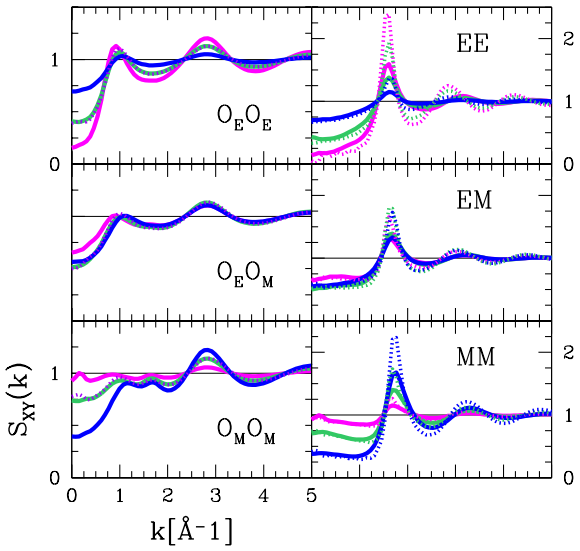

Figure 4.6.: Selected site-site structure factors for the correlations shown in Figure 4.5, with same line and color conventions. Left panels: OO structure factors. Right panels: methyl-methyl structure factors (full lines) and LJ structure factors (dashes).

Apart from the main peak, there is also a pre-peak for all three OO structure factors. This pre-peak is positioned at around $k_{PP} \approx 0.8\ \AA^{-1}$for ethanol and cross structure factors and $k_{PP} \approx 1 - 1.5\ \AA^{-1}$for methanol. The pre-peak hints at much larger objects - clusters formed by the hydrogen bond. Since this pre-peak indicates cluster-cluster interactions, we have named it the cluster peak. The shape and location of the cluster peak in the O_EO_E and O_MO_M structure factors is very similar to that in neat ethanol and methanol (shown in Figure A.5), indicating that ethanol and methanol preserve their neat liquid clustering in the mixture, once again indirectly confirming the perfect mixing of the components.

In contrast, the site-site structure factors of the carbon groups (right panels of Figure 4.6) don't have this cluster pre-peak. Their main feature is the main peak, which corresponds to the size of the carbon united atom ($k_{MP} = \frac{2\pi}{\sigma} \approx 1.7\ \AA^{-1}$ for $\sigma_C \approx 3.4$ Å). Once again, this demonstrates that the non-polar groups are randomly arranged in the system, much like LJ particles are, and that they do not participate in the building of Hbonded clusters.

However, the sole existence of clusters in this system indicates an an inherent complexity which is absent from the simple Lennard-Jonesium mixture. The fact that this complexity is hidden behind several apparent signatures of simplicity is worth further examination through thermodynamic properties.

It's also important to notice the $k = 0$ behavior in the site-site structure factors. The only species with structure factors that show somewhat of a raise at $k = 0$ is methanol (especially at $x_E = 0.8$), which is at variance with the trends of the other

species. However, the data globally indicates very small concentration fluctuations, which is reminiscent of simple systems. This seems to be a signature of clustered systems - the structure factor curve decaying in in the $k = 0$ limit, while having a cluster peak at a small k value. This can also imply that clustering means the "transfer" of the fluctuations at $k = 0$ to small k.

On a sidenote, the TraPPE model structure factors (dotted purple lines) in the left panels of Figure 4.6 and are seen to be very similar to the OPLS data.

4.2. Thermodynamical analysis

4.2.1. Volumes and energies

Figure 4.7 presents the intermolecular energies (upper panel), molar volumes (lower panel), as well as associated excess quantities (as insets) for the ethanol-methanol mixture (OPLS and TraPPE models), as a function of ethanol mole fraction. The results for the LJ mixture are also added, alongside the experimental volumetric data [164] in the lower panel.

In terms of molar volumes, both the OPLS and the TraPPE models perform fairly well in comparison with the experimental results. Since the LJ mixture's spheres are tailored according to the molar volumes of ethanol and methanol, the molar volumes of that mixture closely follow the experimental results and are comparable to those of the simulated systems. However, the real test of forcefield accuracy comes when excess properties are calculated. In that sense, neither the OPLS nor the TraPPE forcefield are accurate enough to reproduce the realistic behavior of the excess volume. While the OPLS data shows a positive excess volume, it significantly overestimates the values obtained by experiment. The TraPPE data is closer to the experimental values, but only in the ethanol rich region. In the ethanol poor region it completely changes trend and becomes negative. A negative excess volume is the hallmark of hard sphere mixtures [1], and the LJ mixture shows exactly that.

This discrepancy between experiment and models could be the consequence of several issues, such as the neglect of polarisability. One can search after models that can reproduce better experimental data. However, in a past work, the group has studied several models of ethanol and found that none of them reproduced accurately the experimental enthalpies and volumes of water-ethanol mixtures [149]. Despite those inaccuracies, the global microscopic structure of the mixture is reproduced well.

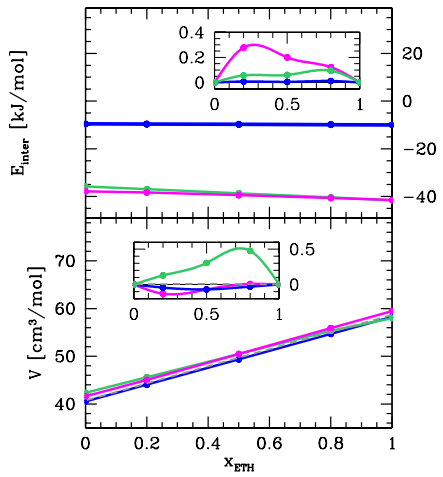

Figure 4.7.: Intermolecular energies (upper panel), molar volumes (lower panel) and corresponding excess quantities (insets) for the studied systems. Green for the OPLS model, magenta for the TraPPE model, and blue for the LJ model. The experimental data for the volumes and excess volumes [164] are equally shown in dashed grey lines.

The upper panel of Figure 4.7 reveals that the intermolecular energies of the ethanol-methanol mixtures are (about -40 kJ/mol) far below that of the LJ mixtures (about -10 kJ/mol). A LJ system cannot achieve such negative energy and stay liquid; increasing the well depth ε would likely lead to crystallization. These large negative energies of the alcohol mixtures are therefore a signature of a hidden complexity.

As for the excess energies, they are positive for all types of mixtures, indicating that the mixing is slightly less favourable than the neat states. Interestingly enough, the TraPPE force field overestimates the value on the methanol rich side, while OPLS does the same thing on the ethanol rich side. This indicates the low performance of force fields as far as excess thermo-physical properties go.

4.2.2. Kirkwood-Buff integrals

Ideality in mixtures can be considered through concentration fluctuations. If molecules from different species interact very similarly, their relative distributions will be similar to the respective pure liquid, rendering the concentrations fluctuations small. Ideal mixtures have been investigated through the Kirkwood-Buff theory in the literature [165, 166, 167]. Ploetz et al. [167] have studied ideal and non-ideal mixtures in comparison with the associated pair correlations. They noted that ideal mixtures tends to have very little variation of their correlations in mixing condition with respect to that of their respective pure states, which is what one would expect if all the interactions would be very similar.

Through the section on structural analysis, we've seen that pair correlation functions of the ethanol-methanol mixture indeed conform to this trend. Now we turn to the KBI results to see whether or not they are in accord with the trend in ideal mixtures. The calculated KBIs for the ideal case (lines) and the KBIs obtained from simulation (symbols) are reported in Figure 4.8. The ideal KBIs are calculated by setting the $D(x)$ from Equation 2.32 to 1.

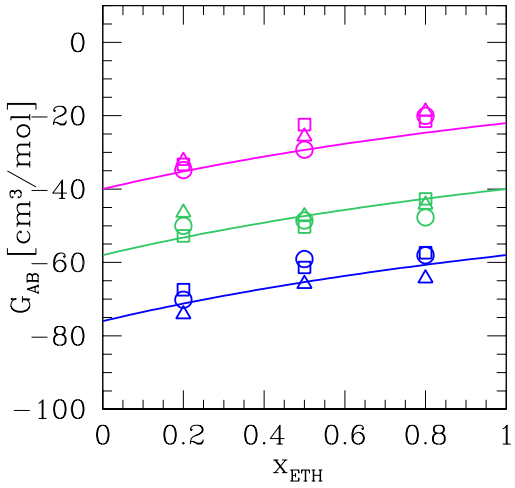

Figure 4.8.: Kirkwood-Buff integrals for the alcohol (OPLS in open dots, TraPPE in open squares), LJ (open triangles and ideal KBI in lines) mixtures. The solvent-solvent (methanol) KBI are in magenta, the solute-solute (ethanol) in blue, and the cross in green.

Both the alcohol mixture and LJ mixture exhibit similar behavior in terms of KBI. All of the data sets fall quite close to the calculated ideal KBI values. This finding indicates that these mixtures are ideal from thermodynamic point of view, with very little concentration fluctuations. The near absence of concentration fluctuations in the ethanol-methanol mixture was pointed out in studies of the diffusion constants in the mixture [66, 168].

In the case of the LJ mixture, these low concentration fluctuations go hand in hand with a uniform distribution of the molecular species, and this is the scenario seen in simple liquids [1]. The ethanol-methanol mixture displays strong clustering at every mole fraction, accompanied by much more negative energies, yet it also seems to be thermodynamically ideal.

However, the presence of clusters in the system is not opposed to the concept of thermodynamic ideality. The fact that ethanol and methanol share the same hydroxyl group and, by consequence, the same Hbonding interactions and preferences, will lead to them mixing almost perfectly. Since alcohols have a tendency to form clusters, simultaneously reducing the concentration fluctuations, the final result is a mixture which is ideal on the surface, but hides complex structuring beneath it.

4.3. The methanol-1-propanol mixture

So far, we've seen that the hydroxyl group interactions play an important role in the ethanol-methanol mixture, both in the structural and thermodynamic sense. However, the difference in alkyl tail length between ethanol and methanol is not great, so it naturally poses the question what would happen if alcohols with longer carbon chains were used. If we were to mix methanol with 1-propanol, there would be a bigger asymmetry of the non-polar tails, and it would be interesting to see how this effect would compete with the identical interaction between the hydroxyl groups.

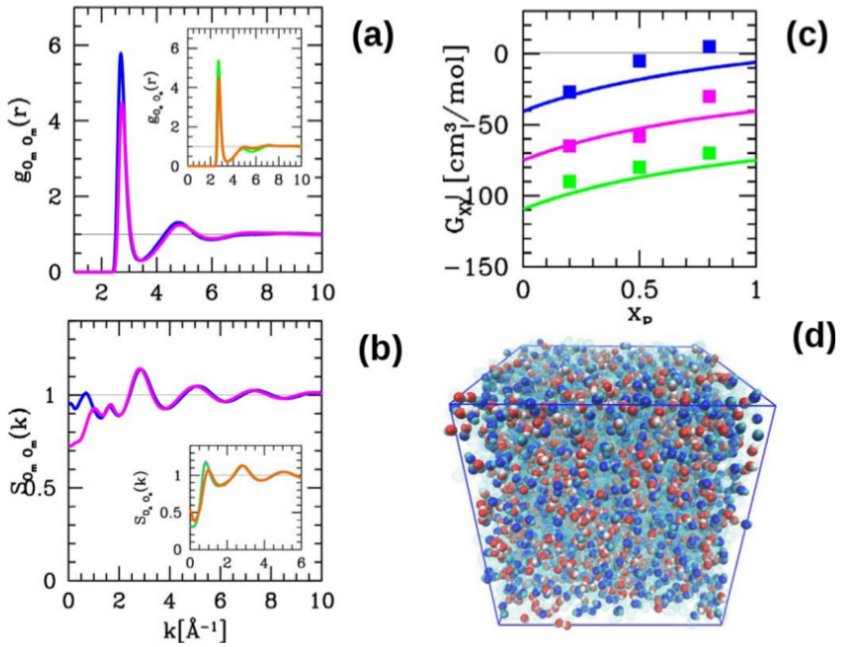

Figure 4.9.: (a) Plot of the methanol oxygen-oxygen correlation functions $g_{OO}(r)$ (blue) from the equimolar methanol-1-propanol mixture, compared with the methanol $g_{OO}(r)$ in the methanol-ethanol equimolar mixture (magenta). The inset shows $g_{OO}(r)$ for 1-propanol (green) compared with ethanol's $g_{OO}(r)$ in equimolar methanol-ethanol mixture (orange). (b) The structure factors corresponding to $g_{OO}(r)$ data in (a). (c) The KBI for the methanol-1-propanol mixture: methanol in blue, 1-propanol in green, and cross in magenta (lines for the calculated ideal curves and symbols for simulations). (d) Snapshot of the equimolar methanol-1propanol mixture. Methanol oxygens shown in red, hydrogens in white, 1-propanol oxygens in blue, and hydrogens in cyan. All methyl united atom groups show as semi-transparent cyan spheres.

Figure 4.9 summarizes the main results for the methanol-1-propanol mixture. Only the data for the equimolar mixture was featured, as other concentrations show an overall similar trend to ethanol-methanol. Figure 4.9a) shows the OO correlation functions of methanol in methanol-1-propanol (blue) and methanol-ethanol mixtures

(magenta curve) in the main panel and the OO correlation functions 1propanol (green) and ethanol (orange curve) in the inset. One can immediately notice the same main features as in Figure 4.5, in the form of tall and sharp first neighbor peaks, characteristic of Hbonding. The second neighbor peak shows some differences, which are expected because of the difference between the molecules. As for the structure factors (presented in Figure 4.9b) with the same color code as in panel a)), they all have cluster peaks which are very similar for these two systems. The only differences are at very small k-values, or in long range correlations. These two panels in Figure 4.9 confirm that the hydroxyl group correlations are the same for both mixtures.

The clustering in the methanol-1-propanol system is also visually observable. In Figure 4.9d) we have one snapshot of the mixture, with the hydroxyl groups of methanol shown in red (oxygen) and white (hydrogen), while those of 1propanol are shown in blue (oxygen) and cyan (hydrogen). The methyl groups are shown in transparent cyan. Similar to the middle panel of Figure 4.1, we notice the extensive and indiscriminate chain-like clustering of hydroxyl groups.

Figure 4.9c) contains the KBIs from the simulation (symbols), alongside the calculated ideal KBI (lines). The KBIs obtained from the simulation agree with the ideal KBIs, indicating that the concentration fluctuations are close to ideal. However, it must be noted that there are small but systematic deviations from pure ideality, more noticeable than in the ethanol-methanol mixture. This quantity implies that mixing closely related alcohols will result in a quasi-ideal mixture, with the ideality stemming from the dominating hydroxyl group energies. As soon as alcohols' non-polar tails start to diverge, there is a shift from ideality.

4.4. Conclusions

In this chapter we have studied mixtures between methanol and either ethanol or 1-propanol, with a particular accent on the ethanol-methanol mixture. Through the structural analysis, we have shown that this mixture has a rich organization, stemming from its hydroxyl groups and their tendency to form Hbonded clusters. With the hydroxyl groups being identical, both alcohols participate in the building of clusters equally, resulting in a system which is interspersed with such "mixed" clusters. This is proven through the results of the cluster probability distributions, but also through the site-site structure factors. The site-site structure factors for all combinations of oxygen sites bear the characteristic signature of clustering - a pre-peak which we dubbed the cluster peak.

However, it's important to note that clustering in this sense involves only the functional groups of the alcohols, while the non-polar parts of the molecules are organized randomly, similar to spheres in a Lennard-Jones mixture. The site-site structure factors of the carbon united atoms are devoid of the cluster peak.

In context of the previous chapter on simple and complex disorder, we need to make a few distinctions. Complex disorder was exemplified through the mixture of ethanol-benzene, where we had the microsegregation of the associating species - ethanol - in relation to the non-polar component. In that case, the whole ethanol molecule participated in the building of much larger objects: domains. These domains had a signature in the site-site structure factors of ethanol in the form of a pre-peak, but it's not the same pre-peak as the one studied in this chapter. The pre-peaks from the previous chapter were positioned at a much smaller k value, hinting at bigger objects, and were more intense.

In the case of ethanol-methanol, the pre-peak in the partial structure factors is solely due to the presence of specific clusters, which do not involve the micro-segregation of the entire species. These specific clusters can also be observed via scattering experiments, which were done on neat alcohols [153, 155, 169, 170]. Our calculated scattering intensities also show the signature of clusters [73].

With such structural features, the ethanol-methanol mixture differs considerably from the example of simple disorder, also described in the previous chapter. But, this richness in structure is hidden behind the apparent thermodynamical ideality of the mixture. Even though thermodynamical ideality is primarily linked to simple systems [1], it's possible to attain it in mixtures such as ethanol-methanol. Its constituents have identical interactions which govern the system and dictate cluster formation, which seems to be a mechanism for lowering concentration fluctuations and rendering the system close to ideality.

Indeed, the key to identifying an ideal mixture is the lack of concentration fluctuations, as demonstrated by the KBI results. Textbook examples of ideality will inevitably include systems with non-interacting or weakly interacting constituents, giving the impression that the absence of interactions is necessary for a mixture to be ideal. However, throughout this chapter we've seen that strong interactions in a system can coexist with ideality, and that the absence of concentration fluctuations is what makes the mixture ideal. This notion promotes concentration fluctuations, and not interactions, as the indicator of ideality, opening the road to understanding micro-heterogeneity as an enhanced form of concentration fluctuations.

As we increase the difference between the alkyl tails of the alcohols in the mixture, like in the methanol-1-propanol case, there is a more pronounced competition between the asymmetry of the non-polar parts and the strong and identical interaction between the hydroxyl groups. The results indicate that there is a shift from pure ideality, hinting that the shift will be more pronounced as the gap between the alcohols' non-polar parts widens.

5. Microheterogeneity versus clustering

Through the Introduction and previous chapters, we've seen that concentration fluctuations, observable at $S_{ab}(k) = 0$, are not to be confused with micro-heterogeneity, which manifest at $S_{ab}(k) \neq 0$, but close to $k = 0$. In a way, micro-heterogeneity is a concentration fluctuation. This perhaps subtle distinction becomes very clear when considering the mathematical definition of the pair correlation, as related to fluctuations of the local microscopic density $\rho_a(\vec{r})$ for species a. One writes this local density in terms of a fluctuation $\delta\rho_a(\vec{r})$ with respect to the macroscopic density ρ_a:

$$\rho_a(\vec{r}) = \rho_a + \delta\rho_a(\vec{r}) \tag{5.1}$$

Then, the two-body density function between species a and b is defined as the correlation between the respective two microscopic variables considered as random variables, and evaluated as a statistical ensemble average [11]:

$$\rho_{ab}^{(2)}(\vec{r}, \vec{r}') = \langle \rho_a(\vec{r})\rho_b(\vec{r}') \rangle \tag{5.2}$$

For a macroscopically homogeneous system, this definition leads to [11]:

$$\rho_{ab}^{(2)}(\vec{r}, \vec{r}') = \rho_a\rho_b g_{ab}\left(|\vec{r} - \vec{r}'|\right) + \alpha\delta\left(\vec{r} - \vec{r}'\right)\delta_{ab} \tag{5.3}$$

The structure factor expresses the same fluctuation, but in the k-space. The last term in the equation comes from the fact that, for same species, the self-correlation term must be excluded by definition.

In this chapter, which draws upon the content from our PCCP paper [74], we delve deeper into the concept of micro-heterogeneity and confront it with the more commonly spread concept of cluster. Clustering happens naturally in any interacting molecular system, when some particles are grouped together through attractive interaction forces. This term is connected to the structuring in associated

liquids, in particular to neat alcohols. Clustering in neat alcohols leaves a distinct signature in the form of the pre-peak in the experimental X-ray and neutron scattering intensity, a fact that has been well known throughout the years [153, 155, 161, 162, 169, 170, 171, 172, 173].

What happens when we mix a clustering liquid, such as ethanol, with solvents of different nature? How does this clustering differ from micro-heterogeneity or concentration fluctuations?

For that reason, we will be probing in depth the properties of ethanol-hydrocarbon mixtures and ethanol-water mixtures. Even though Chapter 3 has given us much insight into the ethanol-benzene mixture, we will show that the general characteristics of that mixture apply to other mixtures of ethanol with non-polar solvents, such as pentane and hexane. When mixed with hydrocarbons, ethanol's hydroxyl groups form energetically favorable hydrogen bonded structures [174, 175]. Since ethanol is immersed in a non-polar environment, the only bonding possibilities are between the ethanol molecules themselves, and the resulting structures are well-defined. A typical ethanol cluster found in the ethanol-benzene mixture, where $x_{BEN} = 0.8$, can be seen in the left panel of Figure 5.1.

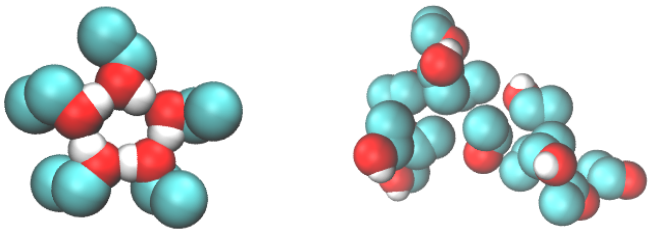

Figure 5.1.: Ethanol structuring present in: 80% mole fraction of benzene (left panel) and 80% mole fraction of water (right panel). The color code for element is the same as in Figure 3.2.

However, when mixed with water, ethanol molecules can bond not only among themselves, but with water molecules as well. In all classical force fields, the values of partial charges located on the water molecule are larger than those of the ethanol hydroxyl group [176, 177, 178]. For that reason, water molecules will prefer to Hbond with themselves, rather than with ethanol [38, 149, 148]. The wealth of bonding choices will destroy ethanol's chain-like clusters, relegating them to fuzzy aggregated structures - an example of which is shown in the right panel of Figure 5.1.

Thoughout this chapter, we will connect the ideas behind the visual findings from Figure 5.1 to the signatures of their structuring in the site-site structure factors. Different features of the structure factor are associated to concentration fluctuations, clustering and micro-heterogeneity, as we will show. In addition, cluster probabil-

ity distributions of these systems will be evaluated, and this method of structural analysis will be compared to the structure factor one.

5.1. Snapshot analysis

Snapshots shown here are for illustrative purposes only. Since a snapshot corresponds to one configuration at a given point in time, it cannot be used to draw conclusions about the general behavior of a mixture. However, for micro-heterogeneous systems (such as the ones investigated in this chapter) snapshots can be quite useful. MH is a constant property of a system. In a simulation, it may realize itself somewhat differently from configuration to configuration, but the overall segregation pattern stays the same. For that reason, a single microstate in our MH mixtures can provide ideas about the structuring in the mixture.

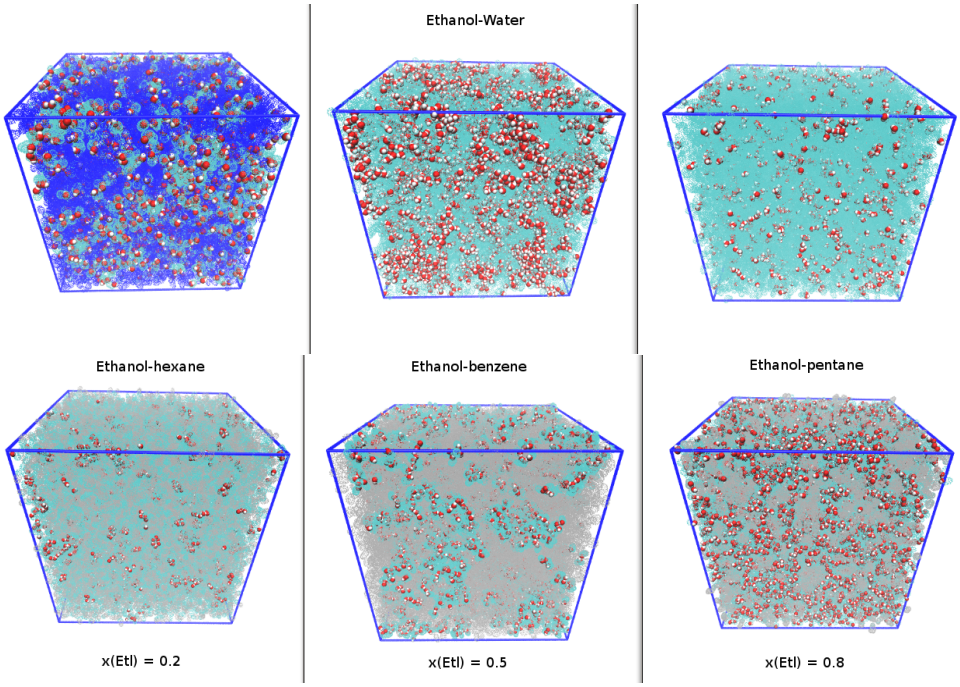

Figure 5.2.: Selected snapshots of aqueous-ethanol (top figures) and hydrocarbon-ethanol (lower figures) mixtures. Figures on the right correspond to 20% mole fraction of ethanol, in the middle for 50% ethanol and on the right for 80% ethanol. See the text for details on color conventions for different molecules.

Figure 5.2 expands the statement in the introduction about typical ethanol structuring in two different types of environment. It shows the the morphology of the ethanol-water (upper row) and ethanol-hydrocarbon mixtures (lower row), each for 3 mole fractions of ethanol, namely $x_{ETH} = 0.2$ (left column), 0.5 (middle column) and 0.8 (right column).

For the case of aqueous ethanol mixtures, the $x_{ETH} = 0.2$ mole fraction reveals that ethanol molecules (depicted in red (oxygen), white (hydrogen) and semi-transparent cyan (methyl groups)) form loose domains in water (shown as semi-transparent dark blue environment). Moreover, the ethanol hydroxyl groups are not so bonded among themselves - they also bond with the surrounding water molecules. As a result, despite segregation, the ethanol domains are rather fuzzy. The other two mole fractions, $x_{ETH} = 0.5$ and 0.8, show explicitly the water molecules, while ethanol is in semi- transparent representation. We notice that water is segregated in loose domains, despite the apparent hydrogen bonding amongst itself. The general picture that emerges from these 3 snapshots is that both water and ethanol form fuzzy micro-segregated domains, with the fuzziness originating from the incomplete self-hydrogen bonding of each species with its own kind. From this observation, we expect that the cluster distributions will not show any peak at some particular cluster size.

The lower panel of Figure 5.2 with the ethanol-hydrocarbon mixtures tells a different tale. The left figure shows ethanol molecules (same respresentation as in the upper panel) at $x_{ETH} = 0.2$ in hexane (semi-transparent gray representation). Although it's immediately apparent that ethanol molecules are segregated from hexane, we can see another important detail - ethanol's hydroxyl groups are oriented towards each other and from chains and loops. In fact, almost all hydroxyl groups are bound into such a shape. The middle picture shows $x_{ETH} = 0.5$ in benzene, with a representation of the molecules analogous to the previous snapshot. This figure follows the trend seen in the previous one - there is a segregation in species domains, as well as chain/loop clusters of the hydroxyl groups inside the ethanol domains. The lower right picture shows $x_{ETH} = 0.8$ in pentane, where the ethanol molecules are shown entirely. Again we observe a domain segregation by species, and geometric clusters of the hydroxyl groups. Moreover, the clustering of ethanol in a non-polar environment strongly resembles that in pure ethanol.

5.2. Correlation function analysis

Figure 5.3 shows the correlation functions in aqueous ethanol. The main panel contains the ethanol OO correlations, for 3 different concentrations of ethanol, while the inset shows the correlations between the oxygen sites of water. The pure liquid correlations are also shown in black. All cases are characterized by a sharp and narrow first peak, a feature tied to underlying hydrogen bonding between hydroxyl groups. Although these findings suggest strong associations of the species, that is more easily confirmed by considering the long-range correlations, which will be done in the next section.

It's imporant to observe that water O_WO_W correlations increase with the decrease of water content, which was observed for other aqueous mixtures before [33, 38, 114]. That trend is opposite for ethanol, as its correlations at contact tend to decrease with

decreasing ethanol concentration. This interesting feature is not limited to water. In fact, it's observed for any associating molecule mixed with a less associating one.

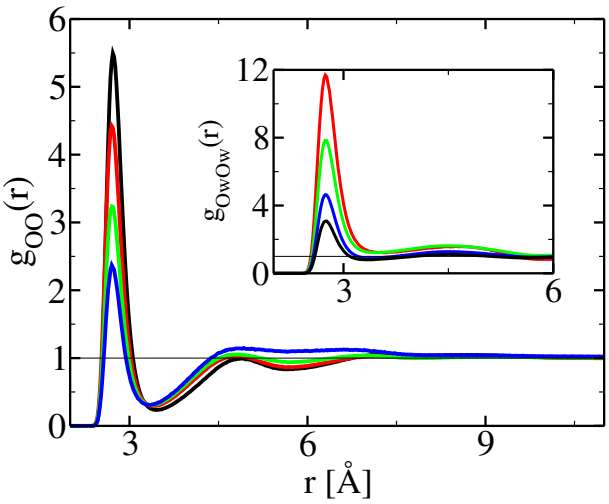

Figure 5.3.: Oxygen–oxygen correlation function in ethanol–water mixtures. Main panel for ethanol, the inset for water. Blue curves for 20% mole fraction of ethanol, green for 50% ethanol and red for 80% ethanol. The pure component is shown in black. These color conventions are preserved in all subsequent figures.

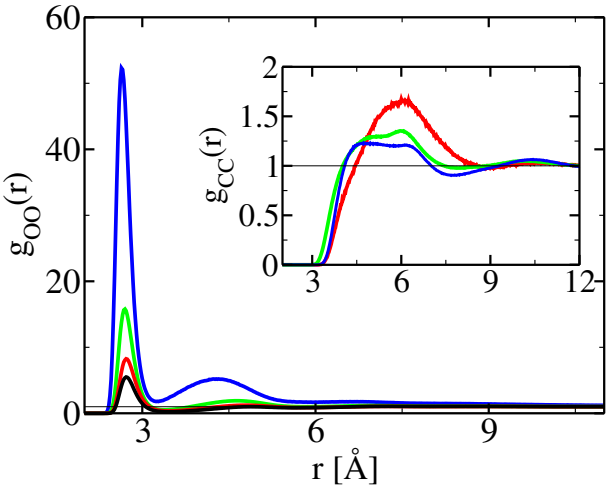

Figure 5.4.: Site–site correlations in ethanol–alkane mixtures. Main panel: ethanol oxygen–oxygen correlation function. Inset: Carbon united atom correlations (blue for pentane, green for benzene and red for hexane). Color convention according to ethanol mole fraction as in Figure 5.3.

That is demonstrated in Figure 5.4, which shows the correlations between the oxygen sites of ethanol in non-polar solvents. In the latter case, ethanol takes the role of the associating species, which is directly mirrored in the correlation functions. The

ethanol oxygen *g(r)*s, presented in the main panel, have a first peak which increases with decreasing ethanol content. The various alkane correlations – shown in the inset – show the opposite trend, although these correlations concern very different alkanes. Moreover, the sharp first peak in the ethanol OO *g(r)* is much higher and stronger than the peaks in Figure 5.3, indicating the stronger hydrogen bonding of the hydroxyl groups of ethanol when mixed with non-polar solutes. Their association is energetically favorable, giving rise to the "hair-out" micelle analogy mentioned in the introduction of this chapter.

5.3. Structure factor analysis

Figure 5.5 presents the structure factors corresponding to the *g(r)*s in Figure 5.3, with the same color code. The black lines denote the oxygen–oxygen structure factors of the neat components, which help us to evaluate the changes in the microstructure compared to the pure liquid.

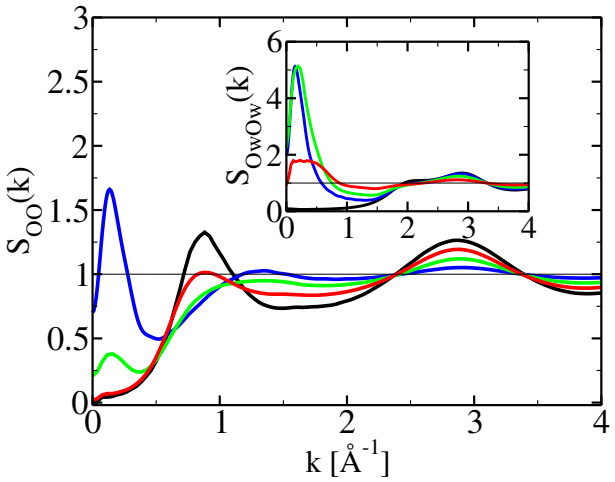

Figure 5.5.: Structure factors for the correlation functions shown in Figure 5.3, with the same color conventions. Structure factors of neat liquids shown in black. Main panel: ethanol; inset: water.

In the case of water (the inset of Figure 5.5), we notice the characteristic double peak of neat water [179] decreasing as the ethanol concentration is increased. The Hbond peak at $k \approx 3$ Å^{-1}decreases progressively with the addition of ethanol, while the main peak at $k \approx 2$ Å^{-1} doesn't change much until $x_{ETL} = 0.8$, when it is almost decimated. Both of those facts reveal that water molecules are less and less hydrogen bonded when the ethanol concentration is increased. However, there is one more important feature in Figure 5.5- a pre-peak located at $k \approx 0.2 - 0.4$ Å^{-1}, which corresponds to domain sizes of $d \approx 12 - 30$ Å. This pre-peak occurs for all ethanol mole fractions, although the pre-peaks at $x_{ETL} = 0.2$ and 0.5 are much stronger than for $x_{ETL} = 0.8$. That is in line with the large water domains one observes

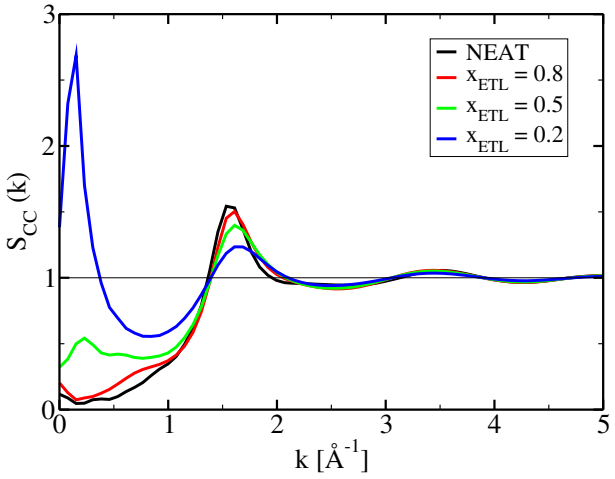

Figure 5.6.: Site-site structure factors of ethanol methyl groups in water. The color code is the same as in Figure 5.3.

in the snapshots (Figure 5.2) for the two former concentrations, and smaller water domains for the latter ethanol fraction. The small water segregated domains (at large ethanol concentrations) have less hydrogen bonded water molecules than in pure water, implying that bonding with ethanol is occurring, which confirms the idea of fuzzy water clusters introduced above.

As for the ethanol structure factors (the main panel of Figure 5.5), there are several peaks to take note of. The OO structure factor of neat ethanol has a main peak $k \approx 2.8$ Å^{-1}, which corresponds to the hydrogen bonding distance, and a pre-peak located at $k \approx 0.8$ Å^{-1}, which corresponds to the chain and ring clusters [149]. Under mixing conditions, the Hbonding peak of ethanol decreases strongly with the increase of water content. The cluster peak recedes as more water is added, turning non-existant at $x_{ETL} = 0.5$, while a domain pre-peak at $k \approx 0.1 - 0.2$ Å^{-1}emerges for mole fractions $x_{ETL} = 0.5$ and 0.2. Even though these two peaks seem similar, the mechanisms behind them are very different. The cluster peak, as its name says, detects cluster formations brought on by the oxygens in ethanol, which are characteristic of the neat liquid and mixtures where ethanol is prevalent. The origin of the domain pre-peak is different - when ethanol becomes the minority, its hydroxyl groups bond more with water, rather than among themselves, which in turn prompts the hydrophobic methyl sites to group together. This is a direct manifestation of the so-called hydrophobic effect [180, 181], which can be seen even more clearly through the structure factors of the methyl groups in ethanol. In Figure 5.6, there is a domain peak for the two lowest ethanol concentrations, yet no cluster peak for the high ethanol content. That confirms the picture of different origins of the two pre-peaks.

Figure 5.7 shows the structure factors calculated from the *g(r)*s from Figure 5.4. The OO structure factors of ethanol, presented in the main panel, retain the main peak at $k \approx 2.8$ Å^{-1}, which has the same intensity regardless of the alkane concen-

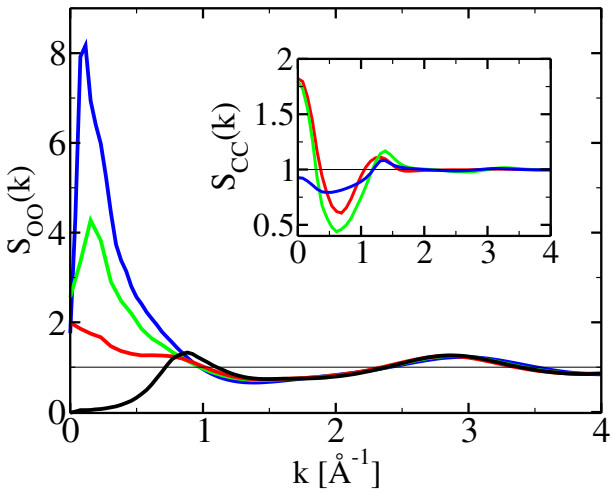

Figure 5.7.: Structure factors for the correlation functions shown in Figure 5.4, with same conventions.

tration. Clearly, the ethanols' Hbond is the dominant interaction in this case and is not affected by mixing with alkanes. The cluster peak of neat ethanol, however, gradually gets absorbed into a domain pre-peak at small k-values $k \approx 0.1 - 0.15$ Å^{-1}as more hydrocarbons are added. This result indicates that ethanol domains in alkanes are made up of hydroxyl group clusters (similar to the left example shown in Figure 5.1), which ties in with the visual information from Figure 5.2.

All hydrocarbon structure factors, in the inset of Figure 5.7, have one characteristic feature - the main peak placed at $k \approx 1.4$ Å^{-1}, which translates to the diameter of the united atom methyl sites in various force field models ($\sigma_C \approx 4$ Å). Although the hydrocarbon molecules are different, their structure factors look nearly the same around this value of k. Furthermore, the increase in domain segregation of ethanol causes an increase of these structure factors but only at $k = 0$. Contrary to associating species, these non-polar liquids witness solely concentration fluctuations.

5.4. Cluster distribution analysis

Figure 5.8 shows the cluster distribution of water oxygen atoms in aqueous-ethanol, for different concentrations of ethanol. Knowing that aqueous mixtures of alcohols are microheterogeneous, one expects to notice that in the cluster distribution. However, the curves in the main panel show that the probability of a small size cluster occuring is always greater than that of a larger size cluster. That type of behavior is characteristic of simple liquids [121, 123], as seen in the upper inset of Figure 5.8, where the cluster distribution of a Lennard-Jones mixture is shown. The LJ mixture taken in account is actually a model for carbon tetrachloride ([182]), which is treated as a mixture by changing the names of the molecules. The lower inset of Figure 5.8 depicts the probability distribution of clusters of the pentane carbon

atom in ethanol–pentane mixtures, for different ethanol concentrations, which are again trivial cluster distributions.

Judging from the data in Figure 5.8, it turns out that there are almost no differences in these various distributions, which is very counter-intuitive in light of the strong micro-segregation in aqueous-ethanol mixtures.

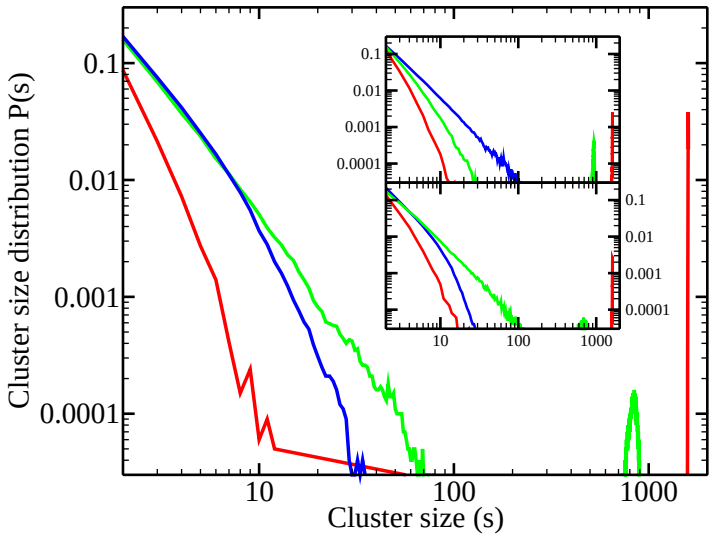

Figure 5.8.: Cluster distribution functions. Main panel, for water oxygen atoms in aqueous ethanol mixtures (color conventions according to the ethanol mole fraction as in Figure 5.3). Top inset: Cluster distributions in a binary Lennard-Jones type mixture (see the text). Lower inset: Cluster distribution for the pentane central carbon atom in ethanol–pentane mixtures.

Figure 5.9 presents a comparison of the cluster distribution of ethanol oxygen atoms in pentane (main panel) and water (inset), for different concentrations of ethanol, including pure ethanol (shown in black). Pure ethanol has a peak in its cluster probability distribution, witnessing the preferential cluster size of 4-6 ethanol molecules. When ethanol is mixed with pentane, that pure ethanol cluster peak increases with decreasing ethanol concentrations, confirming the clustering trend observed through visual inspection of the system and also the pre-peak analysis of the structure factors in Figure 5.7. The inset, on the contrary, shows only the trivial clustering akin to that in Figure 5.8, despite the micro-segregation present in aqueous-ethanol.

From the difference of ethanol clustering, we see that the cluster distribution calculation is only able to detect sharp, well-defined clusters such as those present in ethanol-alkane mixtures, while fuzzy clusters in aqueous ethanol cannot be observed. To use the analogy mentioned in the introduction of this chapter, we could say that cluster analysis is more performing for the surfactant in oil, rather than the surfactant in water.

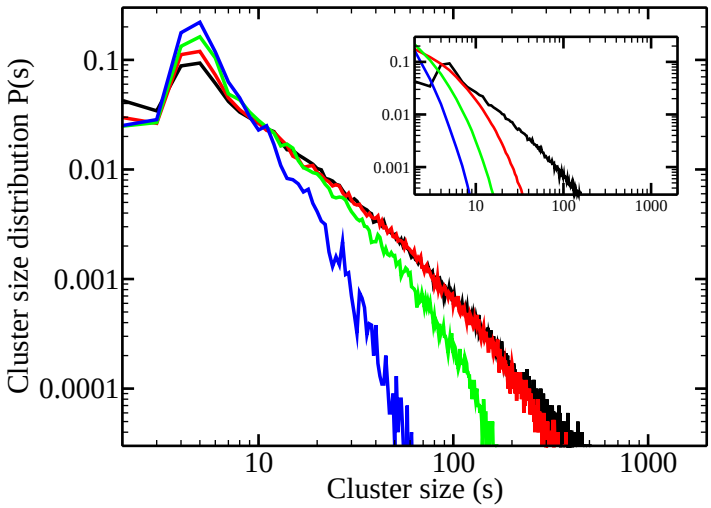

Figure 5.9.: Cluster distribution functions. Main panel, for ethanol oxygen atoms in ethanol–pentane mixtures. Inset, for ethanol oxygens in aqueous mixtures (color conventions according to the ethanol mole fraction as in Figure 5.3).

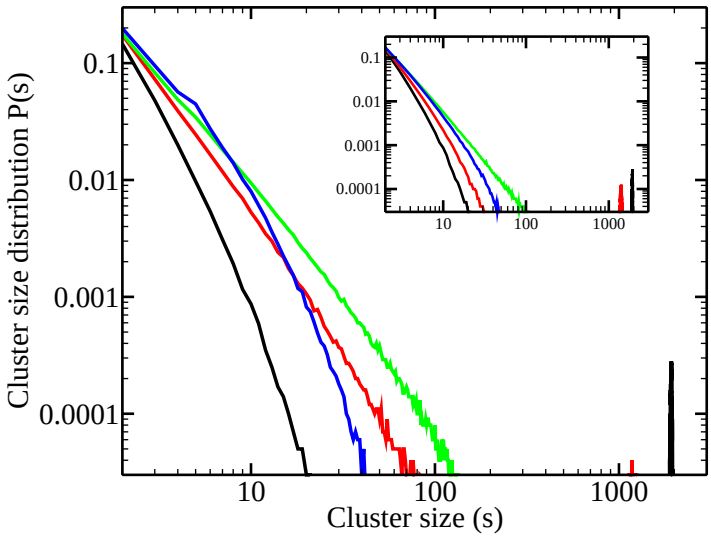

Figure 5.10.: Cluster distribution functions for the ethanol methyl group. Main panel, for ethanol–pentane mixtures. Inset, for aqueous-ethanol mixtures (color conventions according to the ethanol mole fraction as in Figure 5.3).

Figure 5.10 shows a comparison of the clustering of the methyl group in ethanol-pentane mixtures, and aqueous-ethanol (inset). These methyl groups are randomly distributed in pure ethanol, as shown by the black curve. This random distribution

is present in both aqueous ethanol and alkane-ethanol. The cluster probability distributions for both mixtures look very similar, even though they differ among themselves.

5.5. Conclusions

In this chapter, we have compared the difference in structuring between two complex mixtures - one with both associating species (aqueous ethanol) and one with a single associating species (ethanol-hydrocarbon).

Figure 5.3 and Figure 5.4 show two universal features in mixtures of associating liquids. When there is only one associating species in the mixture, it will exhibit the typical behavior i.e. it will bind with itself more and more as its concentration decreases. But, when we have two associating species in the mixture, the strength of their binding affinity strongly influences the structuring. The less associating species bonds less and less with itself with the increase of concentration of the more associating species, while the more associating species bond more and more with itself when its concentration decreases.

Another important issue is the comparison between the correlation function formalism and the direct cluster analysis. We have seen that the study of structure factors reveals rich structuring for both types of mixtures; cluster calculation, on the other hand, has success with the ethanol-hydrocarbon mixture, while it has no remarkable results for aqueous ethanol.

The crux of the matter lies in the intrinsic differences between the mixtures. Cluster calculation is able to detect ethanol clusters driven by Hbonding. In the neat liquid, clusters of ethanol are the only structure there is; in the mixture with hydrocarbons, clusters are the building blocks of ethanol domains. Because of that, cluster analysis can hint to the presence of ethanol domains through the existence of ethanol clusters. In aqueous ethanol, however, microsegregated domains are not reducible to the Hbond clusters of which they are made. That's why the fuzzy domains present in that mixture cannot be detected via cluster calculation.

The different origins of microsegregation make cluster analysis a less suitable tool for exploring MH in all its cases. The correlation function analysis, and particularly the structure factor analysis, can pick up the signatures of clustering and microsegregation unerringly. On top of that, the structure factor analysis can differentiate between concentration fluctuations (which manifest at $k = 0$ and can be connected to thermodynamic observables through the KBI formalism) and segregated domain structures (which manifest as a pre-peak at small k) - something cluster analysis cannot do.

6. Aqueous alcohol mixtures in cold conditions

In this chapter, we shift our attention towards mixtures with water. Up to this point, two different types of water structuring were observed in aqueous mixtures, depending on the type of co-solvent it is added to. The first one is when water forms two-dimensional, chain-like clusters, which occur in aqueous DMSO mixtures [34]. The second one is when water forms globular domains, which is a hallmark of aqueous alcohol systems, for example *tert*-butanol-water [39, 41, 183, 184]. The strong MH displayed in these systems is often accompanied by considerable CF, as shown by the KBI experiments [26, 185]. We've seen that the difference between MH and CF is the most visible in the structure factor, with the former manifesting as a pre-peak in the small k region of the structure factor, and the latter being the $k = 0$ part of the structure factor.

What happens to these manifestations with the change in temperature? This question is especially pertinent in the case of lowering the temperature. Decreasing temperature increases in interaction forces through the Boltzmann factor in classsical statistical mechanics. However, this increase might affect the different types of interaction, namely the Lennard-Jones interactions and the Coulomb interactions, in a different manner. Is there such a change, and how would it affect the structure of the mixture?

To answer those questions, we start with the aqueous methanol mixture. This is the first mixture which was reported to have MH [186, 187] and which continues to garner attention to this date, as evidenced by the considerable body of literature, both in terms of simulations and experiments [16, 21, 36, 58, 61, 62, 66, 65, 64, 188]. This mixture could be considered a good starting point for studying micro-heterogeneity, for we have shown that it is not so much pronounced under ambient conditions [189]. Also, there is another point of interest in investigating the temperature dependence of this mixture in particular.

Mixtures with an upper critical solution temperature (UCST) demix when the temperature is lowered below this critical temperature. This is the case for a few aqueous mixtures, like aqueous acetonitrile [190] or aqueous 2-butoxyethanol [191]. The water-methanol mixture does not undergo demixing at any temperatures for which they are liquid. However, there have been speculation about the existence of a hidden UCST at temperatures lower than ambient [126]. In that light, it would be

interesting to study the behavior of concentration fluctuations. Also, that would help to clarify how does MH evolve with decreasing temperatures.

To get a broader picture, we will also look into the water-ethanol and water-*tert*-butanol mixture.

Simulating systems at low temperatures has its own set of challenges. The discussion concerning that can be found in Appendix B.

The work given in this chapter has been the subject of two publications [75, 76]. The aqueous methanol results were presented as a poster on the conference "WaterX - exotic properties of water under extreme conditions" (July 2016.) and as a talk on the 13th International school of biophysics "Greta Pifat Mrzljak" (September 2016.). The results on aqueous ethanol and aqueous TBA were featured on a poster for the "Joint EMLG/JMLG Annual Meeting" (September 2017).

6.1. Aqueous methanol mixture

6.1.1. Correlation functions

Figure 6.1 shows the evolution of oxygen-oxygen atom correlations with decreasing temperature. We notice that the correlations increase with decreasing temperatures, both for water and methanol, and for every concentration.

That is expected because of the drop in the kinetic energy, which has the effect of the Coulomb interactions being more dominant than at room temperature. This results in a tightening of the H-bonds in our classical description [135]. This is consistent with the results of Bako et al. [129], who reported for the high water mole fractions. Also, the two species behave differently. Water oxygen correlations increase with decreasing water concentrations, while that of methanol decrease with decreasing methanol concentrations (noticed before for aqueous alcohol mixtures [40, 114, 149], and also discussed in chapter 5). Furthermore, water displays a larger relative increase of correlations of the first neighbours than methanol. Also, second neighbor correlations behave peculiarly - they go through a maximum at 200 K for water (green curves)-for all methanol concentrations, while for methanol, this happens at 150 K (red curves). At low water concentration, water-water correlations at second and higher neighbours tend to oscillate sightly below unity, which indicates a decrease of the number of neighbours and is in line with Soper's previous report [126]. That can be acertained from the coordination number of water in Figure 6.2. One sees clearly that the H-bonding coordination of water decreases below that of methanol at the highest methanol content (right panel), which is especially pronounced for $T = 200$ K (lower row). On top of that, there is a flattening of the water coordination, which implies the existence of the chain-like clusters. On the other hand, methanol coordinations at the two lower concentrations are quite low,

while at $x_M = 0.8$ they resemble those of neat methanol, suggesting the existence of methanol chains.

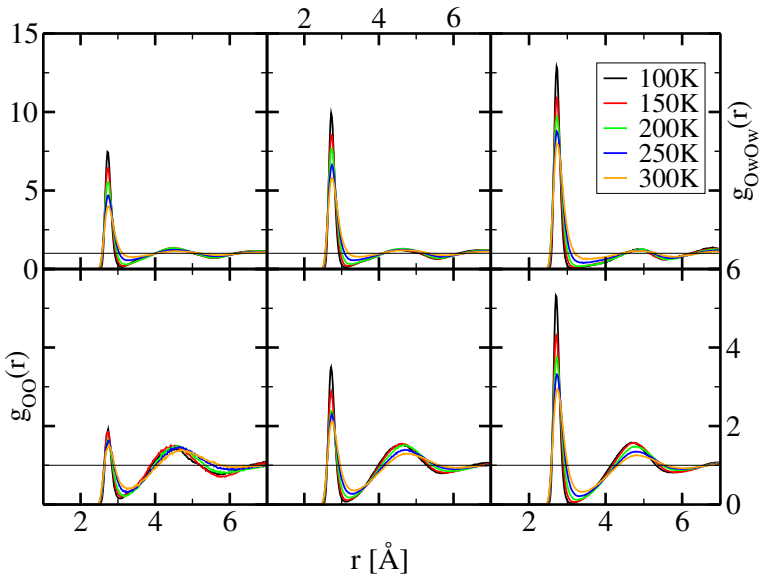

Figure 6.1.: Temperature dependence of the oxygen-oxygen correlation functions for water (upper row) and methanol (lower row). Left, middle, and right panels correspond to methanol mole fractions of 0.2, 0.5 and 0.8, respectively. The color code is contained in the legend.

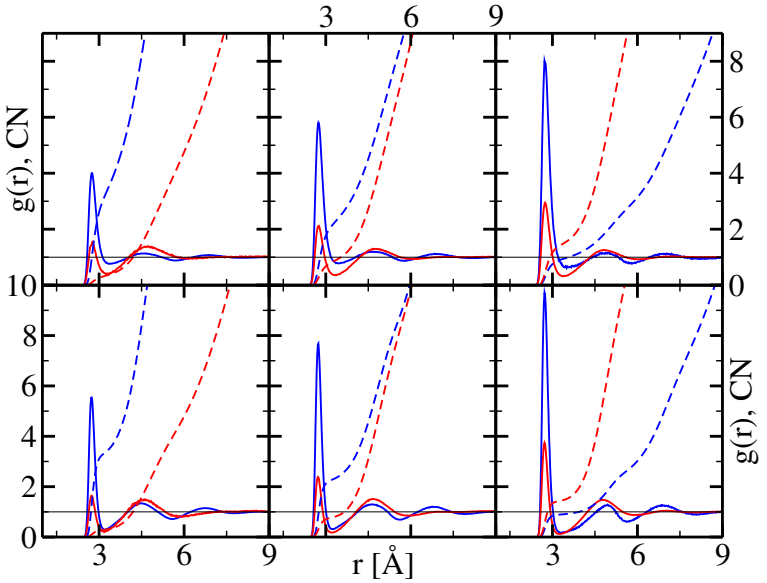

Figure 6.2.: Oxygen-Oxygen correlation functions (solid lines) and corresponding coordination numbers (dashed lines). Water is shown in blue and methanol in red. Top panels for $T = 300$ K and lower panel for $T = 200$ K. Left figures for methanol mole fractions x = 0.2, middle for x = 0.5 and right for x = 0.8.

6.1.2. Cluster probability distributions

Figure 6.3 shows the temperature evolution of the cluster distribution probabilities for the oxygens in methanol (upper row) and in water (lower row). The cluster distributions fall monotonously with the increasing cluster size, displaying the trivial behavior characteristic of simple systems [121, 123]. With the decrease in temperature, the changes to the probability distributions in methanol are negligible. Water undergoes more changes, especially at $x_M = 0.2$ mole fraction, but overall, there is no specificity in the distribution. The result shown for water probability distributions at $x_M = 0.5$ (lower row, middle panel) agrees with the data in [126].

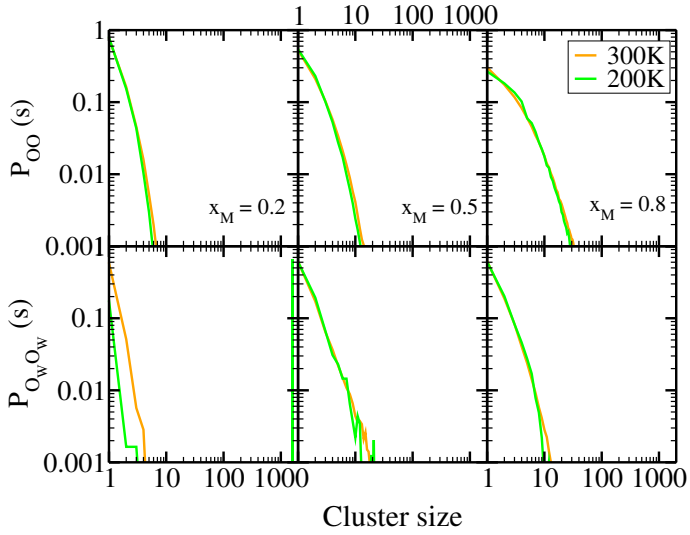

Figure 6.3.: Cluster probability distributions for methanol (upper row) and water (lower row). The mole fractions of methanol are 0.2 (left panel), 0.5 (middle panel) and 0.8 (right panel). The color code for the temperatures is contained in the legend of the image.

The cluster analysis of aqueous methanol at ambient temperature yielded results similar to those of aqueous-ethanol (presented in the previous chapter).

6.1.3. Structure factors

The structure factors, presented in Figure 6.4, are organized in the same way as in Figure 6.1. In the upper panel, we observe that, at $T = 300$ K, water oxygen-oxygen structure factors show mostly concentration fluctuations, as seen from the large $k = 0$ raise. With the decrease in temperature, the CF decrease and an intermediate broad pre-peak structure emerges, in the range $k = 0.2$ - 1 Å^{-1}. This range corresponds to domains of size 6 - 30 Å. This pre-peak feature has small oscillatory sub-structures. For small methanol mole fractions ($x_M = 0.2$, left panel),

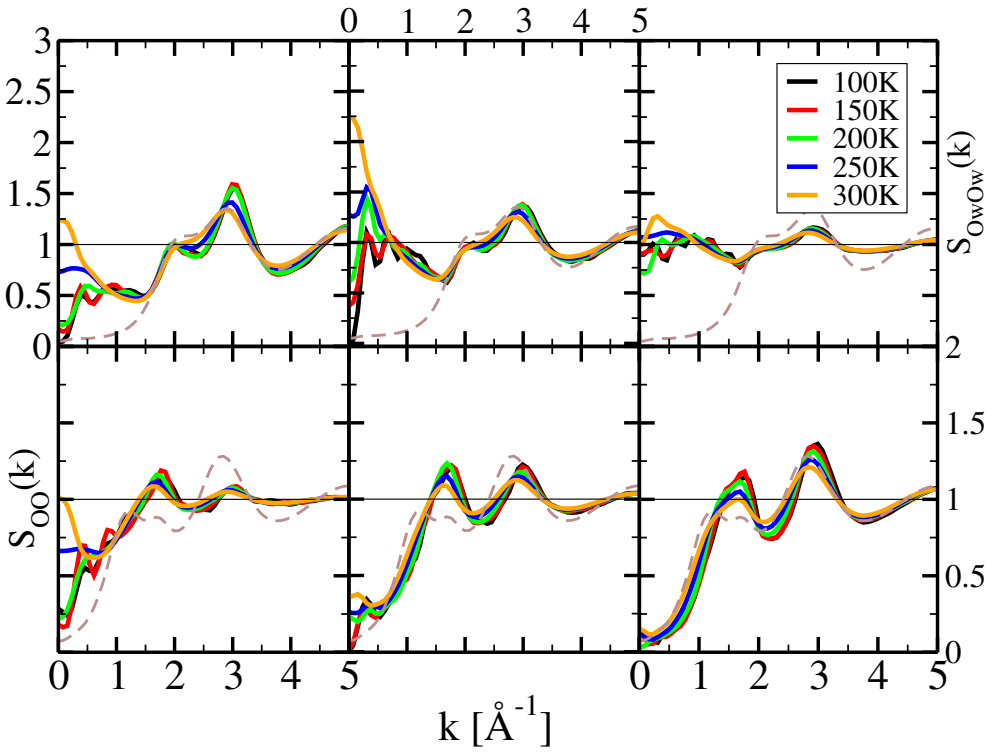

Figure 6.4.: Temperature dependence of the oxygen-oxygen structure factors corresponding to the correlation functions in Figure 6.1. The organization of panels and color code are the same as in Figure 6.1. The dashed brown lines respresent the structure factors of the neat liquids at $T = 300$K.

the pre-peak resembles more a plateau, while for the two other concentrations it looks more like a bump, hinting at better defined water domains.

The other interesting feature is the main peak of water. At $T = 300$ K, water structure factor shows the characteristic double peak [179], with one peak at $k = 2$ Å^{-1} and the other at $k = 3$ Å^{-1}. At $x_M = 0.5$ and $x_M = 0.8$, this double-peak structure changes little with temperature, but at $x_M = 0.2$, this structure is enhanced, indicating that water tightens its H-bond structure.

These small peaks found at lower temperatures contrast the large pre-peak we observe for aqueous mixtures of higher alcohols [33, 40, 192]. This may be linked to the linear water clusters we note here, rather than the bulky globular domains seen at room temperature aqueous alcohol mixtures. There are some cases where water shows this tendency to form linear structures, notably in aqueous-DMSO [34] and aqueous propylamine [77], where the pre-peak resembles the one in cold aqueous methanol.

The structure factors of methanol (lower panel of Figure 6.4) show a different behavior. Neat methanol at $T = 300$ K (dashed brown line) has a main peak at $k = 3$ Å^{-1}and a flat, broad cluster peak at $k = 1 - 1.5$ Å^{-1}[124, 125], which corresponds to H-bonded clusters of 4 – 6 Å. As the temperature goes down, both the main peak

and cluster peak become more prominent, especially for $x_M = 0.8$ and to a degree $x_M = 0.5$. For those two concentrations, the peaks are closer together in cold conditions than in ambient ones. Contrary to water, methanol structure factors don't show a domain pre-peak, hinting only at consistent cluster structuring. The CF are rather small in those two cases. As for $x_M = 0.2$, the structure factor shows less accentuated evolution of these 2 peaks, as well as a broad raise at $k = 0$, all of this suggesting indeed loose cluster structure between mere concentration fluctuations and chain structures.

6.1.4. Kirkwood-Buff integrals

So far, the structure factors presented in Figure 6.4 have indicated that the concentration fluctuations are rather small. To confirm that, we turn to the KBIs. Figure 6.5 shows the temperature dependence of the KBI of the aqueous methanol mixtures for $T = 300$ K (left), $T = 200$ K (middle), and $T = 100$ K (right). The room temperature KBIs (reported previously [189]), show a sizeable deviation from ideal behavior, especially water. But, as the temperature is gradually lowered, the calculated KBIs start following ideal behavior trends.

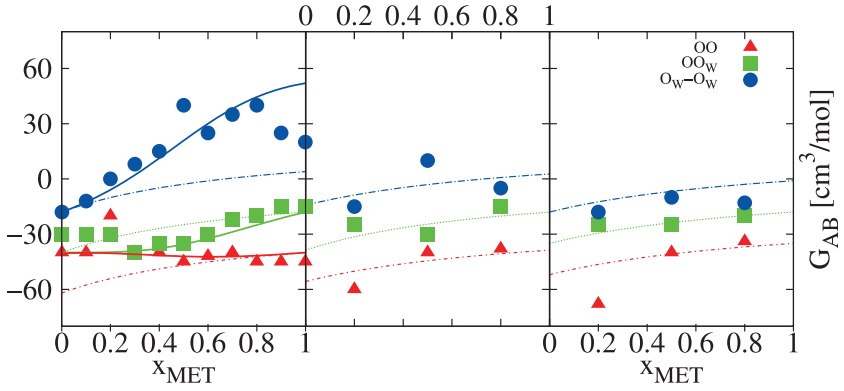

Figure 6.5.: Kirkwood-Buff integrals of the aqueous methanol mixtures for $T = 300$ K (left), $T = 200$ K (middle), and $T = 100$ K (right panel). Symbols are the KBI computed from computer simulations, full lines are experimental data [26], and dashed lines are ideal KBI. The color code is contained in the legend.

Interestingly, ideal or quasi-ideal KBI behavior is also found in aqueous-DMSO [34] and aqueous propylamine [77], especially in the the low water content region. Those findings hint at the possible link between low CF and the occurence of linear water clusters.

Finally, we can conclude that concentration fluctuations decrease with temperature, which does not agree with the predicted UCST behaviour and the associated increase of critical concentration fluctuations [126].

6.2. Aqueous ethanol and aqueous tert-butanol mixture

6.2.1. Correlation functions

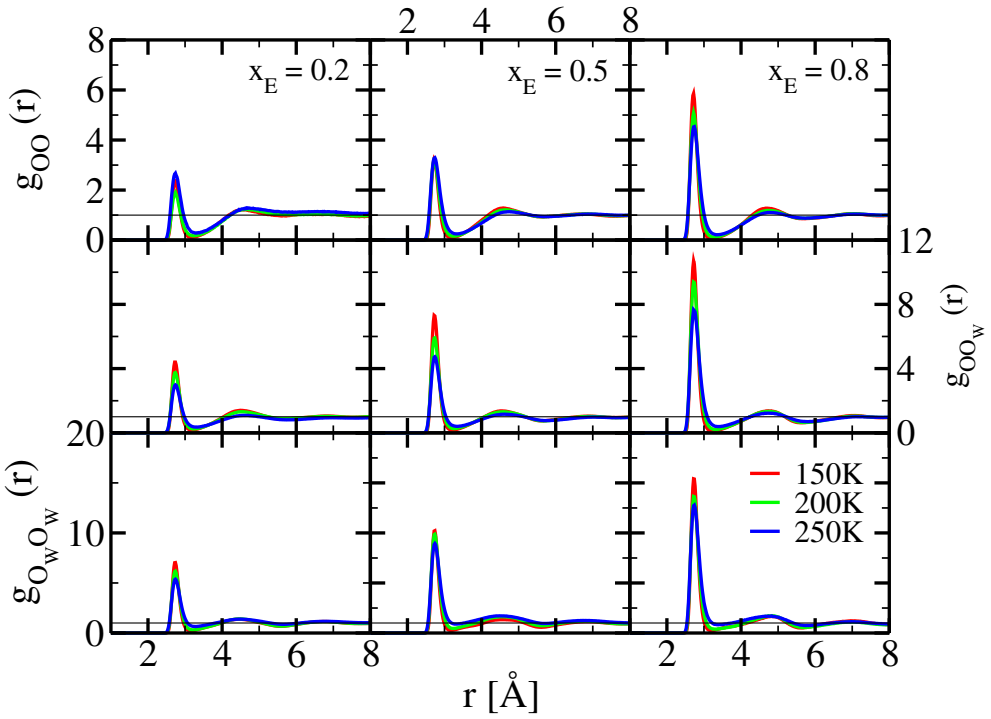

Figure 6.6.: Site-site correlation functions between the oxygen atoms of aqueous ethanol mixtures. Ethanol oxygens (upper row) and water oxygens (lower row) and cross correlations (middle row). The corresponding temperatures are shown in the figure legend. Three typical alcohol mole fractions are represented: 0.2 (left panel), 0.5 (middle panel) and 0.8 (right panel).

Figure 6.6 and Figure 6.7 show the site-site correlation functions between oxygens for ethanol-water and TBA-water, respectively. Just like in many examples before, the first peak of the water-water correlations increases as water becomes scarce, while the opposite is true for the solute species. The cross oxygen atom correlations of both mixtures (middle rows) share the same trend with alcohols, but it's important to note that the height of the first RDF peak is between those of water and alcohol (depending on the concentration). That indicates that: a) there is significant cross binding between the different species, b) water may preserve tetrahedrality by binding with the oxygens of the alcohol molecules, while chain-binding with itself.

Another general characteristic of these correlation functions is a high and narrow first peak, followed by comparatively small second and higher neighbor shells. That behavior is typical for Hbond associations, which seem to be the principal mechanism

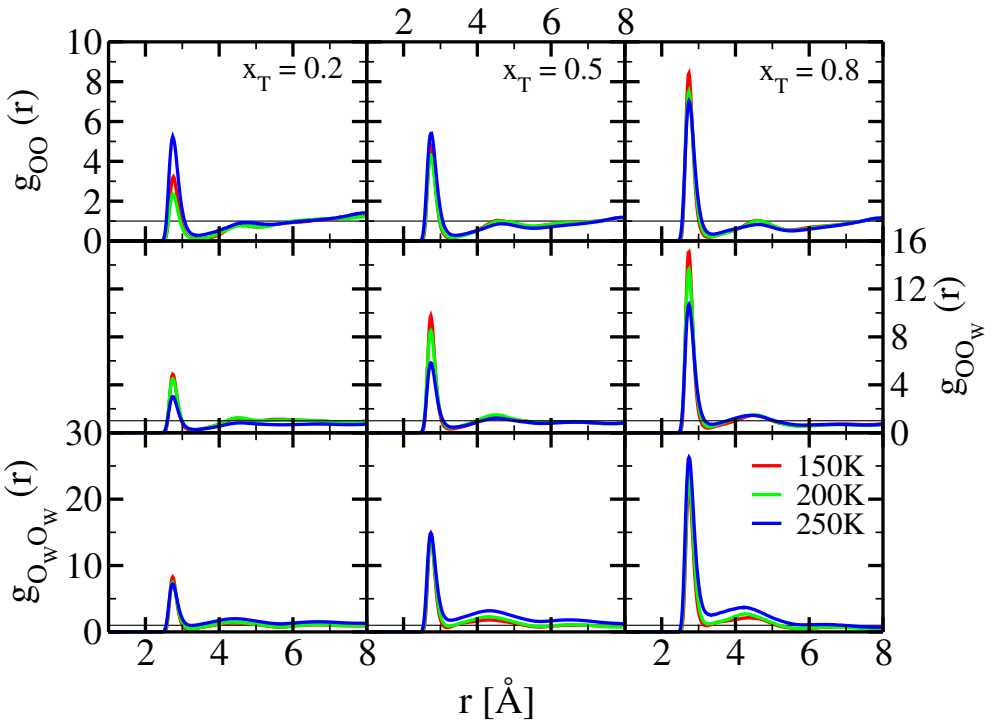

Figure 6.7.: Site-site correlation functions between the oxygen atoms of aqueous TBA mixtures, organized as in Figure 6.6.

at low temperatures. This trend was also noted by Ghosh and Bagchi [193], who presented results for the ethanol-water mixture at low temperatures and for low ethanol mole fractions.

Taken into account the behavior of methanol-water as well, we can conclude that the first peaks are always higher for water-water correlations than alcohol-alcohol. Also, the peaks are higher for the higher alcohol. Since all alcohols have the same partial charges on the hydroxyl sites, it's evident that the increase in the carbon united atom "cargo" the hydroxyl groups carry plays an important role in the organization of alcohols. In TBA, the neutral groups are the bulkiest and therefore introduce constraints which promote more Hbonding between the closest oxygen atoms.

The significance of the neutral groups can also be appreciated indirectly through the second neighbors correlations. Out of the three alcohols, the higher order neighbour correlations of TBA appear depleted, being lower than 1 for a large spatial range. The depletion of correlations beyond the first neighbors points to the lower oxygen Hbonding [74]. TBA's bulky non-polar part takes up more space in the mixture and hampers the organization of the second oxygen neighbors.

Water, due to bigger partial charges and hence stronger Coulomb interactions, will enforce its own bonding pattern first, leaving the alcohol to adjust. If, as in the case of TBA, the alcohol has a large neutral group, the hydroxyl group has an additional constraint which dictates the bonding.

6.2.2. Cluster probability distributions

The figures containing the cluster distribution probabilities are in Appendix B, Figure B.7, since the general trend of the results is the same as in Figure 6.3. As in the case of methanol-water, the alcohol cluster probabilities show very little temperature dependence. On the whole, water cluster probabilities show more change as the temperature decreases, which is, again, in line with the behavior water has in methanol-water. It also demonstrates indirectly the sensitivity to temperature of the water clustering. However, this present analysis confirms that cluster analysis is not the most adequate tool to study micro-segregation [74].

6.2.3. Structure factors

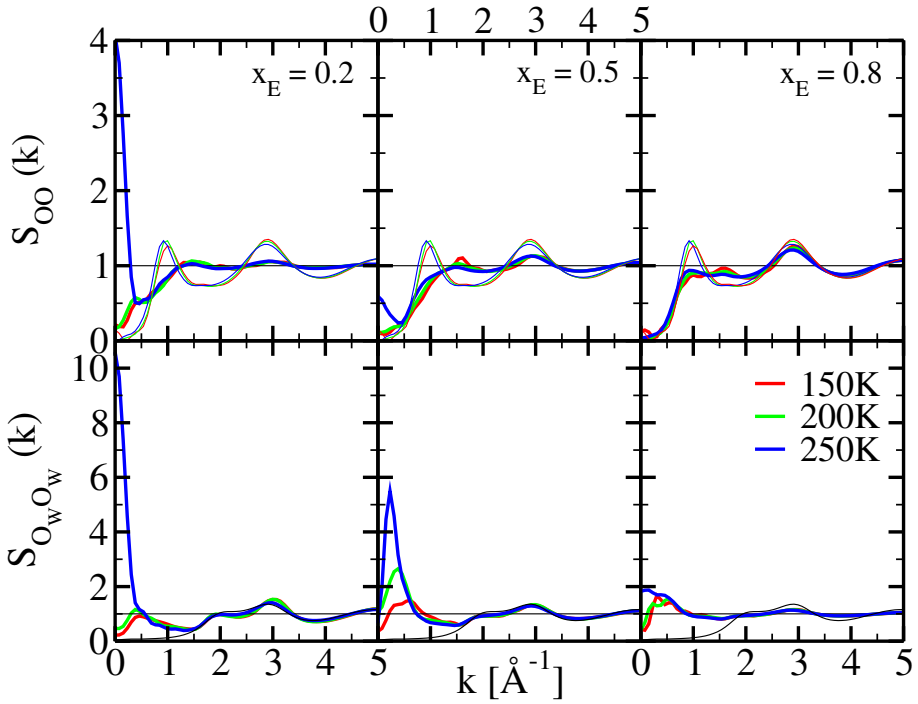

Figure 6.8.: Site-site structure factors of aqueous ethanol, calculated from the correlation functions in Figure 6.6 (cross structure factors not shown), with the same organization of rows, panels and temperature color codes. The thinner lines in the upper panel are oxygen-oxygen structure factors of neat ethanol, for same 3 temperatures. The thinner black line in the lower panel is for pure water at $T = 300$K.

The structure factors for aqueous ethanol and aqueous TBA are depicted in Figure 6.8 and Figure 6.9. The two important features seen in aqueous methanol (Figure 6.4) are present in these systems as well.

Firstly, there is a significant diminishing of concentration fluctuations. As the temperature decreases from $T = 250$ K to $T = 200$ K, the $k = 0$ part of the structure

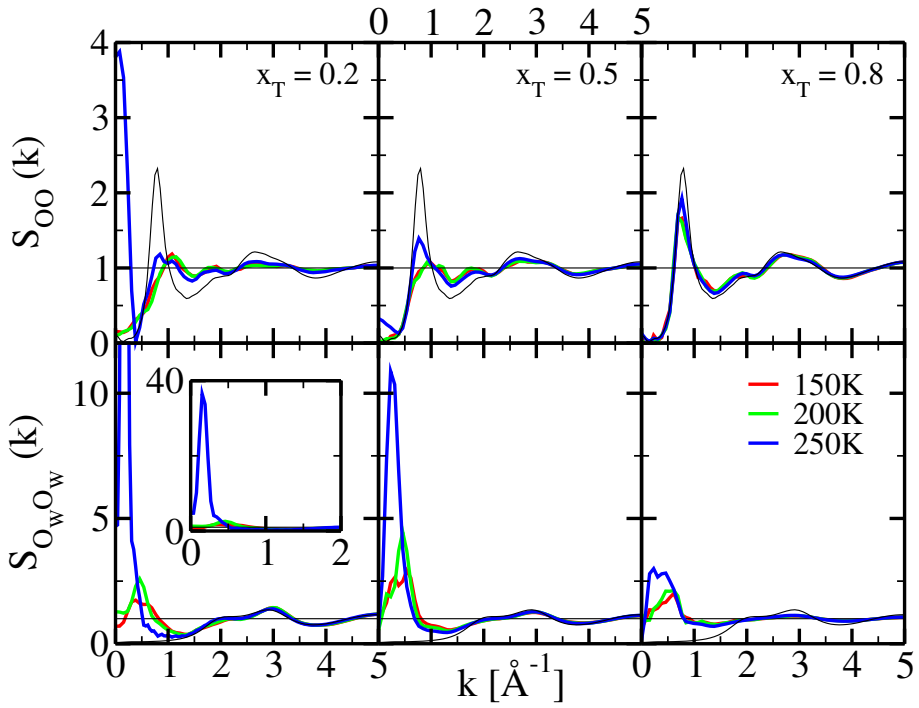

Figure 6.9.: Site-site structure factors of aqueous TBA, calculated from the correlation functions in Figure 6.7. The figure is organized as Figure 6.8.

factors is lowered for both water and ethanol oxygen atoms. That is especially visible for alcohol molar fraction of 0.2, but is also present for the other two concentrations.

Secondly, pre-peaks at small k values appear in the structure factors for both mixtures. The water structure factors (lower rows of Figure 6.8 and Figure 6.9) develop pre-peaks positioned at around $k_{\mathrm{P}} \approx 0.5$ - 0.9 Å^{-1}, which implies smaller domains than those present at ambient conditions ($k_{\mathrm{D}} \approx 0.05 - 0.1$Å^{-1}). The height of these pre-peaks varies substantially with the mole fraction of alcohol.

As for alcohol structure factors, the trends observed here are similar to those seen in Figure 6.4 for methanol. At low alcohol content (left panels of Figure 6.8 and Figure 6.9), the structure factors are flat and nearly structureless in comparison with the neat alcohol. As the alcohol content is increased, the structure factors acquire a structure similar to that of the neat alcohol. At $\mathrm{x_{ALC}} = 0.8$, TBA structure factors are almost identical as the neat TBA (thin black line in Figure 6.9). On a sidenote, the neat alcohol *S(k)* practically don't vary with temperature, as demonstrated for neat ethanol (plotted in thin lines in the upper panels of Figure 6.8).

However, there is one significant trend happening to both species with the drop in temperature: the transfer of fluctuations from $k = 0$ to k_{P}. This occurs naturally in neat alcohols, which are known to form specific clusters [153, 161, 170]. Another example where this happens are mixtures of two similar monools, which are considered to be close to thermodynamic ideality [159]. While a mixture of methanol and ethanol will have small CF, it will also have a rich cluster structure hidden beneath

thermodynamic ideality [73], thus illustrating perfectly the storing of fluctuations into supra-molecular entities.

Unlike alcohols, neat water at room temperature will have a diverse bonding pattern, since it's not inhibited by the neutral groups. Water's larger degrees of freedom of bonding will enable the molecules to form domains when a solute is added, thus increasing the $k = 0$ part of the structure factor. However, in the case of cold aqueous mixtures, water molecules seem to be forming linear clusters which lock the fluctuations, just like in alcohols. This explains the lower $S(k = 0)$ for water oxygens for x = 0.5 and x = 0.8. For those concentrations, water displays a pre-peak similar to that in neat alcohols. The likeness is glaring for TBA-water at $x_{ALC} = 0.8$, where the pre-peak located at $k_P \approx 0.8 - 1$ Å^{-1}(Figure 6.9, lower right panel).

6.2.4. Kirkwood-Buff integrals

Figure 6.10 and Figure 6.11 show the KBIs for two temperatures: 200 K (left panel) and 150 K (right panel). It is obvious that for both cases the KBI obtained in simulations (symbols) fall onto the calculated ideal KBI (dashed lines), similar as in aqueous methanol. This behavior is in stark contrast with the KBI of room temperature ethanol-water [26, 134] and TBA-water [134]. It may seem strange that mixtures with such strong directional interactions and consequential structuring display very little concentration fluctuations, but that just shows that concentration fluctuations should be analysed through their entire k-vector dependence.

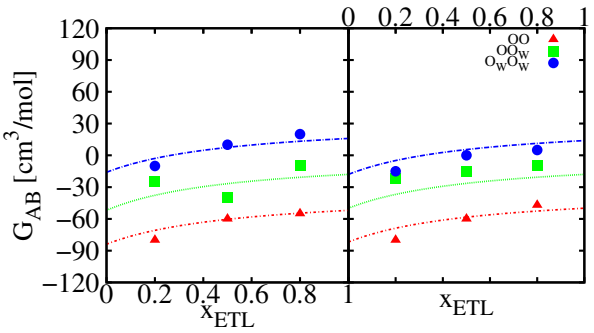

Figure 6.10.: Kirkwood-Buff integrals of the aqueous-ethanol mixture, depicted for two temperatures: 200 K (left panel) and 150 K (right panel). Color code is as follows: red for ethanol-ethanol, blue for water- water and green for the cross KBI. Symbols correspond to KBIs from present simulations, while dashed lines represent ideal KBI.

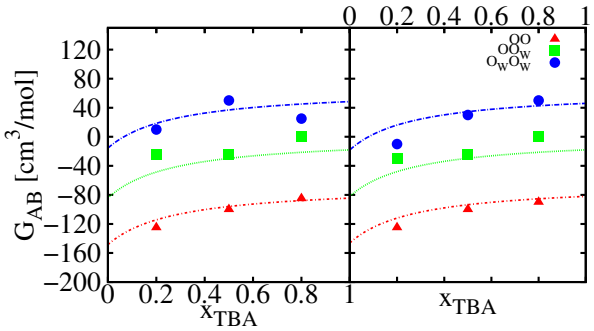

Figure 6.11.: Kirkwood-Buff integrals of the aqueous TBA mixture, depicted for two temperatures: 200 K (left panel) and 150 K (right panel). The figure is organized identically as Figure 6.10.

6.3. Conclusions

Three alcohols, differing only in their neutral groups, were mixed with water and simulated well below room temperature. All three mixtures have shown an appreciable decrease in CF with the lowering of temperature, apparent from the ideal behavior of the calculated KBIs.

The low temperature has decreased the thermal agitation in the mixtures, thus facilitating certain bonding choices. The fuzzy domains present in aqueous alcohol mixtures at $T = 300$ K have gradually transformed into sharper, more defined objects. That is especially evident in mixtures at high alcohol content, where we clearly see alcohol clusters interspersed with linear water clusters (most notably for TBA-water). While structuring in the form of chains is a hallmark of alcohols, it is quite unusual for water, due to its molecular topology and abundance of binding possibilities. However, the drop in the temperature has spurred water into forming linear clusters, resulting in a transfer of fluctuations from $k = 0$ to small k. That is in line with the calculated ideality of the KBIs. These mixtures demonstrate that it's possible to have both strong interactions in the system and ideal KBIs, simply because the entropic and enthalpic contributions cancel each other out.

These systems show, yet again, that fluctuations have to be analysed over the entire k range, and not only at $k = 0$.

7. The case of the aqueous propylamine mixture

Throughout the previous chapters, the spotlight was put on alcohols and their binary mixtures. The amphiphilic nature of alcohol enables it to mix with both water and non-polar solvents, displaying different types of structuring depending on the environment. However, alcohols are not the only group of amphiphilic molecules relevant in biological processes. Amines, organic compounds that contain nitrogen atoms, are a part of proteins and many vitamins and hormones [32]. This diverse group of compounds plays an important role in industrial [194, 195, 196] and pharmacological [197, 198] applications, yet the studies of structuring in neat amines and their binary mixtures are rather scarce. Unlike their alcohol counterparts, amine investigations are few and far in between. Kusalik et al. [199] have reported on methylamine and aqueous methylamine, while Lachet et al. [200] have studied a large variety of alkanolamines and their aqueous mixtures, proposing a new force field as well.

Monoalkylamines (primary amines connected to one alkyl chain) quite resemble mono-ols, albeit with one caveat. Their functional group is NH_2, which has two donors and one acceptor, instead of the one donor - one acceptor structure of OH hydroxyl group of linear alcohols. So far, we're acquainted with the behavior of neat mono-ols and their aqueous mixtures. However, we don't know if amines will behave according to the same blueprint. How will the difference in the amine functional group affect the Hbonding properties and therefore the micro-structure of neat amines and aqueous amine mixtures? What will be the behavior of the aqueous amine mixture in terms of concentration fluctuations and micro-heterogeneity? Does a small change in the functional group lead to small or significant changes in structuring in comparison with aqueous alcohol mixtures?

In the following chapter we focus on propylamine, a liquid monoalkylamine which is fully miscible with water [201]. Also, it is the first amine in the sequence which is liquid at ambient conditions, unlike methylamine and ethylamine which are gaseous (and not miscible with water in every proportion). Through the study of neat propylamine and its aqueous mixture we will shed light on the importance of the functional group in the shaping of the structural and thermodynamic features of the mixture.

Details about the modelling of neat propylamine, simulations performed and thermodynamic results can be found in Appendix A, while details about the aqueous

propylamine mixture are listed in Appendix B.

The work presented in this chapter has been the subject of one publication [77].

7.1. Neat propylamine

The left panel of Figure 7.1 shows a snapshot of the neat propylamine system, where the functional groups are shown in full color, while the carbon united atoms are transparent. One can observe chain-like structures built by the amino group in propylamine. However, the bonding pattern of propylamine is somewhat different than that of alcohols, as evidenced by the example of 1-propanol in the right panel of Figure 7.1. In the case of 1-propanol, the hydroxyl group forms distinct chain-like clusters; the amino group, on the other hand, allows for considerable branching and polydispersity, due to the double hydrogens on the nitrogen site.

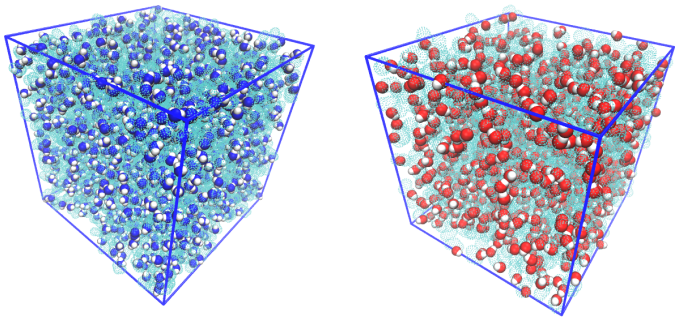

Figure 7.1.: Snapshots of neat propylamine (left panel) and 1-propanol (right panel). The functional groups are shown in full, with nitrogen being blue, hydrogen white and oxygen red. The carbon tails are transparent cyan.

This notion can be followed through quantifiable means, such as the cluster distribution probabilities (Figure 7.2). Once again, we look at the comparison of propylamine and its alcohol counterpart, 1-propanol. The cluster distributions of 1-propanol show a clear peak around cluster size of 4–6, which is a typical signature of alcohols that was discussed in previous chapters. In contrast, the cluster distribution of the nitrogen sites of propylamine have a rather weak shoulder about the same cluster size. Also, the occurrence of monomers is higher for propylamine than 1-propanol. Although these results may seem startling, they are just confirming the observation from Figure 7.1. Simple, linear chains will produce a characteristic mark in the cluster probability distribution. As soon as a functional group allows for choice of bonding, the end result will be branched chains, which tend to blur

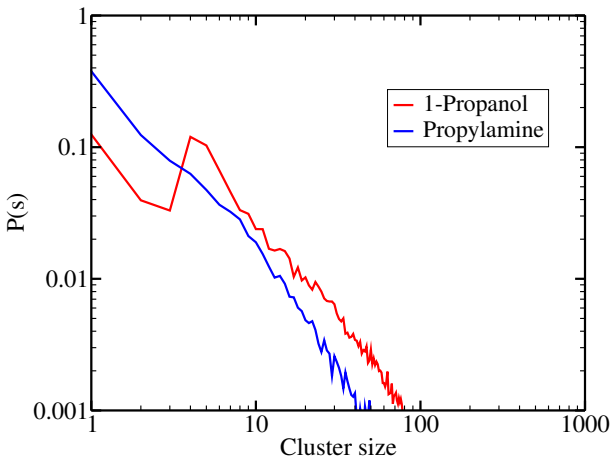

Figure 7.2.: Cluster distribution probabillities for the nitrogen atoms of propylamine (blue line) and the oxygen atoms of 1-propanol (red line).

the distribution of aggregated atoms and produce a weak broadened feature instead. This finding also leans onto the discussion in the previous chapter regarding cluster probability calculations. It seems like cluster distributions are not the best tools for cases with extensive branching in the system.

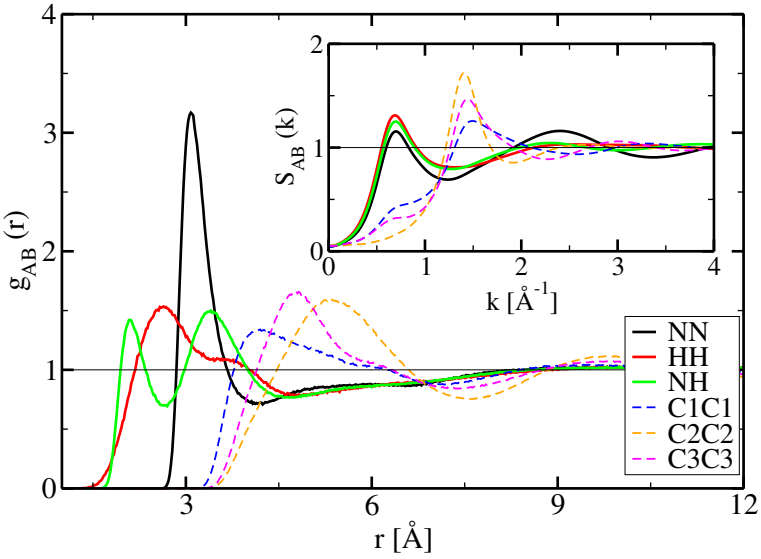

Figure 7.3.: Main panel: pair correlation functions of selected site-site combinations in neat propylamine, with the color code contained in the legend. Inset: Site-site structure factors calculated from the g(r)s from the main panel, with the same color code.

For that reason, we turn to the analysis of correlation functions and site-site structure factors. The side-by-side comparison with 1-propanol is not directly included here, as the 1-propanol data is shown in Appendix A. Figure 7.3 shows the various pair correlation functions of neat propylamine in the main panel. The correlations stemming from the functional group are depicted in thick lines; the ones from car-

bon united atoms are dashed. The NN correlation function has a high and narrow first peak, characteristic of hydrogen bonding liquids, which is in line with the behavior of neat alcohols [124, 125]. The HH correlations, however, are smaller and broader than in neat alcohols, with the first peak positioned at roughly $r = 2.5$ Å and a shoulder at $r = 4$ Å. Both features are a consequence of having two hydrogen atoms attached to the nitrogen. Furtermore, the NH correlations are significantly lower than NN correlations and are split into two peaks. The first peak corresponds to direct NH bonding while the second one is due to the existence of the second hydrogen on a fixed distance from the first hydrogen. As expected, the correlation functions of carbon sites are similar to those seen in alcohols (Figure A.4, and also [124, 125]).

The inset of Figure 7.3 contains the site-site structure factors of corresponding correlation functions. It's immediately evident that the Hbonding site combinations - NN, NH and HH - all possess cluster peaks located at $k \approx 0.65$ Å^{-1} and of a similar intensity. This would correspond to a structure of approximately 10 Å, confirming the existence of Hbonded clusters observed in the snapshot. Apart from the cluster peak, these structure factors have a main peak, centered about $k \approx 2.5$ Å^{-1}, which corresponds to the Hbonding distance of $r_{HB} = 2$ Å. In contrast, the carbon sites' structure factors display main peaks at $k \approx 1.4$ Å^{-1}, which correspond to the mean diameter of the site.

As for 1-propanol, the OO structure factor (Figure A.7) has a higher pre-peak than the NN in propylamine. This indicates that for the same number and same topology of the methyl sites, the hydrogen bonding difference between straight and branched chains tends to weaken the pre-peak of branched chains.

This analysis shows that correlations, both in direct and reciprocal space, can describe an Hbonding cluster structure which may be elusive to other types of calculations. Despite the same origin of the cluster structures in alcohols and amines, differences arise from the two donor hydrogen sites the amino group possesses.

7.2. Aqueous propylamine

After the study of neat propylamine, we tackle its mixture with water. For the sake of simplicity, the snapshots that will be presented are of the 2k system, while all the other data in subsequent images is calculated from the 16k system.

7.2.1. Snapshots

Figure 7.4 shows three configurations of propylamine water mixtures, for three different amine mole fractions: $x_P = 0.2$ (left panel), 0.5 (middle panel) and 0.8 (right panel). The structural evolution of the mixture with concentration is very graphic.

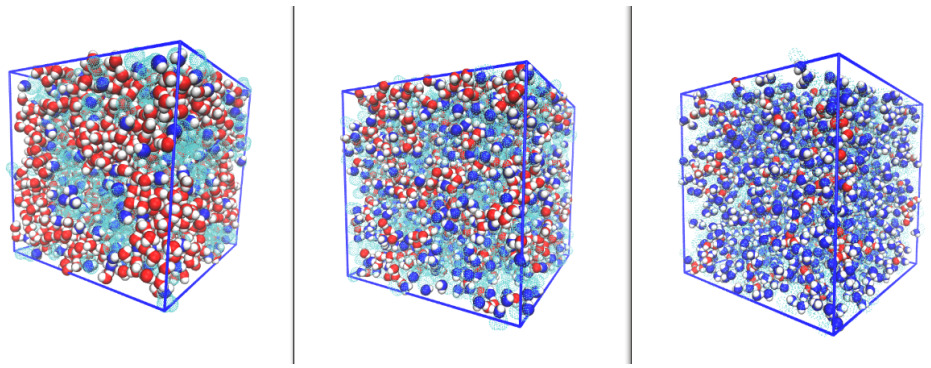

Figure 7.4.: Snapshots of three typical mole fractions of propylamine: $x_P = 0.2$ (left panel), 0.5 (middle panel) and 0.8 (right panel). Water molecules are depicted in red and white (for oxygen and hydrogen sites, respectively), propylamine's amino group in blue and white (for nitrogen and hydrogen), while propylamine's non-polar tail is in transparent cyan.

At low amine content, the propylamine molecules have formed domains in which the hydophobic tails are grouped together in the core of the domain, while the amine functional groups act as a sort of interface with the surrounding water molecules. Amine domains, albeit smaller, are also present at $x_P = 0.5$, and at this concentration, the water domains appear like rows of chains. At x_P =0.8, branched chains formed by the amine groups dominate the mixture, with a number of water molecules integrated in their chains. Also, water molecules among themselves form linear clusters. The latter is a significant departure from what was observed in the case of aqueous alcohol mixtures, hinting at the importance of the chemical makeup of the functional group of the molecule.

7.2.2. Cluster probability distributions

Figure 7.5 shows the cluster probability distribution for propylamine sites (left panel) and oxygens of water (right panel). The general trends resemble those in aqueous ethanol, shown in the previous chapter. As soon as water is added to propylamine, the nitrogen cluster distribution loses its weak shoulder and becomes a decaying function similar to that of ethanol's oxygen in aqueous ethanol. As the mole fraction of propylamine decreases, the probability of monomers increases, while the cluster size lessens.

The cluster distribution of the carbon united atom (calculated for the last methyl group in the chain, the farthest away from the functional group) for neat propylamine shows a Lennard-Jones type of behavior. As propylamine is rarified, the cluster distributions show a decrease in the cluster size, as well as a lessened probability of those clusters occuring. At $x_P = 0.2$, there is a small, yet observable probability of larger clusters formation, which is more than what was seen in the cluster probability distribution of ethanol's methyl group (previous chapter).

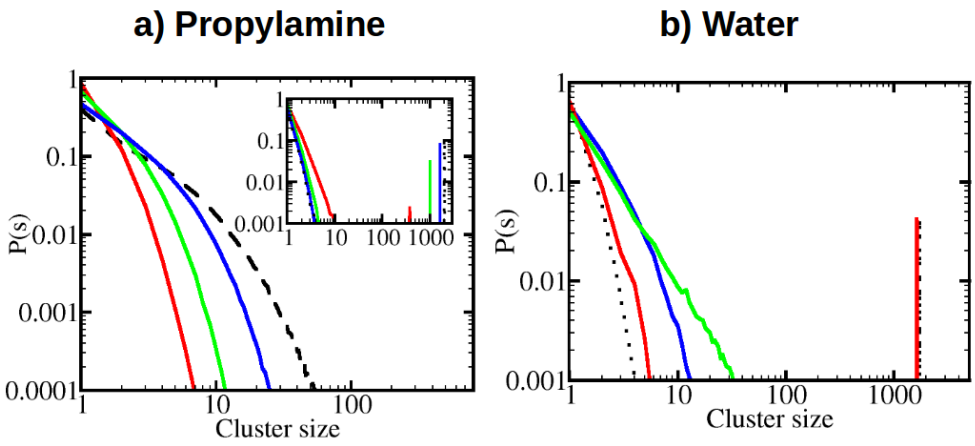

Figure 7.5.: Cluster probability distributions for: a) propylamine NN sites (main panel) and CC sites (inset), b) water OO sites. The color code is the following: $x_P = 0.2$ (red), $x_P = 0.5$ (green) and $x_P = 0.8$ (blue). Black lines represent the data for the neat compound (dashed for propylamine and dotted for water).

The cluster probability distributions for the water oxygens show functions characteristic for simple mixtures. At first glance, the behavior of water oxygens in aqueous propylamine is similar to that in aqueous ethanol. However, there is a subtle difference for the equimolar mixture. In aqueous ethanol, there is a considerable probability for the occurance of large water clusters (cluster size around 1000 sites), while in aqueous propylamine the same distribution has the lowest probability of larger clusters (cluster size considerably less than 100 sites). This finding may indicate the lack of globular water domains seen in the snapshots.

7.2.3. Pair correlation functions

Figure 7.6 shows the most representative correlation functions of the aqueous propylamine mixture, for the typical amine mole fractions $x_P = 0.1$, 0.2, 0.5 and 0.8. The left panel shows the NN correlations, where the first peak decreases as the amine mole fraction decreases. This is the same behavior pattern shown by alcohols when mixed with water. However, there are differences between alcohol OO and amine NN correlations, for we see that NN correlation functions are very small and depleted at contact for $x_P = 0.1$ and 0.2. This hints at the fact that, at small amine concentrations, propylamine molecules tend to Hbond with water rather than with themselves. Indeed, this is confirmed when assessing the middle panel of Figure 7.6, where the cross correlations between propylamine and water are presented. For all amine mole fractions, NO_w correlations are significantly higher than NN correlations. Also, the first peak decreases as the amine concentration decreases. However, these correlations are depleted beyond second neighbours, hinting at the short ranged correlations between opposite species. The evolution of the cross correlation functions indicates that, when amines are in the majority, water has a high likelihood

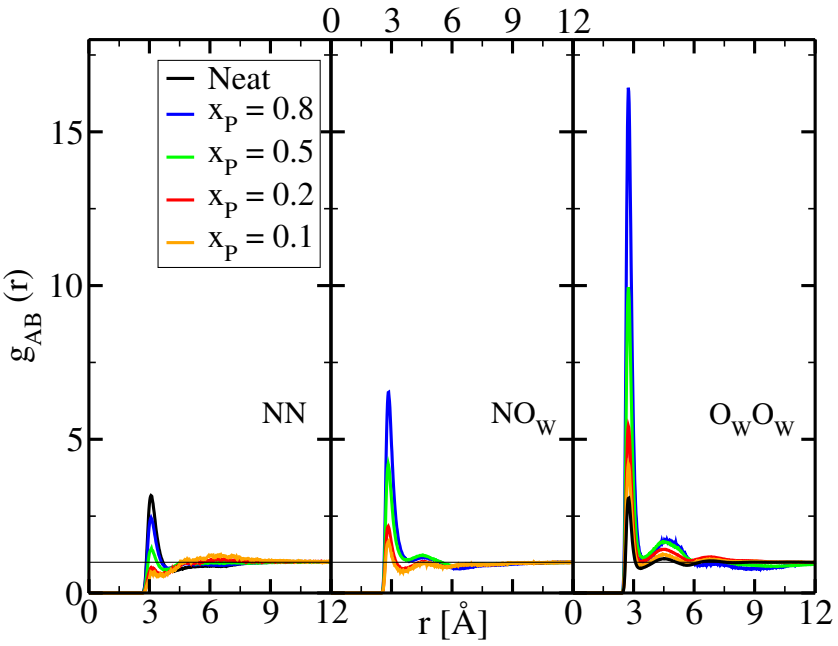

Figure 7.6.: Pair correlation function for aqueous propylamine. Propylamine's NN correlations are featured in the left panel, the cross NO_w correlations in the middle panel, and water's O_wO_w correlations are in the right panel. The color code is contained in the legend of the Figure.

of forming hydrogen bonds with the surrounding amines, which aligns well with the snapshots in Figure 7.4.

The O_wO_w correlation functions, shown in the right panel of Figure 7.6, display the typical water behavior seen in many aqueous mixtures. The first and second neighbour correlations increase with decreasing water content, and they are much higher than cross or NN correlations, revealing once again the preference water has for bonding with itself, even when it's in the minority. Yet, there is an interesting feature not observed in other aqueous systems - a shallow minimum beyond the third neighbour correlations. This feature makes sense given that water doesn't seem to form bulky, globular domains when mixed with propylamine. Instead, it forms chains with appreciable cross binding, as seen for $x_P = 0.8$ in Figure 7.4, which result in such a noticeable depletion in the correlation function, especially visible for $x_P = 0.8$.

7.2.4. Structure factors

Site-site structure factors, calculated from the pair correlation functions in Figure 7.6, are displayed in Figure 7.7. The left panel shows the NN structure factors and their evolution with the change in molar fraction of propylamine. It's seen that the main peak gradually decreases as the propylamine content decreases, almost flattening for

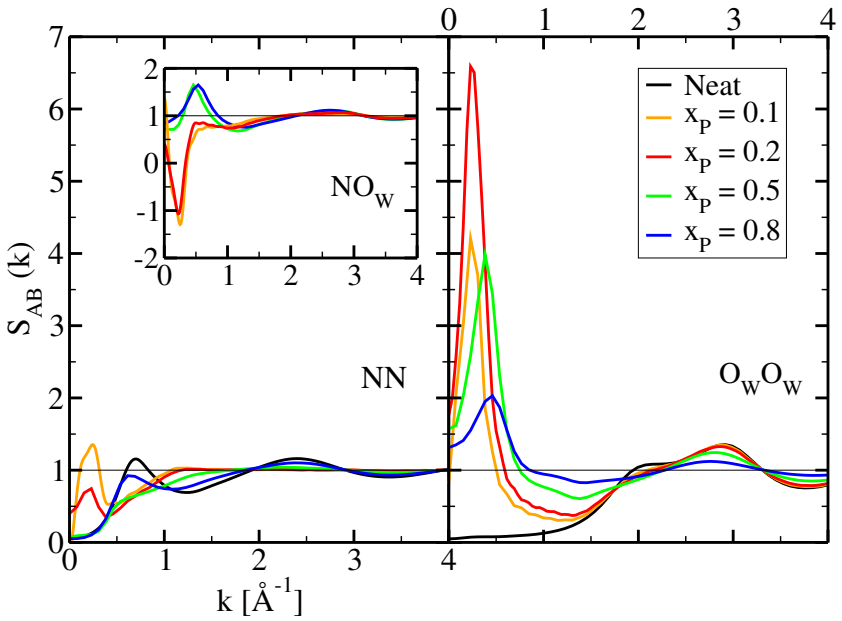

Figure 7.7.: Site-site structure factors calculated from the pair correlation functions from Figure 7.6. The NN structure factors are shown in the left panel, while the O_wO_w are in the right panel. The inset in the left panel contains the cross structure factors. The color code is contained in the legend of the Figure.

$x_P = 0.2$ and 0.1, which is to be expected from the information given by the pair correlation functions. The behavior of the features at small k values is much more interesting. The cluster peak of neat propylamine starts diminishing as soon as water is added. While the cluster peak still persists at $x_P = 0.8$, it wanes at $x_P = 0.5$ - the same concentration where a kernel of a domain pre-peak is observed. This domain pre-peak is prominent for $x_P = 0.2$ and especially $x_P = 0.1$. This pattern of different pre-peaks is indicative of the inner structural changes going on in the mixture. At high amine content, the predominant structural organization are branched chains formed by the amine group, while at low amine content, the propylamine molecules gather in domains. In these domains, the alkyl tails are grouped together towards the center of the domain, while the amino functional groups form a kind of interface with water (a pictorial representation is in Figure 7.4). This type of behavior was already observed in the case of ethanol-water, described in the previous chapter.

The right panel of Figure 7.7 contains the O_wO_w structure factors. For all concentrations, the site-site structure factors show a pre-peak feature, which is absent for neat water (black line in Figure 7.7). At $x_P = 0.1$ and 0.2, the domain pre-peak is located at $k \approx 0.25$ Å^{-1}, corresponding to domains of roughly 25 Å. As more propylamine is added, the domain pre-peak of water shifts to the right, falling at $k \approx 0.5$ Å^{-1} for both $x_P = 0.5$ and 0.8. The evolution of the pre-peak aligns well with the more bulky water domains observed for low amine content (Figure 7.4, left panel) and the linear water clusters when propylamine is in the majority (Figure 7.4, right panel). It's interesting to notice that the domain pre-peaks in water structure factors

are more intense than those of propylamine. Also, the trend in pre-peak intensity varies with concentration, with the pre-peak at $x_P = 0.2$ being the most intense.

As for the main peak, which in neat water has the split peak feature [179], we note that the outer peak disappears for every amine mole fraction. Only the inner Hbond peak at $k \approx 3$ Å^{-1} (corresponding to $r_{HB} \approx 2$ Å) survives, although it decreases with amine content increase.

Finally, the inset in Figure 7.7 shows the NO_wstructure factors, which are seen to have both positive and negative pre-peaks, depending on the concentration. At high and intermedate amine content there are positive pre-peaks, which is not surprising considering the type of structuring the same species exhibit and the number cross correlations between the species. At $x_P = 0.2$ and 0.1 we have anti-pre-peaks. This negative pre-peak has been reported before for cases of room temperature ionic liquids [202, 203], where it's typical of domain segregation. In the context of aqueous propylamine, it's clear that water and propylamine form same-species domains with comparably less cross-species contact at long range, which produces this negative pre-peak feature.

7.2.5. Kirkwood-Buff integrals

So far, the aqueous propylamine mixture has shown interesting structural features which have lots of commonalities with the aqueous ethanol mixture. Therefore, one might expect high KBI values that vary strongly with concentration, a hallmark of aqueous alcohol mixtures [26]. However, Figure 7.8, which contains the KBIs calculated from the simulations, tells a different tale. The KBI values are quite small in magnitude and, when compared to the computed ideal KBIs (dashed lines), nearly ideal in the range $0.3 < x < 1$. This implies that the concentration fluctuations are small in this range of concentrations, which makes sense considering the chain-like structuring observed for both propylamine and water. This behavior of KBIs is also reminiscent of another water mixture: aqueous dimethylsulfoxide (DMSO), which also has close to ideal KBIs [26]. Looking into the microstructure of water-DMSO one finds chain-like water clusters at high DMSO content [34], hinting at the ability of linear clusters to lower the concentration fluctuations.

Water specific interactions are strongest in the range $0 < x < 0.3$, as seen from the non-ideal KBI. As for propylamine KBIs, they are also non-ideal in that mole fraction range. When the *D(x)* is calculated to fit that KBI trend, one obtains the function in the inset of Figure 7.8. This *D(x)* has a maximum at $x_P \approx 0.15$, which is flanked by two concentrations, $x_P = 0.1$ and 0.2, which have signatures of bulky domains in the site-site structure factors.

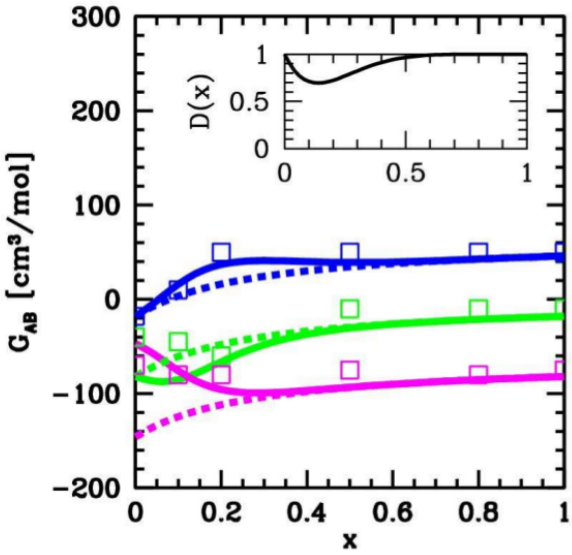

Figure 7.8.: Kirkwood-Buff integrals for aqueous propylamine, with respect to the mole fraction of propylamine. The species are colored as follows: blue for water-water, magenta for propylamine-propylamine and green for the cross KBI. Open squares are the KBI calculated from the present simulations, dashed lines represent the ideal KBIs, while full lines correspond to the KBIs calculated with the D-coefficient shown in the inset.

7.3. Conclusions

The study of neat and aqueous propylamine has introduced interesting new findings in the puzzle of microheterogeneity. Since propylamine is an amphiphilic compound, one has expected it to share common structuring traits with mono-ols. However, the introduction of a different functional group, with two donors and one acceptor, has increased the binding possibilites of the NH_2 group. In neat propylamine, this results in branched chains, as opposed to linear chains in alcohols. These branched chains are difficult to observe via cluster calculations. However, the site-site structure factors of the amine functional group reveal cluster pre-peaks, albeit of a lesser intensity than those of the hydroxyl group in 1-propanol, pointing to the existence of branched chains.

The propylamine-water mixture has several features in common with aqueous alcohols. The trends in short-range behavior are similar, with water pair correlation functions increasing as the water content decreases, while it's the opposite for propylamine. This is typical of aqueous mixtures and occurs in aqueous alcohols as well. In terms of long range behavior, the evolution of propylamine's structure factors with concentration mirrors that of ethanol's structure factors. Both compounds transition from a chain-like cluster structuring at high concentrations to domain formation at low concentrations. Their respective site-site structure factors witness the decrease of the cluster pre-peak as more water is added, and the emergence of a

domain pre-peak when water is in the majority.

However, the behavior of water in the amine mixture breaks the mold. Up to $x_P = 0.3$, water forms bulky domains, similar to those we have observed in aqueous alcohols, which are marked by a prominent domain pre-peak in the oxygen-oxygen structure factor. After $x_P = 0.3$, water forms linear clusters, similar to those in aqueous DMSO [34], and leading to smaller structure factor pre-peaks and near ideal KBI. The lowering of the concentration fluctuations brought on by the formation of linear chains is an interesting feature that illustrates the plasticity of water.

8. The microstructure of neat 1,n-diols and their mixtures

Up to this point, a good portion of the research in our group was focused on small alcohols which are fully miscible in water and alkanes. The alcohols in question were mono-ols, alcohol compounds containing one hydroxyl group [32]. However, these are not the only alcohols occurring in nature. Alcohols have diversified into sub-categories depending on the number of attached functional groups. Compounds with two hydroxyl groups are called diols, while those with three hydroxyl groups are called triols [32]. These two families have a wide range of application purposes. For example, 1,2-ethanediol or ethylene glycol is the major component of antifreeze [204] and the precursor for synthetizing PET fibers [205]. 1,2,3- propanetriol or glycerol is a staple of the cosmetic industry and is used as an additive in the food industry [206]. Glycerol is also the basis for the synthesis of triacylglycerols and phospholipids, thus having biological importance.

In comparison with mono-ols, additional hydroxyl groups in diols and triols should complexify the structural landscape of aqueous mixtures, as is hinted by experiments. In a series of experimental papers, Teixeira and D'Arrigo have investigated aqueous mixtures of such complex co-solvent surfactant, with the use of neutron scattering techniques, in order to interpret the various presence and absence of domain pre-peaks as a function of the complexification of the alcohols [207, 208, 209]. However, the alcohols studied by D'Arrigo et al. would represent a big leap in the level of complexity when considering the compounds we have dealt with in the previous chapters. In computer simulations, the main problem is to find reliable force fields for such complex alcohols. Transferability works only for small molecules and it's usually necessary to improve the force field parameters when modelling more complex compounds [200].

For that reason, we will explore a model which is rather well confirmed before we tackle something similar to the work of D'Arrigo et al., staying in the realm of short diols. That way, one is able to make points of reference with the previous work on small mono-ols and their mixtures.

However, this now poses another question, and that is the placement of the second hydroxyl group in diols. This position can vary from close to the first hydroxyl group, leading to 1,2-diols, all the way to positioning it at the other end, leading to 1,n-diols (Figure 8.1). A point can be made that 1,2-diols will share similar behaviors with mono-ols, as the hydroxyl groups are concentrated on one side of the

molecule and the alykl tail is somewhat free. On the other hand, 1,n-diols present a particular interest, since the two hydroxyl groups are attached to an alkyl chain in between. What is the role of the alkyl chain, and how does it affect the clustering properties of the neat 1,n-diols?

This question is addressed in the first part of this chapter, which describes the underlining micro-structure of 1,n-diols, particularly in comparison to neat mono-ols. The present work has revealed an important finding: the calculated scattering intensities, obtained from simulation results, show no no pronounced pre-peak. This is in variance with mono-ols, which are known to exhibit pre-peaks in scattering intensities [153, 155, 161, 162, 169, 170, 171, 172]. A subsequent experimental paper from Tomšič et al. [210] has confirmed our prediction.

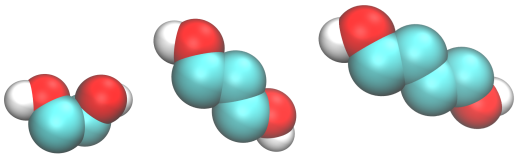

Figure 8.1.: Graphic depiction of 1,n-diol models: 1,2-ethanediol (left), 1,3-propanediol (center) and 1,4-butanediol (right panel). The atom colors correspond to the following elements: cyan - carbon, red - oxygen and white - hydrogen. The molecules are shown for demonstrative purposes only, for they are not in the exact proportions with one another.

In the second part of this chapter we study mixtures of 1,n-diols. Once again, the principal idea is to ascertain how does the constraint in the form of an alkyl tail influence the organization in these mixtures. For that reason, we mix 1,n-diols with water and ethanol, respectively. Since we're already acquainted with the ordering present in water-ethanol mixtures and its signatures, we can observe the differences in mixtures with diols and draw parallels.

Without much surprise, we find that 1,n-diols mix rather well with either water or ethanol and do not form segregated domains. However, this apparent structural homogeneity contains a twist, which is visible through the shape of the structure factors near $k = 0$. These mixtures have neither high CF nor domain pre-peaks in their site-site structure factors, and generally appear as to be borderline to a clustering system. This represents a new form of disorder which we call the Lifshitz state. Its name is inspired by the Lifshitz point in field theory [211], which separates a disordered phase from two types of ordered phases. This point represents the continuous transition between the disordered and the ordered phase [211]. However, the Lifshitz point is not permanent, for it can be reached by moving through the phase diagram. In contrast, the Lifshitz state is a permanent physical state, where the system is stuck in a disorder without clustering.

It may be worth mentioning that the Lifshitz points can take on a more elaborate interpretation in micro-emulsion studies from a theoretical point of view, with the Lifshitz points being analogous to spinodal points at $k \neq 0$.

The work presented in this chapter has been the subject of two separate publications [78, 79]. The study of neat 1,n-diols has also been featured on a poster for the Liquid Matter Conference (July 2017), while the results for the 1,n-diol mixtures were presented as a poster for the Joint EMLG/JMLG Annual Meeting (September 2017).

8.1. Neat 1,n-diols

As mentioned in the introduction, this section will deal with the structural properties of 1,2-ethanediol (ethylene glycol) and 1,4-butanediol, in comparison with methanol and ethanol, respectively. Not only are methanol and ethanol the first two alcohols in the series, but "combining" two methanols (or ethanols) would yield ethanediol (or butanediol).

Results for 1,3-propanediol and 1,5-pentanediol are not shown in their entirety. The most notable result - the calculated scattering intensity - is reported for all four diols. The simulation details for the neat species can be found in Appendix A.

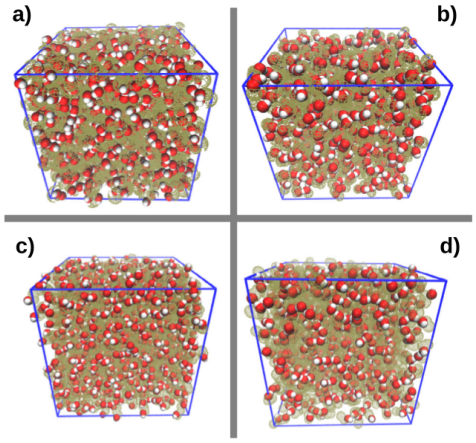

Figure 8.2.: Snapshots: (a) ethanediol, (b) methanol, (c) butanediol, (d) ethanol. Oxygen atom is shown in red, hydrogen in white and methyl and methylene united atoms as semi- transparent tan.

Figure 8.2 shows snapshots of the ethanediol and methanol (upper row) and butanediol and ethanol (lower row). The characteristic pattern of chains formed by hydroxyl groups is present in all alcohols and is especially prominent for ethanol and butanediol. However, ethanediol seems to have less chains and these tend to be shorter than in methanol. Also, ethanediol has a new feature, previously unseen in

alcohols: there are a few chains aligned next to each other. That feature is already a sign of the important role the alkyl chain plays in diols, and is visible precisely because of ethanediol's short, two-methylene group chain.

Although not shown here, propanediol and pentanediol show chain behaviour similar to butandiol, with a more pronounced chaining for pentanediol.

8.1.1. Cluster distribution probabilities

To quantify the visual findings in Figure Figure 8.2, we performed the the cluster probability distribution analysis for neat 1,n-diols. The main panel of Figure Figure 8.3 displays the cluster probability distributions of the hydroxyl oxygen atoms, for 1,2-ethanediol, 1,4-butanediol and their mono-ol counterparts. It's known that methanol and ethanol oxygen distributions have a cluster peak which corresponds to cluster sizes from 4-6 [124, 125], and we notice that the cluster distribution in butanediol is similar to that of the mono-ols. But, the probability of monomer occurence is smaller in butanediol than in the mono-ols, which infers that hydroxyl groups are less free in butandiol than in the mono-ols. This is somewhat counter-intuitive, since we expect that the constraint imposed by the alkyl chain would leave more hydroxyl groups free. Yet, we observe that there are more bound hydroxyl groups in diols than in the mono-ols. This is also true for propanediol and pentanediol (inset), which both show the cluster peak corresponding to the observed chaining of the hydroxyl groups.

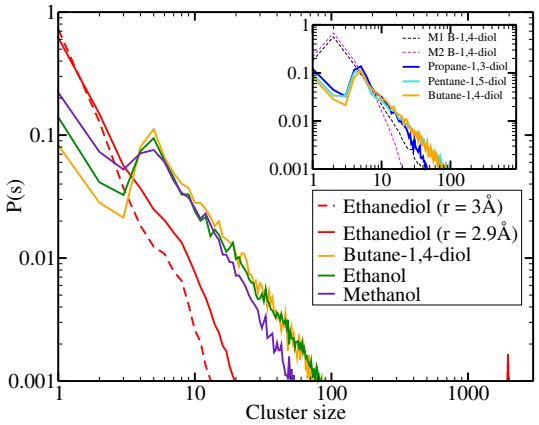

Figure 8.3.: Cluster probability P(s) versus cluster size s. The cutoff parameter is taken to be r = 3.6 Å, except for ethanediol for which r = 3 Å and r = 2.9 Å are reported in dashed and full red lines. Main panel shows a comparison between mono-ols and diols. The inset shows higher diol oxygen distrubutions (full lines) and distribution of the methylene sites (M1 and M2) for butanediol.

The results for ethanediol contrast those of the other alcohols. Instead of a distinct peak, there is a shoulder in the cluster distribution. This can be rationalized in

terms of the constraint imposed by the alkyl chain: the number of free hydroxyl monomers is indeed larger than for the other alcohols.

As for the methyl/methylene groups of diols, they have a monotonously decaying cluster distribution (dashed lines in the inset of Figure Figure 8.3), the same as in mono-ols. Since these groups go in pairs in each molecules, the monomer distribution is slightly lower than the dimers. This overall monotonous cluster distribution implies that, despite the constraint of being tied to the clustered hydroxyl groups, these non-polar groups are essentially randomly distributed.

8.1.2. Pair correlation functions

Figure 8.4 shows the pair correlation functions for ethanediol (left panel) and methanol (right panel). As expected, the oxygen and hydrogen pair correlations of ethanediol have the typical sharp and narrow first peak, followed by depleted pair correlations of the nearest next neighbours. This depletion has been observed in neat mono-ols before [124, 125], and it's connected to the charge distribution and topological setup of the whole molecule. The hydroxyl group in alcohols contains point charges of positive and negative sign, whose preference in structuring would be somewhat resemblant of charge ordering. Charge ordering refers to distributions of alternating positive and negative charges, most characteristic for ionic liquids [212]. However, alcohols also contain a neutral group attached to the hydroxyl group, which obstructs the otherwise isotropic distribution of plus and minus charges. Due to the constraint of the neutral "cargo", the plus and minus charges in the OH group associate into chains, producing the characteristic increase in the first neighbors and depletion in the second neighbors. This type of correlation function will produce a pre-peak in its corresponding structure factor [34].

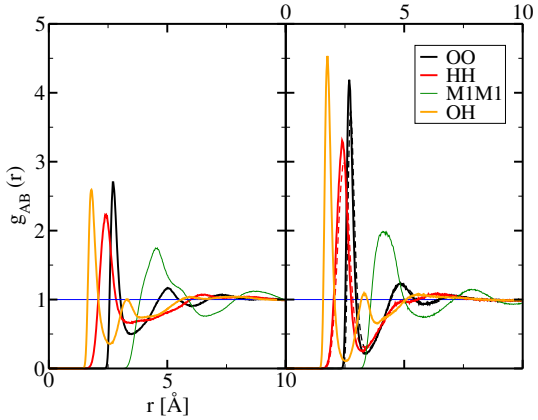

Figure 8.4.: Site-site pair correlation functions for ethanediol (left panel) and methanol (right panel). The species are described in the legend. The dashed lines in the right panel represent methanol modeled with another forcefield (OPLS-UA).

The main difference between these two alcohols is the height of the first peaks, and perhaps a more marked depletion in the case of second neighbors. Both are a signature of the constraint ethanediol's alkyl chain imposes. As expected, for both alcohols, the carbon group pair correlations behave in an LJ-like fashion.

Figure 8.5 presents the pair correlation for butanediol (left panel) and ethanol (right panel). The main features of the correlation functions follow the trends of those in Figure 8.4. However, the first peaks of the Hbonding species are higher than in the respective previous cases and the depletion is quite similar, hinting at the more pronounced chaining action. Also, the correlations of the mono-ol are higher than that of the diol. Another interesting observation concerns the alcohols' neutral groups. The correlation functions of ethanol's carbon groups are aligned, with their first peaks located at ~5 Å. In the case of butanediol, the corresponding correlation functions are out of phase - their first peaks are separated by roughly 1 Å. This is another indicator of the importance of the carbon chain in diols, and it will have interesting implications when considering the following data.

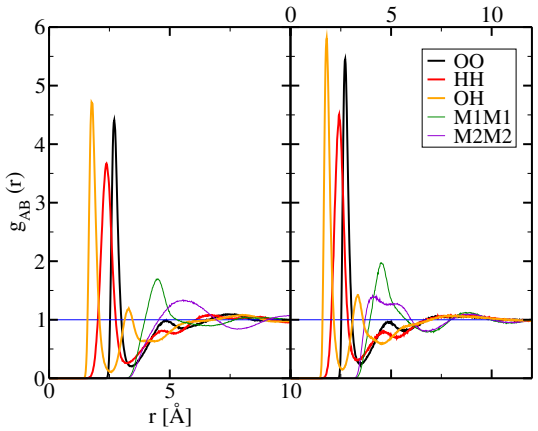

Figure 8.5.: Site-site pair correlation functions for butanediol (left panel) and ethanol (right panel).

8.1.3. Structure factors

Figure 8.6 shows the site-site structure factors obtained from the pair correlation functions from Figure 8.4. Both alcohols have a pre-peak at $k_P \approx 1$ Å^{-1} occuring in their Hbonding species' structure factors, while their carbon structure factors only have a main peak located at $k_M \approx 1.8$ Å^{-1}. So far, we've shown that diols have the characteristic features observed in mono-ols. However, the pre-peak is more pronounced for methanol than for ethanediol, and both alcohols share the particular double-peak shape of the $S_{OO}(k)$, which stems from the contributions of $S_{OH}(k)$ and $S_{MM}(k)$. The $S_{OO}(k)$ of ethanediol, obtained from neutron scattering, shows the same position of the pre-peak and a similar function shape [213].

The structure factors of butanediol and ethanol in Figure 8.7 correspond to their correlation functions from Figure 8.5. The pre-peak is much more prominent than in the case of ethanediol and methanol, indicating more pronounced clusters and and confirming general trends deduced from previous analysis. Once again, it's important to notice the trends in the carbon-carbon structure factors - for butanediol, they are out of phase, while for ethanol they are in phase.

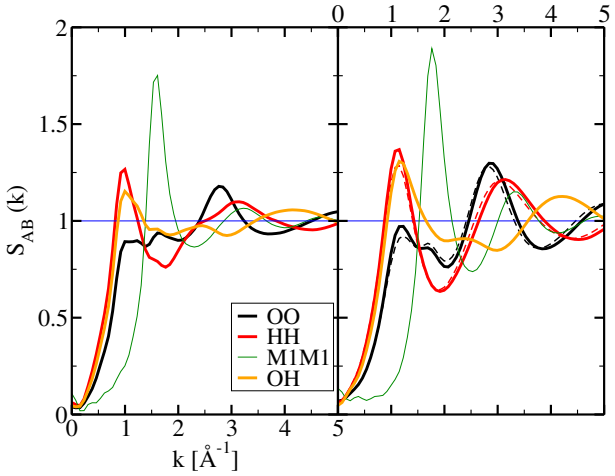

Figure 8.6.: Site-site structure factors corresponding to the pair correlations shown in Figure 8.4 for ethanediol (left panel) and methanol (right panel).

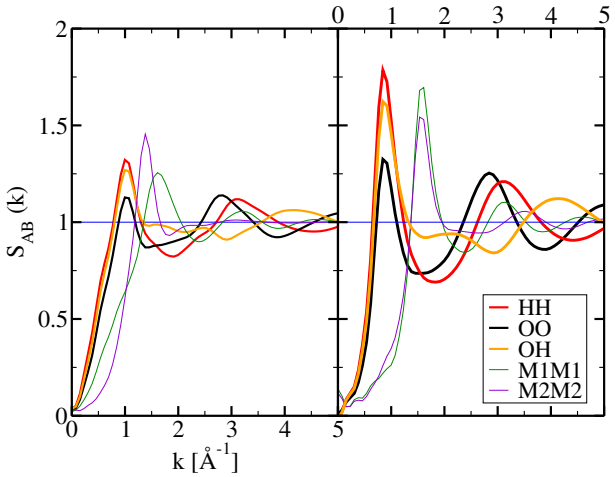

Figure 8.7.: Site-site structure factors corresponding to the pair correlations shown in Figure 8.5 for butanediol (left panel) and ethanol (right panel).

8.1.4. Scattering intensity

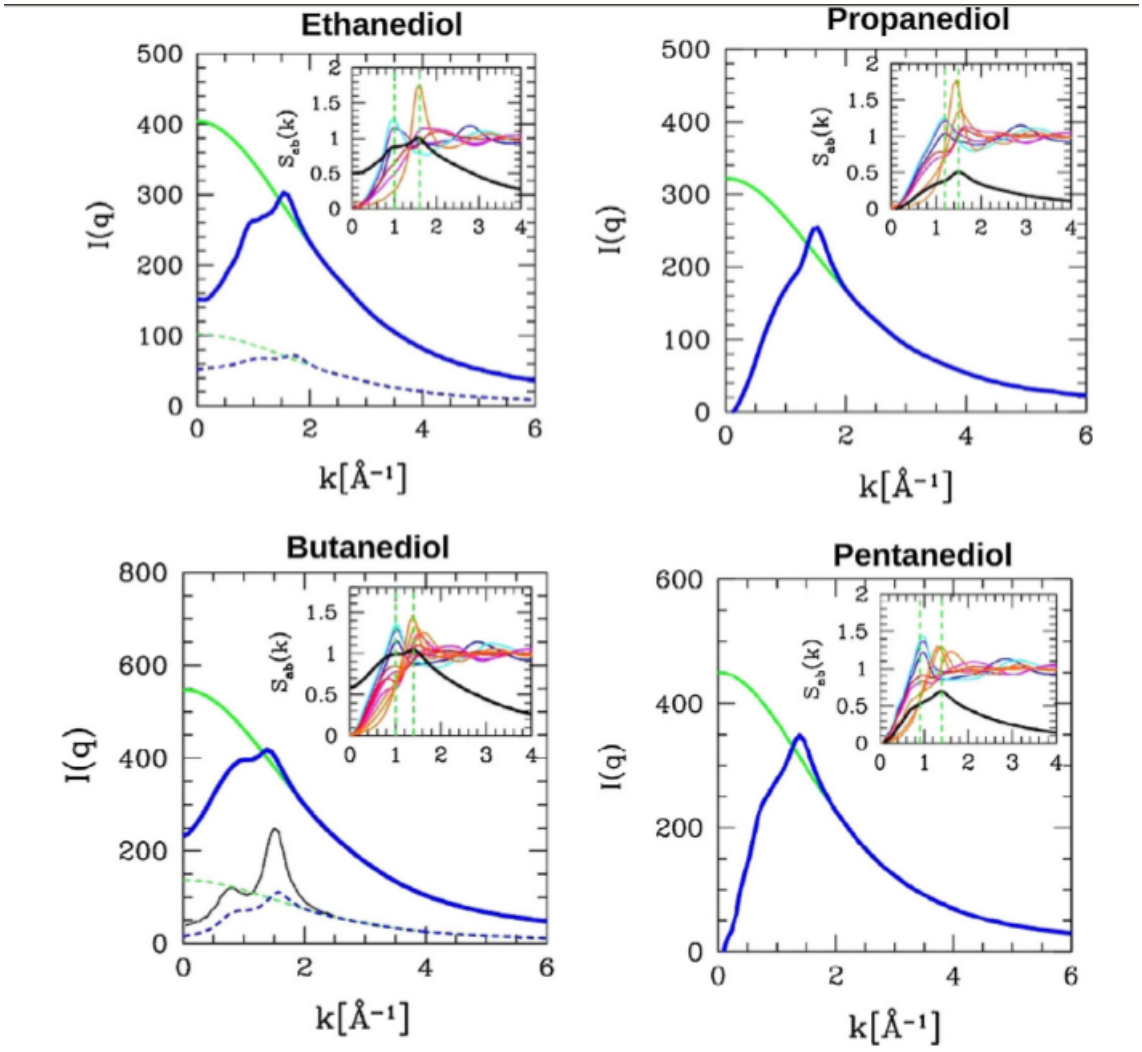

Figure 8.8.: Calculated X-ray scattering intensity I(k) for diols (in blue). The green curve is the ideal contribution (see text). The scattering curves for mono-ols (methanol and ethanol) are shown in dashed lines under those of ethanediol and butanediol. The experimental X-ray data for ethanol [170] is shown in black line. The insets show typical atom-atom structure factors (see text) with a scaled I(k) (in thick black line), with vertical lines indicating the position of the pre-peak and main peak.

The X-ray scattering intensities in Figure 8.8 were obtained from the atom-atom structure factors (part of them shown in the previous section) via the methodology explained in subsection 2.2.3. The data in Figure 8.8 shows the results for all four diols, together with those calculated for the mono-ols, and experimental SAXS data [170] for ethanol. In each panels, the main intensity $I(k)$ is reported in blue lines, and the ideal intensity $I_{ideal}(k)$ in green lines (dashed lines for the mono-ols).

It can be noticed that, even though the pre-peak in the structure factor is more pronounced for butanediol than for ethanediol, the scattering intensity doesn't have a marked contribution of the pre-peak. This trend becomes more apparent for propanediol and pentanediol, for which only the main peak is apparent, and the pre-peak is just a shoulder. In linear mono-ols it's experimentally known that the pre-peak and main peak become more defined the higher we go in the series [170], which seems not to be the case in 1,n-diols.

The reason for such behavior is hidden in the carbon chain which binds the two hydroxyl groups. The higher we go in the diol series, the more carbon sites contribute to the scattering intensity, and those sites produce structure factors which are out of phase for the longer diols and distributed between k_P and k_M. This essentially causes an enhancement of the contributions at k_M , while smearing that at k_P.

This finding has interesting implications in regards to what can and cannot be detected in scattering experiments. Microemulsions are notorious for exhibiting a peak at very small k values [214], which is linked to the objects (domains/droplets) formed in such systems. Pre-peaks are found in certains neat liquids, such as mono-ols [153, 155, 170] and room temperature ionic liquids [202], and can be connected to the existence of clusters in such liquids. As one might expect, pre-peaks are absent in the cases of simple liquids [11], but also for pure water [215] and aqueous mono-ol mixtures [21, 216]. Since the constraint in diols causes the pre-peak and main peak to basically merge into a single peak, scattering experiments may be rendered unable to show a clear signature of the underlying chain-like organization. This provokes the question whether there is a similar effect present in water and its alcohol mixtures.

8.2. Mixtures with 1,n-diols

In the following sections, the results for mixtures with 1,2-ethanediol and 1,3-propanediol with either water or ethanol are presented and discussed. A portion of the data, concerning cluster distribution probabilities and basic thermodynamic results, can be found in Appendix B for all mixtures.

8.2.1. Mixtures with water

8.2.1.1. Structural features

Through snapshots in Figure 8.9 we can visually appraise the organization in ethanediol-water. The snapshots show three typical mole fractions of ethanediol, demonstrated for the $N = 2$k system. In the upper row of Figure 8.9 we show each of the species with different colors, which helps visualise species segregation. The snapshot shows that the species are somewhat segregated into small chain-like clusters, but that the

overall distribution is quite homogeneous. This is particularly striking for water, since it tends to self- segregate into very large pockets when mixed with mono-ols [33, 38, 41, 39, 189]. The same snapshots can be observed with a different coloring convention - by emphasizing the water molecules and hydroxyl groups, while muting the non-polar sites of the diol (lower row of Figure 8.9). This way, we can see that hydrogen bonding is abundant in the mixture, indiscriminately of the species.

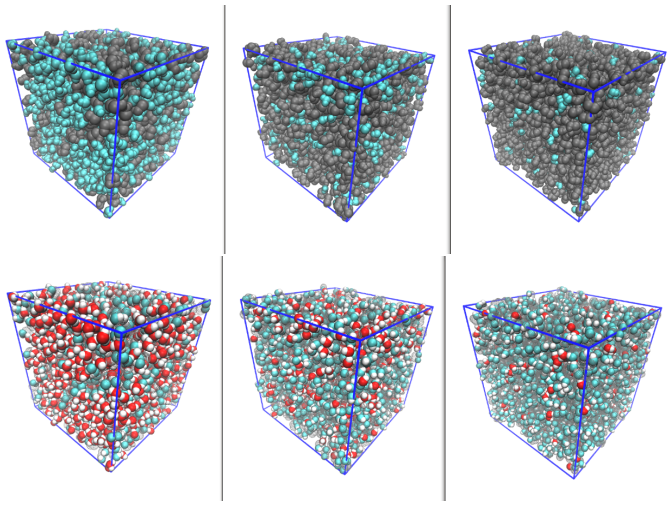

Figure 8.9.: Snapshots of the 1,2-ethanediol-water system, at the following diol mole fractions: $x_{DIOL} = 0.2$ (left panel), $x_{DIOL} = 0.5$ (middle panel) and $x_{DIOL} = 0.8$ (right panel). The upper row contains the full molecule representation, with water being in cyan and the diol in gray. The lower panel has the identical snapshots, but with only the water molecules (red-white) and hydroxyl groups (cyan-white) fully represented. The diol's non-polar chain is in transparent gray.

Figure 8.10 shows the characteristic oxygen–oxygen pair correlations (left panel) and their corresponding structure factors (right panel), for three diol mole fractions in the ethanediol-water system. In terms of pair correlation functions, it's noticeable that water oxygen–oxygen correlations are the strongest, followed by the cross correlations and then the diol correlations. Also, water's correlations become stronger with decreasing water content. The opposite is true for diol correlations, i.e. the first peak decreases with decreasing diol content. This is not surprising, as it fits into the mold of aqueous mixtures, which has been reported previously in various contexts [21, 23, 38, 189].

However, the results for the oxygen-oxygen structure factors (left panel of Figure 8.10) give an interesting new twist in comparison with aqueous mono-ol mixtures. The diol and cross structure factors possess a cluster pre-peak (or plateau), yet there is no domain pre-peak for small diol concentrations (which would be present in aqueous mono-ol mixtures). Conversely, the water structure factor shows a rather enhanced $k = 0$ raise, with no clear sign of a domain pre-peak. It seems that the water correlations ''waver'' between a pre-peak and a concentration fluctuation $k = 0$ peak. This is one of the signatures of the Lifshitz state.

It's interesting to note that the increase of the $k = 0$ peak is coupled to the behaviour at larger k-values. The oxygen structure factors of the diol show an increase of both the $k = 0$ and the cluster pre-peak when the diol content decreases ($x_{DIOL} = 0.2$), which is also accompanied by a decrease of the main peak at $k_M \approx 2.7$ Å^{-1}. A similar effect is also observed for the water oxygen correlations.

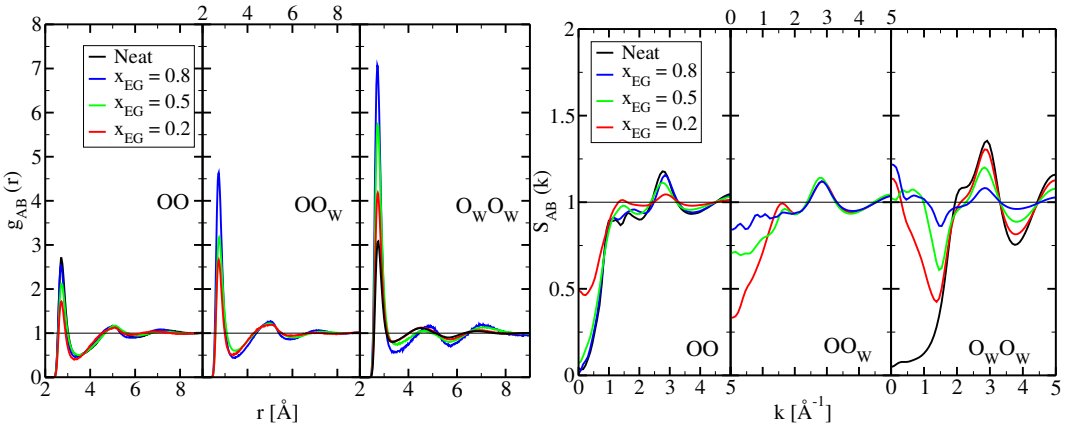

Figure 8.10.: Oxygen–oxygen correlation functions (left panel) and structure factors (right panel) for the aqueous–ethanediol mixtures. The diol concentrations are shown in blue for x = 0.2, green for x = 0.5 and red for x = 0.8. Pure solvent data are shown in black. The left panel for the oxygen atoms of the diol, the middle panel for the cross-correlations and the right panel for the oxygen atoms of water.

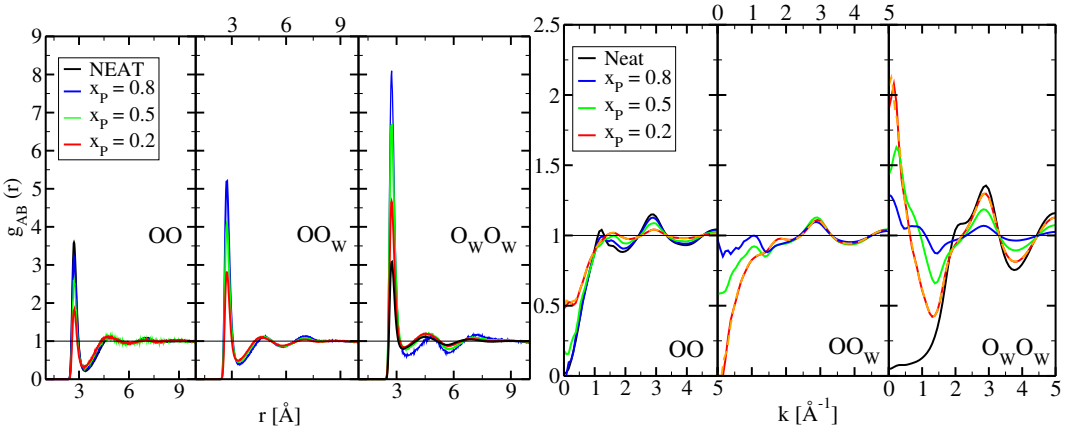

Figure 8.11.: Oxygen–oxygen correlation functions (left panel) and structure factors (right panel) for the aqueous–propanediol mixtures, with the same color conventions as in Figure 8.10. The dashed yellow curve is for N = 16 000 particles in the case of x = 0.2.

As for aqueous–propanediol mixtures, Figure 8.11 displays the data analogous to those in Figure 8.10, with the same arrangement of panels and color code. The overall trend in that Figure is very similar to that in Figure 8.10. The pair correlation functions (left panel of Figure 8.11), show a higher first peak for aqueous-

propanediol than for aqueous–ethanediol. Since the charges on the oxygen atoms are the same between the 2 models, the increase in the oxygen correlations comes from the presence of an additional methylene group for the propanediol. In terms of structure factors (right panel of Figure 8.11), propanediol's oxygen atoms show a more pronounced cluster peak than ethanediol. This is also true for the neat liquids (Figure 8.8), and is a consequence of the surplus methylene group, which enforces oxygen atom correlations through hydrophobic effects. Once again, water oxygen atom structure factors show no sign of a clear pre-peak, but rather an increase in the $k = 0$ region. This confirms the findings in the case of aqueous ethanediol.

Aqueous 1,n-diol mixtures display significant hydrogen bonding in the short range, both between the same species and cross species, which shows that they are not simple disorder. However, this short-range bonding does not produce sufficient local order, i.e. domains, which would then give rise to a domain pre-peak in the structure factor. Due to the absence of domain–domain correlations, and the analogy to the disappearance of the pre-peak in the micro-emulsion when approaching the Lifshitz point from the side of the layer ordered phase, this new type of disorder is named the Lifshitz state.

To close this section, we compare the structure factors calculated from a system with $N = 16\ 000$ particles (Figure 8.11, orange dashed curve) with that from a 2k system, for the $x_{DIOL} = 0.2$ molae fraction. It's apprent that the domain pre-peak type feature vanishes for the larger system, indicating that such a feature is a numerical artifact.

8.2.1.2. Kirkwood-Buff integrals

The Kirkwood-Buff integrals for both aqueous diol mixtures are displayed in Figure 8.12. The KBIs calculated from simulations (symbols) are in good agreement with the ideal KBIs obtained from the equation Equation 2.32, where $D(x) = 1$ (full lines). In the case of ethanediol (Figure 8.12, left panel), the results are well-aligned with the experimental data (dotted lines) reported by Marcus [217]. The latter data is the only experimental KBI data on binary mixtures with diols in literature. A simulation study by Geerke and van Gusteren [218] has included KBI results for ethanediol-water in the small concentration regime, which is also in good agreement with Marcus' experimental data.

The ideality which we perceive in the KBIs shows that these mixtures have low concentration fluctuations, in addition to being very homogeneous. There is more uncertainty in the data for water than the diol and cross KBIs. This is a direct consequence of the slowness of the dynamics and the statistics.

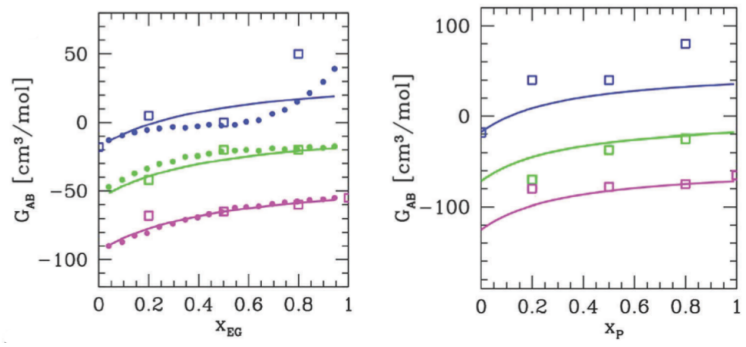

Figure 8.12.: Kirkwood–Buff integrals, versus the diol mole fractions, of the aqueous ethanediol (left panel), and aqueous propanediol mixtures (right panel). Blue line is for solvent–solvent, green for solvent–diol and magenta for diol–diol KBI. The squares represent the simulation results, the full lines correspond to D = 1. The dots in the left panel are experimental KBI results [217].

8.2.2. Mixtures with mono-ols

8.2.2.1. Structural features

Figure 8.13 contains the snapshots of the ethanediol-ethanol system, organized similarly to Figure 8.9. The upper row of Figure 8.13 has both compounds shown explicitely, while in the lower row only the hydroxyl groups are shown in full. Just like in Figure 8.13, one can observe the abundant Hbonding present in the system, regardless of the species. There also seems to be visual evidence of Hbonded chains, which also means there is no self-segregation of the species and no domains.

The oxygen–oxygen correlations and structure factors of the ethanol–ethanediol mixtures are shown in Figure 8.14, left and right panel, respectively. Looking at the pair correlation functions, we notice that the main peak of the diol correlations increases with decreasing concentrations of the diol, while it is the opposite for ethanol correlations. It seems like the diol is taking the role of water, while ethanol is behaving as if it's in an aqueous mixture in terms of short range structuring. Up to this point, we know the trademarks of short range features for both aqueous mono-ol mixtures and mixtures of mono-ols with non-polar solutes. This situation, where two associating species (none of them water) are being mixed is a novel one in terms of investigating the microstructure.

We know that both pure ethanol and ethanediol have pre-peaks in their oxygen-oxygen structure factors, so we expect a similar feature in the case of their mixture. Indeed, in Figure 8.14 (right panel), we observe pre-peaks at $k_P \approx 1$ Å^{-1}, which confirm that clusters characteristic for alcohols are present in the mixtures. However, at even smaller k-values there are also pre-peaks. Granted, these pre-peaks are of smaller magnitude than those observed in micro-heterogeneous systems like ethanol-benzene. In the latter system, the pre-peaks were due to long range oscillations in

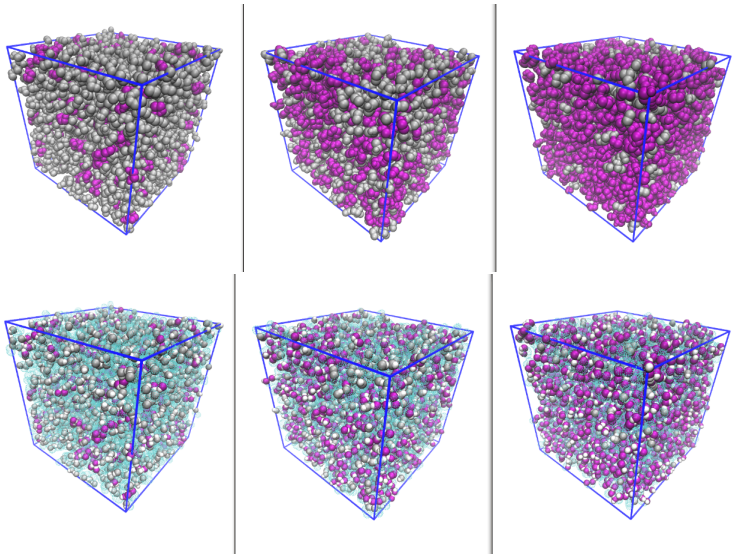

Figure 8.13.: Snapshots of the 1,2-ethanediol-ethanol system, at the following diol mole fractions: $x_{DIOL} = 0.2$ (left panel), $x_{DIOL} = 0.5$ (middle panel) and $x_{DIOL} = 0.8$ (right panel). The upper row contains the full molecule representation, with the diol in purple and ethanol in silver. The lower panel has the identical snapshots, but with only the hydroxyl groups fully represented (silver-white for ethanol and purple-white for ethanediol). The non-polar sites of both compounds are in transparent cyan.

the correlation functions, caused by the formation of domains. But in the case of ethanol-ethanediol, there are no observed medium-to-long-range correlations which would correspond to these small pre-peaks. In all likelihood, these pre-peaks are artifacts of the Fourier transforms, which stem from small irregularities in the flat asymptotic region of $g_{ab}(r)$. These are probably caused by small system size in conjunction with the general sluggishness of these mixtures. The orange curves in the right panel of Figure 8.14, which respresent the structure factors calculated from the 16k system at $x_{EDO} = 0.8$, show that these artifacts tend to disappear.

The ethanol-propanediol mixture follows the trends set out by ethanol–ethanediol. As evidenced in the left panel of Figure 8.15, the correlation functions for all species behave similarly to those observed in Figure 8.14. Once again, the diol correlations behave like those of water, but with a smaller magnitude. This is likely caused by the length of the alkyl chain linking the two hydroxyl groups. The non-polar chain is longer for 1,3-propanediol than 1,2-ethanediol, so it's to be expected that the compound with the shorter chain will exhibit features closer to those of water.

The site-site structure factors for this mixture, shown in the right panel of Figure 8.15, highly resemble those found in ethanol-ethanediol. There are cluster peak at $k_P \approx 1$ Å^{-1} seen in the structure factors of all three species, once again indicating the existence of clusters typical for alcohols and appreciable cross binding between the species. A small pre-peak for small k values is noticeable, especially in the case of ethanol structure factors. Just like in the case of ethanol-ethanediol, the problem is

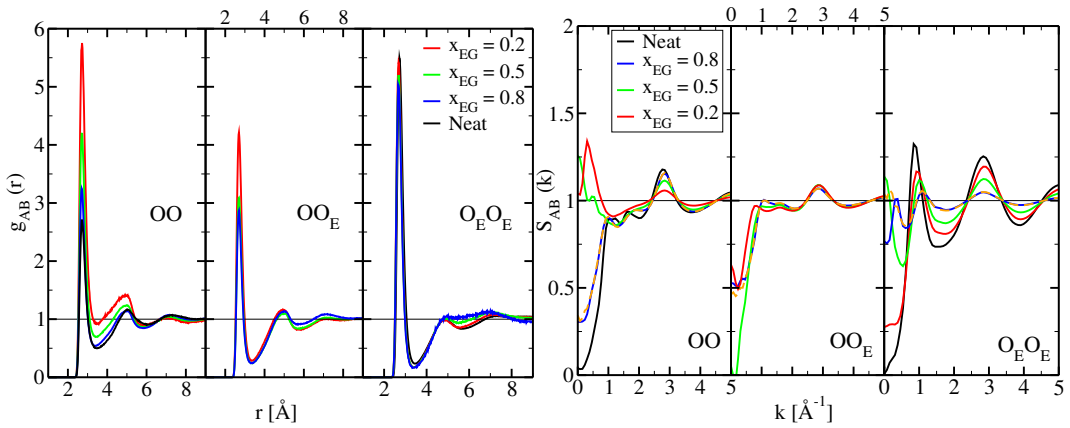

Figure 8.14.: Oxygen–oxygen correlation functions (left panel) and structure factors (right panel) for the ethanol–ethanediol mixtures, with the same color conventions as in Figure 8.10. The dashed orange curves in the structure factor plots correspond to data calculated from 16k systems, for molar fractions of $x_{EDO} = 0.8$.

chalked up to the system's slowness and resulting statistical problems in the asymptotes of $g_{ab}(r)$, accompanied by the small system size. The orange dashed curves, calculated from 16k systems for two mole diol fractions, 0.2 and 0.8, indicate that these small pre-peaks will vanish.

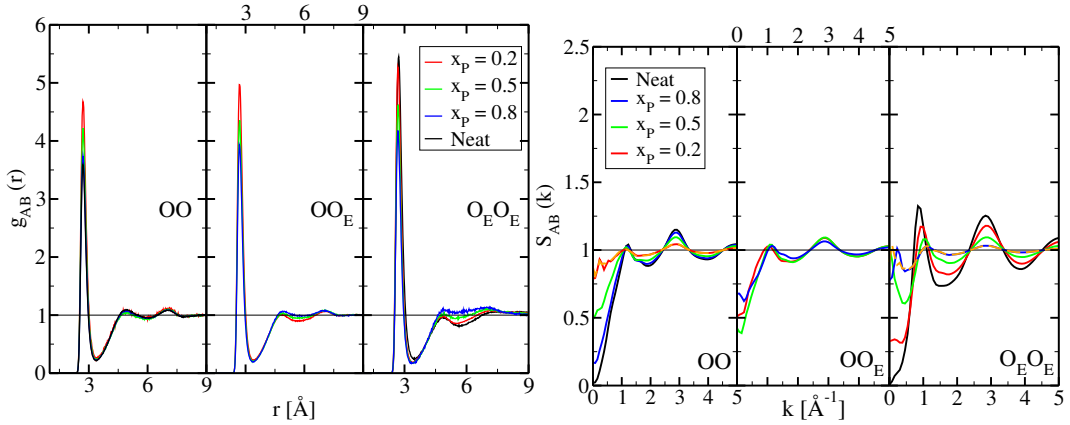

Figure 8.15.: Oxygen–oxygen correlation functions (left panel) and structure factors (right panel) for the ethanol–propanediol mixtures, with the same color conventions as in Figure 8.10. The dashed orange curve is for N = 16 000 particles in the case of x = 0.2.

8.2.2.2. Kirkwood-Buff integrals

Figure 8.16 presents the KBI results for ethanol-ethanediol (left panel) and ethanol-propanediol (right panel). Unlike aqueous mixtures of diols, featured in Figure 8.12, mono-ol-diol mixtures show a weak non-ideality. The results calculated from the

simulations (symbols) somewhat contrast the calculated ideal KBIs with $D(x) = 1$ (dashed lines). This is more apparent for the case of ethanol-ethanediol, since its ideal KBIs are grouped close together, due to the similar molar volumes of neat ethanol and ethanediol.

Generally speaking, the functions *D(x)*, shown in the respective insets of Figure 8.16, show small deviations from $D(x) = 1$, the latter of which is the ideal value corresponding to ideal chemical potential. Also, the KBI values these mixtures yield are at variance with the KBIs from micro-heterogeneous systems. Aqueous alcohol mixtures, for example, usually have a maximum in the water–water KBIs which can reach from 400 to 10000 cm^3/mol, depending on the alcohol [26, 29]. Monool-diol mixtures, on the other hand, lack these high KBIs, pointing to small concentration fluctuations. This is consistent with the visual homogeneity observed in the snapshots.

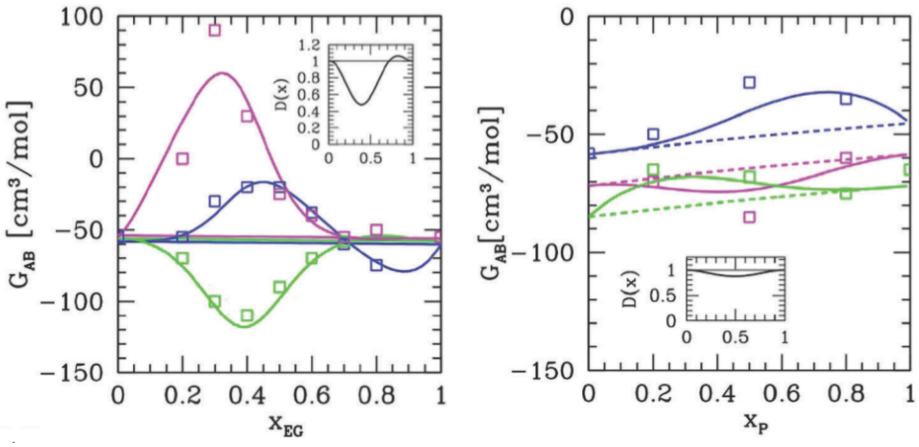

Figure 8.16.: Kirkwood–Buff integrals versus the diol mole fractions, of the ethanol–ethanediol (left panel), and ethanol- propanediol mixtures (right panel). Blue line is for solvent–solvent, green for solvent–diol and magenta for diol–diol KBI. The squares represent the simulation results, the full lines correspond to D(x), which are shown in the inset.

However, aqueous diol mixtures appear to be more ideal than ethanol–diol mixtures. This is rather counter-intuitive, as one would expect that the presence of non-polar groups in ethanol would help randomize these mixtures much more than in the case of water. In fact, the alkyl groups of the ethanol molecules hinder the structuring which would be produced if only the hydroxyl groups were present. This hinderance produces an apparent fluctuation and non-ideality, which is seen in the KBIs, but also in the sluggishness of the dynamics of these ethanol–diol mixtures. Aqueous diol mixtures, on the other hand, have a strong short-range order, produced by the abundance of hydrogen bonding choices. Despite the constraint that the alkyl chain in 1,n-diols pose, the hydroxyl groups are able to disperse themselves in water. This results in no domain segregation and the decrease of concentration fluctuations.

8.3. Conclusions

The study of neat 1,n-diols has yielded several interesting results and clarified notions about the role of the alkyl chain in these compounds.

The existence of a carbon chain of varying length, which binds two hydroxyl groups, leads one to assume that the clustering of the hydroxyl groups in diols would be hindered. Indeed, that seems to be true to a degree, especially in comparison with mono-ols, where the chaining of hydroxyl groups is a trademark of their microstructure. However, the hydroxyl groups still manage to associate into chains, albeit less prominently than mono-ols. This is shown through several structural features, such as the pair correlation functions and structure factors.

The most interesting findings are those pertaining to the calculated scattering intensity. While mono-ols have the tell-tale signature of hydroxyl group clustering in their scattering intensities, embodied in a pre-peak located at roughly $k_P \approx 1$ Å^{-1}, 1,n-diols don't share the same trait. In fact, these diols possess a shoulder-like feature at the same position, which may seem puzzling when one recalls the existence of chains in 1,n-diols. This is where the existence of carbon chains comes into play. Unlike free carbon tails in mono-ols, the carbon sites in diols are spread between their respective hydroxyl groups, thus contributing to the scattering intensity at various k values which lie between the main peak and the pre-peak. This broadening at the main peak seems to mask the signal of the pre-peak, which is a noteworthy finding considering the value and widespread usage of scattering experiments. This was confirmed in the subsequent experimental study of Tomšič *et al.* [210].

Binary mixtures with 1,n-diols have also given interesting information. In terms of short-range structuring, diol alcohols exhibit a duality of behaviors, depending on the nature of the other component in the mixture. When mixed with water, diols will show the signatures characteristic of monool alcohols in aqueous mixtures, i.e. the first peak of the pair correlation function will decrease with the decrease of diol content. But, if 1,n-diols are mixed with monools, they will essentially take over the role of water, while the monool behaves as in aqueous mixtures. However, other quantities indicate a difference between the behavior of diol mixtures and typical complex mixtures like aqueous alcohols.

Unlike aqueous alcohols, mixtures with diols exhibit small concentration fluctuations, as evidenced by the KBIs. Furthermore, there are no signatures of domain pre-peaks in the site-site structure factors, but more of a flattening of the S(k). This absence of a pre-peak in S(k) as a signature of the Lifshitz state, where the system is trapped in a disorder, but which is not a random disorder either, precisely because of the strong hydrogen bonding tendencies. The Lifshitz state represents a novel form of disorder, an intermediate state between random disorder and domain order, in a globally disordered homogeneous liquid. It is one step further to classify different forms of disorder in liquids, which could be of importance in classifying different types of disorder, particularly in the context of soft and bio-matter.

9. Conclusions and outlook

The main aim of this thesis is to connect the chemical properties of molecules to the statistical description of liquids and mixtures containing them. This connection links the nature of the atom-atom interactions in the molecular species to the diversity of the supra-molecular structuring formed inside liquid mixtures. These interactions are twofold; being the Lennard-Jones interactions and Coulomb interactions. In Chapter 3, we show that LJ interactions alone lead to simple disorder, which is the usual type of disorder one expects in liquids, random disorder. The introduction of Coulomb interactions imposes a new form of disorder. This form of disorder is expressed differently in ionic melts, room temperature ionic liquids or polar molecules, which is based on charge order. The fact that polar molecules can be modeled as a group of charged atomic sites imposes severe geometrical constraints to the charge ordering, leading to micro-heterogeneity in mixtures. Different aspects of MH were explored through various systems in this thesis.

We have suggested that micro-heterogeneity can be considered as a supra-molecular entity, linked by a non-covalent bond, such as the hydrogen bond, which is classically represented through Coulomb interactions. Mixtures can be viewed at several levels of descriptions: the atomic level, the molecular level, the heterogeneous level and finally the macroscopic liquid level. The unified description of these levels cannot be encompassed by the usual methods of chemistry or statistical physics approaches alone. A striking demonstration of this impossibility is the interpretation of the experimental scattering intensity in these mixtures, as we have seen in subsection 2.2.3 of Chapter 2. This description contains the form factors which represent the atomic level, but all the other levels appear through the various frequency peaks present in the spectrum. Since these peaks are the product of atom-atom structure factor peaks, the entanglement in the final information is complex, and requires a detailed interpretation through the atom-atom structure factors, which are not experimental observables by themselves. This is why computer simulations are necessary, along with reliable force field models.

The representation of real liquids in the classical force fields, based solely on LJ and Coulomb interactions, is a subject of investigation in and of itself, undertaken since the very beginning of simulations. It is interesting to note that earlier simulations of liquid argon through LJ interactions [219] remain valid to this date, while earlier simulations of water or aqueous mixtures are not [220, 221, 222]. This is already a hint of what we have discussed in Chapter 3, through the concepts of simple and complex disorder. While simple disorder requires little modeling and computational

effort, the exact nature of the effort required to describe complex disorder is not very clear. It would appear that most researchers in the field study these mixtures solely from the point of view of simple disorder neglecting the inherent local heterogeneity of these mixtures.

Yet, it is obvious that water has many anomalies, all of which are scattered in the phase diagram at many levels of description, thermodynamic, structural or dynamic [14, 15, 223]. The exact nature of the structure of water is still unknown [224]. It is interesting that earlier models of water invoked the two-state model, with water being both in ordered ice-like and disordered dense forms of liquids [225, 226]. These two forms are quite reminiscent of the idea of simple and complex disorder that we propose. While a lot of conceptual progress remains to be made, the present work can be considered as a step in a promising direction. One of the promising directions where this type of research might have an impact is biophysics.

As mentioned in the Introduction, a significant part of molecular biophysics is about how various large molecules associate, move and interact in a rich solvent environment. Such molecules are often macromolecules or polymer molecules, which fold, separate or assemble to form other types of molecules [227]. The assembling interactions are often of the hydrogen bond type, which is smaller in magnitude than a covalent bond, but large enough to resist thermal destruction for an amount of time needed for the molecules to function and accomplish tasks [228]. The physical background behind the structuring in liquid mixtures and the assembly of biomacromolecules is the same, even though the scales and objects themselves are different. The work presented in thesis could be a stepping stone towards understanding the assembly of macromolecules and also the role of complex mixtures in the biological environment.

This thesis discusses only the structural aspect of complex liquids. It seems that understanding the kinetics and the dynamics in micro-heterogeneous liquids would be not only useful, but necessary in obtaining a comprehensive approach to biomolecular processes. The dynamic part of the micro-heterogeneity is still in its infancy, and the first steps are being undertaken by the Split and Paris groups. New and exciting results in that field are expected in the future.

The topic of future research surpasses the limits of this thesis, so we would like to take this opportunity to look inward and discuss the other side of the medal. The results' section is populated by many different mixtures which spawned new ideas, but these were not the only projects that were tackled throughout the course of this thesis. There was a number of interesting projects which promised to answer important questions, but didn't fully come to fruition due to modelling or computational obstacles. A brief account of two such topics is given.

Pyridine, piperidine and their aqueous mixtures The pyridine-water and piperidine-water mixtures are notable examples of being too complex for the current time frame. Both pyridine and piperidine are six-membered ring molecules, with the ring

composed of five carbon atoms and one nitrogen atom. However, they belong to different species: pyridine is an aromatic compound, while piperidine is a secondary amine. Both molecules are miscible with water in all proportions [229] and KBI experiments for both mixtures [26] have similar trends. There are appreciable concentration fluctuations and segregation in the concentration range $x_{PIP,\,PYR} = 0$ - 0.4 for both mixtures, while beyond that range the KBIs become flat and close to the ideal values (Figure 9.1).

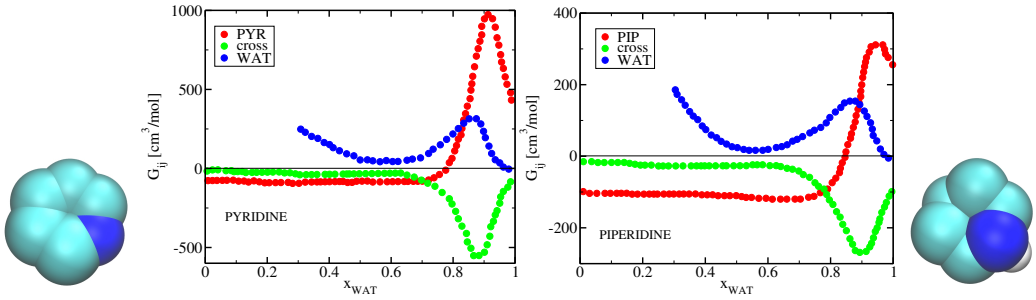

Figure 9.1.: The KBI results for aqueous pyridine (left panel) and aqueous piperidine mixture (right panel). The experimental results were taken from Matteoli and Lepori [26]. The color code is contained in the figure.

Yet, SANS measurements done on both water mixtures show a remarkable difference: piperidine-water shows a small-k pre-peak in the scattering intensity for the piperidine mole fraction interval $0.2 < x_{PIP} < 0.5$ [230], while the same feature is absent in pyridine-water for all pyridine mole fractions [231]. The peculiarity of this experimental result gave us the motivation to delve deeper into the structure of these two mixtures at the molecular level and shed light on what kind of structuring will give rise to a pre-peak in the scattering intensity.

In order to do that, it was necessary to simulate these mixtures. We tested the majority of available force fields for both molecules; namely OPLS-AA[232], TraPPe-AA [233] and Gromos-AA [234] for pyridine and OPLS-AA [235] and OPLS-UA [236] for piperidine. The calculated thermodynamic properties for those systems can be found in Appendix A, where they are discussed. Suffice to say that, due to their performance, the TraPPe-AA model for pyridine and OPLS-UA model for piperidine were chosen for further simulations.

However, the aqueous mixtures of both molecules have proven to be particularly challenging. Initial simulations of aqueous pyridine and aqueous piperidine showed either demixing or strong segregation of the solute molecules in water for all proportions, regardless of the water model used (SPC/E [177], TIP4P/2005 [178] or TIP5P [237]).

So, the first key step in this investigation was to attain the proper mixing of pyridine and piperidine with water. The specific KBI behavior of these mixtures became one of the guidelines for force field modification. The idea was to modify the existing

pyridine and piperidine models in such a way that they mix with water and reproduce the correct KBIs, all the while maintaining the volumes and enthalpies of vaporization close to experimental values. The full account of the force field modification, the rationale behind it and the resulting new force fields is the subject of a pending paper. Nevertheless, achieving the correct miscilibity of pyridine or piperidine with water was only the beginning. At low solute concentrations, the domains formed by piperidine or pyridine proved to be too large to be properly sampled in a 16k system. Both of these systems require an even larger simulation box to fully capture the domain oscillations in the tale of the $g(r)$. With the current results, we could not have concluded the study in a satisfactory manner.

The ternary mixture of methanol-1-propanol-benzene Another project foiled by computational limitations was the ternary mixture of methanol-1-propanol-benzene. Originally, the work was envisioned as the extension of the research done on ethanol-non-polar solutes [72, 74], where ethanol is being replaced by a mixture of two alcohols. Since methanol and 1-propanol form a quasi-ideal mixture [73], it behaves as a pseudo one-component which micro-segregates from the alkane. However, the asymmetry in alkyl chain length between methanol and 1-propanol introduces a new moment in the mixture. By varying not only the total alcohol concentration, but also the concentration of the respective alcohols, a fine structure of the otherwise micro-heterogeneous organization was to be brought forth. But, the 16k system was also proven too small to properly capture the domains formed at low alcohol content. Like in the cases of aqueous pyridine and piperidine, doubling the existing box sizes would be necessary to obtain proper results. However, this means going from 16k molecules to 128k, which increases the computational cost beyond our current means.

Apart from those two open-ended projects, there was work undertaken in collaboration with other groups, with a thematic related to this thesis, but still going beyond its scope.

The MB methanol model This is the investigation of the two-dimensional model of methanol, based on the Mercedes-Benz (MB) model of water [238, 239]. The research, which yielded one publication [240], proposes a new methanol model, with the hydroxyl group modelled as a sphere with two hydrogen bonding arms and the methyl group represented by a non-polar Lennard-Jones disk. A comparison was done between the new model and an existing one [241], as well as with experimental results and 3D models of methanol.

Finally, there were projects which came into the picture towards the end of this thesis, exceeding its temporal limits.

Other alcohol binary mixtures One such subject is the ethanol-heptane mixture, which possesses an unusual trend in the experimental KBI measurements [242] - two

distinct maxima, corresponding to two different ethanol concentrations. This was never observed in other micro-heterogeneous mixtures presented in this thesis. It poses the question - what microscopic organization gives rise to such macroscopic features? This will be explored further down the line.

The other topic that merits exploration is the aqueous mixture of 2,2,2-trifluoroethanol (TFE). This mixture is of high biological relevance, as it's known to promote the secondary structuring in peptides and proteins [243], cause beta to alpha transitions [244] and stabilize the secondary structuring of proteins for circular dichroism (CD) and the liquid NMR structure determinations [245, 246]. For all of these applications, the mixture with 30% volume fraction of TFE is commonly used. At this particular fraction, the micro-heterogeneous nature of TFE-water is the most pronounced, as witnessed by scattering experiments [247, 248, 249, 250]. The main idea would be to connect the underlying structuring of TFE-water with observable, macroscopic properties and gain some insight into why aqueous TFE affects biomacromolecules as it does on the molecular level. The latter may prove to be difficult, as TFE-dependent conformational changes are protein specific [250]. Nevertheless, this investigation is just one step in the direction of connecting assemblies at the molecular level with those on the cellular level, guiding this type of research more into the domain of biophysics.

A. Supplementary simulation results for neat liquids

A.1. Simulation protocol

Molecular dynamics simulations were performed with the program package Gromacs [71]. The simulation protocol has been the same for all neat systems. The initial configurations were generated by random molecular positioning, with the program Packmol [251]. Initial configurations were first energy minimized, and then equilibrated in the NpT ensemble from 1 ns to 5 ns, depending on the system. Finally, production runs from 1 ns to 10 ns were performed, when the data for analysis was gathered (1000 configurations was the minimum number collected, although on average, 2500 to 5000 was the usual number of configurations). The length of the production run depended on the convergence of both termodyamic values and the long range tail of the atom–atom correlation functions.

Unless specified, all of the simulations were done under ambient conditions, *i.e.* with T = 300 K and p = 1 bar. Temperature was maintained constant using mostly the Berendsen [104] or Nose–Hoover [105, 106] thermostat, while pressure was maintained with the Parrinello–Rahman barostat [108, 109]. The temperature algorithms had a time constant of 0.2 ps, while the pressure algorithm was set at 2 ps.

Typically, the integration algorithm of choice was the leap-frog [94] at every time-step of 2 fs. The short-range interactions were calculated within the 1.5 nm cut-off radius and the dispersion correction was included in the energy calculations. When employed, the electrostatics were handled with the PME method [100], and the constraints with the LINCS algorithm [99].

For pure liquids, the question of system size is not crucial. Systems of N = 1000 particles provide sufficient structural and thermodynamic information.

A.2. Neat liquids - various results

A.2.1. Benzene

Benzene is a planar, ring-like molecule with a particular electron distribution [151]. From the seventies onward, there have been many efforts to model liquid benzene and reproduce its thermodynamic, structural and dynamic behavior [142, 233, 252, 253, 254, 255, 256, 257, 258]. Those efforts include different approaches in terms of number of sites, electrostatic interactions (or lack thereof) and van der Waals interactions. Comparisons of available forcefields have been done before [259, 260], with the intentions of finding the most accurate model of liquid benzene.

However, the best benzene model was not necessary for our purposes in investigating simple and complex disorder. We chose to test three models: the all atom and united atom representations of the OPLS forcefield[256, 142] and the united atom respresentation of Trappe [257]. The OPLS-AA forcefield explicitely models the hydrogen atoms on carbons, therefore requring the computation of twelve LJ centers of force and twelve point charges. On the other hand, the OPLS-UA and Trappe-UA forcefields use six sites and have no charges, which renders them highly computationally efficient.

The simulated pure systems were comprised of 2000 molecules (in the case of the OPLS-UA forcefield) and 1000 molecules (in case of the OPLS-AA and TraPPe forcefield). All simulations were performed in the NpT ensemble. The pressure of 1 bar and temperature of 300 K were kept constant thanks to the Parrinello-Rahman barostat[108, 109] and v-rescale thermostat[261]. In the case of the OPLS-AA model, which is possesses charges, the long-range electrostatics were handled with PME [100]. The simulation protocol was the same for all systems. After energy minimization, 1 ns of equilibration was done. Production runs, from which the results were calculated, lasted 5 ns.

Model	Density [kg/m^3]	H_{VAP} [kJ/mol]
OPLS-AA	865.0 (+/- 5.2)	33.85 (+/- 0.42)
OPLS-UA	885.7 (+/- 3.0)	34.62 (+/- 0.17)
Trappe-UA	855.5 (+/- 5.3)	29.52 (+/- 0.24)
Experiment[229]	876.5	33.83

Table A.1.: Thermodynamic results for tested benzene models.

Table A.1 gives the average values of densities and energies of the tested pure liquids, as well as the corresponding experimental values. In terms of energy, the OPLS-AA model performs the best, reproducing the H_{vap} to the first decimal. The OPLS-UA model comes in as a close second with a 3% deviation, while the Trappe-UA is last with a 13% deviation.

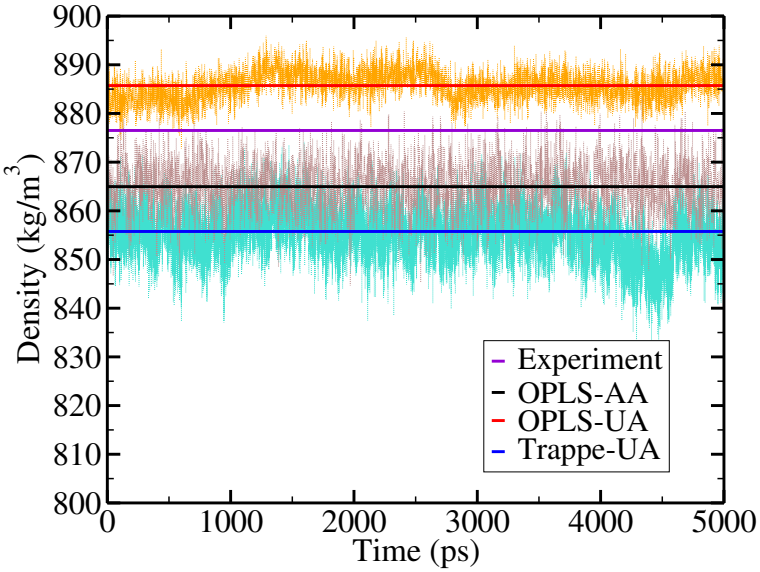

Figure A.1.: Average densities for the tested pure benzene systems (full lines) and their fluctuations. The values were calculated for production runs of already equilibrated systems.

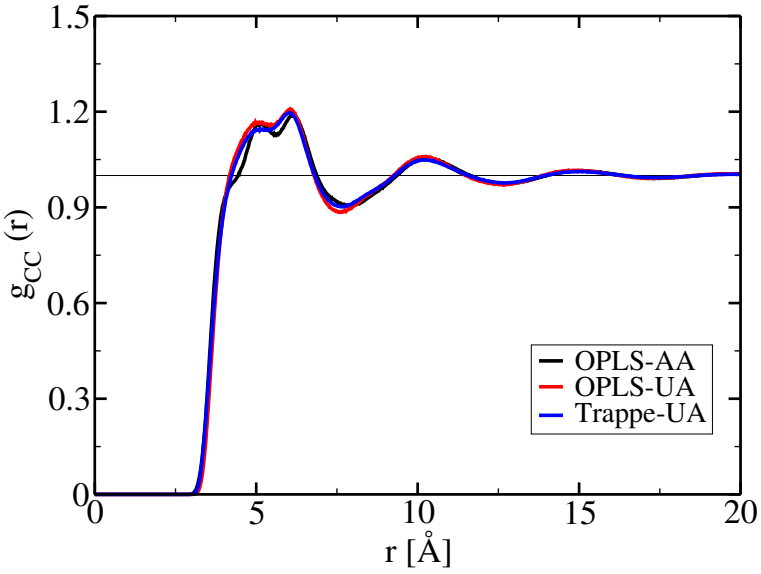

Figure A.2.: Hydrocarbon united atom radial distribution functions for the tested pure benzene systems.

As for the densities, all three models show solid agreement. The OPLS models are within percent deviations of 1%, and the Trappe model is within less than 3%. Figure A.1 shows the change in density over time for the production runs. The full lines denote the average values from Table A.1. We notice that the OPLS-UA

forcefield shows less fluctuations than the other two, but in general, the density behaves well over time.

Figure A.2 displays the relevant radial distribution functions. The united atom models have virtually identical RDFs, which are in small variance with the all atom model. The differences between the AA and UA models are seen only in the structure of the first peak. Although both UA and AA models show a split peak structure, with two small peaks located at 5 Å and 6 Å, the OPLS-AA benzene has a more distinct peak at 5 Å. However, all three models reproduce the most important features of the RDF obtained from Narten's scattering experiments [262].

Since all three models perform reasonably well in modelling liquid benzene, it was possible to forgo the computationally expensive OPLS-AA model in favor of the UA models.

A.2.2. Acetone

Acetone is the simplest ketone, i.e. it has a bivalent carbonyl group bonded to two carbon substituents [151].

We tested several models for pure acetone, once again seeking resonably reproduced thermodinamical and structural behavior tempered by computational efficiency. The chosen models were: the classic united atom OPLS[263] and Trappe [264] forcefields, alongside a modified OPLS forcefield. The latter combined the partial charges parametrized for the all atom OPLS ketone model [236] with the united atom representations of the methyl groups[142]. In brief, the major difference between the classic OPLS-UA model and our modified OPLS-UA model is the distribution of partial charges on the sites, as can be ascertained from Table A.2.

Model	Site	q [e]	σ [Å]	ε [kJ/mol]
OPLS-UA[263]	C	0.300	0.3750	0.439
	O	-0.424	0.2960	0.879
	M	0.062	0.3910	0.670
Trappe-UA[264]	C	0.424	0.3820	0.332
	O	-0.424	0.3050	0.657
	M	0.0	0.3750	0.814
Modified OPLS-UA[236]	C	0.470	0.3750	0.439
	O	-0.470	0.2960	0.879
	M	0.0	0.3775	0.866

Table A.2.: Parameters used for tested acetone models. The sites are: C - central carbon atom; O - oxygen atom; M - methyl group united atom.

The system sizes of pure acetone were: 1000 molecules for the classic OPLS-UA forcefield and 2000 molecules for the other two forcefields tested. The simulations

were done in the NpT ensemble at ambient conditions, utilizing the same thermostat and barostat as for pure benzene. The long-range electrostatics were handled with PME [100]. The simulation protocol was the same for all systems. After energy minimization, 1 ns of equilibration was done, followed by 1 ns of production.

Model	Density [kg/m^3]	H_{VAP} [kJ/mol]
Modified OPLS-UA	818.5 (+/- 3.3)	33.3 (+/- 0.16)
OPLS-UA	738.8 (+/- 5.1)	18.0 (+/- 0.11)
Trappe-UA	761.6 (+/- 4.1)	31.7 (+/- 0.17)
Experiment[229]	784.5	30.99

Table A.3.: Thermodynamic results for tested acetone models.

Table A.3 summarizes the calculated thermodynamic properties for the simulated acetone models. Density-wise, the Trappe-UA acetone performs the best, slightly underestimating the density, but being in the 3% deviation. It's followed closely by the modified OPLS acetone, which is within 4% deviations, while the classic OPLS-UA is the last at 6% deviations. In terms of energy, the ranking of forcefields is the same. The Trappe forcefield is proven is within percent deviations of 2% for H_{VAP}, while the modified OPLS model is within 7%. The classic OPLS-UA model significantly underestimates the value of H_{VAP} with a 40% deviation from the experimental value.

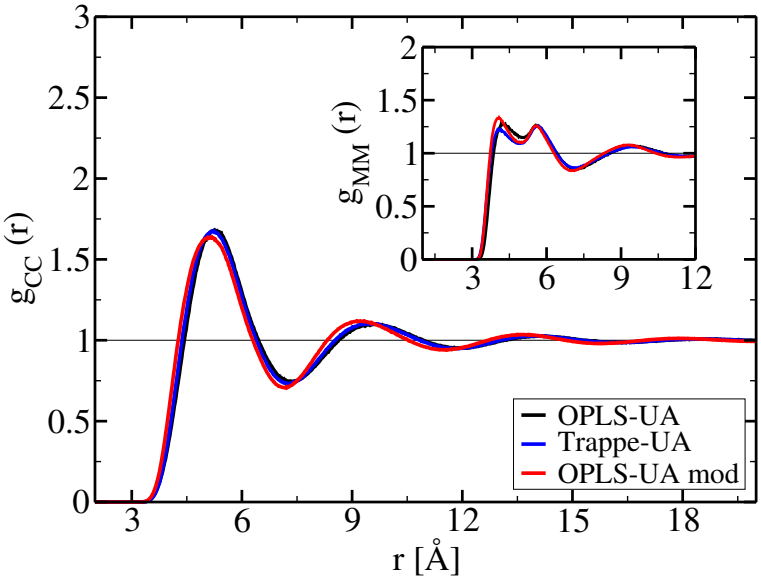

Figure A.3.: Main panel: C-C (central carbon atom) radial distribution functions for the tested acetone models. Inset: Methyl-methyl RDFs.

Figure A.3 contains the relevant pair correlation functions for all three models: the RDFs of acetone's central carbon atom in the main panel, and the RDFs of the

methyl groups in the inset. The RDFs in the main panel show significant overlap, with the only difference being the slight shift to the left in the second neighbor shell for the modified OPLS-UA model. The RDFs of the methyl groups have a double peak feature in the first neighbor shell, coming from the fact that the acetone molecule has two methyl groups flanking the central carbon atom. The first small peak, located at ~4 Å, differs in height from one model to another, but from that position onward, the RDFs are identical for all the models.

A.2.3. Alcohols

A.2.3.1. Mono-ols

Mono-ols are a subgroup of alcohols which consist of one hydroxyl group (-OH) connected to a hydrocarbon tail. Their dual nature (having a hydrophyllic part and a hydrophobic part) enables their rich structuring in binary mixtures, depending on the solvent.

Since mono-ols play an important role in our inquiries, it was, once again, important to find forcefields and models which adequately reproduce their properties while keeping the computational costs reasonable. The first two mono-ols in the series, methanol and ethanol, were extensively tested. The objective was twofold: to compare the difference between the united atom models of OPLS [265] and Trappe [266], and also to compare the performance of the OPLS forcefield's united atom [265] and all atom [236] models. The higher alcohols (1-propanol, 2-propanol, 1-butanol and tert-butanol) were done only in the Trappe-UA forcefield.

The simulated systems contained mostly 1000 or 2000 molecules. All the alcohols were simulated in ambient conditions, which were kept constant with the thermostat and barostat designated in the introduction of the Appendix. The simulation times were in the range mentioned in the introduction. Additional simulations of ethanol at low temperatures were done as well, with the minimum production runs of 5 ns.

Table A.4 contains the relevant thermodynamic data for the tested models. In the case of methanol, the densities are within percent deviation of 5% in comparison to the experiment, while the heats of vaporization are within 8% deviation from the experimental value.

For ethanol, the density values deviate at most 2% from the experimental value for all models. However, when it comes to H_{VAP}, the united atom models perform much better than the all atom model: the united atom values are within 4% deviation from the experiment, in comparison with the 26% percent deviation of the all atom model.

Alcohol	Model	Density [kg/m^3]	Exp. Den. [kg/m^3]	H_{VAP} [kJ/mol]	Exp. H_{VAP} [kJ/mol]
Methanol	OPLS-UA	756.4 (+/- 7.0)	791.4	38.28 (+/- 0.22)	37.43
	Trappe-UA	770.5 (+/- 7.2)		40.34 (+/- 0.21)	
	OPLS-AA	769.1 (+/- 5.2)		36.37 (+/- 0.22)	
Ethanol	OPLS-UA	780.0 (+/- 9.1)	789.3	44.10 (+/- 0.66)	42.32
	Trappe-UA	774.4 (+/- 6.2)		42.87 (+/- 0.25)	
	OPLS-AA	795.2 (+/- 7.7)		56.94 (+/- 0.48)	
1-propanol	Trappe-UA	793.7 (+/- 4.7)	799.7	47.47 (+/- 0.26)	47.45
2-propanol	Trappe-UA	760.4 (+/- 4.1)	780.9	45.14 (+/- 0.19)	45.39
1-butanol	Trappe-UA	836.0 (+/- 5.0)	809.5	48.81 (+/- 0.36)	52.35
Tert-butanol	Trappe-UA	782.2 (+/- 3.5)	788.7	49.24 (+/- 0.19)	46.69

Table A.4.: Thermodinamical properties for tested mono-ol forcefields. The experimental values at 25 °C are taken from [229].

Structure of neat ethanol and methanol The site-site correlation functions, shown on Figure A.4, demonstrate the structural similarity between the united and all atom models for both ethanol and methanol. In both cases, the UA and AA models differ mostly in the height of the first peak in the OO correlations. The OO structure factors of both models (Figure A.5) reproduce the position of the cluster pre-peak in both alcohols. However, the UA model of ethanol shows are more intense pre-peak than its AA counterpart. In the case of methanol, the UA model has a split pre-peak feature, which is missing from the AA model. The correlation functions and structure factos of the methyl and methylene groups for both alcohols are extremely similar.

Given the thermodynamic and structural results above, it's was not necessary to employ the AA model of the OPLS forcefield over the UA model, since the UA model reproduces well the traits of the pure liquids. As for the difference between forcefields, both Table A.4 and Figure A.6 show that the differences between the forcefields are minor.

From those basic results, one can conclude that the united atom models from both

OPLS and Trappe forcefields work well and it's not necessary to use the all atom model to achieve the same results.

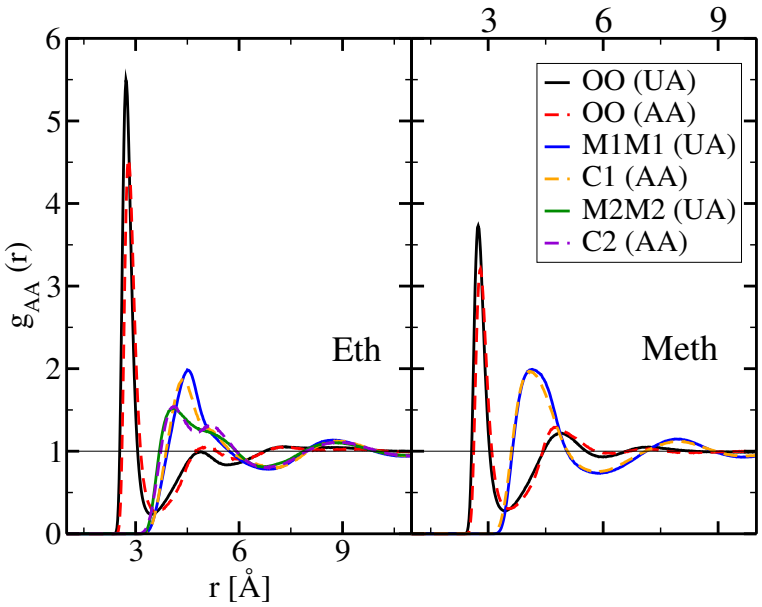

Figure A.4.: Selected site-site RDFs for pure ethanol (left panel) and pure methanol (right panel). The united atom (full lines) and all atom (dashed lines) are compared.

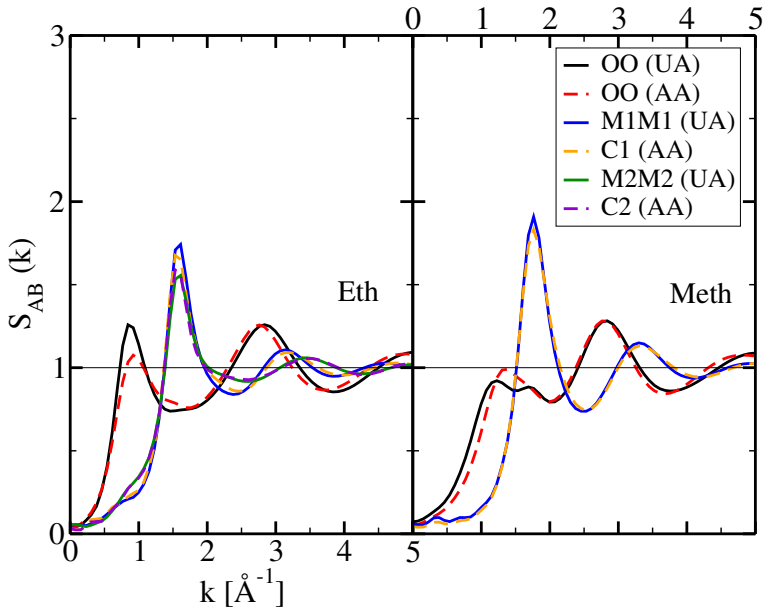

Figure A.5.: Selected site-site structure factors for pure ethanol (left panel) and pure methanol (right panel). The united atom (full lines) and all atom (dashed lines) are compared.

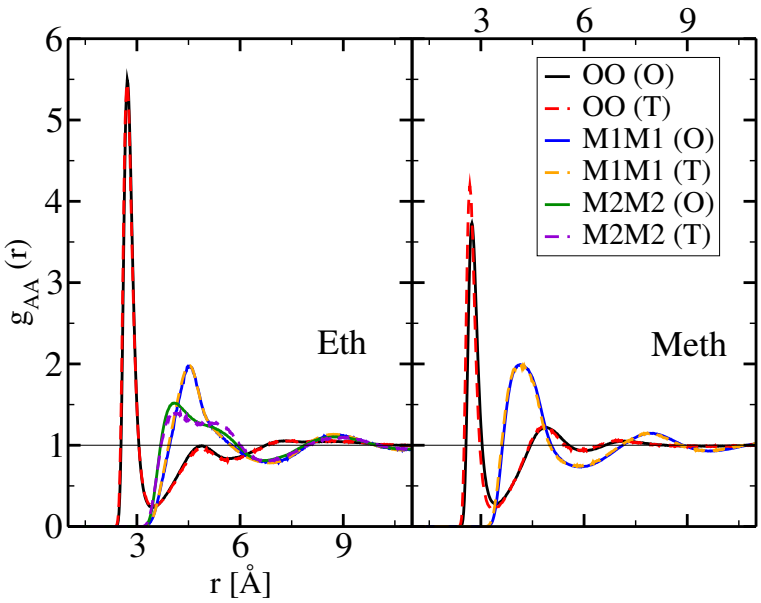

Figure A.6.: Selected site-site RDFs for pure ethanol (left panel) and pure methanol (right panel). The performance of OPLS-UA (full lines) and Trappe-UA (dashed lines) forcefields is compared.

Structure of higher mono-ols Figure A.7 shows characteristic site-site correlation functions and structure factors for three higher monools: 1-propanol, 2-propanol and *tert*-butanol.

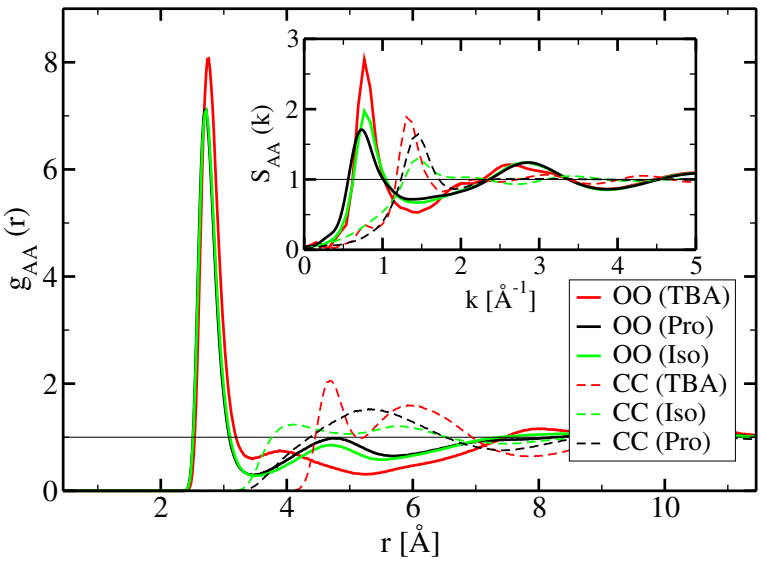

Figure A.7.: Selected site-site correlation functions (main panel) and structure factors (inset) for 1-propanol, isopropanol and tert-butanol. The color code for specific site-site combinations is contained in the legend.

The site-site combinations were OO and CC, where the carbon groups were the

second (central) methylene group for the propanols and the central carbon atom for TBA. The OO correlations for all alcohols feature a high and narrow first peak, typical for the Hbond, which increases with the size of the alcohol. These three alcohols have a bigger neutral group cargo attached to the hydroxyl group than ethanol and methanol; also, apart from the linear 1-propanol, the neutral tail is differently configured for the other two alcohols. The influence of the neutral tail, its size and compactness is reflected in the second neighbors (which is glaring for the case of TBA). The OO structure factors all feature prominent cluster peaks positioned at around $k \approx 0.7\,\mathring{A}^{-1}$, indicative of the cluster formations in these alcohols. The CC structure factors, as expected, have only a main peak, located between $k \approx 1.3 - 1.5\,\mathring{A}^{-1}$.

A.2.3.2. Diols

Diols are a subgroup of alcohols which are characterized by two hydroxyl groups and a hydrocarbon chain. We chose to look into diols whose hydroxyl groups are placed at the ends of the carbon chains, i.e. 1,2-ethanediol, 1,3-propanediol etc. The chosen forcefield was Trappe-UA [264]. In comparison with mono-ols, the diol family was less studied throughout the years. 1,2-ethanediol, also known as ethylene glycol, was investigated via classical computer simulations by several authors [17, 267, 268, 269], mostly focusing on the thermodynamics and short-range structuring in the liquid. All of the authors mentioned above used OPLS or OPLS-based forcefields [236, 265, 270] to model 1,2-ethanediol, which yield the same short-range structural features as the Trappe forcefield. In terms of the basic thermodynamic values, the Trappe-UA forcefield performs reasonably well, as evidenced in Table A.5.

Alcohol	Model	Density [kg/m^3]	Exp. Den. [kg/m^3]	H_{VAP} [kJ/mol]	Exp. H_{VAP} [kJ/mol]
1,2-ethanediol	Trappe-UA	1121 (+/- 4.8)	1113.5	81.52 (+/- 0.29)	63.9
1,3-propanediol	Trappe-UA	1031.42 (+/- 4.1)	1053.8	63.65 (+/- 0.32)	69.8
1,4-butanediol	Trappe-UA	998.2 (+/- 4.2)	1017.1	88.57 (+/- 0.39)	77.1
1,5-pentanediol	Trappe-UA	986.3 (+/- 3.6)	991.4	84.68 (+/- 0.40)	83.0

Table A.5.: Thermodinamical properties for tested diol forcefields. The experimental values at 25 °C are taken from [229].

A.2.4. Water

Over the last forty years, there have been many efforts to create explicit water models which would reproduce water's exact properties. These models widely differ in the number of sites, rigidity versus flexibility and the inclusion of polarizability. For our purposes, we have considered rigid, non-polarizable water models. These models describe water interactions in an approximate way and therefore can't reproduce *all* of the properties of water. However, the main goal was to repoduce the structural behavior of water at room temperature while keeping the computational costs reasonable.

Model	Density [kg/m^3]	Exp. Den. [kg/m^3]	H $_{VAP}$ [kJ/mol]	Exp. H $_{VAP}$ [kJ/mol]
SPC/e [177]	995.30 (+/- 6.2)	997.05	49.21 (+/- 0.16)	43.98
TIP4P2005 [178]	991.97 (+/- 8.2)		50.23 (+/- 0.22)	
TIP5P [237]	977.17 (+/- 12.1)		42.84 (+/- 0.38)	

Table A.6.: Thermodinamical properties for tested water forcefields. The experimental values at 25 °C are taken from [229].

The tested models are contained in Table A.6, along with the experimental results for selected thermodynamic values. The results are in line with those presented in Vega's work [271]. The results for the correlation functions (not shown here) are also consistent with those in [271].

A.2.5. Other neat liquids

The thermodynamic properties of miscellaneous neat liquids, along with the chosen forcefields, are catalogued in Table A.7. This category includes pentane and carbon tetrachloride, both of which were constituents of mixtures in Chapter 3. Heptane is another close relative, which has been mentioned in the context of the ethanol-heptane mixture in the Conclusion. The only associating compound in the bunch is propylamine, the structure of which is discussed at length in Chapter 7.

Compound	Model	Density [kg/m^3]	Exp. Den. [kg/m^3]	H_{VAP} [kJ/mol]	Exp. H_{VAP} [kJ/mol]
Pentane	OPLS-UA [142]	628.3 (+/- 6.7)	626.2	27.78 (+/- 0.37)	26.43
	TraPPe-UA [272]	614.5 (+/- 5.1)		29.55 (+/- 0.20)	
Heptane	TraPPe-UA [272]	682.6 (+/- 4.2)	679.5	43.82 (+/- 0.22)	36.57
CCl_4	OPLS-AA [182]	1536.3 (+/- 6.3)	1594.0	32.28 (+/- 0.28)	32.43
Propylamine	Gromos 53a6 [234, 273]	737.5 (+/- 3.2)	717.3	37.09 (+/- 0.22)	31.27

Table A.7.: Thermodynamic properties for tested forcefields. The experimental values at 25 °C are taken from [229].

A.2.6. Pyridine and piperidine

As mentioned in the Conclusion, simulations were performed for neat pyridine and piperidine, respectively. In the case of pyridine, the following forcefields were tested: OPLS-AA[232], TraPPe-AA [233] and Gromos-AA [234]. For piperidine, the available OPLS-AA [235] and OPLS-UA [236] models were tested. The calculated thermodynamic properties for those systems - volume and enthalpy of vaporization - are presented in Table Table A.8. Due to their performance, the TraPPe-AA model for pyridine and OPLS-UA model for piperidine were chosen for further simulations.

	Volume [cm^3/mol]	H_{VAP} [kJ/mol]
Pyridine		
OPLS - AA [232]	79.70 (+/- 0.25)	29.89 (+/- 0.31)
Trappe - AA [233]	81.00 (+/- 0.28)	38.94 (+/- 0.25)
Gromos - AA [234]	80.94 (+/- 0.21)	45.36 (+/- 0.21)
Experiment [229]	80.6	40.17
Piperidine		
OPLS - AA [235]	102.76 (+/- 0.36)	34.46 (+/- 0.37)
OPLS - UA [236]	99.72 (+/- 0.30)	38.07 (+/- 0.15)
Experiment [229]	98.78	39.25

Table A.8.: Thermodynamic results for neat compounds, both original and modified.

B. Supplementary simulation data for mixtures

B.1. Simulation protocol, system size and simulation time

The methodology for simulating neat liquids is applicable for binary mixtures as well. The program package and simulation protocol are the same. However, the addition of one more component adds another level of complexity to the mixture. The question of system size becomes much more imporant than for neat liquids.

For mixtures that fall into the category of simple disorder, system sizes of $N \sim 2000$ particles are sufficient for obtaining satisfactory results. Simple disorder systems have little to no interaction, and their are governed purely by entropic contributions. Thus, they have no discernable structural pattern on the local or global scale, and their correlation functions have the typical liquid-like behavior, with the first neighbour shell being the most pronounced, and subsequent shells diminishing until they reach unity. Naturally, they lack domain oscillations since there are no domains formed.

Complex disorder systems are more tricky. As the majority of complex mixtures involve more advanced structuring (either clustering or domain formation), it's advisable to opt for $N \sim$ 16k systems. That way, the box size length is doubled in comparison with the corresponding $N \sim$ 2k system, enabling better detection and sampling of large, globular domains.

The simulation time also an issue to consider. The occurrence and evolution of complex structuring inevitably imply that the dynamics of these objects has to be taken into account when simulating. These structures can have slow temporal fluctuations, so it's necessary to employ long equilibration times (at least 5 ns) and long production runs (5-10 ns) in order to better sample the system.

B.2. Mixtures with benzene as the common solvent

B.2.1. LP shift

The LP correction, described in subsection 2.2.1, is shown visually in the following Figures for selected binary mixtures. For the sake of convenience, the quantities presented are the site-site structure factor (main panel) and the rKBIs (inset). The curves are shown for both species and the cross. The corrected curves are in full lines, while the uncorrected curves are in dotted lines. This is also the format used for subsequent Figures demonstrating the LP correction.

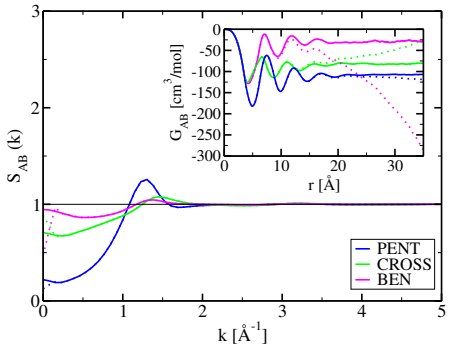

Figure B.1.: The LP correction for the benzene-pentane mixture, $x_{BEN} = 0.2$. Main panel: site-site structure factors for selected combinations, with full lines denoting the corrected curves, and the dottes ones the uncorrected curves. Inset: rKBIs for the same species combinations as in the main panel. The color code is in the legend of the Figure.

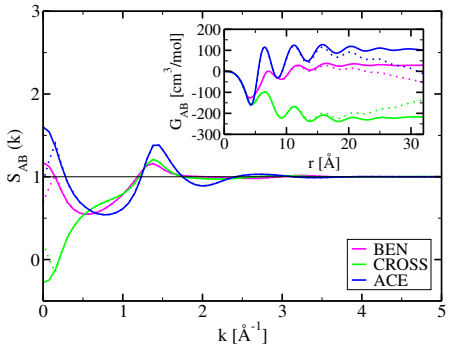

Figure B.2.: The LP shift demonstrated for the benzene-acetone mixture, $x_{BEN} = 0.5$. As in Figure B.1, the main panel contains the corrected (full lines) and uncorrected (dotted lines) site-site structure factors for selected site-site combinations. The inset shows the rKBIs for the same site-site combinations as in the main panel.

B.3. The ethanol-methanol mixture

B.3.1. LP shift

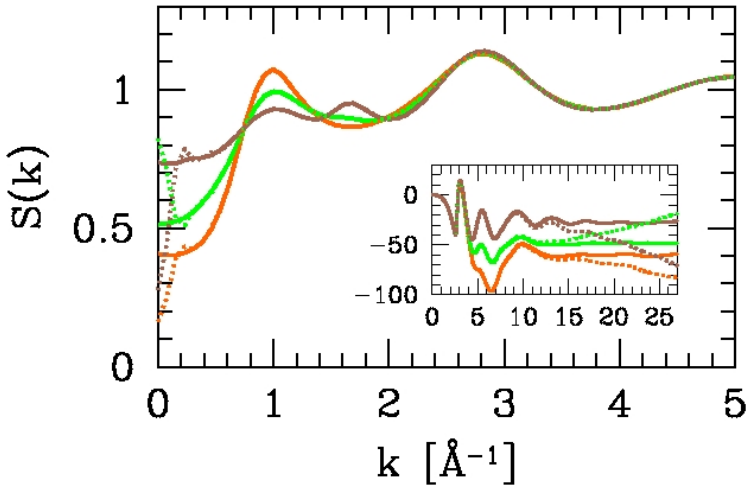

Figure B.3.: Structure factors (main panel) and rKBI (inset) for the equimolar ethanol-methanol mixture, demonstrating the LP correction. Methanol correlation is show in brown, ethanol in orange, and cross correlations in green. As always, the full lines are the corrected data, while the dotted ones are uncorrected data.

B.4. Aqueous alcohol mixtures in cold conditions

B.4.1. Simulations at low temperatures

Computer simulations are an excellent tool for investigating the behavior of liquid mixtures below the freezing point. It's difficult to obtain a crystalline phase below the experimental freezing point for aqueous mixtures [274, 275]. The crux lies in forming hydrogen bonded complexes with the correct crystalline symmetry, so one would have to use specific sampling techniques [275] or models [178]. Since we do not use such techniques here, we obtain supercooled and glassy phases for very low temperatures.

However, simulating liquid mixtures far below room temperature is demanding in other aspects. With the reduction in temperature comes the reduction in kinetic energy, so the particles will move sluggishly and it will take more time to properly sample the phase space. The existence of strong energetic interactions in the system (the Hbond, for example), will add an additional level of difficulty. When the particles are in a energetically favorable configuration, they will be less likely to break free out of it at low temperatures. The tendency to stay in those energetic

minimums hampers the exploration of the phase space, so a lot of time is necessary for adequate sampling. However, Figure B.4 and (Figure B.5) clearly show different configurations at different points in time, confirming that systems don't stay locked in the same place and will undergo their evolution with enough time.

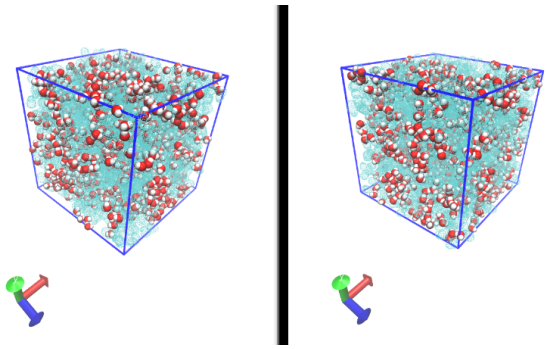

Figure B.4.: Snapshots of the equimolar ethanol-water system for $T = 200$ K, before and after a 5 ns run, taken under the same angle (as demonstrated by the lab frame arrows at the left lower corners). Water is highlighted with red and white balls, while ethanol is in transparent blue.

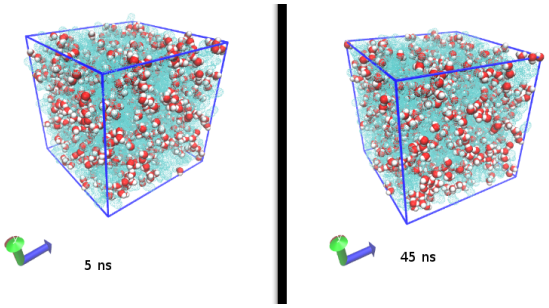

Figure B.5.: Snapshots of the equimolar ethanol water system at $T = 150$ K, taken 40 ns apart and at the same angle. As in the previous figure, water is highlighted with red and white balls, while ethanol is in transparent blue.

Along those notes - one of the potential pitfalls is the question of the starting configuration. When tackling a system with strong interactions, or a system which is confirmed to display MH at room temperature, it's advisable to start simulations from random configurations. That way, the system can evolve naturally at the low temperature. If one simulates an MH system at room temperature and then quenches it to a low temperature of choice, the system will have already formed domains and/or clusters. Since the system has found itself in an energetic minimum, it's questionable whether it will ever break out of it. That being said, in the case of cold aqueous alcohol mixture, we started simulating from random configurations.

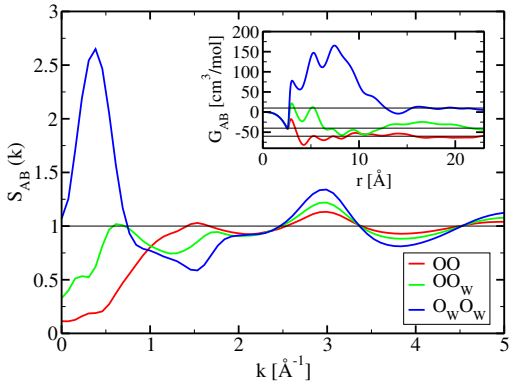

Figure B.6.: A detailed look at selected site-site structure factors (main panel) and rKBIs (inset) for the equilmolar ethanol-water mixture, at $T = 200$K. The color code is shown in the legend. The rKBIs are particularly interesting, for they show the stabilization of the curves around an asymptotic value.

B.4.2. Cluster distribution probabilities

Figure B.7 shows the cluster analysis for ethanol-water and TBA-water mixtures, organized as in Figure 6.3. As in the case of methanol-water, the cluster probabilities of ethanol-water are monotonous functions of cluster size. For the most part, TBA-water behaves exactly like that, with one exception - the cluster distribution TBA at $x_T = 0.8$ (Figure B.7, right image, upper right panel). There is a plateau-like feature for cluster sizes from 1 to 10 for the two lowest temperatures, which evolves into a tiny peak for T=250 K. Pure monool alcohols have a peak in their cluster probability distribution, centered around the size 4-6 [124, 125], which is a signature of their characteristic chains and rings. It seems like 80% tbutanol retains some such clusters, which account for the plateau and peak seen in Figure B.7.

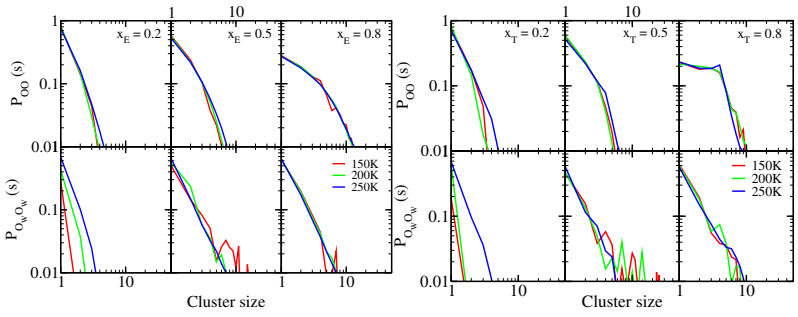

Figure B.7.: Cluster size distribution probabilities versus cluster size for the: aqueous ethanol (left panel) and aqueous- tert-butanol mixture (right panel). The cluster size distributions for alcohol sites (upper row) and water oxygen sites (lower row) are depicted for various temperatures (color code is in the legend). Three typical alcohol mole fractions are represented: 0.2 (left panel), 0.5 (middle panel) and 0.8 (right panel).

B.5. Propylamine-water mixture

B.5.1. LP shift

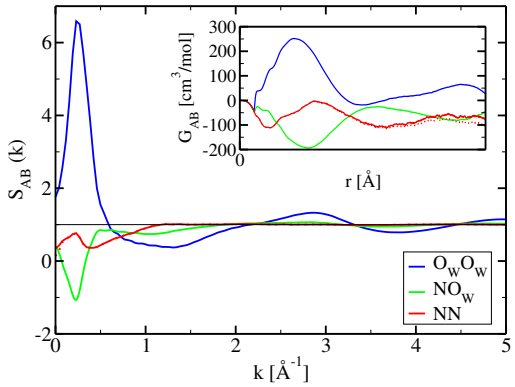

Figure B.8.: LP shift shown for aqueous propylamine, $x_{PROP} = 0.2$, for site-site structure factors (main panel) and rKBIs (inset). The water-water and cross correlations didn't need the LP correction done, but just the NN ones (dotted lines for the uncorrected data).

B.6. Mixtures with 1,n-diols

B.6.1. LP shift

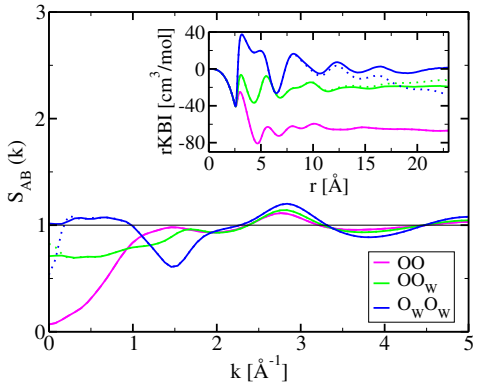

Figure B.9.: The LP shift, demonstrated for the equimolar mixture of 1,2-ethanediol-water. Main panel: site-site structure factors. Inset: rKBIs. The species are represented by the following color code: ethanediol - magenta; cross - green; water - blue. In the case of ethanediol's OO g(r), no correction was necessary. Otherwise, full thick lines represent the corrected data, while the dotted lines are uncorrected data.

B.6.2. Cluster distribution probabilities

Figure B.10 and Figure B.11 show the cluster distribution of the oxygen atoms inside the aqueous diol and ethanol-diol mixtures, respectively. The oxygen atoms of the diols are presented in the the main panel and the solvent oxygen atoms in the insets, all of them for 3 different diol mole fractions. Each figure contains curves with a decaying distribution, similar to what is seen in LJ systems [121, 123]. Unlike neat alcohols and alcohol-non-polar solvent systems, where the cluster distribution clearly has a peak denoting the higher probability of finding specific-sized clusters, the results for these mixtures are devoid of such a feature. Of course, this finding (or lack thereof) doesn't exclude MH, since aqueous-mono-ol mixtures are highly microheterogeneous and yet their structural make-up is not suitable for detection via cluster calculations.

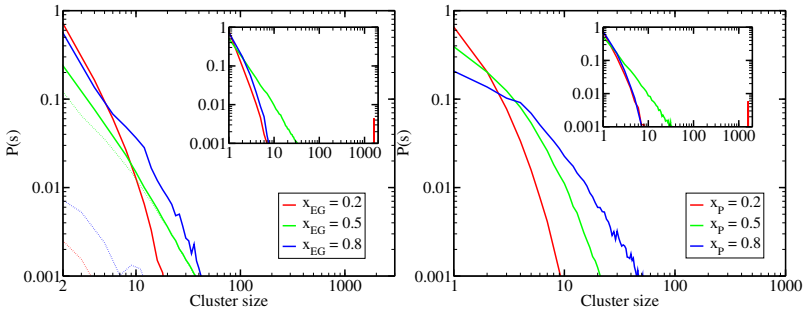

Figure B.10.: Clusters distributions of the diol oxygen sites (main panels) and water oxygen sites (insets), versus the cluster size. Results for ethanediol are shown in the left panel, and results for 1,3-propanediol in the right panel. The diol concentrations are shown in red for x = 0.2, green for x = 0.5 and blue for x = 0.8.

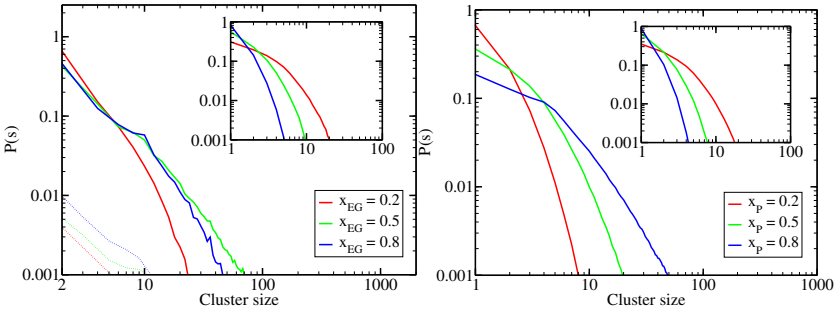

Figure B.11.: Clusters distributions of the diol oxygen sites (main panels) and ethanol oxygen sites (insets), versus the cluster size. Results for ethanediol are shown in the left panel, and results for 1,3-propanediol in the right panel. The diol concentrations are shown in red for x = 0.2, green for x = 0.5 and blue for x = 0.8.

B.6.3. Thermodynamic results

In Figure B.12 we present the thermodynamic results for 1,n-diol mixtures. The molar volumes are contained in the upper row, while the enthalpies of vaporization are in the lower row. Experimental data for all of these mixtures was scarce. The only relevant data were the total densities of the mixtures [276, 277, 278, 279], which are depicted with thick black lines in Figure B.12. As we can see, the simulated molar volumes agree well with the experimental data, confirming that the Trappe forcefield is successful in reproducing this property of 1,n-diol mixtures. The enthalpies of vaporization for water or ethanol mixtures with a given diol are close together in values and have a similar trend. It's important to note that the H_{VAP} of diols is higher than those of water and ethanol (i.e. the potential energy is more negative). That implies that two bound hydroxyl groups exert a big influence over the energetics of the system and are most likely responsible for the sluggishness of these systems.

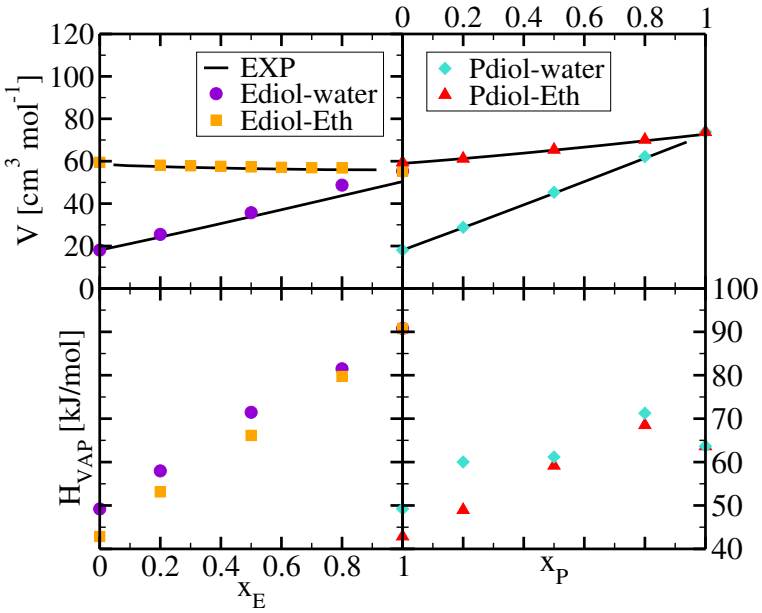

Figure B.12.: Thermodynamic properties for mixtures with 1,n-diols. Volumes are contained in the upper two panels, enthalpies of vaporization in the lower two. Black lines represent experimental data [276, 277, 278, 279], purple circles aqueous-ethanediol, gold squares ethanol–ethanediol, cyan diamonds aqueous–propanediol and red triangles ethanol–propanediol.

Summary

The topic of this thesis is to analyze the rich variety of disorder present in liquids. The majority of the research features binary mixtures involving at least one hydrogen bonding component. Hydrogen bonding liquids, such as water or alcohols fall into the category of complex liquids. The mixtures of water and alcohol are notorious for being micro-heterogeneous (MH), *i.e.* their components are segregated at the molecular level [186, 187]. While there is a substantial body of work on the topic of simple liquids (the typical example being liquid argon) [1, 11], it is not so with complex liquids and their mixtures. A good number of authors in the field focus on thermodynamic or transport properties [16, 20, 58, 60, 61, 62, 63, 64], and if they work on the structural organization in liquids, these investigations are usually limited to the short range organization [18, 19, 22, 59, 128]. The novelty of the work in this thesis is that it pays particular attention to the medium to long range ordering. The main goal is to connect the nature of the atom-atom interactions in the molecular species to the diversity of the supra-molecular structuring formed inside various mixtures. The methods of statistical physics are employed in this research, and it's shown that the same statistical tools used to study simple liquids can give new information and perspectives on the complexity present in binary mixtures.

This wealth of information on studied binary systems is accessed via molecular dynamics (MD) simulations [67], which were performed in the program package Gromacs [110]. A general theoretical introduction into MD and important results from statistical physics as well as a description of the methods used are contained in Chapter 2. An in-depth discussion of relevant simulation details can be found in Appendices A and B, for neat liquids and liquid mixtures, respectively.

The first important concept of this thesis, that of simple and complex disorder in mixtures, is presented in Chapter 3 [72]. It is described through binary mixtures with benzene as the common solvent, where the co-solvents are molecules of different physico-chemical characteristics (alkanes as inert, neutral molecules; acetone as a dipolar molecule; ethanol as an Hbonding molecule). Benzene, modeled as a simple liquid, enabled us to see more clearly the effects produced by the solute molecules, which was very challenging in the case of aqueous mixtures [148, 149, 189]. Based on the structural anaysis, as well as the KBI results, the three different mixtures could be categorized in the following way. The benzene-alkane system is an example of simple disorder, where the components have similar interactions and the mixture as a whole has near ideal concentration fluctuations (CF) and no noticeable local or global ordering. The benzene-acetone system is a regular mixture, as it possesses

short range ordering and its CF deviate from the ideal case, due to acetone's dipolar interactions. The benzene-ethanol mixture falls into the category of complex disorder. Ethanol's Hbond interactions drive the extensive clustering and domain formation, which can be detected in site-site structure factors as pre-peaks at small k values. Also, the CF in this system are large and vary strongly with concentration. Apart from defining various types of mixtures, these results have shown that interactions are paramount. In this case, it's the interactions between one species that generate complex disorder and subsequently MH, while the influence of the molecular shape of the inert solvent is almost negligible. This study demonstrates the importance of observing structuring over the entire k range, and not only at $k = 0$.

Chapter 4 deals with the concept of ideal mixtures, studied through the perspective presented in Chapter 3 [73]. The main focus is placed on the mixture of methanol and ethanol, which is a textbook example of an ideal mixture. The structural analysis has shown a rich organization in this mixture, driven by the hydroxyl group and its tendency to form Hbonded clusters. These clusters are built indiscriminately by the hydroxyl groups of both alcohols, which is witnessed in the results of the cluster probability distributions, but also in the site-site structure factors. In the latter, there is a pre-peak at $k \approx 0.9$ Å which we've called the cluster peak, due to its origin. Because of those structural features, the ethanol-methanol mixture differs considerably from simple disorder, even though it has near ideal CF. Since the constituents of this mixture have identical interactions which promote cluster formation, it is possible to attain this apparent thermodynamical ideality.

In Chapter 5 we further the notions of complex disorder by analyzing and comparing two binary mixtures with ethanol: ethanol-water and ethanol-non-polar solvent [74]. We uncover key differences in the formation and detection of domains in their structuring. In neat alcohols, the hydroxyl group drives the clustering into chains and loops [155, 161, 162, 169, 170], which persist even when molecules of non-polar solvent are added [174, 175]. In the latter case, as more and more non-polar solvent is added, alcohol clusters will form domains. These domains are detectable through both structure factor and cluster distribution analysis, as the domains are reducible to the clusters that build them. On the other hand, in alcohol-water mixtures, domains at low alcohol content are formed by a completely different mechanism (a variant of the hydrophobic effect), thus being noticeable solely through a pre-peak in the site-site stucture factors. Cluster probability distributions, which in this case show results similar to a simple liquid, are not a suitable tool for uncovering domains which are not reducible to clusters.

Chapter 6 deals with the temperature dependance of the structural properties in aqueous mono-ol mixtures. Three mixtures: methanol-water, ethanol-water and *tert*-butanol-water are studied in cold conditions [75, 76]. These aqueous alcohol mixtures all share common traits, such as the decrease in CF with the lowering of temperature, visible from the ideal behavior of the calculated KBIs. With the drop

in temperature, the fuzzy domains which are characteristic of room temperature aqueous alcohols have turned into more defined objects. This is the most apparent for TBA-water, where at high alcohol content linear water clusters can be observed. There is a transfer of fluctuations from $k = 0$ to small k, which enforces the notion of analyzing the structuring over the entire k range.

Chapters 7 and 8 explore mixtures with different types of co-solvents. In Chapter 7, the focus is on propylamine and its aqueous mixture [77]. Propylamine is an amphiphilic compound, just like alcohols, but it has the amine (NH_2) functional group. The two donors and one acceptor in the functional group mean more bonding choices. Its consequences are visible in neat propylamine as the occurrence of branched chains, whereas in alcohols we have linear chains. The aqueous propylamine mixture shares some common traits with aqueous alcohol mixtures, such as the trends in the pair correlation functions. The site-site structure factors of propylamine mirrow the behavior of those of ethanol. However, the main difference comes from the behavior of water. In aqueous propylamine, water displays a duality of structuring. It forms bulky domains up to $x_P = 0.3$, which have a signature of a domain pre-peak in the oxygen-oxygen structure factor. After $x_P = 0.3$, linear clusters of water occur, which lead to smaller structure factor pre-peaks and near ideal KBI.

Chapter 8 discusses diol alcohols, both as neat liquids [78] and in mixtures [79]. Neat 1,n-diols display clustering similar to neat mono-ols, even though it's less prominent, as shown through several structural features. The highlight of the chapter are the calculated scattering intensities for the four 1,n-diols studied. Mono-ol alcohols have a pre-peak at about $k_P \approx 1$ Å^{-1} in their scattering intensities, which is a signature of the hydroxyl group clustering [153, 155, 161, 169, 173, 170]. Diols, on the other hand, have a shoulder-like feature at the same position, which may seem strange in light of the chains present in 1,n-diols [210]. This peculiar result is due to the carbon chains in 1,n-diols, which act as a constraint, forcing the carbon sites' contributions to the scattering intensity to fall at various k values which lie between the main peak and the pre-peak. This broadening at the main peak seems to mask the signal of the pre-peak.

Binary mixtures of 1,n-diols with either water or ethanol were reported as well. Diol alcohols exhibit a duality of behavior in the short range structuring, depending on the nature of the other component in the mixture. In mixtures with water, they behave as a typical mono-ol [17, 59], while in mixtures with mono-ols, the diol takes over the role of water, which is confirmed by pair correlation functions. However, mixtures with diols exhibit small concentration fluctuations, as evidenced by the KBIs, which is a departure from aqueous alcohols. There are no signatures of domain pre-peaks in the site-site structure factors, but more of a flattening of the *S(k)*. This absence of a pre-peak in *S(k)* as a signature of the Lifshitz state, which is a new form of disorder, an intermediate state between random disorder and domain order, in a globally disordered homogeneous liquid.

The conclusion is presented in Chapter 9, where the most salient points of the thesis are synthetized. Also, there is a short exposition of other projects, some of which couldn't be completed for computational or modeling reasons, while others went beyond the temporal limits of this thesis. Finally, further perspectives are discussed, especially those pertaining to biophysics. The physical background behind the structuring in liquids and macromolecular assemblies is the same. Understanding the structuring in liquids could be a stepping stone towards understanding the processes of biomacromolecules and perhaps formulating the theoretical approaches from the point of view of site-site interactions.

Sažetak

Tema ovog doktorskog rada je analiza različitih vrsta uređenja prisutnih u tekućinama. Glavnina istraživanja se bavi binarnim mješavinama koje imaju barem jednu asocijativnu komponentu, tj. koja može tvoriti vodikovu vezu. Asocijativne tekućine, kao što su voda ili alkoholi, spadaju u kompleksne tekućine. Mješavine vode i alkohola su poznate po svojstvu mikro-heterogenosti (MH) - njihove komponente su segregirane na molekularnoj razini [186, 187]. Postoji mnogo literature na temu jednostavnih tekućina (tipičan primjer je tekući argon) [1, 11], dok se isto ne može reći za kompleksne tekućine i njihove mješavine. Veliki broj autora u ovom polju se usredotočuje na termodinamička i transportna svojstva mješavina [16, 20, 58, 60, 61, 62, 63, 64], a ukoliko se bave strukturnom organizacijom, te studije su ograničene na kratkodosežno uređenje [18, 19, 22, 59, 128]. Novost rada predstavljenog u ovoj tezi se očituje u proučavanju dugodosežne organizacije u kompleksnim mješavinama. Glavni cilj je povezati atom-atom interakcije u molekulama s raznolikošću supramolekularnog strukturiranja u različitim mješavinama. U ovom istraživanju su korištene metode statističke fizike te je pokazano da isti statistički alati koji se koriste za opis jednostavnih tekućina mogu dati nove informacije i perspektive o kompleksnosti u binarnim mješavinama.

Tekuće mješavine su se proučavale simulacijama molekulske dinamike (MD) [67], koje su se izvršavale u programskom paketu Gromacs [110]. Opći teoretski uvod u MD i važni rezultati statističke fizike, kao i opis korištenih metoda, su sadržani u Poglavlju 2. Detaljnija diskusija oko relevantnih simulacijskih detalja za čiste tekućine i mješavine se nalazi u Dodacima A i B.

Prvi važan koncept u ovoj tezi je jednostavni i kompleksni nered u mješavinama, koji je predstavljen u Poglavlju 3 [72]. Opisan je kroz binarne mješavine s benzenom kao zajedničkim otapalom, dok su otopljene tvari molekule različitih kemijsko-fizikalnih svojstava (alkani kao inertne, neutralne molekule; aceton kao dipolarna molekula; etanol kao asocijativna molekula). Benzen, modeliran kao jednostavna tekućina, je omogućio da jasnije vidimo efekte otopljenih tvari, što je bilo jako izazovno u slučajevima vodenih mješavina [148, 149, 189]. Na temelju strukturne analize, kao i rezultata Kirkwood-Buff integrala (KBI), te tri različite mješavine se mogu kategorizirati na sljedeći način. Sustav benzen-alkan je primjer jednostavnog nereda, jer komponente imaju slične interakcije, a mješavina kao takva ima gotovo idealne koncentracijske fluktuacije (KF), a nema primjetno lokalno ili globalno uređenje. Benzen-aceton je primjer regularne mješavine, jer ima kratkodosežno uređenje, a KF odudaraju od idealnog slučaja zahvaljujući acetonovim dipolarnim interakci-

jama. Benzen-etanol spada u kategoriju kompleksnog nereda. Etanolove vodikove veze promoviraju klasteriranje i formaciju domena, koje se mogu detektirati kao *pre-peakovi* na malim k vrijednostima u *site-site* strukturnim faktorima. Također, KF u ovom sustavu su velike i snažno ovise o koncentaciji komponenti. Osim što su se definirali različiti tipovi mješavina, ovi rezultati su pokazali da su interakcije od presudne važnosti. Interakcije između jedne vrste su te koje generiraju kompleksni nered i MH, dok je utjecaj molekularne topologije inertnog otapala gotovo zanemariv. Ova studija pokazuje koliko je važno promatrati strukturiranje preko cijelog k prostora, a ne samo u $k = 0$.

Poglavlje 4 se bavi konceptom idealnih mješavina, koje proučavamo kroz perspektivu Poglavlja 3 [73]. Glavni fokus je na sustavu metanol-etanol, koja je udžbenički primjer idealne mješavine. Strukturna analiza pokazuje bogatu organizaciju prisutnu u ovom sustavu, promoviranu od strane hidroksilne skupine i njene tendencije da stvara klastere kroz vodikovu vezu. Klastere grade hidroksilne grupe oba alkohola, bez obzira kojem alkoholu pripadaju, što se vidi u rezultatima distribucije vjerojatnosti klastera, ali i *site-site* strukturnih faktora. U potonjima postoji pre-peak na lokaciji $k \approx 0.9$ Å kojeg smo, zbog svog porijekla, nazvali klaster *peak*. Zbog tih strukturnih značajki, sustav metanol-etanol se znatno razlikuje od jednostavnog nereda, iako ima gotovo idealne KF. Budući da komponente mješavine imaju identične interakcije koje promoviraju klasteriranje, moguće je dobiti prividnu termodinamičku idealnost.

U poglavlju 5 produbljujemo ideje kompleksnog nereda kroz analizu i usporedbu dva sustava s etanolom: etanol-voda i ethanol-nepolarno otapalo [74]. Otkrivamo ključne razlike u stvaranju i detektiranju domena u tim mješavinama. U čistim alkoholima, hidroksilna skupina promovira klasteriranje u lance i petlje [155, 161, 162, 169, 170], koji opstaju i kad se dodaju molekule nepolarnog otapala [174, 175]. U potonjem slučaju, povećavanje molarnog udjela nepolarnog otapala dovodi do toga da se klasteri alkohola organiziraju u domene. Te domene se mogu detektirati kroz strukturne faktore, ali i kroz distribucije vjerojatnosti klastera, jer se domene alkohola mogu reducirati na klastere od kojih su izgrađene. U mješavinama alkohol-voda pri niskim udjelima alkohola, domene alkohola se formiraju posve drukčijim mehanizmom (varijanta hidrofobnog efekta). Stoga, te domene imaju svoj potpis u *site-site* strukturnim faktorima, ali ne i u distribucijama vjerojatnosti klastera. Račun klastera nije pogodan za otkrivanje domena koje se ne mogu reducirati na klastere, što je slučaj kod alkohola-vode.

Poglavlje 6 se bavi temperaturnom ovisnosti strukturnih svojstava u mješavinama mono-ola s vodom. Tri sustava: metanol-voda, ethanol-voda i *tert*-butanol-voda su ispitivana pri niskim temperaturama [75, 76]. Ove tri vodene mješavine imaju slične karakteristike, poput smanjenja koncentracijskih fluktuacija sa smanjenjem temperature, što se vidi iz gotovo idealnog ponašanja KBI-jeva. Sa spuštanjem temperature, *fuzzy* domene, koje su tipične za mješavine voda-alkohol pri sobnoj

temperaturi, postaju puno definiraniji objekti. Ovo je najočitije za *tert*-butanol-vodu, gdje se mogu vidjeti linearni klasteri vode za visoke koncentracije alkohola. Postoji transfer fluktuacija od $k = 0$ do malog k, koji potvrđuje ideju da je strukturiranje potrebno analizirati preko čitavog raspona k prostora.

Poglavlja 7 i 8 istražuju mješavine s otapalima koje nisu mono-olni alkoholi. U Poglavlju 7, žarište je na propilaminu i njegovoj vodenoj otopini [77]. Propilamin je amfifilna molekula, baš kao i alkoholi, no ima amino (NH_2) funkcionalnu skupinu. Dva donora i jedan akceptor u funkcionalnoj skupini impliciraju više mogućnosti za ostvarenje vodikove veze. Posljedice toga su vidljive u čistom propilaminu kroz pojavu razgranatih lanaca, dok su u mono-olima lanci linearni. Mješavina propilamin-voda dijeli zajedničke značajke s mješavinama vode i alkohola, poput trenda ponašanja dvočestičnih korelacijskih funkcija. Također, *site-site* strukturni faktori propilamina zrcale one etanola u vodenoj mješavini. No, glavna razlika je u ponašanju vode. Kod propilamina-vode, voda se organizira dvojako. Do $x_P = 0.3$, voda gradi globularne domene koje imaju svoj potpis u obliku domenskog *pre-peaka* u kisik-kisk strukturnim faktorima. Nakon $x_P = 0.3$, pojavljuju se linearni klasteri vode, koji povlače za sobom manje *pre-peakove* u strukturnima faktorima i gotovo idealne KBI-jeve.

Poglavlje 8 govori o diolnim alkoholima, kako u čistoj formi [78], tako i u mješavinama [79]. Čisti 1,n-dioli pokazuju klasteriranje slično kao u čistim mono-olima, iako nekoliko strukturalnih rezultata pokazuje da je nešto manje izraženo. Glavni rezultat ovog poglavlja su izračunati intenziteti raspršenja za predstavljena četiri 1,n-diola. Mono-oli imaju *pre-peak* lociran oko $k_P \approx 1$ Å^{-1} u svojim intenzitetima raspršenja, što je potpis klasteriranja hidroksilnih grupa u lance i prstene [153, 155, 161, 169, 173, 170]. Dioli, pak, na istom k položaju imaju samo "rame" u izračunatom intenzitetu, što je pomalo začuđujuće zbog prisustva klastera u čistim 1,n-diolima [210]. No, taj neobični rezultat je posljedica lanca metilenskih grupa koje povezuju dvije hidroksilne skupine u molekuli diola, koji djeluju kao veza. Doprinosi CH_2 *siteova* intenzitetu raspršenja padaju na različite k vrijednosti između glavnog *peaka* i *pre-peaka*, što u konačnici rezultira proširenjem glavnog *peaka* i maskiranjem signala *pre-peaka.*

Drugi dio poglavlja se odnosi na mješavine 1,n-diola s vodom odnosno etanolom. Diolni alkoholi pokazuju dualnost ponašanja u kratkodosežnom strukturiranju, ovisno o prirodi druge komponente u mješavini. U mješavinama s vodom, dioli se ponašaju kao tipični mono-oli [17, 59], dok u mješavini s etanolom, dioli preuzmu ulogu vode, što je potvrđeno kroz dvočestične korelacijske funkcije. Rezultati KBI-jeva pokazuju male koncentracijske fluktuacije za sustave s diolima, što je u raskoraku s ponašanjem vodenih mješavina mono-ola. *Site-site* strukturni faktori diolnih mješavina nemaju domenski *pre-peak*, već postaju plosnati prema $k = 0$. Odsustvo *pre-peaka* u $S(k)$ je znak Lifshitz stanja - nove vrste nereda, koja predstavlja stanje između nasumičnog nereda i domenskog reda.

Zaključak je predstavljen u Poglavlju 9, gdje su sažete najzanimljivije točke ove

teze. Nakon toga, ukratko su predstavljeni drugi projekti, neki od kojih nisu bili dovršeni zbog poteškoća s modeliranjem ili računanjem ili su pak prešli vremensko trajanje ove teze. Nadalje, govori se o perspektivama koje otvara ovaj rad, naročito u polju biofizike. Fizikalna pozadina iza strukturiranja u tekućinama i formiranja makromolekula je ista. Razumijevanje strukturiranja u tekućinama može biti korak naprijed prema razumijevanju biomakromolekularnih procesa i formuliranju teoretskih pristupa iz perspektive atom-atom interakcija.

Resumé

Le but de cette thèse est d'analyser la riche variété de désordres présents dans les liquides. La majorité de la recherche comporte des mélanges binaires avec au moins un composant de liaison hydrogène. Les liquides à liaison hydrogène, tels que l'eau ou les alcools, entrent dans la catégorie des liquides complexes. Les mélanges d'eau et d'alcool sont connus pour être micro-hétérogènes, c'est-à-dire que leurs composants sont ségrégés au niveau moléculaire [186, 187]. Bien qu'il existe un corpus important sur le sujet des liquides simples (l'exemple typique étant l'argon liquide) [1, 11], il n'en va pas de même pour les liquides complexes et leurs mélanges. Un bon nombre d'auteurs dans le domaine se concentrent sur les propriétés thermodynamiques ou de transport [16, 20, 58, 60, 61, 62, 63, 64] et, s'ils travaillent sur l'organisation structurelle dans les liquides, ces investigations se limitent généralement à l'organisation à courte portée [18, 19, 22, 59, 128]. La nouveauté du travail dans cette thèse est qu'il porte une attention particulière à l'organisation à moyenne et longue portée. L'objectif principal est de relier la nature des interactions atome-atome chez les espèces moléculaires à la diversité de la structuration supramoléculaire formée dans différents mélanges. Les méthodes de physique statistique sont employées dans cette recherche et nous montrons que les mêmes outils statistiques utilisés pour étudier des liquides simples peuvent donner de nouvelles informations et perspectives sur la complexité présente dans les mélanges binaires.

Cette mine d'informations sur les systèmes binaires étudiés est accessible au travers des simulations de dynamique moléculaire (MD) [67] effectuées dans le logiciel Gromacs [110]. On trouvera au Chapitre 2 une introduction théorique générale à la MD et des résultats importants de la physique statistique, ainsi qu'une description des méthodes utilisées. On trouvera en annexes A et B une analyse approfondie des détails pertinents spécifiques à la simulation pour les liquides purs et les liquides mélanges, respectivement.

Le premier concept important abordé dans cette thèse, concerne les notions de désordre simple et complexe dans les mélanges, tel qu'elles sont présentées au Chapitre 3 [72]. Ces notions sont introduites par l'étude des mélanges binaires avec le benzène comme solvant commun, les co-solvants étant des molécules de caractéristiques physico-chimiques différentes (les alcanes en tant que molécules neutres inertes, l'acétone en tant que molécule dipolaire, l'éthanol en tant que molécule faisant les liaisons hydrogène). Le benzène, modélisé comme un liquide simple, nous a permis de voir plus clairement les effets produits par les molécules de soluté, ce qui est très difficile dans les mélanges aqueux, à cause de la nature de la ségrégation. Sur la base

de l'analyse structurelle, ainsi que des résultats des Kirkwood-Buff intégrales (KBI), les trois mélanges différents pourraient être classés de la manière suivante. Le système benzène-alcane est un exemple de désordre simple, dans lequel les composants ont des interactions similaires, le mélange a des fluctuations de concentration (CF) quasi-idéales, et aucune organisation locale ou globale notable n'apparait. Le système benzène-acétone est un mélange régulier, car il possède une organisation à courte distance et ses CF s'écartent du cas idéal, en raison des interactions dipolaires de l'acétone. Le mélange benzène-éthanol relève de la catégorie de désordre complexe. La liaison hydrogène de l'éthanol est à l'origine du regroupement et de la formation de domaines importants, qui peuvent être détectés dans les facteurs de structure *site-site* sous la forme de pré-pics à des petits k. De plus, les CF dans ce système sont importantes et varient fortement avec la concentration. Outre la définition de différents types de mélanges, ces résultats ont montré l'importance capitale des interactions de type association. Ce sont ces dernières qui génèrent un désordre complexe et la MH, alors que l'influence de la forme moléculaire du solvant inerte est presque négligeable. Cette étude démontre l'importance d'observer la structure sur toute la gamme k, et pas seulement à $k = 0$.

Le Chapitre 4 traite du concept de mélanges idéaux, étudiés à partir de la perspective présentée au Chapitre 3 [73]. L'accent est mis sur le mélange méthanol-'éthanol, qui est un exemple classique de mélange idéal. L'analyse structurale de ce mélange a montré une organisation riche, induite par le groupe hydroxyle et sa tendance à former des agrégats *(clusters*). Ces agrégats sont construits par les groupes hydroxyles sans distinction entre les deux alcools, comme en témoignent les résultats des distributions de probabilité des *clusters*, mais aussi les facteurs de structure *site-site*. Dans ce dernier cas, il y a un pré-pic à $k \approx 0.9$ Å que nous avons appelé le pic de *cluster*, en raison de son origine. Grâce à ces caractéristiques structurelles, le mélange éthanol-méthanol diffère considérablement du simple désordre, même s'il a les CF proche de l'idéal. L'idéalité thermodynamique n'est donc qu'apparente, puisque les constituants de ce mélange ont des interactions fortent qui favorisent la formation des *clusters,* et donc une forte hétérogénéité dans la distribution moléculaire.

Au Chapitre 5, nous approfondissons les notions de désordre complexe en analysant et en comparant deux mélanges binaires avec l'éthanol: éthanol-eau et éthanol-solvant non polaire [74]. Nous découvrons les principales différences dans la formation et la détection des domaines dans leur structuration. Dans les alcools purs, le groupe hydroxyle entraîne le regroupement en chaînes et en boucles [155, 161, 162, 169, 170], qui persistent même lorsque des molécules de solvant non polaire sont ajoutées [174, 175]. Dans ce dernier cas, au fur et à mesure de l'ajout de solvant non polaire, on observe la formation de domaines de *clusters* d'alcool. Ces domaines sont détectables grâce à l'analyse des facteurs de structure et de la distribution des *clusters*, car les domaines sont réductibles aux *clusters* qui les construisent. D'autre part, dans les mélanges alcool-eau, les domaines à faible concentration de l'alcool sont formés par un mécanisme complètement différent (une variante de l'effet hy-

drophobe), perceptible uniquement par un pic des facteurs de structure *site-site*. Les distributions de probabilités des *clusters*, qui dans ce cas montrent des résultats similaires à un liquide simple, ne constituent pas un outil approprié pour découvrir des domaines qui ne sont pas réductibles aux *clusters*.

Le Chapitre 6 traite de la dépendance en température des propriétés structurelles dans les mélanges alcool-eau. Trois mélanges: méthanol-eau, éthanol-eau et *tert*-butanol-eau sont étudiés en conditions froides [75, 76] pour des températures bien en dessous de celle ambiante. Ces mélanges d'alcools aqueux ont tous des traits communs, tels que la diminution des CF avec l'abaissement de la température, visible d'après le comportement idéal des KBI calculés. Avec la chute de température, les domaines peu définis, qui sont une caractéristiques des alcools aqueux à température ambiante, deviennent des objets plus définis, tels que des agrégats linéaires. Ceci est le plus apparent pour l'eau à *tert*-butanol, où des *clusters* d'eau linéaires à haute concentration en alcool peuvent être observées. Il y a un transfert de fluctuations de $k = 0$ à petit k, ce qui renforce la notion d'analyse de la structure sur toute la gamme k.

Les Chapitres 7 et 8 explorent des mélanges avec différents types de co-solvants. Au Chapitre 7, l'accent est mis sur la propylamine et son mélange aqueux [77]. La propylamine est un composé amphiphile, tout comme les alcools, mais elle possède le groupe fonctionnel amine (NH_2). La présence des deux donneurs et d'un accepteur dans le groupe fonctionnel impliquent plus de choix de liaisons hydrogène. Ses conséquences sont visibles dans la propylamine pure lors de l'apparition de chaînes ramifiées, alors que dans les alcools, nous avons des chaînes linéaires. Le mélange aqueux de propylamine partage certains traits communs avec les mélanges d'alcool aqueux, tels que les tendances dans les fonctions de corrélation de paires. Les facteurs de structure *site-site* de la propylamine reflètent le comportement de ceux de l'éthanol. Cependant, la principale différence provient du comportement de l'eau. Dans la propylamine aqueuse, l'eau présente une dualité de structuration. Il forme des domaines globuleux allant jusqu'à la concentration en propylamine $x_P = 0{,}3$, et qui ont une signature de domaine pré-pic dans le facteur de structure oxygène-oxygène. Au delà de $x_P = 0{,}3$, des *clusters* linéaires d'eau se produisent, ce qui conduit à des facteur de structure moins structurés et à un KBI proche de l'idéal.

Le Chapitre 8 traite des di-alcools (diols), à la fois en tant que liquides purs [78] et en mélanges [79]. 1,n-diols purs présentent un regroupement similaire aux mono-ols purs, même s'il est moins proéminent, comme le montrent plusieurs caractéristiques structurelles. Les points forts du chapitre sont les intensités de diffusion calculées pour les quatre 1,n-diols étudiés. Les alcools mono-ol ont un pré-pic environ $k_P \approx 1$ $Å^{-1}$ dans leurs intensités de diffusion, qui est une signature du groupement hydroxyle en chaînes et boucles [153, 155, 161, 169, 173, 170]. Les diols, par contre, présentent une caractéristique d'épaulement du facteur de structure à la même position, ce qui peut paraître étrange prenant en considération les chaînes présentes dans 1,n-diols [210]. Ce résultat particulier est dû aux chaînes de carbone dans 1,n-diols,

qui agissent comme une contrainte, forçant les contributions des sites de carbone à l'intensité de diffusion à tomber à différentes valeurs k qui se situent entre le pic principal et le pré-pic. Cet élargissement au pic principal semble masquer le signal du pré-pic.

Des mélanges binaires de 1,n-diols avec de l'eau ou de l'éthanol ont également été étudiés. Les diol alcools présentent une dualité de comportement dans la structuration à courte distance, en fonction de la nature de l'autre composant dans le mélange. Dans les mélanges avec de l'eau, ils se comportent comme un mono-ol [17, 59], alors que dans les mélanges avec les mono-ol, le diol joue le rôle de l'eau, ce qui est confirmé par les fonctions de corrélation des paires. Cependant, les mélanges avec des diols présentent de faibles CF, comme en témoignent les KBI, ce qui constitue un écart par rapport aux mono-ols aqueux. Il n'y a pas de signatures de pré-pics de domaine dans les facteurs de structure *site-site*, mais plutôt un aplatissement du $S(k)$. Cette absence de pré-pic dans $S(k)$ est une signature de *l'état de Lifshitz*, qui est une nouvelle forme de désordre que nous avons introduite - un état intermédiaire entre désordre simple et ordre de domaine, dans un liquide homogène globalement désordonné.

La conclusion est présentée au Chapitre 9, où les points les plus marquants de la thèse sont mis en avant. En outre, nous avons ajouté une courte présentation d'autres projets, dont certains n'ont pas pu être complétés pour des raisons de temps de calcul ou de modélisation, tandis que d'autres dépassaient les limites temporelles de cette thèse. Enfin, d'autres perspectives sont discutées, en particulier celles concernant la biophysique. La physique derrière la structuration dans les assemblages liquides et macromoléculaires reste la même. La compréhension de la structuration dans les liquides pourrait être un tremplin pour comprendre les processus incluant des biomacromolécules et aider à formuler les approches théoriques de ces systèmes, de la perspective des interactions atome-atome.

List of Figures

1.1. The 2D structures of: MBBA (upper panel) and sodium stearate (lower panel). 1

1.2. KBIs of aqueous TBA (left) and aqueous DMSO (right) as function of water mole fraction (taken from Matteoli and Lepori [26]). 4

1.3. Snapshpot of equimolar aqueous TBA system (left panel) and aqueous DMSO (right panel). 4

2.1. The different approaches to computing interactions. 13

2.2. Illustration of the periodic boundary conditons, taken from [90] . . . 14

2.3. An example of the LP shift for the case of carbon united atom correlations in benzene, for the benzene-pentane mixture at $x_{BEN} = 0.2$. . 21

2.4. Schematic of X-ray scattering on a sample. 22

2.5. rKBIs results for the carbon united atom correlation function of benzene, from the benzene-pentane mixture at $x_{BEN} = 0.2$. 26

3.1. The model of the benzene molecule. 32

3.2. Models of molecules: pentane (left), acetone (center) and ethanol (right). 32

3.3. Snapshots of the benzene-pentane mixture at three different mole fractions. 33

3.4. Site–site correlations between the carbon atoms of benzene (upper panel) and between the end methyl groups of heptane (lower panel). . 34

3.5. Kirkwood–Buff integrals G_{AB} for the benzene–pentane system (upper panel) and benzene heptane system (lower panel). 35

3.6. Upper panel: running Kirkwood–Buff integrals $G_{AB}(r)$ for the benzene-pentane system. Lower panel: site-site structure factors corresponding to the rKBIs in the upper panel. 35

3.7. Snapshots of the benzene-acetone mixture, for three different benzene mole fractions. 36

3.8. Kirkwood–Buff integrals for the benzene–acetone system. 37

3.9. Site–site correlations (top) for the equimolar benzene–acetone mixtures... 37
3.10. (Main panel) Ethanol oxygen–oxygen correlations $g_{OO}(r)$ in benzene–ethanol mixtures. 39
3.11. Kirkwood–Buff integrals for the benzene–ethanol system. 40
3.12. Structure factors for the benzene–ethanol system. 41
3.13. Snapshots of the benzene-ethanol system. 41
3.14. Models of solvent molecules: benzene (left), pentane (center) and CCl_4 (right). 42
3.15. Kirkwood–Buff integrals for the acetone-pentane (left) and acetone-CCl_4 system (right). 43
3.16. Correlation functions (left) and their corresponding structure factors (right) for the equimolar acetone-CCl_4 (top) and acetone-pentane mixture (bottom). 44

4.1. Snapshots for the ethanol-methanol mixture 48
4.2. Snapshots for the ethanol-methanol mixture (upper row) and Lennard-Jones mixture (lower row) 49
4.3. Cluster distribution of the oxygen atoms (main panel) and carbon atoms (inset) 50
4.4. Cluster probability distributions calculated for all oxygen atoms in the system, regardless of the molecule. 51
4.5. Selected site-site correlation functions in the methanol-ethanol mixture. 52
4.6. Selected site-site structure factors for the correlations shown in Fig. 4.5 53
4.7. Intermolecular energies (upper panel), molar volumes (lower panel) for the studied systems. 55
4.8. Kirkwood-Buff integrals for the alcohol and LJ mixtures. 56
4.9. The methanol-1-propanol mixture data 57

5.1. Ethanol structuring present in high benzene and water content. . . . 62
5.2. Selected snapshots of aqueous-ethanol (top figures) and hydrocarbon-ethanol (lower figures) mixtures. 63
5.3. Oxygen–oxygen correlation function in ethanol–water mixtures. . . . 65
5.4. Site–site correlations in ethanol–alkane mixtures. 65
5.5. Structure factors for the correlation functions shown in Fig. 5.3. . . . 66
5.6. Site-site structure factors of ethanol methyl groups in water. 67

5.7. Structure factors for the correlation functions shown in Fig. 5.4. . . . 68
5.8. Cluster distribution functions for various sites in the studied systems. 69
5.9. Cluster distribution functions for ethanol OO sites in the studied systems. 70
5.10. Cluster distribution functions for the ethanol methyl group 70

6.1. Temperature dependence of the oxygen-oxygen correlation functions for water (upper row) and methanol (lower row). 75
6.2. Oxygen-Oxygen correlation functions (full lines) and corresponding coordination numbers (dashed lines). 75
6.3. Cluster probability distributions for methanol (upper row) and water (lower row). 76
6.4. Temperature dependence of the oxygen-oxygen structure factors corresponding to the correlation functions in Fig. 6.1. 77
6.5. Kirkwood-Buff integrals of the aqueous methanol mixtures 78
6.6. Site-site correlation functions between the oxygen atoms of aqueous ethanol mixtures. 79
6.7. Site-site correlation functions between the oxygen atoms of aqueous TBA mixtures 80
6.8. Site-site structure factors of aqueous ethanol, calculated from the correlation functions in Fig. 6.6 81
6.9. Site-site structure factors of aqueous TBA, calculated from the correlation functions in Fig. 6.7. 82
6.10. Kirkwood-Buff integrals of the aqueous-ethanol mixture 83
6.11. Kirkwood-Buff integrals of the aqueous TBA mixture 84

7.1. Snapshots of neat propylamine (left panel) and 1-propanol (right panel). 86
7.2. Cluster distribution probabillities for the nitrogen atoms of propylamine (blue line) and the oxygen atoms of 1-propanol (red line). . . 87
7.3. Pair correlation functions and site-site structure factors of selected site-site combinations in neat propylamine 87
7.4. Snapshots of three typical mole fractions of propylamine 89
7.5. Cluster probability distributions for: a) propylamine NN sites (main panel) and CC sites (inset), b) water OO sites. 90
7.6. Pair correlation function for aqueous propylamine. 91
7.7. Site-site structure factors calculated from the pair correlation functions from Fig. 7.6. 92

7.8. Kirkwood-Buff integrals for aqueous propylamine, with respect to the mole fraction of propylamine. 94

8.1. Graphic depiction of 1,n-diol models 98
8.2. Snapshots of neat 1,n-diol alcohols. 99
8.3. Cluster probability P(s) versus cluster size s for neat 1,n-diols. 100
8.4. Site-site pair correlation functions for ethanediol (left panel) and methanol (right panel) 101
8.5. Site-site pair correlation functions for butanediol (left panel) and ethanol (right panel). 102
8.6. Site-site structure factors corresponding to the pair correlations shown in Fig. 8.4 for ethanediol (left panel) and methanol (right panel). . . 103
8.7. Site-site structure factors corresponding to the pair correlations shown in Fig. 8.5 for butanediol (left panel) and ethanol (right panel). . . . 103
8.8. Calculated X-ray scattering intensity I(k) for diols 104
8.9. Snapshots of the 1,2-ethanediol-water system 106
8.10. Oxygen–oxygen correlation functions (left panel) and structure factors (right panel) for the aqueous–ethanediol mixtures. 107
8.11. Oxygen–oxygen correlation functions (left panel) and structure factors (right panel) for the aqueous–propanediol mixtures 107
8.12. Kirkwood–Buff integrals of the aqueous ethanediol (left panel), and aqueous propanediol mixtures (right panel). 109
8.13. Snapshots of the 1,2-ethanediol-ethanol system 110
8.14. Oxygen–oxygen correlation functions (left panel) and structure factors (right panel) for the ethanol–ethanediol mixtures 111
8.15. Oxygen–oxygen correlation functions (left panel) and structure factors (right panel) for the ethanol–propanediol mixtures 111
8.16. Kirkwood–Buff integrals of the ethanol–ethanediol (left panel), and ethanol- propanediol mixtures (right panel). 112

9.1. The KBI results for aqueous pyridine (left panel) and aqueous piperidine mixture (right panel). 117

A.1. Average densities for the tested pure benzene systems (full lines) and their fluctuations. The values were calculated for production runs of already equilibrated systems. 123
A.2. Hydrocarbon united atom radial distribution functions for the tested pure benzene systems. 123

A.3. Main panel: C-C (central carbon atom) radial distribution functions for the tested acetone models. Inset: Methyl-methyl RDFs. 125

A.4. Selected site-site RDFs for pure ethanol (left panel) and pure methanol (right panel), concerning UA and AA models. 128

A.5. Selected site-site structure factors for pure ethanol (left panel) and pure methanol (right panel), concerning UA and AA models. 128

A.6. Selected site-site RDFs for pure ethanol (left panel) and pure methanol (right panel), concerning the forcefield 129

A.7. Selected site-site correlation functions (main panel) and structure factors (inset) for 1-propanol, isopropanol and tert-butanol. 129

B.1. The LP correction for the benzene-pentane mixture, $x_{BEN} = 0.2$. . . . 134

B.2. The LP shift demonstrated for the benzene-acetone mixture, $x_{BEN} = 0.5$. 134

B.3. Structure factors (main panel) and rKBI (inset) for the equimolar ethanol-methanol mixture, demonstrating the LP correction. 135

B.4. Snapshots of the equimolar ethanol-water system for $T = 200$K . . . 136

B.5. Snapshots of the equimolar ethanol water system at $T = 150$ K . . . 136

B.6. A detailed look at selected site-site structure factors (main panel) and rKBIs (inset) for the equilmolar ethanol-water mixture, at $T = 200$K. 137

B.7. Cluster size distribution probabilities versus cluster size for the: aqueous ethanol (left panel) and aqueous- tert-butanol mixture (right panel).137

B.8. LP shift shown for aqueous propylamine, $x_{PROP} = 0.2$, for site-site structure factors (main panel) and rKBIs (inset). 138

B.9. The LP shift, demonstrated for the equimolar mixture of 1,2-ethanediol-water. 138

B.10. Clusters distributions of the diol oxygen sites (main panels) and water oxygen sites (insets), versus the cluster size. 139

B.11. Clusters distributions of the diol oxygen sites (main panels) and ethanol oxygen sites (insets), versus the cluster size. 139

B.12. Thermodynamic properties for mixtures with 1,n-diols. 140

List of Tables

A.1. Thermodynamic results for tested benzene models. 122

A.2. Parameters used for tested acetone models. The sites are: C - central carbon atom; O - oxygen atom; M - methyl group united atom. . . . 124

A.3. Thermodynamic results for tested acetone models. 125

A.4. Thermodinamical properties for tested mono-ol forcefields. The experimental values at 25 °C are taken from [229]. 127

A.5. Thermodinamical properties for tested diol forcefields. The experimental values at 25 °C are taken from [229]. 130

A.6. Thermodinamical properties for tested water forcefields. The experimental values at 25 °C are taken from [229]. 131

A.7. Thermodynamic properties for tested forcefields. The experimental values at 25 °C are taken from [229]. 132

A.8. Thermodynamic results for neat compounds, both original and modified. 132

Curriculum vitae

Martina Požar

Education

- **M.Sc. in Biophysics** (2011 - 2013)

  University of Split, Split, Croatia
- **B.Sc. in Physics** (2008 - 2011)

  University of Split, Split, Croatia

Employment

- **Doctoral fellow** (January 2015 – Nov 2018)

  University of Split, Split, Croatia

  Part of the Croatian Science Foundation project UIP-4514 “Multi-scale description of meso-scale domain formation and destruction”, P.I. dr. sc. Larisa Zoranić

Awards and grants

- **L’Oreal grant "For women in science"** (2018.)
- **French government grant** (2015./16. and 2017./18.)
- **Award for the best young scientist** given by the Faculty of science, University of Split (for 2016. and 2017.)
- **Dean’s award**, given for outstanding GPA after finishing Master studies (2014.)

List of publications

- M. Požar, J-B. Seguier, J. Guerche, R. Mazighi, L. Zoranić, M. Mijaković, B. Kežić-Lovrinčević, F. Sokolić and A. Perera. Simple and complex disorder in binary mixtures with benzene as a common solvent. **Phys. Chem. Chem. Phys.**, 2015, **17**, 9885-9898
- M. Požar, B. Lovrinčević, L. Zoranić, M. Mijaković, F. Sokolić and A. Perera. A re-appraisal of the concept of ideal mixtures through a computer simulation study of the methanol-ethanol mixtures. **J. Chem. Phys.**, 2016, **145**, 064509
- M. Požar, B. Lovrinčević, L. Zoranić, T. Primorac, F. Sokolić and A. Perera. Micro-heterogeneity versus clustering in binary mixtures of ethanol with water or alkanes. **Phys. Chem. Chem. Phys.**, 2016, **18**, 23971-23979
- M. Požar, A. Kerasidou, B. Lovrinčević, L. Zoranić, M. Mijaković, T. Primorac, F. Sokolić, V. Teboul and A. Perera. The microscopic structure of cold aqueous methanol mixtures. **J. Chem. Phys.**, 2016, **145**, 144502
- M. Požar and A. Perera. On the micro-heterogeneous structure of neat and aqueous propylamine mixtures: A computer simulation study. **J. Mol. Liq.**, 2017, **227**, 210-217
- M. Požar and A. Perera. On the existence of a scattering pre-peak in the mono-ols and diols. **Chem. Phys. Lett.**, 2017, **671**, 37-43
- M. Požar and A. Perera. Lifshitz phase: the microscopic structure of aqueous and ethanol mixtures of 1,n-diols. **Phys. Chem. Chem. Phys.**, 2017, **19**, 14992-15004
- M. Požar and A. Perera. Evolution of the micro-structure of aqueous alcohol mixtures with cooling: A computer simulation study. **J. Mol. Liq.**, 2017, **248**, 602-609
- T. Primorac, M. Požar, F. Sokolić, L. Zoranić, T. Urbic. A Simple Two Dimensional Model of Methanol. **J. Mol. Liq.**, 2018, **262**, 46-57
- M. Požar and L. Zoranić. The structuring in mixtures with acetone as the common solvent. Submitted to **Phys. Chem. Liq.** in September 2018.

Bibliography

[1] Rowlinson, J.; Swinton, F. *Liquids and Liquid Mixtures;* Butterworth Scientific, London, 1982.

[2] Sage, I. In *Ullmann's Encyclopedia of Industrial Chemistry;* American Cancer Society, 2000; chapter Liquid Crystals, pages 2015–246.

[3] Kosswig, K.; American Cancer Society, 2000; chapter Surfactants, pages 431–501.

[4] Schumann, K.; Siekmann, K. In *Ullmann's Encyclopedia of Industrial Chemistry;* American Cancer Society, 2000; chapter Soaps, pages 241–261.

[5] Hargreaves, A. *Chemical Formulation*, RSC Paperbacks; The Royal Society of Chemistry, 2003.

[6] Blinov, L. *Structure and Properties of Liquid Crystals;* Springer, 2011.

[7] Friberg, S., Bothorel, P., Eds. *Microemulsions, structure and dynamics;* CRC Press, 1988.

[8] Chevalier, Y.; Zemb, T. *Reports on Progress in Physics* **1990**, *53*(3), 279.

[9] Pubchem compound database; cid=33363. for Biotechnology Information, N. C.

[10] Pubchem compound database; cid=2724691. for Biotechnology Information, N. C.

[11] Hansen, J.-P.; McDonald, I. *Theory of Simple Liquids;* Academic Press, Elsevier, Amsterdam, 3rd ed., 2006.

[12] Kleman, M.; Lavrentovich, O. *Soft Matter Physics: An Introduction;* Springer, 2003.

[13] Ball, P. *Nature* **2008**, *452*, 291.

[14] Franks, F., Ed. *Water. A comprehensive treatise*, Vol. Volume 1. The Physics and Physical Chemistry of Water; Plenum Press, New York - London, 1st ed., 1972.

[15] Franks, F. *Water: A Matrix of Life;* RSC publishing, 2nd ed., 2000.

[16] Ferrario, M.; Haughney, M.; McDonald, I.; Klein, M. *The Journal of Chemical Physics* **1990**, *93*(7), 5156.

[17] de Oliveira, O.; Freitas, L. *Journal of Molecular Structure: THEOCHEM* **2005**, *728*(1-3), 179.

[18] Jalili, S.; Akhavan, M. *Journal of Computational Chemistry* **2010**, *31*, 286.

[19] Kusalik, P.; Lyubartsev, A.; Bergman, D.; Laaksonen, A. *The Journal of Physical Chemistry B* **2000**, *104*(40), 9533.

[20] Ghoufi, A.; Artzner, F.; Malfreyt, P. *The Journal of Physical Chemistry B* **2016**, *120*(4), 793.

[21] Galicia-Andrés, E.; Pusztai, L.; L., T.; Pizio, O. *Journal of Molecular Liquids* **2015**, *209*, 586.

[22] Gereben, O.; Pusztai, L. *The Journal of Physical Chemistry B* **2015**, *119*(7), 3070.

[23] Chitra, R.; Smith, P. *The Journal of Chemical Physics* **2001**, *114*, 426.

[24] Tolman, R. *The Principles of Statistical mechanics;* Clarendon Press Oxford, 1938.

[25] Weis, J.; Levesque, D. *Physical Review Letters* **1993**, *71*, 2729.

[26] Matteoli, E.; Lepori, L. *The Journal of Chemical Physics* **1984**, *80*(6), 2856.

[27] Ben-Naim, A. *The Journal of Chemical Physics* **1977**, *67*(11), 4884.

[28] Donkersloot, M. C. A. *Journal of Solution Chemistry* **1979**, *8*, 293.

[29] Shulgin, I.; Ruckenstein, E. *The Journal of Physical Chemistry B* **1999**, *103*, 2496.

[30] Ben-Naim, A. *Molecular Theory of Solutions;* Oxford University Press, 2006.

[31] Kirkwood, J.; Buff, F. *The Journal of Chemical Physics* **1951**, *19*(6), 774.

[32] Gorzynski Smith, J. *General, organic, and biological chemistry;* McGraw-Hill, New York, 1st ed., 2010.

[33] Kežić, B.; Perera, A. *The Journal of Chemical Physics* **2012**, *137*(1), 014501.

[34] Perera, A.; Mazighi, R. *The Journal of Chemical Physics* **2015**, *143*(15), 154502.

[35] Perera, A.; Kežić, B.; Sokolić, F.; Zoranić, L.; InTech, 2012; chapter Micro-Heterogeneity in Complex Liquids, pages 193–220.

[36] Allison, S.; Fox, J.; Hargreaves, R.; Bates, S. *Physical Review B* **2005**, *71*, 024201.

[37] Zoranić, L.; Mazighi, R.; Sokolić, F.; Perera, A. *The Journal of Chemical Physics* **2009**, *130*(12), 124315.

[38] Mijaković, M.; Kežić, B.; Zoranić, L.; Sokolić, F.; Asenbaum, A.; Pruner, C.; Wilhelm, E.; Perera, A. *Journal of Molecular Liquids* **2011**, *164*(1-2), 66.

[39] Gupta, R.; Patey, G. N. *The Journal of Chemical Physics* **2012**, *137*(3), 034509.

[40] Kežić, B.; Perera, A. *The Journal of Chemical Physics* **2012**, *137*(13), 134502.

[41] Banerjee, S.; Furtado, J.; Bagchi, B. *The Journal of Chemical Physics* **2014**, *140*(19), 194502.

[42] Atkins, P.; de Paula, J. *Atkins' Physical Chemistry;* Oxford University Press, 8th ed., 2006.

[43] Hasted, J.; Plenum Press, New York - London, 1972; chapter Liquid Water: Dielectric Properties, pages 255–305.

[44] Wallqvist, A.; Mountain, R.; Wiley-Blackwell, 2007; chapter Molecular Models of Water: Derivation and Description, pages 183–247.

[45] Ouyang, J.; Bettens, R. *CHIMIA International Journal for Chemistry* **2015**, *69*(3), 104.

[46] Halgren, T.; Damm, W. *Current Opinion in Structural Biology* **2001**, *11*(2), 236.

[47] Bagchi, B. *Water in Biological and Chemical Processes: From Structure and Dynamics to Function*, Cambridge Molecular Science; Cambridge University Press, 1st ed., 2013.

[48] Poole, P.; Sciortino, F.; Essmann, U.; Stanley, H. *Nature* **1992**, *360*, 324.

[49] Bellissent-Funel, M.-C. *Europhysics Letters* **1998**, *42*(2), 161.

[50] Kumar, P.; Franzese, G.; Stanley, H. *Journal of Physics: Condensed Matter* **2008**, *20*(24), 244114.

[51] Bartels-Rausch, T.; Bergeron, V.; Cartwright, J.; Escribano, R.; Finney, J.; Grothe, H.; Gutiérrez, P.; Haapala, J.; Kuhs, W.; Pettersson, J.; Price, S.; Sainz-Díaz, C.; Stokes, D.; Strazzulla, G.; Thomson, E.; Trinks, H.; Uras-Aytemiz, N. *Reviews of Modern Physics* **2012**, *84*, 885.

[52] Röntgen, W. *Annalen der Physik* **1892**, *281*(1), 91.

[53] Limmer, D.; Chandler, D. *The Journal of Chemical Physics* **2011**, *135*(13), 134503.

[54] Smallenburg, F.; Filion, L.; Sciortino, F. *Nature Physics* **2014**, *10*, 653.

[55] Maestro, L.; MarquÃľs, M.; Camarillo, E.; Jaque, D.; SolÃĺ, J. G.; Gonzalo, J.; Jaque, F.; Valle, J. C. D.; Mallamace, F.; Stanley, H. *International Journal of Nanotechnology* **2016**, *13*(8-9), 667.

[56] Gallo, P.; Amann-Winkel, K.; Angell, C.; Anisimov, M.; Caupin, F.; Chakravarty, C.; Lascaris, E.; Loerting, T.; Panagiotopoulos, A.; Russo, J.; Sellberg, J.; Stanley, H.; Tanaka, H.; Vega, C.; Xu, L.; Pettersson, L. *Chemical Reviews* **2016**, *116*(13), 7463.

[57] Kennedy, D., e. *Science* **2005**, *309*(5731), 78.

[58] Soetens, J.-C.; Bopp, P. *The Journal of Physical Chemistry B* **2015**, *119*(27), 8593.

[59] Gubskaya, A. V.; Kusalik, P. G. *Journal of Physical Chemistry A* **2004**, *108*, 7165.

[60] Freitas, L.; Cordeiro, J.; Garbujo, F. *Journal of Molecular Liquids* **1999**, *79*(1), 1.

[61] Freitas, L. *Journal of Molecular Structure: THEOCHEM* **1993**, *282*(1), 151.

[62] González-Salgado, D.; Zemánková, K.; Noya, E.; Lomba, E. *The Journal of Chemical Physics* **2016**, *144*(18), 184505.

[63] Bley, M.; Duvail, M.; Guilbaud, P.; Penisson, C.; Theisen, J.; Gabriel, J.-C.; Dufrêche, J.-F. *Molecular Physics* **2018**, *116*(15-16), 2009.

[64] Zhang, N.; Shen, Z.; Chen, C.; He, G.; Hao, C. *Journal of Molecular Liquids* **2015**, *203*, 90.

[65] Wensink, E. W.; Hoffmann, A.; van Maaren, P.; van der Spoel, D. *The Journal of Chemical Physics* **2003**, *119*(14), 7308.

[66] Parez, S.; Guevara-Carrion, G.; Hasse, H.; Vrabec, J. *Physical Chemistry Chemical Physics* **2013**, *15*, 3985.

[67] Frenkel, D.; Smit, B. *Understanding Molecular Simulation. From Algorithms to Applications.;* Academic Press, 2002.

[68] Allen, M.; Tildesley, D. *Computer Simulation of Liquids;* Clarendon Press Oxford, 1987.

[69] van der Spoel, D.; Lindahl, E.; Hess, B.; Groenhof, G.; Mark, A.; Berendsen, H. *Journal of Computational Chemistry* **2005**, *26*, 1701.

[70] Hess, B.; Kutzner, C.; van der Spoel, D.; Lindahl, E. *Journal of Chemical Theory and Computation* **2008**, *4*(3), 435.

[71] Pronk, S.; Páll, S.; Schulz, R.; Larsson, P.; Bjelkmar, P.; Apostolov, R.; Shirts, M.; Smith, J.; Kasson, P.; van der Spoel, D.; Hess, B.; Lindahl, E. *Bioinformatics* **2013**, *29*(7), 845.

[72] Požar, M.; Seguier, J.-B.; Guerche, J.; Mazighi, R.; Zoranić, L.; Mijaković, M.; Kežić-Lovrinčević, B.; Sokolić, F.; Perera, A. *Physical Chemistry Chemical Physics* **2015**, *17*, 9885.

[73] Požar, M.; Lovrinčević, B.; Zoranić, L.; Mijaković, M.; Sokolić, F.; Perera, A. *The Journal of Chemical Physics* **2016**, *145*(6), 064509.

[74] Požar, M.; Lovrinčević, B.; Zoranić, L.; Primorac, T.; Sokolić, F.; Perera, A. *Physical Chemistry Chemical Physics* **2016**, *18*, 23971.

[75] Požar, M.; Kerasidou, A.; Lovrinčević, B.; Zoranić, L.; Mijaković, M.; Primorac, T.; Sokolić, F.; Teboul, V.; Perera, A. *The Journal of Chemical Physics* **2016**, *145*(14), 144502.

[76] Požar, M.; Perera, A. *Journal of Molecular Liquids* **2017**, *248*(Supplement C), 602.

[77] Požar, M.; Perera, A. *Journal of Molecular Liquids* **2017**, *227*, 210.

[78] Požar, M.; Perera, A. *Chemical Physics Letters* **2017**, *671*, 37.

[79] Požar, M.; Perera, A. *Physical Chemistry Chemical Physics* **2017**, *19*, 14992.

[80] Gray, C.; Gubbins, K. *Theory of Molecular Fluids. Volume I: Fundamentals*, Vol. 1 of *International Series of Monographs on Chemistry (Book 9);* Oxford University Press, 1st ed., 1985.

[81] March, N.; Tosi, M. *Introduction to Liquid State Physics;* World Scientific, 2002.

[82] Koga, Y. *Solution Thermodynamics and its Application to Aqueous Solutions;* Elsevier Science, 1st ed., 2007.

[83] Alder, B.; Wainwright, T. *The Journal of Chemical Physics* **1957**, *27*(5), 1208.

[84] Alder, B.; Wainwright, T. *The Journal of Chemical Physics* **1959**, *31*(2), 459.

[85] Alder, B.; Wainwright, T. *Physical Review (Series I)* **1962**, *127*(2), 359.

[86] Rahman, A. *Physical Review* **1964**, *136*(2A), A405.

[87] Stillinger, F.; Rahman, A. *The Journal of Chemical Physics* **1974**, *60*(4), 1545.

[88] Levitt, M.; Warshel, A. *Nature* **1975**, *253*, 694.

[89] Beveridge, D.; McConnell, K.; Young, M.; Vijayakumar, S.; Ravishanker, G. *Molecular Engineering* **1995**, *5*, 255.

[90] Hinchliffe, A. *Molecular Modelling for Beginners;* John Wiley & Sons, 2nd ed., 2008.

[91] Rapaport, D. *The Art of Molecular Dynamics Simulation;* Cambridge University Press, 2nd ed., 2004.

[92] Verlet, L. *Physical Review* **1967**, *159*, 98.

[93] Swope, W.; Andersen, H.; Berens, P.; Wilson, K. *The Journal of Chemical Physics* **1982**, *76*(1), 637.

[94] Hockney, R.; Orlando Academic Press, 1970; Vol. 9; chapter The potential calculation and some applications, pages 135–221.

[95] Beeman, D. *Journal of Computational Physics* **1976**, *20*(2), 130.

[96] Griebel, M.; Knapek, S.; Zumbusch, G. *Numerical Simulation in Molecular Dynamics: Numerics, Algorithms, Parallelization, Applications;* Springer, 2007.

[97] Ryckaert, J.-P.; Ciccotti, G.; Berendsen, H. *Journal of Computational Physics* **1977**, *23*(3), 327.

[98] Andersen, H. *Journal of Computational Physics* **1983**, *52*(1), 24.

[99] Hess, B.; Bekker, H.; Berendsen, H.; Fraaije, J. *Journal of Computational Chemistry* **1997**, *18*(12), 1463.

[100] Darden, T.; York, D.; Pedersen, L. *The Journal of Chemical Physics* **1993**, *98*(12), 10089.

[101] Essmann, U.; Perera, L.; Berkowitz, M.; Darden, T.; Lee, H.; Pedersen, L. *The Journal of Chemical Physics* **1995**, *103*(19), 8577.

[102] Hockney, R.; Eastwood, J.; CRC Press, 1988; chapter Particle-Particle-Particle-Mesh (P3M) Algorithms, pages 267–304.

[103] Hünenberger, P.; Springer Berlin Heidelberg, 2005; chapter Thermostat Algorithms for Molecular Dynamics Simulations, pages 105–149.

[104] Berendsen, H.; Postma, J.; van Gunsteren, W.; DiNola, A.; Haak, J. *The Journal of Chemical Physics* **1984**, *81*(8), 3684.

[105] Nose, S. *Molecular Physics* **1984**, *52*(2), 255.

[106] Hoover, W. *Physical Review A* **1985**, *31*(3), 1695.

[107] Fine, R.; Millero, F. *The Journal of Chemical Physics* **1973**, *59*(10), 5529.

[108] Parrinello, M.; Rahman, A. *Physical Review Letters* **1980**, *45*(14), 1196.

[109] Parrinello, M.; Rahman, A. *Journal of Applied Physics* **1981**, *52*(12), 7182.

[110] Gromacs user manual. Abraham, M.; van der Spoel, D.; Lindahl, E.; Hess, B.; the GROMACS development team. version 2016 ed., **2018**.

[111] Humphrey, W.; Dalke, A.; Schulten, K. *Journal of Molecular Graphics* **1996**, *14*, 33.

[112] Schrödinger, L. **2015**.

[113] Lebowitz, J.; Percus, J. *Physical Review* **1961**, *122*(6), 1675.

[114] Perera, A.; Sokolić, F. *The Journal of Chemical Physics* **2004**, *121*(22), 11272.

[115] Gray, C.; Gubbins, K.; Joslin, C. *Theory of Molecular Fluids: Volume 2: Applications*, Vol. 2 of *International Series of Monographs on Chemistry (Book 10);* Oxford University Press, 1st ed., 2011.

[116] Pings, C.; Waser, J. *The Journal of Chemical Physics* **1968**, *48*(7), 3016.

[117] Morrison, P.; Pings, C. *The Journal of Chemical Physics* **1974**, *60*(6), 2323.

[118] Mondello, M.; Yang, H.-J.; Furuya, H.; Roe, R.-J. *Macromolecules* **1994**, *27*(13), 3566.

[119] Tsolou, G.; Harmandaris, V.; Mavrantzas, V. *Macromolecular Theory and Simulations* **2006**, *15*(5), 381.

[120] Migliorati, V.; Serva, A.; Aquilanti, G.; Pascarelli, A.; D'Angelo, P. *Physical Chemistry Chemical Physics* **2015**, *17*, 16443.

[121] Jónsson, H.; Andersen, H. *Physical Review Letters* **1988**, *60*, 2295.

[122] Bakó, I.; Jedlovszky, P.; Pálinkás, G. *Journal of Molecular Liquids* **2000**, *87*(2), 243.

[123] Pugnaloni, L.; Vericat, F. *The Journal of Chemical Physics* **2002**, *116*(3), 1097.

[124] Zoranić, L.; Sokolić, F.; Perera, A. *The Journal of Chemical Physics* **2007**, *127*(2), 024502.

[125] Perera, A.; Sokolić, F.; Zoranić, L. *Physical Review E* **2007**, *75*(6), 060502(R).

[126] Dougan, L.; Hargreaves, R.; Bates, S. P.; Finney, J. L.; Réat, V.; Soper, A. K.; Crain, J. *The Journal of Chemical Physics* **2005**, *122*(17), 174514.

[127] Liu, Y.; Consta, S.; Shi, Y.; Lipson, R.; Goddard, W. *The Journal of Physical Chemistry A* **2009**, *113*(25), 6865.

[128] Anikeenko, A.; Kadtsyn, E.; Medvedev, N. *Journal of Molecular Liquids* **2017**, *245*, 35.

[129] Bakó, I.; Pusztai, L.; Temleitner, L. *Scientific Reports* **2017**, *7*, 1073.

[130] Mondal, S.; Biswas, B.; Sarkar, S.; Singh, P. *Journal of Molecular Liquids* **2017**, *240*, 708.

[131] Hill, T. *The Journal of Chemical Physics* **1955**, *23*(4), 617.

[132] Stillinger, F. *The Journal of Chemical Physics* **1963**, *38*(7), 1486.

[133] Perera, A.; Sokolić, F.; Almásy, L.; Westh, P.; Koga, Y. *The Journal of Chemical Physics* **2005**, *123*(2), 024503.

[134] Perera, A.; Sokolić, F.; Almásy, L.; Koga, Y. *The Journal of Chemical Physics* **2006**, *124*(12), 124515.

[135] Perera, A.; Mazighi, R. *Journal of Molecular Liquids* **2015**, *210*, 243.

[136] Siqueira, L.; Ribeiro, M. *The Journal of Chemical Physics* **2011**, *135*(20), 204506.

[137] Wang, Y.; Voth, G. *Journal of the American Chemical Society* **2005**, *127*(35), 12192.

[138] Wang, Y.; Jiang, W.; Yan, T.; Voth, G. *Accounts of Chemical Research* **2007**, *40*(11), 1193.

[139] Allinger, N. Vol. 13 of *Advances in Physical Organic Chemistry;* Academic Press, 1976; pages 1–82.

[140] Momany, F.; McGuire, R.; Burgess, A.; Scheraga, H. *The Journal of Physical Chemistry* **1975**, *79*(22), 2361.

[141] Brooks, B.; Bruccoleri, R.; Olafson, B.; States, D.; Swaminathan, S.; Karplus, M. *Journal of Computational Chemistry* **1983**, *4*(2), 187.

[142] Jorgensen, W.; Madura, J.; Swenson, C. *Journal of the American Chemical Society* **1984**, *106*(22), 6638.

[143] Cornell, W.; Cieplak, P.; Bayly, C.; Gould, I.; Merz, K.; Ferguson, D.; Spellmeyer, D.; Fox, T.; Caldwell, J.; Kollman, P. *Journal of the American Chemical Society* **1995**, *117*(19), 5179.

[144] de Gennes, P.; Prost, J. *The Physics of Liquid Crystals;* Clarendon Press Oxford, 2nd ed., 1993.

[145] Zoranić, L.; Mazighi, R.; Sokolić, F.; Perera, A. *The Journal of Physical Chemistry C* **2007**, *111*(43), 15586.

[146] Idrissi, A.; Sokolić, F.; Perera, A. *The Journal of Chemical Physics* **2000**, *112*(21), 9479.

[147] Sokolić, F.; Idrissi, A.; Perera, A. *Journal of Molecular Liquids* **2002**, *101*(1-3), 81.

[148] Asenbaum, A.; Pruner, C.; Wilhelm, E.; Mijaković, M.; Zoranić, L.; Sokolić, F.; Kezić, B.; Perera, A. *Vibrational Spectroscopy* **2012**, *60*, 102.

[149] Mijaković, M.; Polok, K.; Kežić, B.; Sokolić, F.; Perera, A.; Zoranić, L. *Molecular Simulation* **2015**, *41*(9), 699.

[150] Allen, P. W.; Bowen, H. J. M.; Sutton, L. E.; Bastiansen, O. *Trans. Faraday Soc.* **1952**, *48*, 991–995.

[151] Orchin, M.; Macomber, R.; Pinhas, A.; Wilson, R. *The vocabulary and concepts of organic chemistry;* John Wiley & Sons, 2nd ed., 2005.

[152] Musso, M.; Giorgini, M.; Torii, H.; Dorka, R.; Schiel, D.; Asenbaum, A.; Keutel, D.; Oehme, K.-L. *Journal of Molecular Liquids* **2006**, *125*(2-3), 115.

[153] Sarkar, S.; Joarder, R. N. *The Journal of Chemical Physics* **1994**, *100*(7), 5118.

[154] Ploetz, E.; Smith, P. *Physical Chemistry Chemical Physics* **2011**, *13*, 18154.

[155] Narten, A. H.; Habenschuss, A. *The Journal of Chemical Physics* **1984**, *80*(7), 3387.

[156] Engel, T.; Reid, P. *Physical Chemistry;* Pearson, 3rd ed., 2013.

[157] Lebowitz, J.; Rowlinson, J. *The Journal of Chemical Physics* **1964**, *41*(1), 133.

[158] Kranendonk, W.; Frenkel, D. *Molecular Physics* **1991**, *72*(3), 715.

[159] Mortimer, R. *Physical Chemistry;* Elsevier Academic Press, 3rd ed., 2008.

[160] Privat, R.; Jaubert, J.-N. *Chemical Engineering Science* **2012**, *82*, 319.

[161] Magini, M.; Paschina, G.; Piccaluga, G. *The Journal of Chemical Physics* **1982**, *77*(4), 2051.

[162] Benmore, C.; Loh, Y. *The Journal of Chemical Physics* **2000**, *112*(13), 5877.

[163] Liu, Y.; Consta, S.; Ogeer, F.; Shi, Y.; Lipson, R. *Canadian Journal of Chemistry* **2007**, *85*(10), 843.

[164] Benson, G.; Pflug, H. *Journal of Chemical and Engineering Data* **1970**, *15*(3), 382.

[165] Matteoli, E. *The Journal of Physical Chemistry B* **1997**, *101*(47), 9800.

[166] Shulgin, I.; Ruckenstein, E. *The Journal of Physical Chemistry B* **2006**, *110*(25), 12707.

[167] Ploetz, E.; Bentenitis, N.; Smith, P. *The Journal of Chemical Physics* **2010**, *132*(16), 164501.

[168] Guevara-Carrion, G.; Nieto-Draghi, C.; Vrabec, J.; Hasse, H. *The Journal of Physical Chemistry B* **2008**, *112*(51), 16664.

[169] Vahvaselkä, K. S.; Serimaa, R.; Torkkeli, M. *Journal of Applied Crystallography* **1995**, *28*, 189.

[170] Tomšič, M.; Jamnik, A.; Fritz-Popovski, G.; Glatter, O.; Vlček, L. *The Journal of Physical Chemistry B* **2007**, *111*(7), 1738.

[171] Warren, B. *Physical Review* **1933**, *44*, 969.

[172] Pierce, W.; MacMillan, D. *Journal of the American Chemical Society* **1938**, *60*(4), 779.

[173] Yamaguchi, T.; Hidaka, K.; Soper, A. *Molecular Physics* **1999**, *96*(8), 1159.

[174] Murdoch, K.; Ferris, T.; Wright, J.; Farrar, T. *The Journal of Chemical Physics* **2002**, *116*(13), 5717.

[175] Balanay, M.; Kim, D.; Fan, H. *The Journal of Chemical Physics* **2016**, *144*(15), 154302.

[176] Berendsen, H.; Postma, J.; van Gunsteren, W.; Hermans, J.; Reidel, Dordrecht, 1981; chapter Interaction models for water in relation to protein hydration, pages 331–342.

[177] Berendsen, H. J. C.; Grigera, J. R.; Straatsma, T. P. *The Journal of Physical Chemistry* **1987**, *91*(24), 6269.

[178] Abascal, J.; Vega, C. *The Journal of Chemical Physics* **2005**, *123*(23), 234505.

[179] Perera, A. *Molecular Physics* **2011**, *109*(20), 2433.

[180] Lum, K.; Chandler, D.; Weeks, J. *The Journal of Physical Chemistry B* **1999**, *103*(22), 4570.

[181] Chandler, D. *Nature* **2005**, *437*, 640.

[182] Duffy, E.; Severance, D.; Jorgensen, W. *Journal of the American Chemical Society* **1992**, *114*(19), 7535.

[183] Banerjee, S.; Bagchi, B. *The Journal of Chemical Physics* **2013**, *139*(16), 164301.

[184] Lee, M.; van der Vegt, N. *The Journal of Chemical Physics* **2005**, *122*(11), 114509.

[185] Chitra, R.; Smith, P. *The Journal of Chemical Physics* **2001**, *114*(1), 426.

[186] Dixit, S.; Crain, J.; Poon, W.; Finney, J.; Soper, A. *Nature* **2002**, *416*, 829.

[187] Guo, J.-H.; Luo, Y.; Augustsson, A.; Kashtanov, S.; Rubensson, J.-E.; Shuh, D. K.; Ågren, H.; Nordgren, J. *Physical Review Letters* **2003**, *91*, 157401.

[188] Zhong, Y.; Warren, G.; Patel, S. *Journal of Computational Chemistry* **2008**, *29*(7), 1142.

[189] Perera, A.; Zoranić, L.; Sokolić, F.; Mazighi, R. *Journal of Molecular Liquids* **2011**, *159*, 52.

[190] Schneider, G. *Zeitschrift fÃijr Physikalische Chemie* **1964**, *41*(5-6), 327.

[191] Aizpiri, A.; Monroy, F.; del Campo, C.; Rubio, R.; Diaz Pena, M. *Chemical Physics* **1992**, *165*(1), 31.

[192] Perera, A. *Pure and Applied Chemistry* **2016**, *88*(3), 189.

[193] Ghosh, R.; Bagchi, B. *The Journal of Physical Chemistry B* **2016**, *120*(49), 12568.

[194] Rochelle, G. *Science* **2009**, *325*(5948), 1652.

[195] Rao, A.; Rubin, E. *Environmental Science & Technology* **2002**, *36*(20), 4467.

[196] Ruiz-Capillas, C.; Jiménez-Colmenero, F. *Critical Reviews in Food Science and Nutrition* **2005**, *44*(7-8), 489.

[197] Silla Santos, M. *International Journal of Food Microbiology* **1996**, *29*(2), 213.

[198] Hallifax, D.; Houston, J. *Drug Metabolism and Disposition* **2007**, *35*(8), 1325.

[199] Kusalik, P.; Bergman, D.; Laaksonen, A. *The Journal of Chemical Physics* **2000**, *113*(18), 8036.

[200] Orozco, G.; Nieto-Draghi, C.; Mackie, A.; Lachet, V. *The Journal of Physical Chemistry B* **2011**, *115*(49), 14617.

[201] Stephenson, R. *Journal of Chemical and Engineering Data* **1993**, *38*(4), 625.

[202] Triolo, A.; Russina, O.; Bleif, H.-J.; Di Cola, E. *The Journal of Physical Chemistry B* **2007**, *111*(18), 4641.

[203] Annapureddy, H.; Kashyap, H.; De Biase, P.; Margulis, C. *The Journal of Physical Chemistry B* **2010**, *114*(50), 16838.

[204] Rebsdat, S.; Mayer, D. In *Ullmann's Encyclopedia of Industrial Chemistry;* American Cancer Society, 2000; chapter Ethylene Glycol, pages 531–544.

[205] K̈opnick, H.; Schmidt, M.; Brügging, W.; Rüter, J.; Kaminsky, W. In *Ullmann's Encyclopedia of Industrial Chemistry;* American Cancer Society, 2000; chapter Polyesters, pages 623–646.

[206] Christoph, R.; Schmidt, B.; Steinberner, U.; Dilla, W.; Karinen, R. In *Ullmann's Encyclopedia of Industrial Chemistry;* American Cancer Society, 2006; chapter Glycerol, pages 67–81.

[207] D'Arrigo, G.; Giordano, R.; Teixeira, J. *Langmuir* **2000**, *16*(4), 1553.

[208] D'Arrigo, G.; Giordano, R.; Teixeira, J. *The European Physical Journal E* **2003**, *10*(2), 135.

[209] D'Arrigo, G.; Giordano, R.; Teixeira, J. *The European Physical Journal E* **2009**, *29*(1), 37.

[210] Tomšič, M.; Cerar, J.; Jamnik, A. *Journal of Molecular Liquids* **2018**, *259*, 291.

[211] Hornreich, R. M.; Luban, M.; Shtrikman, S. *Physical Review Letters* **1975**, *35*, 1678.

[212] Perera, A. *Physical Chemistry Chemical Physics* **2017**, *19*, 1062.

[213] Abdelmoulahi, H.; Ghalla, H.; Nasr, S.; Bahri, M.; Bellissent-Funel, M.-C. *Journal of Molecular Liquids* **2016**, *220*(Supplement C), 527.

[214] Teubner, M.; Strey, R. *The Journal of Chemical Physics* **1987**, *87*(5), 3195.

[215] Head-Gordon, T.; Hura, G. *Chemical Reviews* **2002**, *102*(8), 2651.

[216] Nishikawa, K.; Iijima, T. *Journal of Physical Chemistry* **1993**, *97*, 10824.

[217] Marcus, Y. *Journal of Molecular Liquids* **2003**, *107*(1), 109.

[218] Geerke, D.; van Gunsteren, W. *Molecular Physics* **2007**, *105*(13-14), 1861.

[219] Hansen, J.-P.; Verlet, L. *Physical Review* **1969**, *184*, 151.

[220] McDonald, I.; Klein, M. *The Journal of Chemical Physics* **1978**, *68*(11), 4875.

[221] Impey, R.; Klein, M.; McDonald, I. *The Journal of Chemical Physics* **1981**, *74*(1), 647.

[222] Reimers, J.; Watts, R.; Klein, M. *Chemical Physics* **1982**, *64*(1), 95.

[223] Debenedetti, P.; Stillinger, F. *Nature* **2001**, *410*, 259.

[224] Amann-Winkel, K.; Bellissent-Funel, M.; Bove, L.; Loerting, T.; Nilsson, A.; Paciaroni, A.; Schlesinger, D.; Skinner, L. *Chemical Reviews, American Chemical Society* **2016**, *116*, 7570.

[225] Frank, H.; Wen, W.-Y. *Discussions of The Faraday Society* **1957**, *24*, 133.

[226] Némethy, G.; Scheraga, H. *The Journal of Chemical Physics* **1962**, *36*(12), 3382.

[227] Jackson, M. *Molecular and Cellular Biophysics;* Cambridge University Press, 2006.

[228] Israelachvili, J. *Intermolecular and Surface Forces;* Academic Press, 2nd ed., 1991.

[229] Lide, D. R., Ed. *CRC Handbook of Chemistry and Physics, 90th Edition (CD-ROM Version 2010);* CRC Press/Taylor and Francis, Boca Raton, FL, 2010.

[230] Marczak, W.; Holaj-Krzak, J.; Lodowski, P.; Almásy, L.; Fadda, G. *Chemical Physics Letters* **2015**, *619*, 77.

[231] Almásy, L.; Jancsó, G. *Journal of Molecular Liquids* **2004**, *113*(1), 61.

[232] Jorgensen, W.; McDonald, N. *Journal of Molecular Structure: THEOCHEM* **1998**, *424*(1-2), 145.

[233] Rai, N.; Siepmann, J. *The Journal of Physical Chemistry B* **2007**, *111*(36), 10790.

[234] Oostenbrink, C.; Villa, A.; Mark, A.; van Gunsteren, W. *Journal of Computational Chemistry* **2004**, *25*(13), 1656.

[235] Rizzo, R.; Jorgensen, W. *Journal of the American Chemical Society* **1999**, *121*(20), 4827.

[236] Jorgensen, W.; Maxwell, D.; Tirado-Rives, J. *Journal of the American Chemical Society* **1996**, *118*(45), 11225.

[237] Mahoney, M.; Jorgensen, W. *The Journal of Chemical Physics* **2000**, *112*(20), 8910.

[238] Ben-Naim, A. *The Journal of Chemical Physics* **1971**, *54*, 3682.

[239] Ben-Naim, A. *Molecular Physics* **1972**, *24*, 705.

[240] Primorac, T.; Požar, M.; Sokolić, F.; Zoranić, L.; Urbic, T. *Journal of Molecular Liquids* **2018**, *262*, 46.

[241] Hribar-Lee, B.; Dill, K. A. *Acta Chimica Slovenica* **2006**, *53*, 257.

[242] Zielkiewicz, J. *The Journal of Physical Chemistry* **1995**, *99*(10), 3357.

[243] Goodman, M.; Listowsky, I. *Journal of The American Chemical Society* **1962**, *84*, 3770.

[244] Kumar, S.; Modig, K.; Halle, B. *Biochemistry* **2003**, *42*, 13708.

[245] MacPhee, C.; Perugini, M.; Sawyer, W.; Howlett, G. *FEBS Letters* **1997**, *416*(3), 265.

[246] Haney, E.; Hunter, H.; Matsuzaki, K.; Vogel, H. *Biochimica et Biophysica Acta (BBA) - Biomembranes* **2009**, *1788*(8), 1639.

[247] Hong, D.-P.; Hoshino, M.; Kuboi, R.; Goto, Y. *Journal of The American Chemical Society* **1999**, *121*, 8427.

[248] Kuprin, S.; Graslund, A.; Ehrenberg, A.; Koch, M. *Biochemical and Biophysical Research Communications* **1995**, *217*, 1151.

[249] Takamuku, T.; Kumai, T.; Yoshida, K.; Otomo, T.; Yamaguchi, T. *The Journal of Physical Chemistry A* **2005**, *109*, 7667.

[250] Gast, K.; Zirwer, D.; MÃijller-Frohne, M.; Damaschun, G. *Protein Science* **1999**, *8*, 625.

[251] Martínez, J.; Martínez, L. *Journal of Computational Chemistry* **2003**, *24*(7), 819.

[252] Evans, D.; Watts, R. *Molecular Physics* **1976**, *32*(1), 93.

[253] Claessens, M.; Ferrario, M.; Ryckaert, J.-P. *Molecular Physics* **1983**, *50*(1), 217.

[254] Steinhauser, O. *Chemical Physics* **1982**, *73*(1-2), 155.

[255] Linse, P. *Journal of the American Chemical Society* **1984**, *106*(19), 5425.

[256] Jorgensen, W.; Severance, D. *Journal of the American Chemical Society* **1990**, *112*(12), 4768.

[257] Wick, C.; Martin, M.; Siepmann, J. *The Journal of Physical Chemistry B* **2000**, *104*(33), 8008.

[258] Bonnaud, P.; Nieto-Draghi, C.; Ungerer, P. *The Journal of Physical Chemistry B* **2007**, *111*(14), 3730.

[259] Smith, G.; Jaffe, R. *The Journal of Physical Chemistry* **1996**, *100*(23), 9624.

[260] Fu, C.-F.; Tian, S. X. *Journal of Chemical Theory and Computation* **2011**, *7*(7), 2240.

[261] Bussi, G.; Donadio, D.; Parrinello, M. *The Journal of Chemical Physics* **2007**, *126*(1), 014101.

[262] Narten, A. H. *The Journal of Chemical Physics* **1977**, *67*(5), 2102.

[263] Jorgensen, W.; Briggs, J.; Contreras, M. *The Journal of Physical Chemistry* **1990**, *94*(4), 1683.

[264] Stubbs, J.; Potoff, J.; Siepmann, J. *The Journal of Physical Chemistry B* **2004**, *108*(45), 17596.

[265] Jorgensen, W. *The Journal of Physical Chemistry* **1986**, *90*(7), 1276.

[266] Chen, B.; Potoff, J.; Siepmann, J. *The Journal of Physical Chemistry B* **2001**, *105*(15), 3093.

[267] Saiz, L.; Padró, J.; Guàrdia, E. *The Journal of Chemical Physics* **2001**, *114*(7), 3187.

[268] Kaiser, A.; Ismailova, O.; Koskela, A.; Huber, S.; Ritter, M.; Cosenza, B.; Benger, W.; Nazmutdinov, R.; Probst, M. *Journal of Molecular Liquids* **2014**, *189*(Supplement C), 20.

[269] Gubskaya, A.; Kusalik, P. *The Journal of Physical Chemistry A* **2004**, *108*(35), 7151.

[270] Kony, D.; Damm, W.; Stoll, S.; Van Gunsteren, W. F. *Journal of Computational Chemistry* **2002**, *23*(15), 1416.

[271] Vega, C.; Abascal, J. *Physical Chemistry Chemical Physics* **2011**, *13*, 19663.

[272] Martin, M.; Siepmann, J. *The Journal of Physical Chemistry B* **1998**, *102*(14), 2569.

[273] Oostenbrink, C.; Juchli, D.; van Gunsteren, W. *Chemphyschem* **2005**, *6*(9), 1800.

[274] Vrbka, L.; Jungwirth, P. *Physical Review Letters* **2005**, *95*, 148501.

[275] Matsumoto, M.; Saito, S.; Ohmine, I. *Nature* **2002**, *416*, 409.

[276] Albuquerque, L.; Ventura, C.; Goncalves, R. *Journal of Chemical & Engineering Data* **1996**, *41*(4), 685.

[277] Moosavi, M.; Rostami, A. *Journal of Chemical & Engineering Data* **2017**, *62*(1), 156.

[278] Zaoui-Djelloul-Daouadji, M.; Mokbel, I.; Bahadur, I.; Negadi, A.; Jose, J.; Ramjugernath, D.; Ebenso, E.; Negadi, L. *Thermochimica Acta* **2016**, *642*, 111.

[279] George, J.; Sastry, N. *Journal of Chemical & Engineering Data* **2003**, *48*, 1529.